UNIVERSITÉ DE STRASBOURG

ÉCOLE DOCTORALE DES SCIENCES DE LA VIE ET DE LA SANTE (ED 414)

Génétique Moléculaire, Génomique, Microbiologie (GMGM) – UMR 7156

THÈSE présentée par :

Myriam Sanjuán Vázquez

soutenue le : **29 Janvier 2018**

pour obtenir le grade de : **Docteur de l'Université de Strasbourg**

Discipline/ Spécialité : Aspects moléculaires et cellulaires de la biologie

Study of proteins implicated in centronuclear myopathies by using the model of yeast *Saccharomyces cerevisiae*

THÈSE dirigée par :

Mme FRIANT Sylvie GMGM, Université de Strasbourg

RAPPORTEURS :

Mme TRONCHERE Hélène Institut des Maladies Métaboliques et Cardiovasculaires, Toulouse

M. BITOUN Marc Institut de Myologie, Paris

AUTRES MEMBRES DU JURY :

M. LESCURE Alain Institut de Biologie Moléculaire et Cellulaire, Strasbourg

Acknowledgements

I am grateful to have had the opportunity of making and completing this doctoral thesis. It has been a process of both professional and personal growth. In the process, several people have participated in this achievement.

I will start by respectfully thanking the members of the jury for accepting to read and evaluate my thesis work, Dr. Alain Lescure, Dr Hélène Tronchère and Dr. Marc Bitoun. I really appreciate your interest.

I would like to thank Dr. Sylvie Friant for accepting me in her research team when I was then “just” an erasmus student; later she gave me the opportunity to continue my studies with a doctorate. I am grateful to Dr. Joern Putz, who as erasmus coordinator, put me in contact with Sylvie Friant to my M2S4 internship and who then informed us about the possibility of applying for an IDEX Fellowship at the University of Strasbourg.

Thanks really to the University of Strasbourg for its policy of opening up to the reception of new students coming out of France and by the IDEX Fellowship which has made it possible to finance me during these 3 years and 3 months. I have very good memories of these years as student in this University and in this city so beautiful that is Strasbourg.

Thanks to the members of the team. Thanks to Bruno Rinaldi, Speedy Gonzales of the team; he has always solutions for all, either for problems in the experiments at the laboratory as in experiments at home. At the beginning, I worked with him to learn the techniques in yeast cells. His good character and generosity has helped me to feel at home in the lab during these 5 years. Thanks to Johan de Craene, who although is not in the team (University of Tours has won a good part) was essential for the successful completion of my master project and my continuation on the team. I appreciated his passion for science, which he transmitted to me and I greatly enjoyed our scientific conversations in which I learned a lot with a great fascination and enthusiasm. Thanks to Séverine Bär also for her support, for your attentive listening and interest in our scientific or not discussions, she is always there to help.

Thanks to other PhD students in the department, all of us have gone through the same thing and at the same time, it's been a very valuable support. Thanks to Matthieu Raess for the calm he transmits to me and for the help throughout these years, with him I have learned to take small thing less seriously and look at the positive side of things many times. Thanks to Gaétan Bader for their friendliness and their help always available at the most needed moments, I am still remembering my

“mi-parcours” of thesis and my beginnings in the OpenLab project. Thanks to Romuald Loutre by his affable character and interesting conversations. Thanks to Sylvain Debard for his interest and advice in my experiments on oxidative stress. By the way, thanks to Dimitri Bertazzi, who although I saw him once and I do not know at all, I've heard and said his name more times what I can remember in last years; He defended his thesis just until I came to the laboratory and his experiments have allowed that I continue with my own. Thanks to Roberto Silva Rojas, student erasmus at the time, with whom I started the dynamin project

Thanks to the rest of the people in the department, each has brought something special: Virgile Jarrige, Damien Jeandard, Anne-Marie Heckel, Hubert Becker, Bruno Senger, Laurence Huck, Frédéric Fischer, Anna Smirnova, Alexandre Smirnov, Nina Entelis, Ivan Tarassov, Benoît Masquida, Denise Stuber, Nathaniel Yakobov, Marine Hemmerle, Daphné Laporte, Yuhei Araiso, Ludovic Enkler, Aline Keilbach, Noemi Bindel.

Thank you to the organizers and responsible members of the OpenLAB operation, especially Serge Potier, Laurence Marechal-Drouard, Vincent Leclerc, Stéphane Vincent et Lucile Schneider. It has been a wonderful and very rewarding experience for 2 years. It has allowed me to share the science in a practical way with the students in the high schools through Alsace.

Thanks to my family and friends; the great strength that supports me and allows me to move forward. It would have been impossible to do this doctorate without them. Thanks to my grandparents who rest in peace, I keep the memory of my grandfather “calacala” saying “go into the bullring with the courage of a bullfighter, with your head high and ready to take the bull by the horns”; my grandmother “aia” who had better memory than me, and reminded me of my past achievements to encourage me in the present. Thanks to my mother, Mari Carmen, who listens to me, understands me, supports me, and who believes in me more than anybody; that is something so valuable that I never be able to give the favor back. Thanks to my father, Ricardo, who gave me the passion for understanding science and the world that surrounds us. The two are an example of perseverance. Thanks to my sisters Cristina and Paloma, from whom there is so much to learn. Thanks to Mari Cruz Colodrón, who unfortunately will not see this completed work, without her I would have never finished not even the Bachelor's degree in biochemistry; she has been essential in my life and a decisive person so that I have reached where I am now.

Abbreviations

CMD congenital muscular dystrophies

CMT Charcot-Marie-Tooth

CNM centronuclear myopathy

DNM2 dynamin 2

ECC excitation-contraction coupling

ER endoplasmic reticulum

ESCRT endosomal sorting complex required for transport

GSH glutathione

HTZ heterozygous

MTM1 myotubularin 1

MVB multivesicular bodies

NO nitric oxide

PI phosphoinositides

PtdIns Phosphatidylnositol

PI3P Phosphatidylinositol 3-monophosphate (or PtdIns3*P*)

PI(3,4)P_2 Phosphatidylinositol 3,4-biphosphate (or PtdIns3,4P_2)

PI(3,4,5)P_3 Phosphatidylinositol 3,4,5-trisphosphate (or PtdIns3,4,5P_3)

ROS reactive oxygen species

RTKs Receptor tyrosine kinase

Vps vacuolar protein sorting

I. Introduction

During my thesis, I have put my efforts on a better understanding at the molecular level of three congenital centronuclear myopathies (CNM): firstly, the x-linked centronuclear myopathy (XLCNM) associated to mutations in the *MTM1* gene, secondly the centronuclear myopathy associated to mutations in *PYROXD1* and thirdly the autosomal centronuclear myopathy associated to mutations in *DNM2*. They have some common characteristics especially at the histological level of the patient muscle and at the physiopathology of the myopathy symptoms, but they have also differences. Three different genes are affected, and the proteins produced by their expression are implicated in specific cellular pathways.

In my opinion, the better we understand a problem, the more we will be able to find a suitable solution. Therefore the aim of my PhD thesis was to acquire more information about the molecular function of these proteins, to better understand these disorders and in the future be able to develop a suitable and targeted therapy for the affected patients.

The aim of this introduction is to get a general view of these three types of centronuclear myopathies, with a specific focus at the molecular level but at the same time trying to find the evidences showing that they are connected. I will first give an overview of the clinical and histological features and then focus on the molecular and cellular functions of the three proteins, MTM1 myotubularin, PYROXD1 oxidoreductase and DNM2 dynamin. I will specifically highlight their functions in the cells and link these to the domains present in these proteins. Moreover, I will present the *Saccharomyces cerevisiae* yeast, as this was the model that I used to study these three proteins.

1.1. The different centronuclear myopathies

Myopathy refers to a pathology affecting muscles. They may originate from many causes, including congenital, metabolic, immunological or inflammatory, idiopathic, infectious, nutritional, endocrine, and drug-induced or toxic myopathies. Centronuclear myopathy (CNM) belongs to the large group of **congenital myopathies (**inherited neuromuscular disorders) and as indicated by its

name, nuclei of the patient's fibers are located in the center. Congenital myopathy should not be confused with congenital dystrophy (CMD), even though both present similar features as hypotonia and muscle weakness. Both CMD and Congenital myopathy are usually either static or slowly progressive. Some symptoms are specific of congenital myopathies, such as marked facial weakness, which is poorly associated to congenital muscular dystrophies (CMDs). It is also unlikely to observe ophthalmoplegia (paralysis of one or more extraocular muscles which are responsible for eye movements) in CMD, although it is a diagnostic clue in some congenital myopathies (Bertini et al, 2011). There are at least 30 types of CMDs and only a small group of them affects proteins directly involved in specific muscle process. Indeed, the majority of CMDs is caused by mutations in genes that code for proteins with a role connected to the extracellular matrix (i.e. integrin-alpha 7 gene, integrin alpha 9 gene, collagen 6…). **Congenital myopathies** can be classified in 5 types, Table 1 shows the different types of disorders and the genes that are implicated.

Disorder	Inheritance	Protein (gene)/locus
Congenital myopathies associated with protein accumulation		
Nemaline myopathy	AD,AR	α-tropomyosin$_{SLOW}$ (TPM3)
	AR	nebulin (NEB)
	AD,AR	skeletal α-actin (ACTA1)
	AD	β-tropomyosin (TPM2)
	AR	troponin T (TNNT1)
	AR	cofilin (CLF2)
Cap disease (variant of nemalin myopathy)	AD	β-tropomyosin (TPM2)
	AD	α-tropomyosin$_{SLOW}$ (TPM3)
	AD	skeletal α-actin (ACTA1)
Zebra body myopathy (variant of nemalin Myopathy)	AD	skeletal α-actin (ACTA1)
Myosin storage myopathy (hyaline body)	AD	slow/β-cardiac myosin heavy chain (MYH7)
Congenital myopathies associated with cores		
Central core disease	AD,AR	Ryanodine receptor (RYR1)
Multi-minicore disease	AD,AR	Ryanodine receptor (RYR1)
Including congenital myopathy with cores	AR	Selenoprotein N (SEPN1)

(both central and minicores)	AD	skeletal α-actin (ACTA1)
Congenital myopathies associated with cores and rods		
Core-rod myopathy	AD,AR	Ryanodine receptor (RYR1)
	AD	Kelch repeat BTB (POZ) domain containing 13 (KBTBD13)
	AR	Nebulin (NEB)
Congenital myopathies associated with centralized nuclei		
Myotubular myopathy	X-linked	Myotubularin (MTM1)
Centronuclear myopathy	AD	Dynamin 2 (DNM2)
	AR, AD	Amphiphysin 2 (BIN1)
	AR	Ryanodine receptor (RYR1)
Congenital myopathies associated only with small type I fibers		
Congenital fiber type disproportion	AD	skeletal α-actin (ACTA1)
	AD	α-tropomyosin$_{SLOW}$ (TPM3)
	AR	Selenoprotein N (SEPN1)
	AD	β-tropomyosin (TPM2)
	X-linked	Xp22.13 to Xq22.1
Abbreviations: AD autosomal dominant, AR autosomal recessive.		

Table 1: Classification of congenital myopathies. Centronuclear myopathy is a subgroup of this kind of neuromuscular disorders. Myopathies due to mutations in PYROXD1 gene have mixed features of the 5 groups. Adapted from (North, 2008; Wang et al, 2012)

The number of cases of newborn or/and children (age<18 years) in the population who are suffering of centronuclear myopathy has been estimated to be <1 in 100 000 distributed among MTM1 (45%), DNM2 (15%), RYR1 (10-15%) and BIN1 (<5%) (Amburgey et al, 2011). The remaining ~20% of cases probably have mutations in yet to be identified genes (Biancalana et al, 2012; Tosch et al, 2010). Currently, next-generation sequencing is used for the molecular diagnosis of these patients suffering of centronuclear myopathy but without an identified causative gene (Tosch et al, 2010; Vasli et al, 2012a).

In order to better understand the histology, I show the hematoxylin and eosin staining of a fiber from skeletal muscle of non-affected individual (figure 1). Skeletal muscles are bundles of muscle fibers (cells), which in turn are composed of myofibrils. Muscle fibers have more than one nuclei located at the periphery.

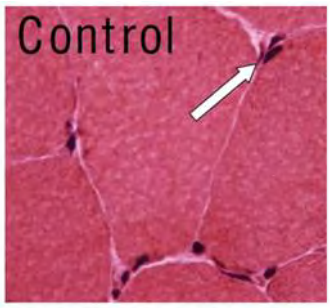

Figure 1: Muscle histology of a healthy person. Hematoxylin and eosin (H&E) staining of a transverse muscle section showing several fibers and the nuclei placed a the periphery (white arrow)

1.1.1. X-linked centronuclear myopathy due to mutations in the *MTM1* gene

The *MTM1* gene is positioned on the X chromosome, at the Xq28 position (Thomas et al, 1990). Due to the genetic inheritance males are mainly affected by this myopathy that is termed X-linked centronuclear myopathy XLCNM or X-linked myotubular myopathy XLMTM. However some rare cases of symptomatic females are also reported (Biancalana et al, 2017). The explanation could be found in the inactivation of the X chromosome that is not the carrier of the mutation (Biancalana et al, 2017). The XLCNM associated to mutations in *MTM1* gene is the most severe form of this type of disorders and the responsible gene was identified for the first time in 1996 by a joint collaboration between three laboratories (Laporte et al, 1996). However, the first clinical case was reported in 1966 in an adolescent boy (Spiro et al, 1966). The disorder was defined as a myotubular myopathy; since the adolescent boy's muscles looked like myotubes characteristic of foetus before 5 months, when their fibers are not mature (Spiro et al, 1966).

The patients' symptoms are generalized muscle weakness, severe hypotonia and severe breathing problems; because of the respiratory distress, patients survive only until childhood. However some individuals with a less severe form of the disease have lived until adulthood. Even before XLCNM patients are born, polyhydramnios (excess of amniotic liquid) can be observed, perhaps due to a swallowing difficulty; normally a foetus swallows a certain amount of amniotic fluid that is metabolized in its body throughout pregnancy. In the absence of normal reflexes the fluid accumulates in the amniotic cavity. Affected newborn males have often an excessive birth weight

and large head. Delayed motor milestones were also reported but not intellectual deficiency (Herman et al, 1999; Jungbluth et al, 2008).

The XLCNM patients have hypotrophic fibers characterized by the nuclei located at the center of the muscle fiber instead at the periphery (figure 2). The central area devoid of myofibrils contains also mitochondria and glycogen. The presence of "necklace" fibers was also observed at least in adults; necklace consisted of smaller myofibrils than normal, surrounded by mitochondria, sarcoplasmic reticulum and glycogen granules (Abath Neto et al, 2016; Bevilacqua et al, 2009). Type I fibers seem to be the most affected, in a healthy person they are characterized by slow contraction, high mitochondria and capillary density, oxidative metabolism, low creatine phosphate and glycogen content, and they are required for lower-intensity exercises such as walking and maintaining posture.

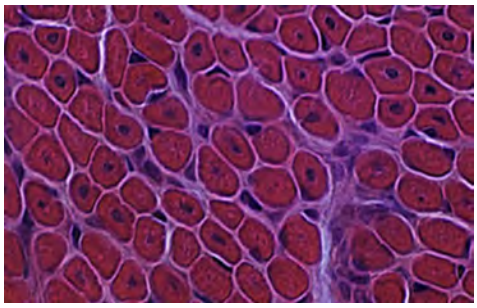

Figure 2: Histology of a patient with X-linked CNM. H&E staining shows hypotrophic fibers characterised by central nuclei. From (Abath Neto et al, 2016)

1.1.2. Centronuclear myopathy due to mutations in the *DNM2* gene

Mutations in the *DNM2* gene are implicated in the mildest form of CNM, which is autosomal dominant (ADCNM) also termed centronuclear myopathy 1 CNM1 (figure 3A). The causative gene is localized at the 19p13.2 position (Bitoun et al, 2005). Recurrent and *de novo* heterozygous missense mutations were identified in the DNM2 gene. Both males and females are affected with hypotonia, muscles weakness, elongated face with ptosis (drooping eyelid) and ophthalmoplegia. Several cases were reported going from the most severe phenotypes with neonatal onset until mild late-onset cases in the childhood and some less severe forms detected in adulthood (Abath Neto et al, 2015; Bitoun et al, 2007; Jeub et al, 2008). In some DNM2 CNM patients, abnormalities in the triad were reported. The triad is the key structure of the skeletal muscle excitation-contraction coupling (ECC) formed by the junction of the muscle T-tubule with the sarcoplasmic reticulum (Fraysse et al, 2016). Other abnormalities have been detected within the cell, i.e. the radiating

sarcoplasmic strands with oxidative enzymes reactions. Fiber type I predominance and hypotrophy were also reported. Usually, DNM2 CNM patients have no abnormalities in the skeletal muscle sarcomere structure; however there are clear differences at the ultrastructural level between the different CNM-related disorders. In order to get a better overview of the muscle biopsy, histoenzymology and electron microscopy are recommended. MRI (magnetic resonance imaging), EMG (electromyogram) and DNA sample for sequencing are also used as diagnostic tests (Biancalana et al, 2012). In the study by Bohm and collaborators, 60 families were described with mutations in the *DNM2* gene leading to a CNM (Bohm et al, 2012). Among these families, the most common mutations are two missense mutations R522H and S619L located in the Pleckstrin Homology (PH) domain of the DNM2 protein.

It is important to mention that mutations in *DNM2* gene also cause neuropathy (OMIM 606482), namely two different types of Charcot-Marie-Tooth (CMT) diseases were described: CMT dominant intermediate B (CMTDIB) and CMT axonal type 2M (Fabrizi et al, 2007; Zuchner et al, 2005) (figure 3B). Charcot-Marie-Tooth neuropathies have two main different forms: demyelinating and axonal. In these forms, the primary defect lies in Schwann cells or neurons, respectively (Pareyson & Marchesi, 2009). However, a complex set of subtypes has been described as the intermediate subtype. In this subtype it is unclear whether an axonal or demyelinating disorder is the culprit of the disease. Nerve loss of conduction, demyelination, and a focal hypermyelination are the molecular signs of the disease. Concerning physical symptoms, patients present two main traits: firstly, legs with inverted champagne bottle appearance; secondly, foot and hand deformities. This could be explained by the fact that limbs muscles cannot receive neuronal transmission properly (Claeys et al, 2009).

A B

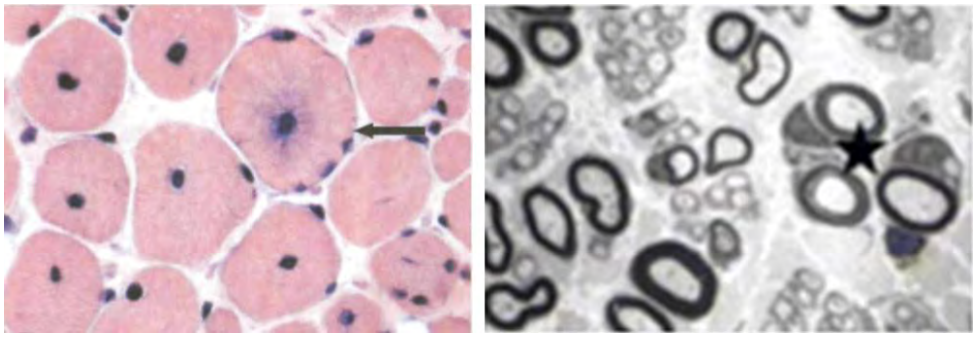

Figure 3: Muscle and nerve biopsies of two patients affected by either DNM2 CNM (A) or DNM2 CMT (B)**.** (A) H&E staining of a muscle section shows the center devoid of myofibrils and occupied by nuclei stained in dark blue, hypotrophic fibers are small and rounder than normal. Black arrow shows a myotube-like fiber. From (Jeub et al, 2008). (B) Electron micrograph showing clusters of non myelinated fibers and two clusters of flattened columns of Schwann cell processes (black star). From (Claeys et al, 2009).

1.1.3. Myopathy due to mutations in the *PYROXD1* gene

Mutations in the PYROD1 gene have been identified as a cause of early-onset myofibrillar myopathy (O'Grady et al, 2016). Patients affected present symptoms at infancy characterized mainly by muscle weakness (slowly progressive), difficulties with running and climbing stairs, and reduction in muscle bulk. Histology showed typical features of centronuclear myopathies, central and minicores diseases, nemaline and myofibrillar myopathies. Indeed, histology analyses have revealed internalized nuclei (figure 4), variation in the size fiber, abnormalities in the center of the fiber (core-like zones) that are devoid of mitochondrial activity, zones of sarcomeric disorganization with absence of aligned thick filaments, and accumulation of thin filaments. Small nemaline rods (electron-dense aggregates) in some small fibers and myofibrillar inclusions positive for desmin, myotilin, alpha-actin and αβ-crystallin were observed by immunohistochemical staining of skeletal muscle (O'Grady et al, 2016). Based on these different observations, this PYROXD1 myopathy is classified as a myofibrillar myopathy type 8 (MFM8, OMIM 617258).

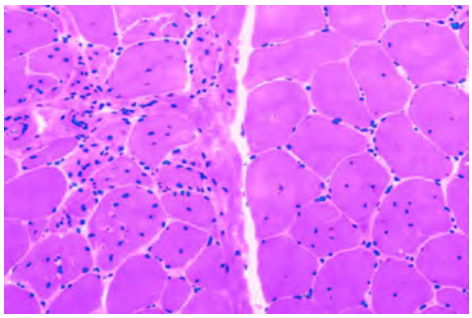

Figure 4. Histology of a skeletal muscle section from a quadriceps biopsy of a Pyroxd1 CNM-related patient. H&E staining shows variation in fiber size, multiple internalized nuclei, and increased fibrous connective tissue. From (O'Grady et al, 2016).

1.1.4. Centronuclear myopathy due to mutations in the *BIN1* gene and in the RYR1 gene

Mutations in two other genes, *BIN1* and *RYR1* also lead to CNM. I will only briefly mention these two myopathies, since I did not study them during my thesis.

Mutations in the *BIN1* gene are responsible for autosomal recessive centronuclear myopathy also termed CNM2 with neonatal or childhood onset (Nicot et al, 2007). However, recent data identified novel mutations in the *BIN1* gene responsible for a dominant form of CNM with depending on the mutation a progressive adult or an early childhood onset (Kouwenberg et al, 2017)). The BIN1 amphiphysin is involved in membrane trafficking and some of the patient mutations disrupt its interaction with the DNM2 dynamin (Nicot et al, 2007).

A *de novo* dominant missense mutation (S4112L) was identified in the *RYR1* gene as responsible for a centronuclear myopathy (Jungbluth et al, 2007). Mutations in the *RYR1* gene are also responsible for other forms on myopathies (Table 1). The *RYR1* gene encodes the ryanodine receptor in the skeletal muscle. However in myopathy patients with histology of centronuclear myopathy, the *RYR1* gene is now considered and tested for mutations.

1.1.5. Current research for treatment for XLCNM myopathies

Nowadays there is no treatment available for patients affected by these centronuclear myopathies. However, several scientific laboratories work hardly in order to better understand this type of myopathy and to find a suitable treatment. Indeed, some therapeutic treatments are either in pre-clinical phase or tested in different animal models, with promising results giving hope to the patients and their families. However, the molecular mechanism of these disorders and how exactly mutations impact the function of the proteins need to be better understood.

Most of the current research projects for CNM treatment are studying XLCNM that has an overall incidence of 1/50 000 newborn males worldwide, while the other CNM are extremely rare. The Mtm1 knockout (KO) mice generated by Ana Buj-Bello and colleagues have allowed to elucidate that XLCNM is not due to impairments in muscle differentiation of the fetus as previously thought by Spiro and colleagues (Spiro et al, 1966), but is due to the preservation of the internal architecture of the myofibers (Buj-Bello et al, 2002). These *Mtm1* KO mice also served as models for the development of new therapies. Among them the AAV (Adeno-Associated Virus) injection of MTM1 in the tibialis anterior (TA) muscle of the *Mtm1* KO mice was shown to rescue the hallmarks of the disease (Buj-Bello et al, 2008). Next, systemic injection of AAV-MTM1 rescued the life span and the myopathy of these *Mtm1* KO mice, showing that this AAV-based treatment might be a good therapeutic option of XLCNM patients (Childers et al, 2014).

The recent results obtained by Ana Buj Bello and colleagues of AAV treatment of Golden Retriever

dogs model of the XLCNM are very promising for a future therapy of this myopathy. These results show that 2 dogs that were followed over 4 years after the AAV-MTM1 treatment were as healthy as the wild type controls, even though a decline in AAV vector copy number and in muscle force was observed (Elverman et al, 2017). In a second study using the Mtm1-N155K canine model, they performed a study to evaluate the efficacy and safety of MTM1 AAV-mediated gene therapy by injecting AAV-MTM1 with MTM1 expression under the control of the muscle-specific desmin promoter in 10 weeks of age dogs showing already signs of the CNM disease. In this study they underwent a dose escalation study with systematic analysis of different parameters and physiological functions in these dogs. Their results show that this systemic AAV-MTM1 gene therapy was safe, efficient with a prolonged life span and a proper skeletal musculature, and this in a dose-dependent manner (Mack et al, 2017). These different studies support the development of AAV-mediated gene therapy clinical trials for XLCNM patients.

A company Audentes Therapeutics (https://www.audentestx.com/at132/) is developing a gene therapy named AT132 derived from these results and based on administration of an AAV carrying the *MTM1* gene to restore long-term expression of the MTM1 myotubularin in XLCNM patients. On September 21, 2017, Audentes Therapeutics announced that the dosing of the first XLCNM patients has begun to evaluate the safety and preliminary efficacy of AT132. At this stage, 12 XLCNM patients less than five years of age will be studied in this Phase 1/2 clinical trial of AT132. The U.S. Food and Drug Administration (FDA) and the European Medicines Agency (EMA) have granted AT132 as an "Orphan medicines". This "orphan medicines" classification was created to facilitate the development and authorization of new medicines for rare disease, since they will benefit of different incentives (protocol assistance, access to centralized authorization procedure, ten years of market exclusivity, and also fee reductions for small- and medium-size enterprises).

The laboratory of Sylvie Friant in collaboration with the laboratory of Jocelyn Laporte (IGBMC, Illkirch) has recently tested complementation by MTMR2, a myotubularin related protein belonging to the same subfamily as MTM1 (Raess et al, 2017a). There are two isoforms of MTMR2, termed MTMR2-S (more similar to MTM1) and MTMR2-L, and their injection with AAV in the TA muscle of *Mtm1* KO mice was effective to rescue the myopathy symptoms, with MTMR2-S showing better rescue properties (Raess et al, 2017a). A patent describing this MTMR2-S based therapy is under evaluation at the European Patent Office (Berlin, Germany).

Another laboratory used another approach based on complementation of the MTM1 phosphatase loss-of-function by inhibition of the phosphatidylinositol 3-kinase (PI3K) producing the phosphatidylinositol 3-phosphate (PtdIns3P) substrate of MTM1 (Kutchukian et al, 2016). This

approach is effective in different animal models of the MTM1 myotubular myopathy (Sabha et al, 2016). Indeed, muscle-specific deletion of PIK3C2B (but not of PIK3C3, another class of PI3K) reverted the CNM muscular phenotypes of Mtm1 KO mice treated before the apparition of the first symptoms or once the symptoms were already observed. These data were confirmed in the zebrafish mtm model were inhibition of PI3K by chemicals such as wortmannin prevented the development of the myopathy phenotypes, and the wortmannin treatment also resulted in prolonged lifespan of Mtm1 KO mice (Sabha et al, 2016).

Belinda Cowling and colleagues have demonstrated that DNM2 is overexpressed in X-linked CNM patients and in *Mtm1* KO mice (Cowling et al, 2011); and that partial reduction of DNM2 levels in *Mtm1* KO mice rescued the XLCNM phenotype (Cowling et al, 2014). Related to these studies, Tasfaout, Cowling and colleagues have injected ASO (antisense oligonucleotides) into affected Mtm1 KO mice in order to reduce DNM2 levels, and this treatment rescued the CNM phenotypes and extent the lifespan of these Mrm1 KO mice that usually die at about 7 weeks of age (Tasfaout et al, 2017). They could observe a rescue in muscle force, mass and histology. Their idea is to translate this pharmacological approach as a therapeutic strategy to be used to regulate DNM2 in CNM-affected patients. A biotechnology company named Dynacure (http://www.dynacure.fr/) was founded to test this new therapeutic approach.

1.1.6. Clinical data and health-care for patients suffering of CNM myopathies

Patients affected by a CNM due to mutations in *MTM1*, *DNM2* or *PYROXD1* gene suffer persistent muscle weakness, respiratory failure and hypotonia. Muscle weakness is defined by an absence of normal muscle contraction even if the person put full efforts it does not produce a normal muscle contraction. Hypotonia is characterized by decreased muscle tone (http://medlineplus.gov); it is the passive movement in opposition to the stretch of the muscle. For example, infants with normal tone can be lifted by adult's hands placed under the armpits. Hypotonic infants tend to slip between the hands.

Most of the clinical data are on patients suffering of XLCNM due to mutations in the MTM1 gene. These patients have an estimated mortality of 50% by 18 months of age, with a strong muscle weakness associated to respiratory failure and feeding difficulties. Diagnosis is based on the clinical observation of the patients combined to histology and genetic testing to show the presence of mutation in the *MTM1* gene.

A recent clinical study termed RECENSUS enrolled 112 boys suffering of XLCNM to expand the data on patients suffering of XLCNM (Beggs et al, 2017). In this RECENSUS study, the data were collected from September 2014 to June 2016 in different medical centers. The mean age of diagnosis was 3.7 months of age. The mortality was 44%, with 64% for the 40 patients being less than 18 months of age and 32% for the 72 patients older than 18 months. At birth, 95% of the patients were hypotonic and 90% required respiratory support with invasive or noninvasive techniques. After the neonatal period, about half of the patients (48%) required 24-hour ventilation, while the others had an average of ventilation of 8.5 hours per day. This clinical study also analyzed the time spent in the hospital by these 112 boys and the number of surgery they undergone. The data show that they spent on average 35% of their first year of life in hospitals and had about 3.7 surgeries during this same time (Beggs et al, 2017). In conclusion, this study shows that XLCNM is associated with high mortality and that the survival of these patients depends on ventilator support and health-care utilization.

1.1.7. The sarcomere structure and the excitation-contraction coupling mechanism of muscles

A muscle fiber or myofiber is a structure of 1 to 40 mm of large and 10 to 50 µm of width. Myofibers are composed of tubular myofibrils bearing repeating sections of sarcomeres (figure 5). Sarcomeres are repeated structures in the cytoplasm where excitation-contraction coupling (ECC) occurs in skeletal muscle. Sarcomeres contain two types of filaments: thick filaments of myosin II and thin filaments of actin. Parallel filaments of actin are embedded with filaments of myosin as shown in figure 6. A myosin head binds actin tightly in the absence of bound nucleotide. Binding of a molecule of ATP to the specific site in the head of the myosin disrupts the myosin-actin bind and the myosin head dissociates from actin filament. Then, the myosin head hydrolyses ATP, which provokes a change in the conformation of the myosin head that moves towards the (+) end of the actin filament and binds a new actin monomer. Then, phosphate (Pi) is released what provokes another conformational change resulting in the movement of the myosin head. This latter is bound to actin filament so this finally provokes the movement of the actin filament. Finally, ADP is released and the cycle can start again.

When the sarcomere is contracted, thin actin filament invades the A band, resulting in the shortening of the sarcomere and contraction of the muscle. The signal that triggers the beginning of this process is the Ca^{2+} (figure 7). Ca^{2+} is mainly stored in fibers within the sarcoplasmic reticulum (SR). At the beginning of contraction, it is released into the cytoplasm where the concentration of

cytosolic calcium increases from 10^{-7} to 10^{-6} and after activation most of the Ca^{2+} released goes back into the SR (Calderon et al, 2014). The resting membrane potential is -85mV. During contraction, membrane depolarization occurs and the electrical conductance and the ion flow may increase the transmembrane voltage until 120 mV. This phenomenon is sequenced in several steps. It begins with the generation of an action potential (AP) along the plasma membrane and the propagation along and inside the fiber via the T-tubule. T-tubules are invaginations of the sarcolemma (plasma membrane muscle) into fibers. In this way electrical information arrives rapidly inside cell.

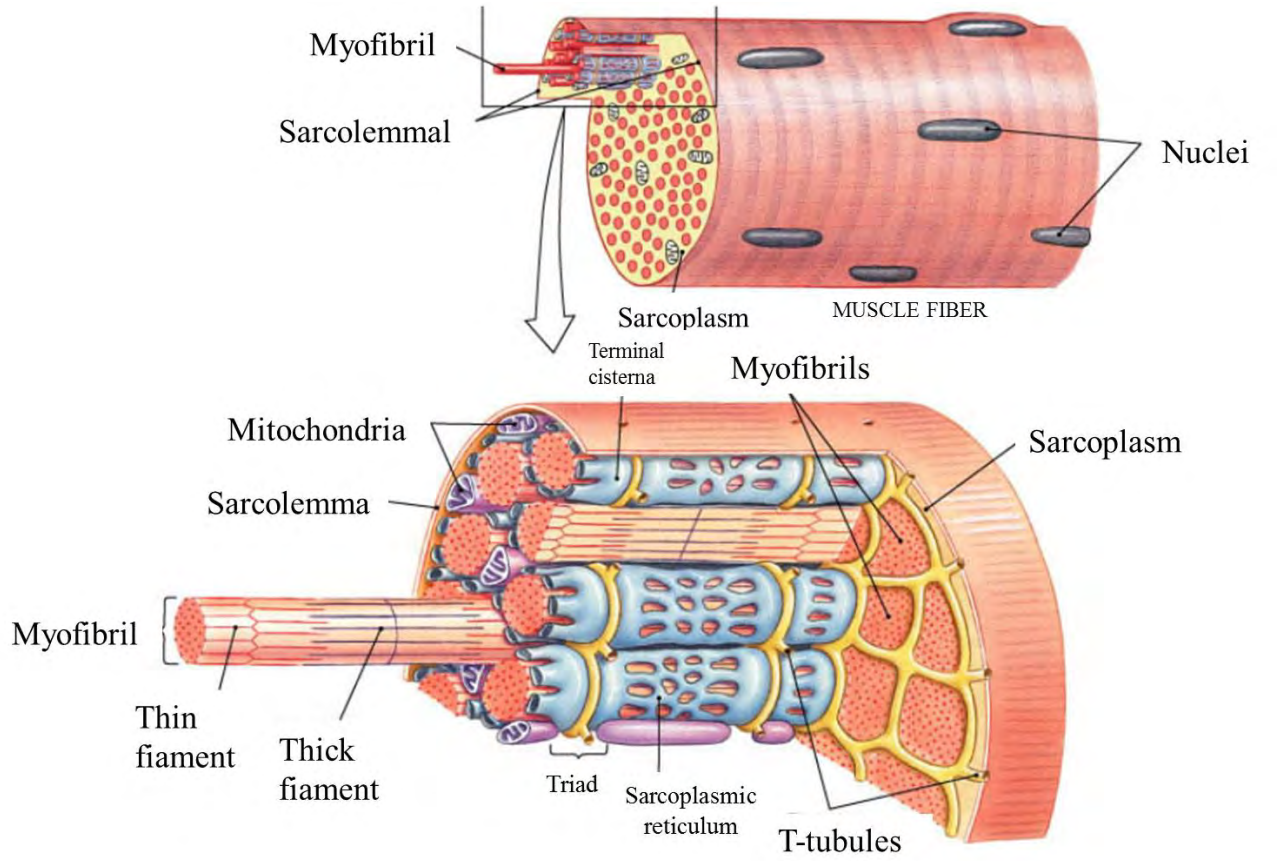

Figure 5: Schematic view of the external and internal organization of a muscle fiber. Muscle fibers are multinucleated. The membrane of the muscle cells is the sarcolemma; there are internal tubular extensions of the sarcolemma into the sarcoplasm called transverse tubules or T tubules.

Source:

http://droualb.faculty.mjc.edu/Lecture%20Notes/Unit%203/chapter_9__skeletal_muscle_tiss%20with%20figures.htm.

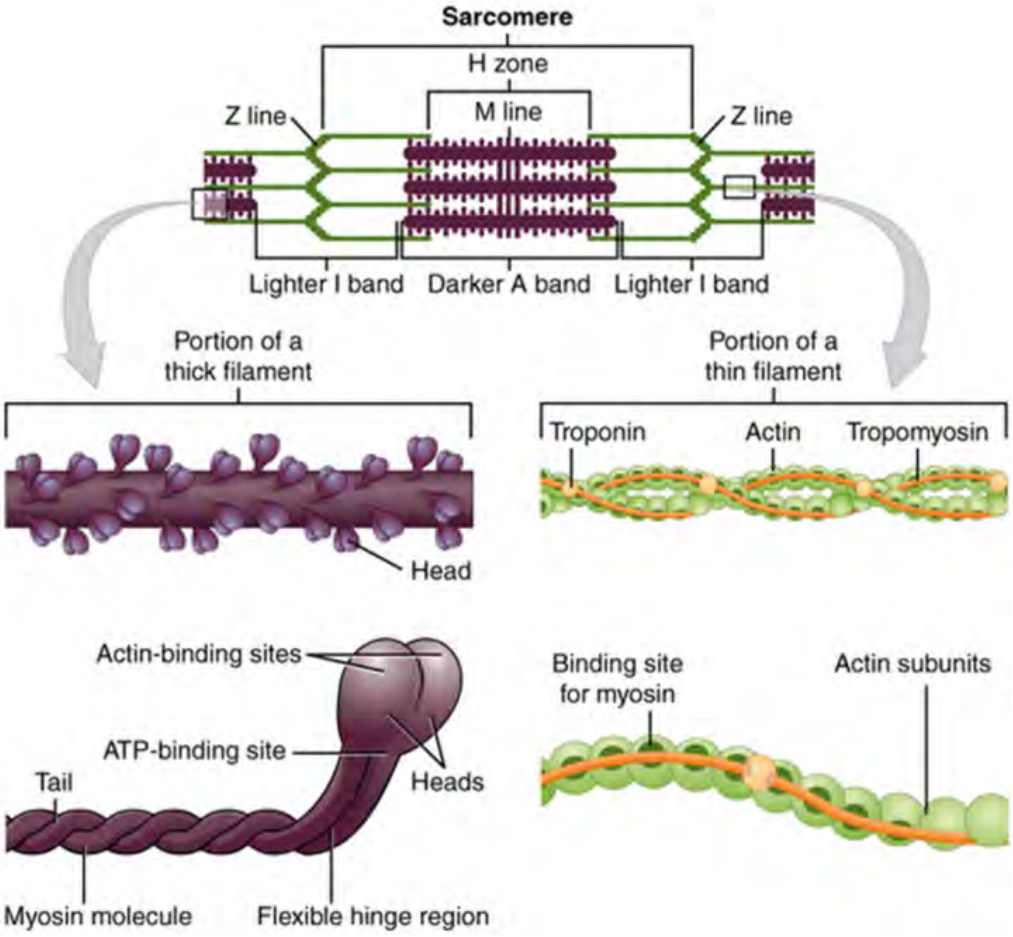

Figure 6: Schematic of the sarcomere structure. The sarcomere is the region from one Z-line to the next Z-line, and it is the functional unit of a skeletal muscle fiber. Thick filaments of myosin and thin filament of actin compose the sarcomere. Troponin and tropomyosin form a complex in the thin filament.

Source: https://cnx.org/contents/FPtK1zmh@8.25:bfiqsxdB@3/Skeletal-Muscle

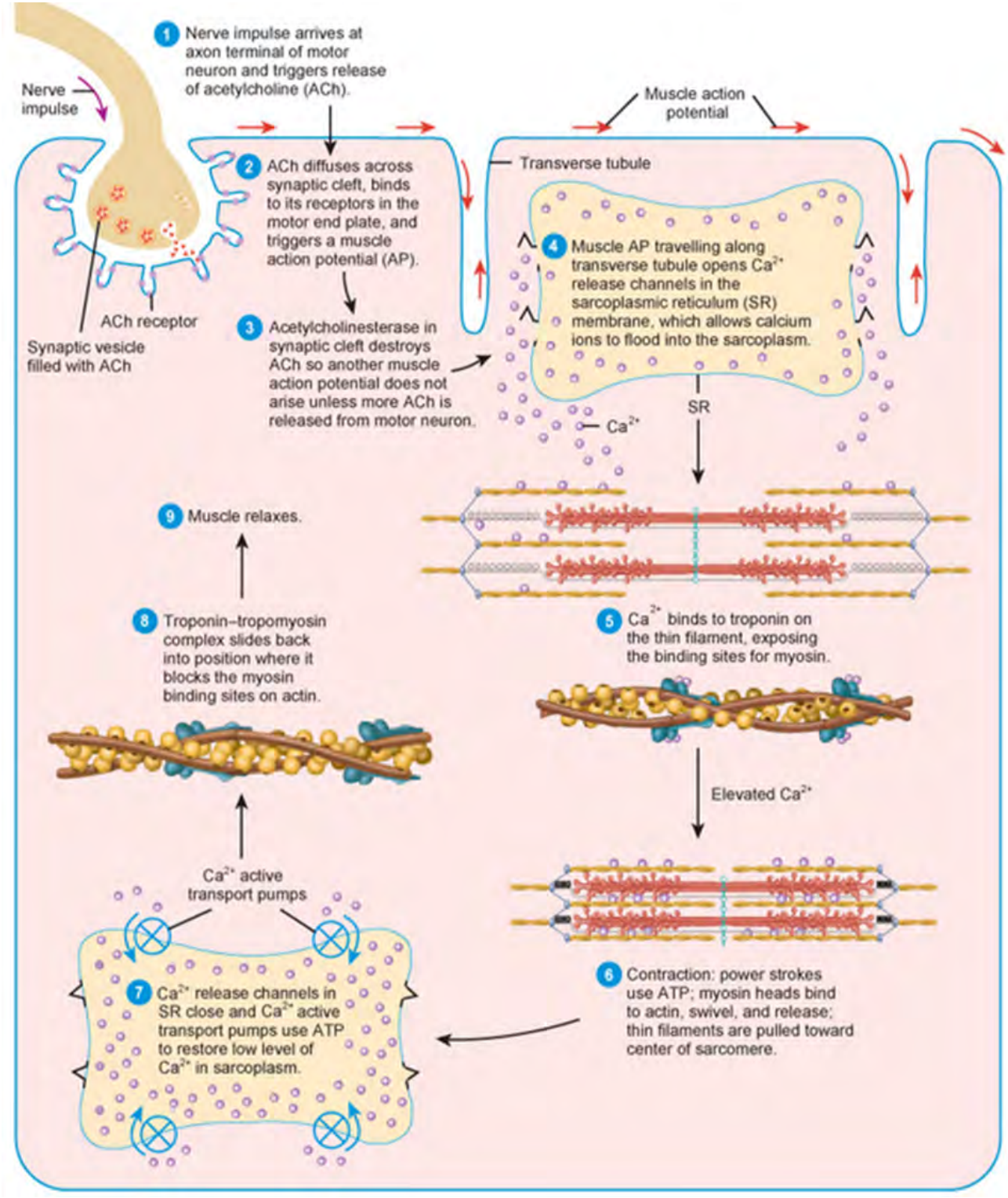

Figure 7: Acetylcholine released at the neuromuscular junction triggers a muscle action potential, which leads to muscle contraction.

Source:

http://higheredbcs.wiley.com/legacy/college/tortora/0470565101/hearthis_ill/pap13e_ch10_illustr_audio_mp3_am/simulations/hear/contraction_relaxation_skeletal_muscle_fiber.html

1.2. The three studied proteins MTM1, DNM2 and PyroxD1.

1.2.1. MTM1 and the myotubularins family of protein

The MTM1 myotubularin protein is an enzyme coded by the *MTM1* gene, localized on the X chromosome at position Xq28. In 1996, Jocelyn Laporte and colleagues identified mutations in *MTM1* as responsible for the XLCNM (Laporte et al, 1996). MTM1 belongs to the subfamily of myotubularins (Raess et al, 2017b). These proteins belong to the big family of lipid phosphatases, specifically protein tyrosine phosphatase (PTP) dual specificity phosphatase. They catalyze the dephosphorylation reaction of the phosphatidylinositol 3-phosphate (PI3*P*) and the phosphatidylinositol (3,5) bisphosphate (PI(3,5)P_2) at the 3 position of the inositol ring. They present a phosphatase motif (CX_5R) in the catalytic domain. There are 14 myotubularins in human cells: MTM1 and the myotubularin-related proteins termed MTMR1 to MTMR13 (Raess et al, 2017b). Some of these myotubularins (MTMR5, MTMR9-13) are catalytically inactive, due to the lack of key residues in the CX_5R motif (Hsu & Mao, 2015). However, it has been shown that catalytic dead myotubularins interact with active myotubularins to regulate their activity (Laporte et al, 2003; Raess et al, 2017b). They can interact between them as homo- or heterodimers. There is a fifteenth 3-phosphatase also implicated in a centronuclear myopathy, the MTMR14/hJumpy, that shares a high homology with myotubularins. However, it is not clear yet whether MTMR14 is the cause of the CNM disease or a modifier of the centronuclear myopathy phenotype caused by mutations in other CNM gene, like DNM2 (Tosch et al, 2006).

Mutations in genes coding for myotubularin related proteins are implicated in other types of neuromuscular diseases. For example, mutations in *MTMR2* and *MTMR13/SBF2* are responsible for Charcot-Marie-Tooth (CMT) neuropathies, types 4B1 and 4B2 respectively (Azzedine et al, 2003; Senderek et al, 2003).

In 2012, about 400 patients were reported with mutations in *MTM1* and suffering of XLCNM. These mutations include point mutations (missense, no sense and splicing mutations), insertions and deletions (Biancalana et al, 2012; Tosch et al, 2010). Many of the mutations found in *MTM1* are associated with a loss of function and often with a decreased level or an absence of MTM1 protein (Laporte et al, 2001; Vasli et al, 2012b).

1.2.1.1. The PH-GRAM and catalytic domains of the MTM1 protein

Myotubularin MTM1 is composed of six different domains (figure 8): PH/GRAM (Pleckstrin Homology-Glucosyltranferase, Rab-like GTPase activator and Myotubularin), RID (Rac-induced recruitment domain), PTP/DSP (Protein tyrosine phosphatase/Dual-specificity phosphatases), SID (SET-protein interaction domain), PDZ binding site mediates protein-protein interactions (PDS-95, a postsynaptic protein, Discs-large, a *Drosophila* tumor suppressor and ZO-1, a tight junction protein) and CC domain (coiled-coil) important for homodimerization and/or heterodimerization of the myotubularin (Bertazzi et al, 2015b; Laporte et al, 2003).

The RID domain (amino acids 161-272 of MTM1) was identified as required for the localization of MTM1 at the plasma membrane in Rac1 GTPase induced membrane deformations termed ruffles (Laporte et al, 2002).

The SID domain (amino acids 435-486 of MTM1) was identified in 1998 by Cui and colleagues in the catalytic-dead myotubularin Sbf1 (SET-binding factor) also named MTMR5. The SID domain binds to proteins with a SET (Suvar3-9, Enhancer of zeste, Tritorax) domain and SET domains are mainly present in proteins involved in epigenetic regulation of genes (Cui et al, 1998).

The CC domain is critical for membrane association and for dimerization of the MTMR2 myotubularin, a close homologue of MTM1 (Berger et al, 2003).

The two domains that I have studied during my PhD, the PH-GRAM (aa 1-170 of MTM1) and the catalytic PTP/DSP (aa 175-538 of MTM1) domain will be presented in more detail below.

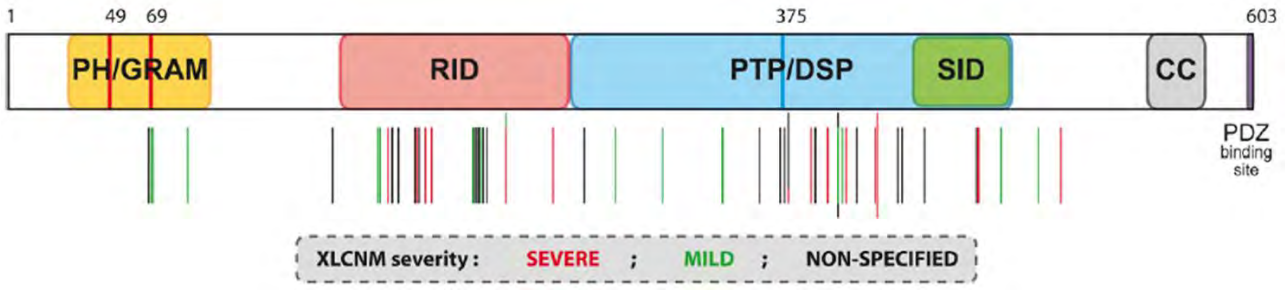

Figure 8: Schematic representation of the domains of human myotubularin MTM1. Colored vertical lines indicate missense mutations according to XLCNM phenotypes (severe, mild or non-specified). From (Bertazzi et al, 2015b).

The PH-GRAM domain

Pleckstrin (Platelet and Leucocyte C Kinase Substrate) was found in platelets as the major target of protein kinase C. It contains about 100 amino acids and similar sequences were termed pleckstrin homology PH domains (Haslam et al, 1993). There are about 285 proteins in the human proteome containing a PH domain. They have been found in several proteins implicated in signal transduction or in cytoskeletal function, such as Ras and Rac proteins, small GTP-binding proteins or serine/threonine kinases (Lenoir et al, 2015). The PH domain is folded in seven up-and-down β strands forming a β barrel and an amphiphilic α helix at its c-terminus (Yoon et al, 1994). All PH domains bind membrane phosphoinositides, however less than 10% of them do it with high affinity and specificity, meaning that most of them bind to several types of PIs (Lemmon, 2007).

The GRAM domain was identified in different proteins among them the MTM1 myotubularin (Doerks et al, 2000). The GRAM domain of myotubularins displays structural similarities with the PH domain, since they share a similar folding. Therefore, this myotubularin GRAM domain identified by bioinformatics studies in 2000 by Doerks and colleagues, was renamed PH-GRAM domain (Doerks et al, 2000). All human myotubularins, even the catalytic dead, share in common the PH-GRAM domain that is about 70 amino acids (Raess et al, 2017b). In the myotubularin MTM1, the PH-GRAM domain is localized at the N-terminus (figure 9).

In vitro, the recombinant PH-GRAM domain of MTM1 can bind PI(3,4,5)P_3, PI(3,5)P_2, PI5*P* and PI3*P* (Schaletzky et al, 2003; Tsujita et al, 2004). However, the MTM1 3-phosphatase has been shown to hydrolyze only PI3*P* and PI(3,5)P_2 (Taylor et al, 2000; Tronchere et al, 2004). Interestingly, *in vitro* the PI5*P*, the product of the dephosphorylation of PI(3,5)P_2 by MTM1 acts as a specific allosteric activator of MTM1 phosphatase, inducing the heptameric homodimerization in a ring of the recombinant purified MTM1 protein. The activity of MTM1 towards PI(3,5)P_2 and PI3*P* is stimulated by PI5*P* via this oligomerization (Schaletzky et al, 2003). Moreover, studies with other myotubularins as MTMR3 have shown that deletion of PH-GRAM domain causes the complete loss of activity of the enzyme (Lorenzo et al, 2005).

It is interesting to mention that even if PH-GRAM domains are expected to bind the PIs, based on the crystal structure of the MTMR2 myotubularin, the size and hydrophobicity of the interface between the MTMR2 PH-GRAM domain and the membrane restricts its interaction with PIs (Begley et al, 2003). Studies have shown that the PH-GRAM domain is required for the membrane binding of the MTMR2 myotubularin (Berger et al, 2003). However, there was no PI binding

observed in the PH-GRAM domain region of MTMR2 in the crystal structure solved in presence of PI(3,5)P_2 and PI3P, suggesting a low affinity interaction with these substrates, a characteristic of the majority of the PH domains (Berger et al, 2006).

A study by Tsujita and colleagues shows that the PH-GRAM domain of MTM1 has the highest affinity for PI(3,5)P_2 (Tsujita et al, 2004). They tested different XLCNM patient mutations affecting the PH-GRAM domain, and their data show that the MTM1-V49F shows a significant decrease in PI(3,5)P_2 binding, whereas the MTM1-R69C, -L70P or -L87P display almost wild-type PI(3,5)P_2 binding (Tsujita et al, 2004). Interestingly, the MTM1-V49F mutation is responsible for a severe form of XLCNM, associated to a twofold decrease in phosphatase catalytic activity, whereas the MTM1-R69C mutation, associated with milder forms of XLCNM, shows almost normal phosphatase activity (Amoasii et al, 2012).

In conclusion, these different studies mostly done on MTM1 and MTMR2 myotubularins show that the PH-GRAM is involved in interaction with membranes, and that its binding to PIs is of low affinity.

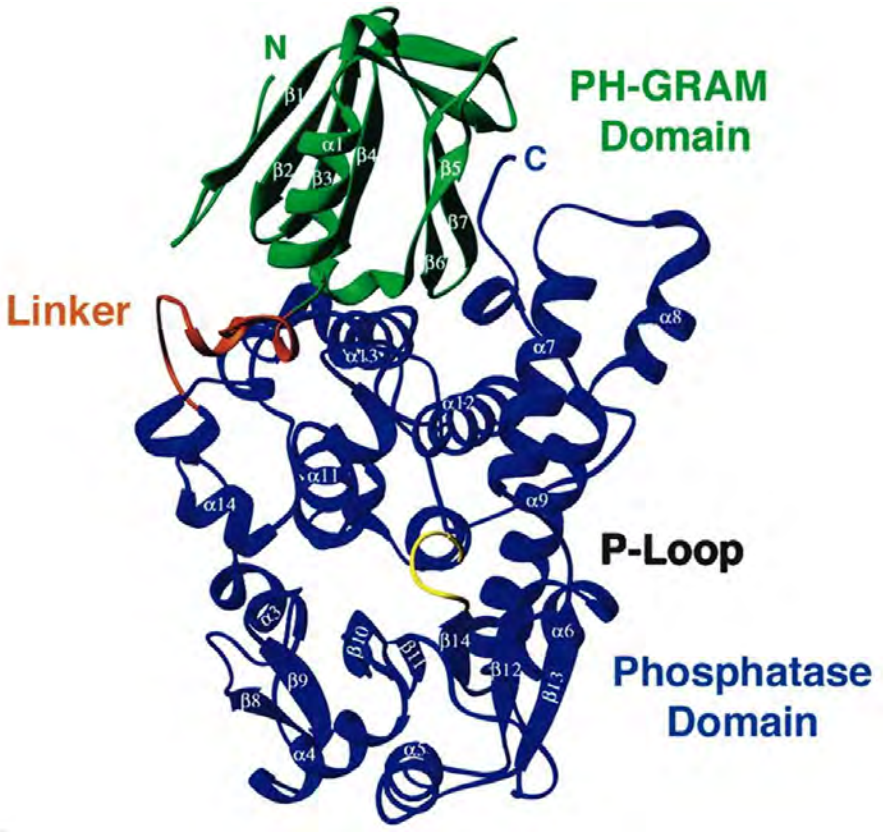

Figure 9: Structure of the human MTMR2 myotubularin solved by X-ray crystallography. The PH-GRAM domain at the N-terminal is shown in green, and the full-length phosphatase domain at the C-terminal is shown in blue with the active p-loop of catalytic site in yellow, and the linker between both domains in orange. From (Begley et al, 2003).

The Catalytic domain

The phosphoinositide phosphatase PTP/DSP catalytic domain is highly conserved among the different myotubularins, both the active and the inactive ones (Raess et al, 2017b). The size of the catalytic domain of myotubularins is much larger than observed for the other protein tyrosine phosphatases PTP, consisting of about 400 amino acids arranged in a central β-sheet sandwiched by α-helices (Begley et al, 2006)(figure 9). The PTPs are characterized by the presence of the consensus motif CX_5R in the active site, where X refers to any amino acid (Denu & Dixon, 1995). The tridimensional structure of CX_5R motif reveals that it is the phosphate-binding loop and that an aspartic acid residue present on the surface loop is important for the catalytic reaction. However, myotubularins do not dephosphorylate tyrosine, threonine or serine residues as the PTP, but they dephosphorylate phosphoinositides lipids, and are termed PTP/DSP for protein tyrosine phosphatase/dual-specificity phosphatases. After searching for four years the protein substrate of MTM1 phosphatase, it was finally shown in 2000 that the MTM1 myotubularin dephosphorylates PI3*P* (Blondeau et al, 2000; Taylor et al, 2000). In 2004, Tronchère and colleagues have shown that *in vitro* and *in vivo* MTM1 also dephosphorylates a second type of PIs, the PI(3,5)P_2 producing PI5*P* (Tronchere et al, 2004).

In the catalytic reaction, the cysteine plays an essential role (Denu & Dixon, 1995). Up to now the crystal structure of MTM1 is not solved due to difficulties to produce large quantities of pure recombinant protein for x-ray crystallography, but the crystal structure of MTMR2 was solved and used to model the catalytic mechanism of myotubularins (figure 10) (Begley et al, 2006; Begley et al, 2003). The thiol group of the cysteine in the CX_5R motif is the nucleophile that attacks via the formation of a thiolate anion ($-S^-$) the phosphate in the position 3 of the inositol ring of the PI3*P* or PI(3,5)P_2 substrate, resulting in a covalent intermediate. Then, the aspartic acid acts first by protonating the dephosphorylated substrate and next as a base, which donates its lone pair of electrons to water, and activates hydrolysis of the phosphor-enzyme intermediate (see figure 10) (Begley et al, 2006; Denu & Dixon, 1995).

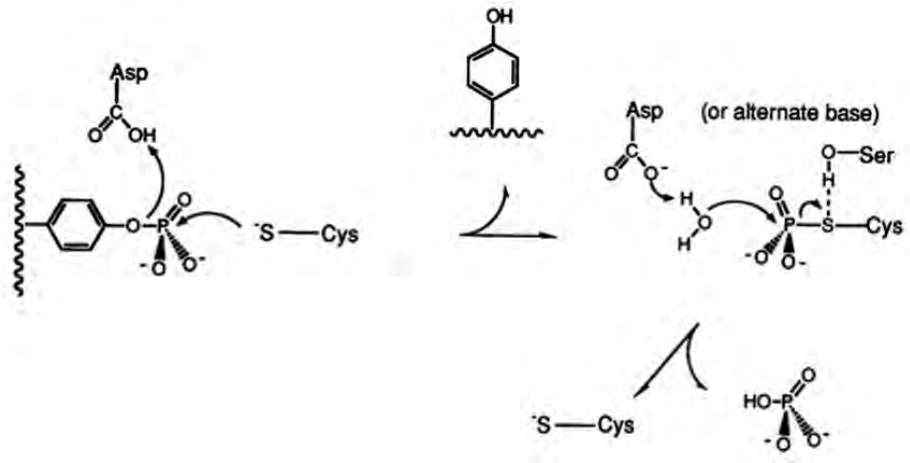

Figure 10: Common chemical mechanism of dual-specific phosphatases. The Cys is the cysteine from the CX_5R motif; the aspartic acid is near the motif and it acts firstly as acid and then as a base favoring the release of the phosphatase from the substrate. Adapted from (Denu & Dixon, 1995).

Begley and colleagues established two interesting characteristics of MTMR2. First, the MTMR2 substrate-binding pocket is deeper and wider than that of other PTPs, explaining the specificity of myotubularins for the large phosphorylated head group of its PI3*P* or PI(3,5)P_2 substrate (Begley & Dixon, 2005; Begley et al, 2006). Second, the surface of MTMR2 is electrostatically polarized, with the surface surrounding the catalytic pocket being electropositive, whereas the remaining surface of the protein is electronegative. Indeed, the PH-GRAM and the catalytic domains of MTMR2 and of the other myotubularins (based on homology models) show electrostatic polarization. The positively charged surface of the myotubularins could favor its interaction with the negatively charged membranes. Moreover, the positive charges could create electrostatic interactions with the negative charges of the phosphoinositides embedded in the membranes (Begley & Dixon, 2005; Begley et al, 2006). In conclusion, the interactions between MTMR2 and the lipid bilayer would be facilitated by the presence of accessible loops surrounding the active-site pocket.

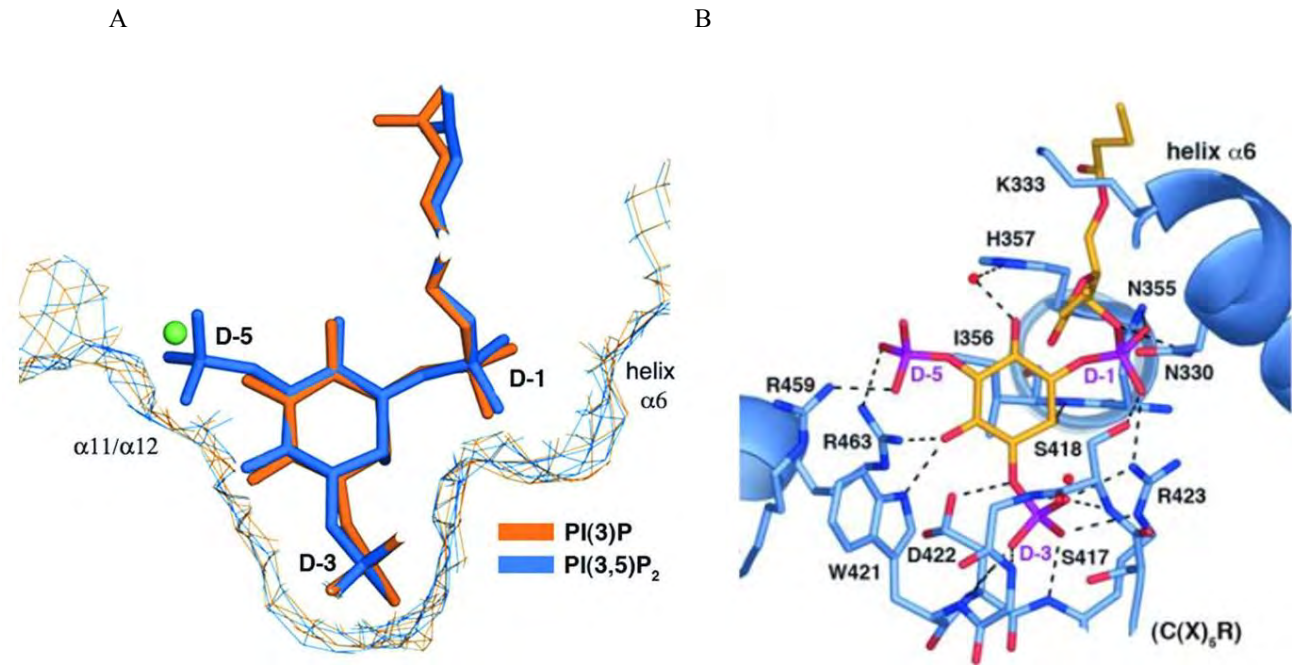

Figure 11 : (A) Representation superimposed of the specific substrates in the catalytic pocket of the myotubularin MTMR2. The PI3*P* is in orange and the PI(3,5)P_2 in blue. (B) The phosphatase domain (blue) interacting with PI(3,5)P_2 (yellow) by non-covalent interactions such as H-bond and salt bridges, is represented by dashed lines; red spheres are water molecules. From (Begley et al, 2006).

1.2.1.2. The reactive oxygen species ROS regulate protein tyrosine phosphatase activity

Redox regulation of protein activity can occur at the cysteine of the conserved CX_5R motif of the PTPs. Indeed, cysteine acts as a nucleophile in the first step of the catalytic reaction, but its capacity to donate an electron pair makes it highly sensitive to inactivation and regulation by reactive oxygen species or ROS (Salmeen & Barford, 2005). ROS are chemical radicals of oxygen, which have an unpaired valence of electrons transforming them into unstable and very reactive species. The thiol group of the cysteine (-SH) via the formation of the thiolate anion ($-S^-$) required for the dephosphorylation reaction, could be reversibly oxidized by ROS into sulfenic acid (S-OH, sulfenylation), and upon exposure to higher concentrations of oxidants, the S-OH is irreversibly oxidized to sulfinic ($S-O_2H$) and further to sulfonic ($S-O_3H$) (Frijhoff et al, 2014). The sulfenic acid intermediate S-OH can be protected from irreversible protein oxidation by thiolation, cysteinylation and S-glutathionylation (GSSG). The GSSG represents the conjugation of glutathione (GSH), a tri-peptide that reacts with the reactive cysteine to protect the proteins from irreversible oxidation and to modify the activity of the protein. Oxidation has been described as a common regulatory mechanism in PTPs activity, but Ross and colleagues have shown in a study the differential sensitivity of each type of PTPs to oxidation under several glutathione GSSG redox buffers.

Interestingly, PTEN the PtdIns 3-phosphatase that dephosphorylates PI(3,4,5)P_3 into PI(4,5)P_2 (Maehama et al, 1998; De Craene et al, 2017), was the most sensitive of the PTPs, whereas MTM1 and MTMR2 show excellent resistance to oxidation, only the strong oxidation conditions using hydrogen peroxide resulted in a significant loss of activity (Ross et al, 2007). These data suggest that the resistance of MTM1 and MTMR2 to oxidation could be required for a specific function, for example to regulate pools of PI3P or PI(3,5)P_2 on ROS-rich membranes.

Redox biology is the study of how the activity, interaction, folding or stability of proteins, lipids, DNA or RNA dependent on the spatial and temporal redox control (Figure 12) (Herrmann & Dick, 2012). Indeed, oxidation-reduction (redox) reactions are used by cells to control fundamental processes. For example, ROS are essential for stem-cell renewal or differentiation and mitochondrial ROS produced from mitochondrial complex I specifically trigger muscle differentiation (Malinska et al, 2012). In a review, Schieber and colleagues suggested that quiescent stem cells present low ROS levels, which increase at the moment of the renewal or differentiation of these stem cells (Schieber & Chandel, 2014). These different studies show that the variation in ROS levels is a cellular mechanism to control different signaling pathways. Indeed, the intracellular or the local levels (at specific compartments or membranes) of ROS can trigger specific cellular responses. Different from these physiological oxidative responses, some excessive or toxic oxidative effects of ROS were also described and these impair key cellular processes leading to disorders and are referred as oxidative stress. Different forms of oxidative stress were reported due to different sources of ROS that includes hydroxyl radical ($^{\bullet}OH$), peroxides ($RO^{\bullet}$), superoxide ($O_2^{\bullet-}$), and singlet oxygen. They are natural products in processes that occur in cells or they can be produced by external oxidants. The internal processes include the respiratory chain, the lipid peroxidation, the NADPH oxidases (NOX) and dual oxidases (DUOX) complexes, or the QSOX (quiescin-sulfhydryl oxidase) and Ero1 (ER-resident oxidoreductases), which drive oxidative protein folding (Figure 12) (Nunes & Demaurex, 2014).

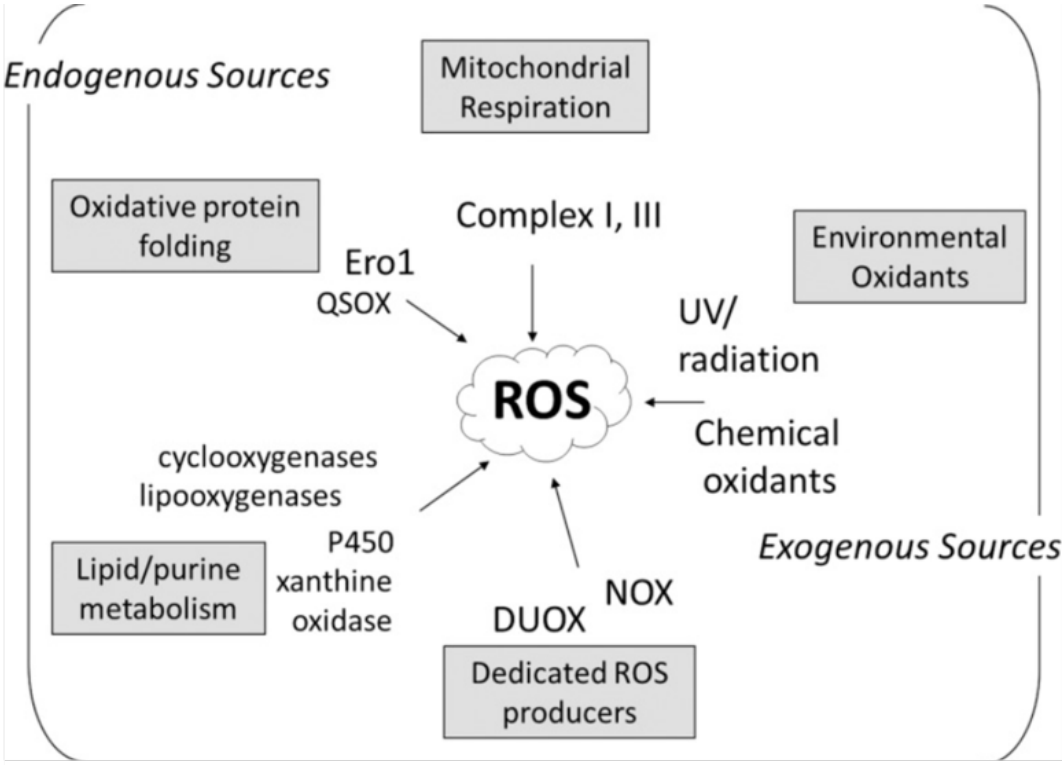

Figure 12: Reactive oxygen species (ROS) sources. ROS are chemical radicals of oxygen, that is, they have an unpaired valence electron what transforms it into unstable and very reactive species. From (Nunes & Demaurex, 2014).

1.2.2. The dynamin DNM2, a GTPase protein

The dynamin DNM2 is a protein belonging to the large family of GTPases. Human DNM2 is a large protein (98 kDa) encoded by the *DNM2* gene located at chromosome 19 in position 19p13.2. Mutations in this gene are associated either with the autosomal dominant centronuclear myopathy AD-CNM or CNM1 or with the neuromuscular Charcot-Marie-Tooth CMT dominant intermediate B (CMTDIB) and CMT axonal type 2M disease (Figure 13) (Bitoun et al, 2009; Bitoun et al, 2005; Zuchner et al, 2005). In mammalian cells there are 3 different types of dynamin encoded by three genes: *DNM1* expressed in neuronal cells, *DNM2* ubiquitously expressed and *DNM3* expressed in brain, testis, lungs and heart (Antonny et al, 2016).

1.2.2.1. The domains of DNM2 protein

The DNM2 dynamin is composed of 5 domains (Figure 13). The catalytic GTPase domain in N-terminal is responsible for GTP binding and hydrolysis and electron microscopy analyses reveal

that GTP hydrolysis induces a conformational change in the protein (Stowell et al, 1999). The middle domain is involved in dynamin self-assembly (Smirnova et al, 1999). The GED or GTPase effector domain and the middle domain participate in the oligomerization and regulation of the GTPase activity. The PH domain of DNM2 binds to lipid membranes but does not show specificity towards PI(4,5)P_2 contrary to what was observed for DNM1 dynamin (Cowling et al, 2017). The PRD or proline rich domain in the C-terminal binds to proteins containing a SH3 (Src homology 3) domains; it is also required for microtubule association. For DNM1 was shown that the PH domain and PRD cooperate to localize dynamin to clathrin-coated pits.

Most of the AD-CNM and CMT patient mutations are found in the Middle and in the PH domain, with 2 CNM patient mutations also localized in the GED domain (Figure 13). Interestingly, a recent report describes the coexistence of histopathological characteristics of the CMT neuropathy and the CNM myopathy in a patient with a DNM2-G359D mutation in the middle domain of DNM2 (Chen et al, 2017). The molecular mechanisms that lead to neuropathy or myopathy remain unsolved.

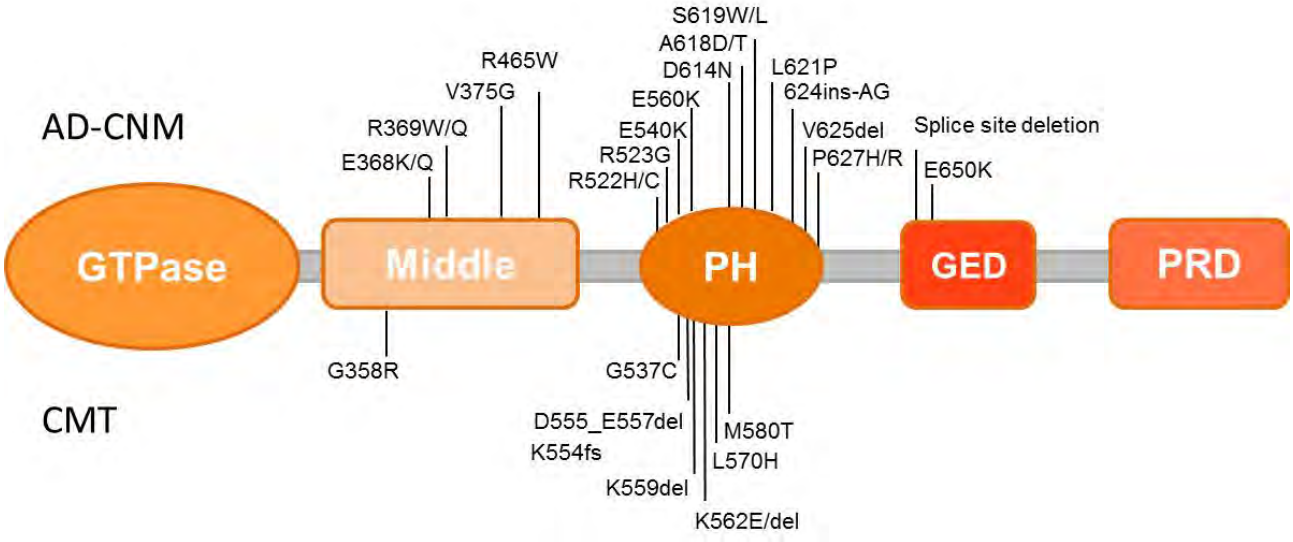

Figure 13: Schematic representation of the domains of human DNM2. Mutations responsible for autosomal dominant centronuclear myopathy (AD-CNM) or for Charcot-Marie-Tooth (CMT) are indicated.

The DNM2 catalytic activity and the DNM2 oligomerization were studied *in vitro* in presence of different CNM mutations located either in the Middle or in the PH domain. These data show that these mutant forms of DNM2 have an increased stability of the oligomers and also an increased GTPase activity (Bitoun et al, 2005; Gonzalez-Jamett et al, 2013).

The PRD domain of DNM2 is associated to actin cytoskeleton functions via recruitment of DNM2 to different actin-rich structures via protein interaction with actin nucleation promoting factors mediated by the PRD-SH3 domain interactions (Gonzalez-Jamett et al, 2013). Interestingly, this PRD domain also mediates the interaction with BIN1 that is involved in CNM, and BIN1 patient mutations resulting in a truncation of the BIN1 C-terminal SH3 domain impaired its association with DNM2 and the recruitment of BIN1 to membrane tubules (Nicot et al, 2007).

1.2.2.2. Activity of the DNM2 protein in mammalian cells

DNM1 is the founding member of the dynamin family and it plays an important role in endocytosis, the process by which cell internalizes extracellular material through invaginations in the plasma membrane. Indeed, DNM1 participates in clathrin-mediated and clathrin-independent endocytosis (Schmid & Frolov, 2011). Endocytosis is the best-characterized role of this protein family.

Based on protein domain conservation, the different dynamins DNM1, DNM2 and DNM3 are supposed to play a role in membrane remodeling and membrane fission events. This dynamin fission mechanism was described in a recent review (Antonny et al, 2016). Indeed, dynamin assembles into helical polymers around the tubular membrane structure between the nascent vesicle and the plasma membrane, then the GTP-hydrolysis provokes a change of conformation in dynamin and this promotes the membrane fission (Ferguson & De Camilli, 2012)(figure 14, figure 15).

A recent study has shown that DNM2 is also implicated in the fission of mitochondria, working in cooperation with the cytoplasmic dynamin-related GTPase DRP1/DNM1L that was previously thought as being the only dynamin required for mitochondria fission (Lee et al, 2016). Using a combination of high-resolution light microscopy and electron microscopy, Lee and colleagues have shown that first DRP1/DNM1L mediates the mitochondrial membrane constriction, and then DNM2 acts and completes this constriction to produce fission of the membrane (Lee et al, 2016). However, this mitochondrial fission event not only requires DNM2 and DRP1 recruitment to outer mitochondrial membrane, but also requires a process named ERMD (ER-associated mitochondrial division) (Lee et al, 2016). This ERMD process is a pre-constriction membrane mechanism where the ER and mitochondria membranes interact and DRP1/DNM1L is recruited to these pre-constricted contact sites, however the precise molecular mechanism directing this specific recruitment is still unclear (Hatch et al, 2014).

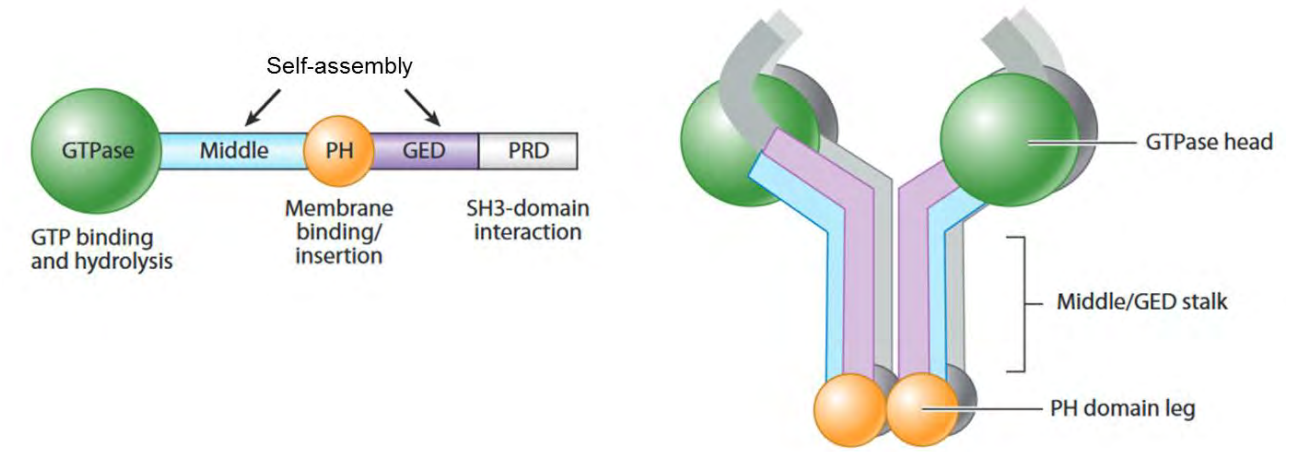

Figure 14: Schematic representation of dynamin and its oligomerization and self-assembly. From (Schmid & Frolov, 2011).

A B

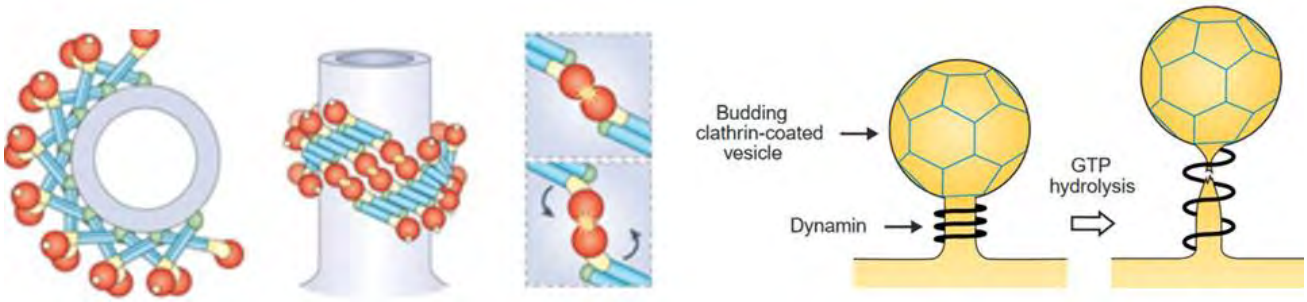

Figure 15: (A) Schematic representation of helical dynamin polymers around a tubular template. The GTPase domain is indicated in red and the PH domain in green. GTP hydrolysis induces a conformational change in the protein. From (Ferguson & De Camilli, 2012). (B) During its role in endocytosis, DNM1 dynamin tubulates around the membrane in order to constrict and allow the fission and release of the endocytic vesicle. From (Stowell et al, 1999).

Now, I will more precisely describe some of the known roles of DNM2 dynamin linked to muscle functions. Durieux and colleagues generated a knock-in (KI) mouse model expressing the most frequent AD-CNM mutation DNM2-R465W at a heterozygous state DNM2-R465W/DNM2. This model showed that DNM2 plays a role in the calcium homeostasis in muscle. Indeed, it has been reported that isolated fibers from flexor digitorum brevis (FDB) muscle from heterozygous Dnm2-R465W KI mice presented a higher cytosolic calcium concentration (Durieux et al, 2010b). Similar studies were performed in dissected fibers of the fast twitch extensor digitorum longus (EDL) and the slow-twitch soleus muscles from Dnm2-R465W KI mice (Fraysse et al, 2016). The results showed a higher cytosolic concentration of Ca^{2+} in EDL muscle from these model mice, an increase of the sarcolemmal permeability to Ca^{2+} and a higher sarcoplasmic reticulum Ca^{2+} content in EDL contrary to the soleus muscle fibers. This suggests that the increase in cytosolic calcium concentration is not the result of a leaky sarcoplasmic reticulum SR. Fraysse and colleagues propose that the plasma membrane permeability is the main factor involved in the calcium

homeostasis disturbances (Fraysse et al, 2016). However it is important to mention that there was no alteration in the kinetics characteristics of the calcium transients associated to the muscular contractile activity in Dnm2-R465W KI muscles, which develop a weaker force; therefore this suggests that calcium homeostasis defect is probably not the cause of the contractile impairment, even if both might be correlated. Interestingly, no differences in calcium homeostasis were observed between the soleus muscle from Dnm2-R465W KI and wild type mice (Fraysse et al, 2016).

A role of DNM2 on the ROS production related to oxidative stress-induced apoptosis in cardiomyocytes has been shown recently (Gao et al, 2016). Indeed, it was previously shown that DRP1/DNM1L inhibition limits ROS production and apoptosis in cardiomyocytes subjected to ischemia/reperfusion injury. Therefore, Gao and colleagues analyzed whether inhibition of DNM2 also limits ROS production. They used specific DNM2 knockdown by shRNA combined to the dynamin-inhibitor Dynasore (a non-selective inhibitor that blocks the GTPase activity of the different DNM1 to DNM3 dynamins). Their results show that inhibition of DNM2 reduces the mitochondrial fission induced by oxidative stress and consequently reduces cell apoptosis in cardiomyocytes (Gao et al, 2016). So, these results suggest that DNM2 is linked to ROS production. Mitochondria participate actively in cell death through different mechanisms and among them the ROS-induced apoptosis (Kamogashira et al, 2015). As already mentioned, DNM2 is required in association with DRP1/DNM1L for the fission of the mitochondria (Lee et al, 2016). Mitochondria are the main organelles producing ROS. All these data highlight a connection between DNM2, mitochondria and ROS production. Even more interesting, the energetic balance between mitochondria fusion and fission is linked to the GTP gradient that also determines a specific cell fate. So a fourth factor comes into this connection: cell fate.

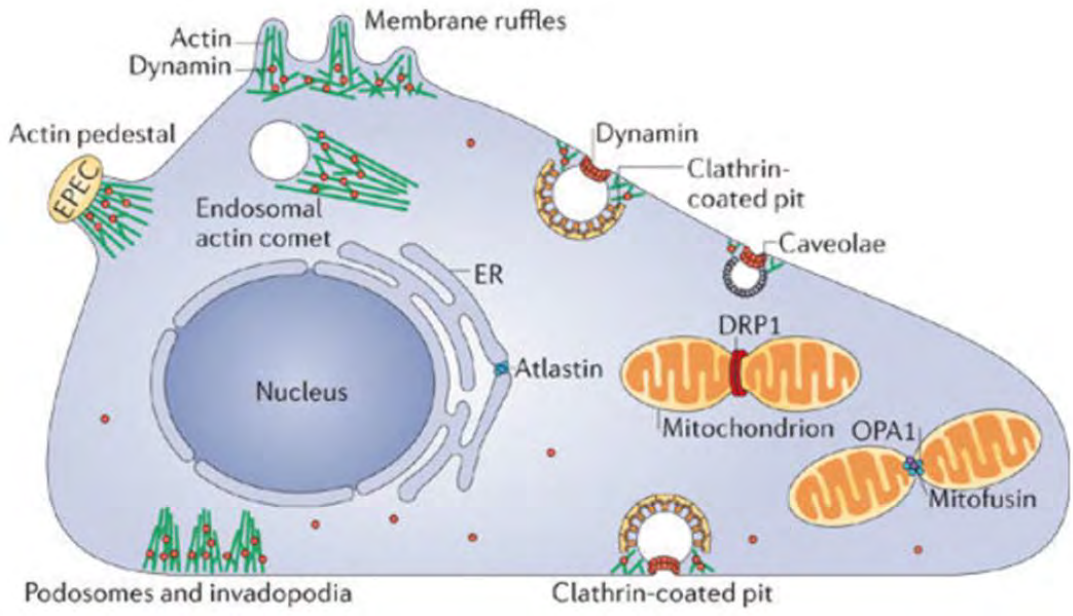

Figure 16: Representation of some of the multiple cellular localizations and functions reported for dynamins and dynamin related proteins (DRPs). Dynamin proteins are indicated as red spheres and the F-actin in green. Atlastin, DRP1/DNM1L, OPA1 and mitofusin are DRPs that localize to sites of intracellular membrane fission and fusion in the endoplasmic reticulum and mitochondria. Adapted from (Ferguson & De Camilli, 2012).

DNM2 was also shown to be involved in autophagy (Durieux et al, 2012). Durieux and colleagues have shown that the Dnm2-R465W KI mice which develop the CNM phenotypes have also a defect in neonatal autophagy with a decrease in autophagy flux prior degradation by the autolysosome, a compartment created by the fusion of the mature autophagosome and the lysosome (Durieux et al, 2012). They also observed that embryonic fibroblasts from the Dnm2 KI mice display an increased ratio of immature autophagomes upon starvation, a condition that induces high levels of autophagy (Durieux et al, 2012).

In hepatocytes, DNM2 plays also a critical role in the regulation of a specific type of autophagy termed lipophagy (figure 17) (Schulze & McNiven, 2014). Lipophagy is defined as the autophagy of cytosolic lipid droplets (LDs). The LDs are engulfed by autophagosomes that fuse with the lysosomes to deliver their intracellular content for degradation and the LDs are then degraded by acid lipases. The autolysosomes result from the fusion between autophagosomes and lysosomes. DNM2 acts in the scission of the autolysosomal membrane tubules resulting in protolysosomes that will finally mature in lysosomes, ready for a new autophagic lysosomal cycle (Schulze & McNiven, 2014). Lipophagy is essential for the regulation of LD catabolism. Perturbations in DNM2 function result in LDs accumulation in hepatocytes and this might be linked to the development of cancers (Schulze & McNiven, 2014).

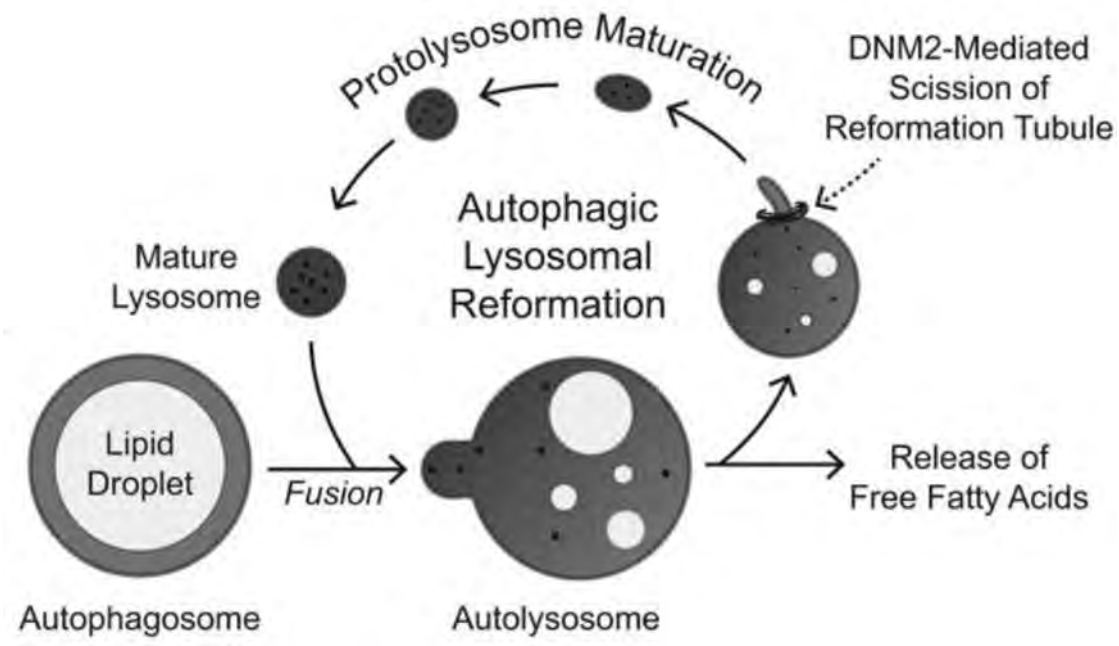

Figure 17: During lipophagy, DNM2 plays a role in membrane scission of reformation tubule (Schulze & McNiven, 2014).

Recent findings show that the GTPase activity of DNM2 is implicated in de novo actin polymerization and also in actin-mediated trafficking of the glucose transporter GLUT4 (Gonzalez-Jamett et al, 2017). GLUT4 is the insulin-regulated glucose transporter found primarily in adipose tissues and striated muscle (skeletal and cardiac). During exercise or muscle contraction, the body needs to convert glucose to ATP to obtain energy. Under insulin signaling, GLUT4 is translocated from intracellular compartments to the plasma membrane in an actin-dependent membrane trafficking pathway. In order to increase glucose levels in the cell, GLUT4 is used as the primary transporter in this facilitated diffusion (Richter & Hargreaves, 2013). Gonzalez-Jamett and colleagues studied the GLUT4 trafficking in RCMH myoblasts, a cell line derived from a skeletal muscle biopsy of a healthy subject (Gonzalez-Jamett et al, 2017). In RCMH cells transfected with DNM2-R369W, -R465W or -R522H, different mutations associated to dominant CNM, there was a decrease in stimulus-induced GLUT4 translocation at the plasma membrane compared to wild type cells. In the same study, Gonzalez-Jamett and colleagues also studied muscles from Dnm2-R465W KI mice and showed that actin organization and polymerization is defective in these dissected muscles. Moreover, they stimulated muscle fibers from wild type mice with insulin and they observed an increased GLUT4 staining along the sarcolemma as a result of its actin-dependent translocation, whereas in Dnm2-R465W KI mice stimulated muscle fibers there was no change in GLUT4 levels compared to the resting state (Gonzalez-Jamett et al, 2017). These data suggest an insulin-induced defective trafficking of GLUT4 vesicles in Dnm2-R465W KI mice. This hypothesis

was confirmed by measuring GLUT4 in biotinylated fractions of insulin-stimulated muscles, indicating its level of expression at the plasma membrane. For Dnm2-R465W KI mice fibers, the GLUT4 expression was significantly reduced in surface membranes compared to wild type mice. Altered distribution of GLUT4 was also observed in skeletal muscle biopsies from DNM2 CNM patients, with abnormal perinuclear localization of GLUT4 (Gonzalez-Jamett et al, 2017).

1.2.3. The oxidoreductase Pyroxd1 protein

PYROXD1 (**pyr**idine nucleotide-disulphide **ox**idoreductase (PNDR) **d**omain-containing protein **1**) is classified as a class I pyridine nucleotide-disulphide oxidoreductase. However unlike the other human PNDRs, such as dihydrolipoamide dehydrogenase (DLD), glutathione reductase (GSR) and thioredoxin reductases 1,2 and 3 (TXNRD1,2,3), PYROXD1 does not present neither the redox motif of the oxidoreductase domain: Gly Gly Thr Cys Val Asn Val Gly Cys in GSR and in TXNRD1,2,3 or Gly Gly Thr Cys Leu Asn Val Gly Cys in DLD, the reactive cysteine disulphide is underlined, nor the conserved c-terminal dimerization domain identified in the class I PNDRs. Instead it presents a highly evolutionary conserved NADH-dependent nitrile reductase domain in c-terminal (figure 18).

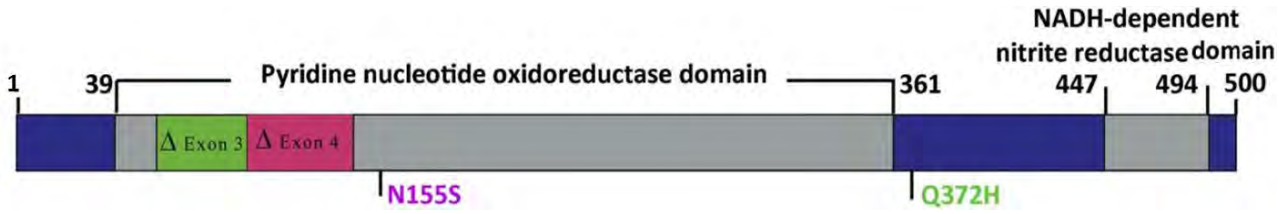

Figure 18: A schematic of PYROXD1 with functional domains and identified missense variants.

Exome sequencing identified two missense mutations in patients, the Gln372His or Q372H and Asn155Ser or N155S (O'Grady et al, 2016). The first mutation is located at the c-terminal and the second is located in the pyridine nucleotide oxidoreductase domain. Also the removal of amino acids encoded by exon 3 or exon 4 appears likely to significantly impact tertiary folding and abolish FAD binding and enzymatic function of the PYROXD1 enzyme (O'Grady et al, 2016).

1.3. The budding yeast *Saccharomyces cerevisiae*, the model of this study

The *Saccharomyces cerevisiae* yeast is a unicellular eukaryote, of the ascomycetes group belonging to the Fungi kingdom. The yeast *Saccharomyces cerevisiae* (specifically the laboratory strain S288c) was the first eukaryote having its genome fully sequenced in 1996; after 4 years of a sequencing project encompassing more than 100 laboratories around the world. Nowadays, it is the best-known annotated eukaryotic genome and the publication data about the regulation of the genes and the role of the protein are stored in a database, the Saccharomyces Genome Database (https://www.yeastgenome.org/).

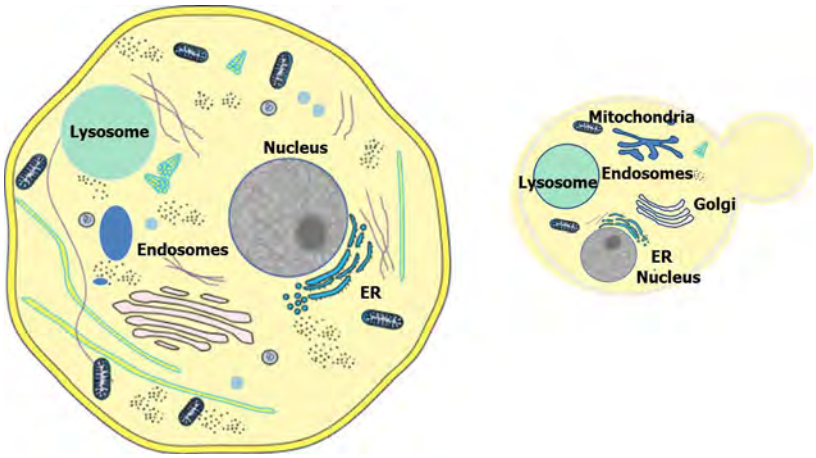

Figure 19: Schematic representation of human (left) and saccharomyces cerevisiae (right) cells. Both are eukaryotes with a similar organization in compartments.

Apart from the use in industry for fermentation processes in wine and beer fabrication or for bread production; yeast is also used as a model organism in research laboratories (Botstein et al, 1997). Growing yeast cells and manipulating its genome in laboratory is well described, fast and low-cost. In addition, the yeast deletion collection strains encompassing the knock-out of each non-essential yeast gene (http://www-sequence.stanford.edu/group/yeast_deletion_project/deletions3.html) is provided for the scientific community by Euroscarf (http://www.euroscarf.de/) (Winzeler et al, 1999). In this collection, we can find a set of yeast deletion strains with the KanMX (Kanamycin) resistance gene of more than 6000 open reading frames (ORFs) in the *S. cerevisiae* genome. This collection allows studying the precise cellular function of each gene in the corresponding deletion strain (Winzeler et al, 1999). In addition *S. cerevisiae* shares a similar intracellular organization with superior eukaryotes (Figure 19). Moreover, about 30% of the yeast ORF have a human orthologue, genes of different species with an ancestral common gene. Therefore, yeast is a the powerful tool for studying human genes (Foury, 1997). I would like to mention that between 2001 and 2013, four Nobel Prizes were awarded for discoveries using the yeast model.

https://www.nobelprize.org/nobel_prizes/medicine/laureates/2013/med_image_press_eng.pdf
https://www.yourgenome.org/stories/using-yeast-in-biology

Researches in congenital myopathies using yeast

The laboratory of Jocelyn Laporte identified that MTM1 was a phosphatase targeting PIs rather that proteins thanks to the yeast *Schizosaccharomyces pombe* model system (Blondeau et al, 2000). Indeed, expression of MTM1 in S. pombe induced an enlarged vacuolar phenotype similar to the one observed for the yeast *vac* mutants, impaired in PI(3,5)P_2 synthesis (Blondeau et al, 2000). Previous studies in the team of Sylvie Friant in collaboration with Jocelyn Laporte were based on a similar approach with expression of human MTM1 in *S. cerevisiae* yeast cells, using an approach now termed as humanization of yeast, as documented in Dimitri Bertazzi PhD thesis "Analyse des mécanismes cellulaires responsables de maladies neurodégénératives dans le modèle de la levure Saccharomyces cerevisiae – Analyse fonctionnelle de myotubularines responsables de pathologies humaines" defended in 2012 and a publication in collaboration with Jocelyn Laporte's team (Amoasii et al, 2012). Walker and colleagues also expressed the active myotubularin MTMR3 in the yeast *S. cerevisiae* and upon as osmotic stress they could identify the production of PI5*P*, identifying a novel PI(3,5)P_2 substrate specificity for MTMR3 (Walker et al, 2001).

Humanization of yeast

Humanization of yeast consists in transforming yeast with human genes or replacing the yeast genes by its human orthologue in order to study its cellular function in a unicellular eukaryote (Kachroo et al, 2015). This approach will be further detailed in the MTM1-ymr1 section of the manuscript.

Kachroo and colleagues have replaced 414 yeast genes with the human orthologues and they confirmed that a substantial portion of them perform similar roles in both organisms (Kachroo et al, 2015). In that way, they showed that functional studies of human proteins could be done in a unicellular eukaryotic yeast cell. During my thesis, I used humanization of yeast to study 3 human proteins implicated in centronuclear myopathies, namely, the myotubularin MTM1, the dynamin DNM2 and the oxidoreductase PYROXD1.

1.3.1. Yeast *Saccharomyces cerevisiae* membrane trafficking

Membrane trafficking is the transport of proteins in vesicles from a donor compartment to an acceptor compartment (figure 20) (Feyder et al, 2015). Indeed, proteins that have to be addressed to the Golgi, endosomes, vacuole or plasma membrane are translocated from the ER and directed to the Golgi apparatus for sorting (figure 21) (Feyder et al, 2015). At the Golgi, there are 3 possible membrane trafficking pathways for these proteins:

1- They can be directed via the SEC secretory/exocytosis pathway to the plasma membrane to be integrated into the plasma membrane for transmembrane containing proteins or secreted into the extracellular medium for soluble proteins.

2 – They can be targeted to the vacuole, directly via the adaptor protein AP-3 dependent pathway termed the alkaline phosphatase ALP pathway or indirectly via the endosomes and the multivesicular body (MVB) for the vacuolar protein sorting VPS pathway termed the carboxypeptidase Y CPY pathway (figure 21). MVBs are a specialized subset of endosomes that contain intraluminal vesicles bearing transmembrane receptors destined for vacuolar degradation after their endocytic internalization for example as for the general aminoacid permease (Gap1) or the uracil permease (Fur4).

3 – They can return to the ER as for the resident ER proteins for example or to be degraded by the unfolded protein response UPR pathway.

Plasma membrane proteins as receptors or permeases can also be internalized by the endocytosis END pathway and delivered into early endosomes EE. From there, proteins can be targeted to vacuole for their degradation or to the Golgi apparatus for their recycling along the recycling RCY pathway. In these different membrane trafficking pathways, vesicle formation and budding at the donor compartment and fusion with the acceptor compartment are strongly regulated by protein-protein interactions encompassing coat (clathrin, COPI or COPII) and adaptor proteins (AP-1, AP-2, AP-3, GGA, Epsin) for formation of the vesicles and sorting of transported cargos, and encompassing SNARE complexes (soluble N-ethylmaleimide–sensitive factor attachment protein receptor) for membrane fusion. For an extended explanation about membrane trafficking in yeast cells, see the review (Feyder et al, 2015).

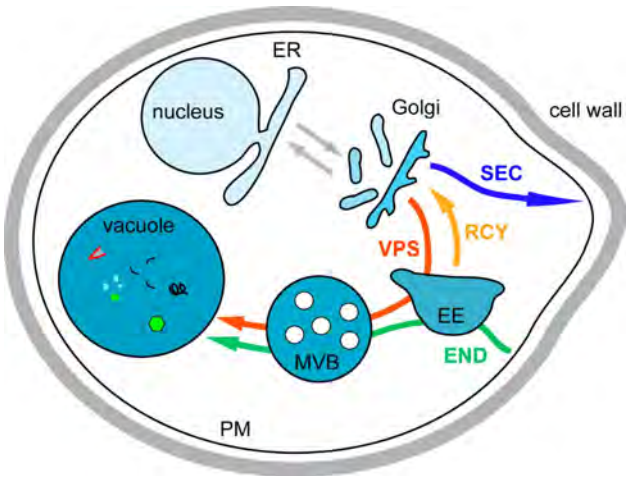

Figure 20: Representation of different trafficking pathways in yeast: the secretory pathway (SEC), the endocytic pathway (END), the vacuolar protein sorting (VPS) and the recycling pathway (RCY). From (Feyder et al, 2015).

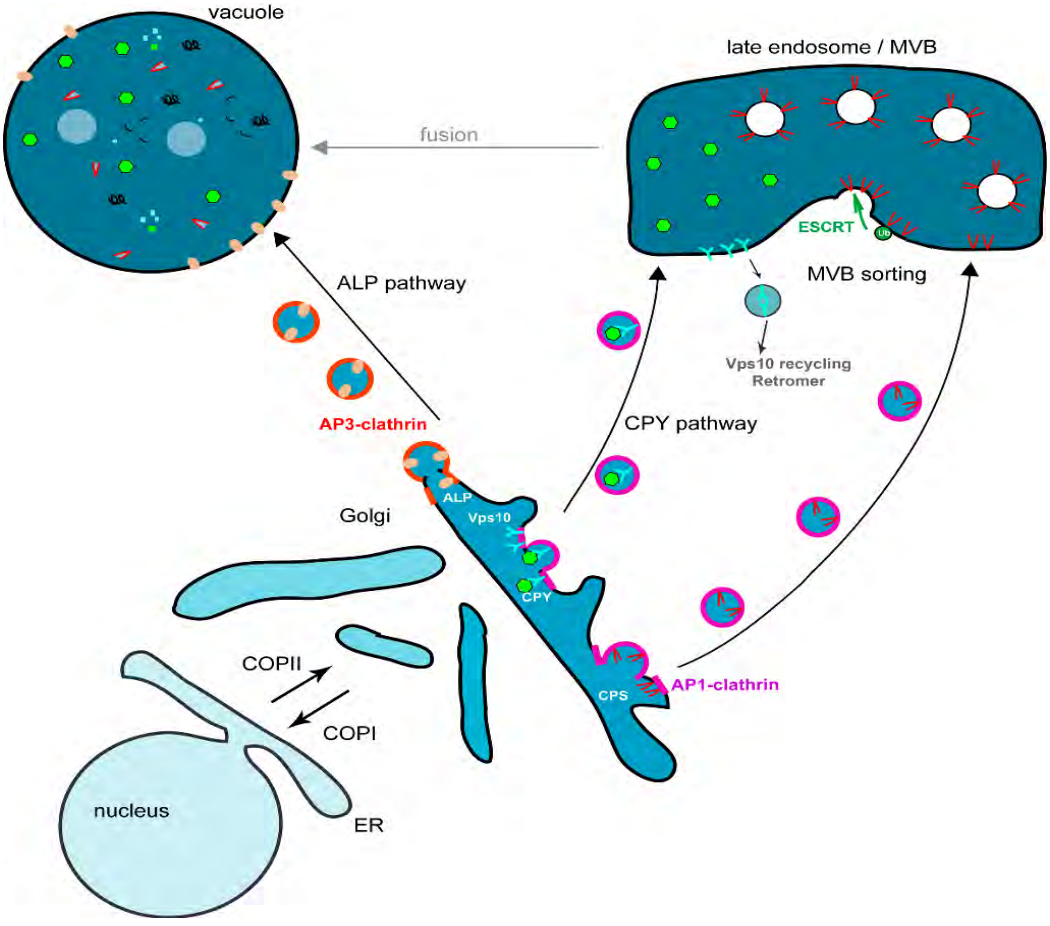

Figure 21: The Golgi to vacuole trafficking pathways. In yeast cells, the Golgi is not stacked. The Golgi to the vacuole transport of cargos can be either direct via the ALP pathway, or via the endosomes for the CPY pathway. COPI and COPII are two protein complexes that coat transport vesicles, COPI in the retrograde transport from the Golgi to ER, and COPII for the anterograde transport from ER to Golgi. From (Feyder et al, 2015).

1.3.2. The yeast vacuole and classification of vacuolar defective yeast mutants

Vacuole is the yeast degradation compartment equivalent to the lysosome in mammalian cells. It stores amino acids, hydrolases, phosphate, calcium, metals and toxins. Vacuole is the main organelle containing Ca^{2+} in yeast and is essential for viability; it plays an important role in homeostasis and stress response. Studies about vacuole sorting in the yeast *Saccharomyces cerevisiae* have helped to better understand the molecular basis of vesicular trafficking and organelle biogenesis. Raymond and colleagues designed 41 *vps* mutants (*vps*, vacuolar protein sorting) to study vacuolar inheritance, morphology and segregation structure (table 2) (Raymond et al, 1992). The terminology *vps* refers to cells lacking the corresponding VPS gene. The *vps* mutants were selected from a yeast temperature-sensitive mutants library based on the phenotype of CPY secretion, in order to identify the mutants showing vacuolar protein sorting (vps) defects characterized by secretion of CPY into the extracellular medium rather than delivery to the vacuole. Vacuole inheritance refers to the process by which mother cell transfer vacuole to daughter cell. Vacuolar segregation structure refers to the morphology of vacuolar extension going from mother cell to the bud during the specific process of bud enlargement (Raymond et al, 1992). In order to classify the *vps* mutants, Raymond and colleagues observed by microscopy the vacuoles after labeling the ALP and the 60 kDa subunit V-ATPase proteins. ALP is an integral membrane protein of the vacuole; antibodies against this protein allowed to delineate the vacuolar membrane. V-ATPase is the vacuolar H^+-ATPase complex; the 60 kDa subunit of the pump is a peripheral membrane protein present at the cytoplasmic face of the vacuole; antibodies against this protein allowed to observe either the proper subunit assembly in the complex (wt) or not (mutants); the latter leading to a diffuse cytoplasmic pattern. They could group the 41 *vps* mutants in 6 classes (class A to E) based on the morphology and segregation of vacuole and the CPY protein sorting (Raymond et al, 1992). They correlated morphological phenotype of the vacuole to the severity of the CPY sorting defect in *vps* mutants. A summary of this classification is shown in the table 2.

Class	*Vps* mutants	Characteristics
Wild type	*Saccharomyces cerevisiae* wild type SF838-9D,SF838-9DR2L1, JHRY20-2C, SEY6210,SEY6211	Vacuole presents 1-10 lobes that cluster together in one region of the cell. During the cell cycle, portions of the mother vacuole extend to developing buds. ALP and the 60 kDa subunit staining pattern are indistinguishable.
Class A	vps8,vps10,vps13,vps29,vps30,	Vacuolar morphology similar to wt, vacuolar segregation

	vps35,vps38,vps44,vps46	structures far less prominent than that wt, V-ATPase complex properly assembled but % CPY secreted different to wt.
Class B	vps5, vps17,vps39,vps41,vps43	A lot of vacuole-like compartments. Despite that, configuration is reminiscent of wt vacuolar segregation structures. No defects in vacuole inheritance. Partial defect in the V-ATPase assembly. High level of newly synthesized CPY. Defective in endosome and vesicle fusion with the vacuole
Class C	vps11, vps16, vps18, vps33	Multiple vesicle-like structures. Not organized vacuole. No cell surface ALP staining. Staining pattern of V-ATPase subunit was diffuse. Strongly defective for CPY sorting.
Class D	vps3,vps6,vps9,vps19, vps21,vps45	Defects in vacuole assembly and in vacuole inheritance. Single spheres that failed to form segregation structures. Buds no receive or little vacuolar material. Nascent vacuolar material produced accumulates as unfused vesicles. High % of newly synthesized CPY secreted.
	vps15,**vps34**	Vps15 and Vps34 take part of this group but they present some important differences with the rest of mutants of class D.
Class E	vps2,vps4,vps20,vps22,vps23, vps24,vps25,vps27,vps28,vps31, vps32,vps36,vps37	Relatively normal appearance of the vacuole. A **separate compartment** was defined. Indeed V-ATPase subunit clustered around this compartment. A-ALP appeared localized to punctate regions typical of Golgi staining in wt. Also the majority of CPY in the compartment. Secreted modesty amounts of newly synthesized CPY.
Class F	**vps1**,vps26	Vacuolar morphology intermediate between wt and class B. Large central vacuole surrounded by smaller vacuole-like. Segregation structures were rarely observed. Vacuole inheritance occurs. V-ATPase assembly OK. Severe CPY sorting defects.

Table 2: Classification of *vps* (vacuolar protein sorting) mutants. The classification is based on different criteria, the CPY sorting, the vacuole inheritance and vacuolar morphology. For the latter, ALP and V-ATPases were marked in order to observe vacuole under microscopy.

They could establish 6 classes and this suggested that the Vps proteins from the same class could participate in the same pathway, biochemical process or interact between them. This classification helped to identify the role of the Vps proteins, for example if a mutation affects the soluble protein sorting process but no other events in vacuole, no disturbances in vacuolar morphology are observed as in the class A *vps* mutants, whereas important defects are observed in protein sorting. Interestingly mutants defective for the fusion of Golgi-derived vesicles with the endosomes form

the Class D, while the ones blocking the membrane fusion with the vacuole form the class B and mutants affected for all fusion events form the class C (Raymond et al, 1992; Weisman, 2003).

This study has also revealed fundamental differences between the different classes of *vps* mutants and latter studies have shown that this was due to differences in the sorting pathway of soluble and integral membrane vacuolar proteins. Indeed membrane proteins are delivered to the vacuole after a sorting step at the MVB requiring their modification by ubiquitin and their sorting into the intralumennal vesicles of the MVB by the ESCRT (endosomal sorting complex required for transport) complexes composed of the class E Vps proteins (Henne et al, 2011). Moreover, microscopy analyses of the class E *vps* mutants has revealed the presence of an enlarged aberrant endosomal compartment near to the vacuole that was termed the class E compartment (Feyder et al, 2015; Henne et al, 2011).

Other *vps* mutant screening studies were done to identify mutants defective in vacuolar inheritance and termed *vac* mutants. They were further subdivided in mutants defective for CPY sorting (*vps* mutants) or not (non *vps* mutants) (Wang et al, 1996; Weisman et al, 1990). Three classes were defined: class I, class II and class III. Classes II and III are subdivided either in *vps* or non *vps* mutants, and class I included only the non *vps* mutants (Weisman, 2003). Studies of the class I mutants have helped to elucidate that the vacuole movements are actin dependent (*act1* mutant) with the class V myosin Myo2 serving as motor (*myo2* mutant). Characteristics of each class are explained in the table 3

Class	Characteristics	Examples of mutants
Class I non *vps*	They appear to have relatively normal vacuole morphology (see wt in table 2), but they are defective in vacuole mobility.	*Act1*, *myo2, vac8 (binds vac17p)*
Class II non *vps*	They present an enlarged vacuole and a spot or arrested segregation on the face of vacuole closest to the bud is usually observed. Vacuole inheritance process is not clearly defined in this group, the *Pho80* mutant is not defective in vacuole inheritance and the function of the other mutants is unknown.	*Vac 5* (Pho80 is the corresponding gene product) (Nicolson et al, 1995)
Class II *vps* (ClassD)	They present a class II vacuole morphology and defects in vacuole biogenesis and vacuole inheritance. Also they are defective in fusion of Golgi-derived vesicles with the late endosomes.	(See table 2) Just a little difference, they include here the vps8 while Raymond and colleagues included it in the Class A
Class III non *vps*	They present a **remarkably enlarged vacuole**. They are defective in vacuole membrane fission, in retrograde traffic out the vacuole, in	***Fab1*, *Vac7*, *Vac14*, *Fig4***

	vacuole acidification and in ion transport.	
Class III *vps*	See class D in the table 2 They are **defective in** the synthesis of **PI3*P***, and thus in the synthesis of **PI(3,5)P_2**.	***Vps15, vps34 (= vac4)***

Table 3: This table complements the table 2. It was done latter and included other mutants than only the *vps* mutant defective for CPY sorting and mutants implicated in vacuole inheritance (*vac*) were also considered.

1.4. The lipid phosphoinositides (PIP) as essential actors of membrane functions.

Membranes are dynamic structures composed mainly by five phospholipids: the phosphatidylcholine (PC), the phosphatidylethanolamine (PE), the phosphatidylserine (PS), the phosphatidylinositol (PtdIns) and the sphingomyelin (SM). Phosphatidylinositols (PtIns) are amphipathic molecules; they have a polar head group composed of an inositol ring and two hydrophobic hydrocarbon tails composed of fatty acids embedded in the membrane layer (figure 22). The inositol ring can be phosphorylated in the 3, 4 or 5 position and this leads to the different species of phosphoinositides, PI3*P*, PI4*P*, PI5*P*, PI(3,4)P_2, PI(3,5)P_2, PI(4,5)P_2, PI(3,4,5)P_3. Phosphoinositides (PIs) are phosphorylated phosphatidylinositols (PtdIns) and these latter represent about 10% of the total phospholipids in eukaryotic cells (Bertazzi et al, 2015a; Payrastre et al, 2001). Phosphorylation and dephosphorylation of each PI are orchestrated by the lipid kinases and phosphatases specific to the different membranes (figure 23) (Bertazzi et al, 2015a). These reactions happen within a spatial and temporal control controlling different cellular functions (Payrastre et al, 2001). Indeed, the different PI are enriched in specific membrane of compartments, to fulfill specific functions, such as the recruitment and/or activation of effector proteins for vesicular trafficking, autophagy or signaling (figure 23) (Bertazzi et al, 2015a; De Craene et al, 2017).

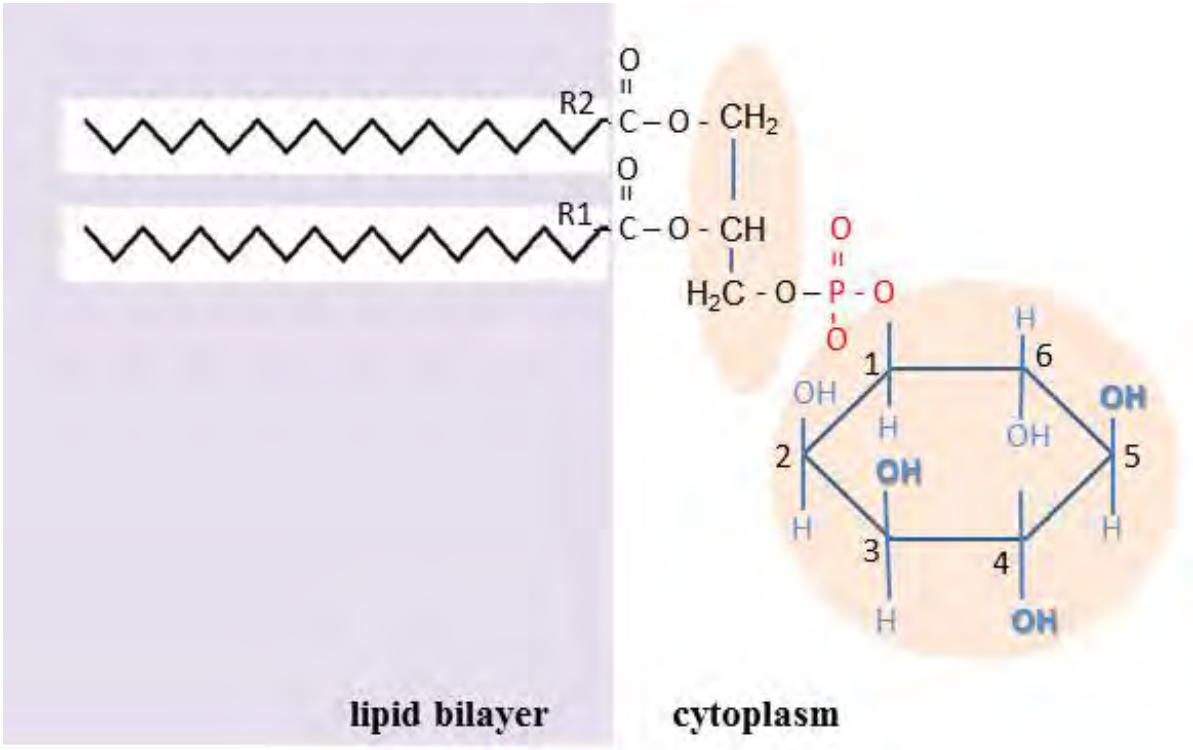

Figure 22: Schematic representation of a phosphatidylinositol, indicated the 2 fatty acid embedded chains in the lipid bilayer, and the glycerol moiety and the inositol ring in the cytoplasm. Adapted from (De Craene et al, 2017).

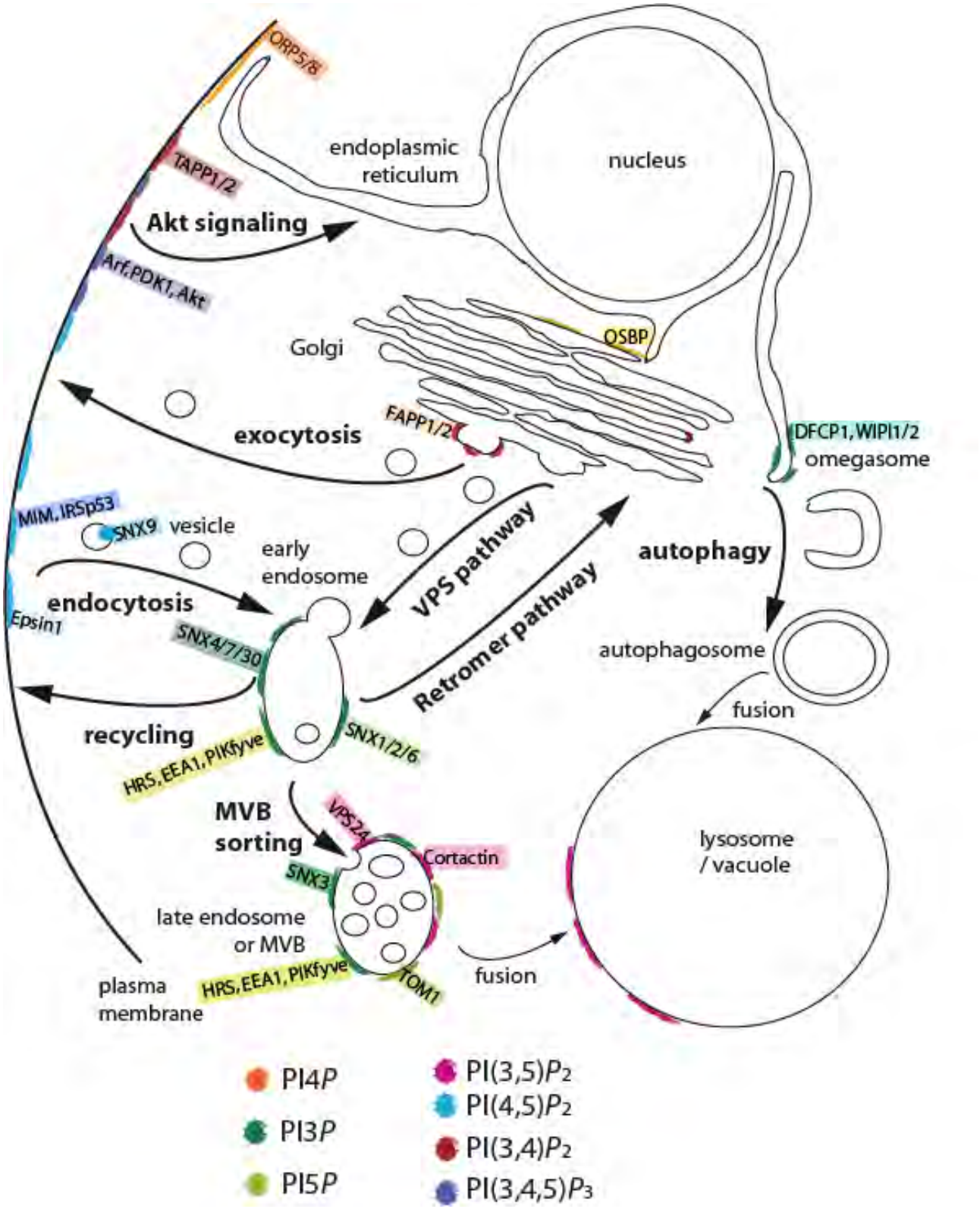

Figure 23: Localization of the different phosphoinositides inside the cell and its implication in each pathway. Each type of phosphoinositide is indicated by a different color. Note that PI(3,4)P_2 and PI(3,4,5)P_3 are absent in yeast. The human proteins interacting with the different PI are indicated in the schema and highlighted in a square with the corresponding color. Adapted from (De Craene et al, 2017).

1.4.1. The phosphoinositide PI3*P*, a substrate of MTM1

In S. cerevisiae, **PI3*P*** is synthesized from phosphorylation of PtdIns in PI3*P*. This reaction is catalyzed by the only phosphoinositide 3-kinase in yeast, the Vps34 (vacuolar protein sorting 34) protein (figure 24) (Schu et al, 1993). PI3*P* is also synthesized from dephosphorylation of PI(3,5)P_2 in PI3*P* by several lipid 3-phosphatases, namely, Fig4 (factor induced gene 4, also known as Sac3), Sjl2/Inp52, Sjl3/Inp53 and Sac1. Regarding human cells, there are up to eight lipid kinases able to phosphorylate PtdIns at the D3 position and also several 3-phosphatases that catalyze the reverse reaction (De Craene et al, 2017; Vanhaesebroeck et al, 2001).

PI3*P* represents 30% of total PI in yeast cells and less than 15% of monophosphorylated PI in human cells (Payrastre et al, 2001). In yeast and mammalian cells, PI3*P* is enriched at endosomal membranes and membranes of the multivesicular body (MVB) (Gillooly et al, 2000). This enrichment allows the recruitment of endosomal effector proteins bearing a PI3*P* binding domain, as the FYVE (Fab1, YGLO23 Vsp27 EEA1) domain for example (Mayinger, 2012). The Endosomal Sorting Complex Required for Transport (ESCRT) machinery was originally identified for its role in the biogenesis of MVBs in the endolysosomal sorting. Indeed, membrane proteins tagged with ubiquitin at the endosomes are recognized by ESCRT-0 to -3 complexes for their endosomal internalization and then packaged into the vesicles budding in the endosomal lumen, thus forming the MVB. Latter they are delivered to the vacuolar lumen after fusion of the MVB with the vacuole (Henne et al, 2011). The ESCRT-0 complex protein Vps27 depends on its interaction with PI3*P* to start the MVB sorting process (De Craene et al, 2017).

PI3*P* is also enriched on the inner membrane of the autophagosome and plays an important role in autophagy by recruitment of Atg (autophagy-related) proteins to autophagic membranes (Obara & Ohsumi, 2011). Indeed, the PROPPIN Atg18 and Hsv2 proteins, which contain two binding sites for PI3*P*, are critical for this process (Baskaran et al, 2012).

Among the human lipid 3-phosphatases, FIG4/SAC3 fulfills similar cellular functions than its yeast Fig4 homologue. Mutations in the human *FIG4* gene cause Charcot-Marie-Tooth CMT type 4J disease, a recessive neuromuscular disease characterized by neuron demyelination (Chow et al, 2007). Other lipid 3-phosphatases are implicated in neuromuscular diseases, as the myotubularins previously mentioned in this manuscript (Hnia et al, 2012). Interestingly, it has been shown that diminution of intracellular PI3*P* levels ameliorates MTM1-related myopathy in a Mtm1 KO mouse

model. Sabha and colleagues obtained this Mtm1 KO CNM phenotypic rescue by inhibition of PIK3C2B, a phosphoinositide 3-kinase in mammal cells (Sabha et al, 2016).

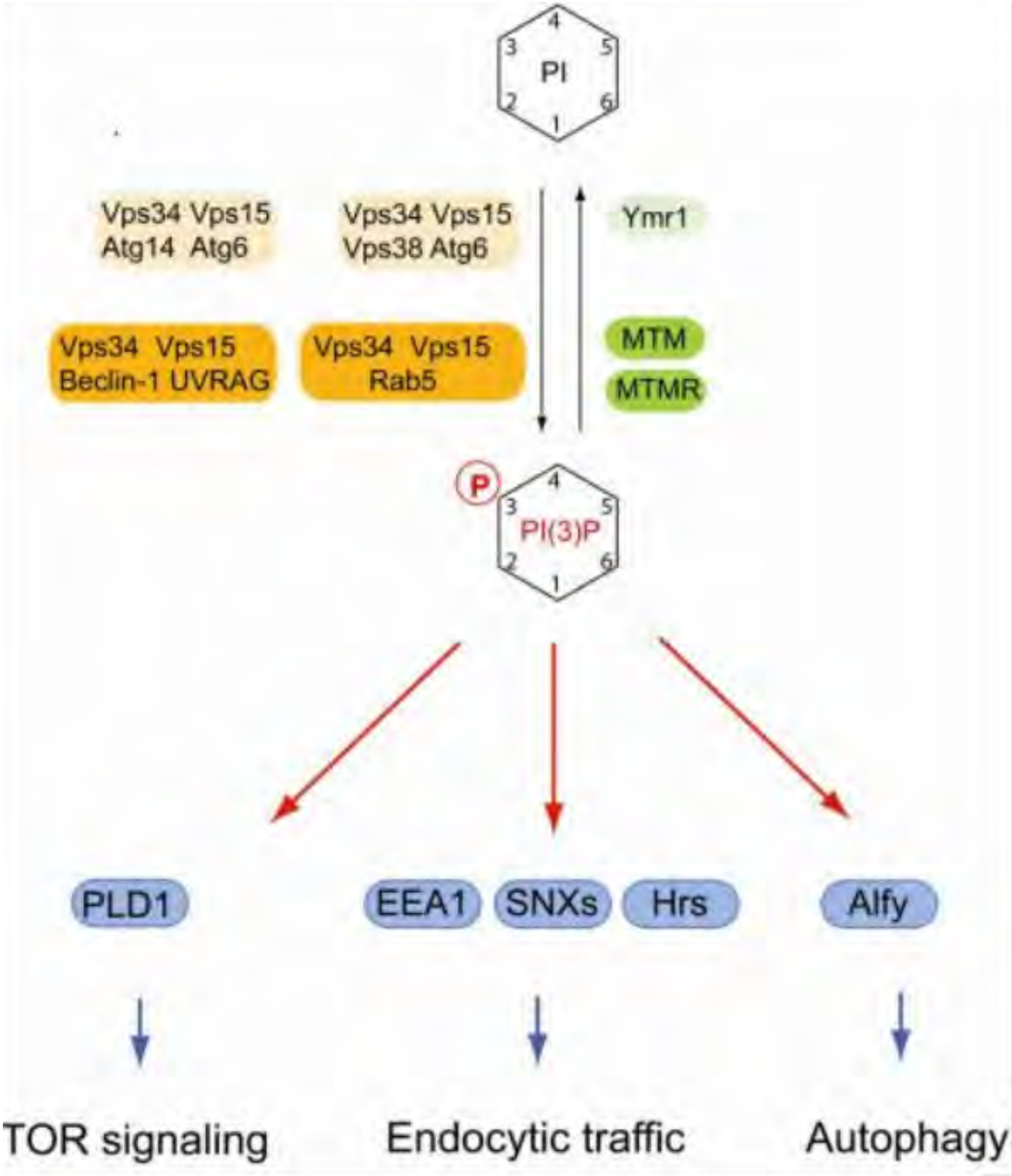

Figure 24: Schematic representation of the functions of PI3*P* in diverse pathways. PI3*P* is synthetized by 3-kinase Vps34 in yeast and in mammals. Vps34 interacts with effectors specific for endosomal trafficking (Vps38) or autophagy (Atg14). PI3*P* is also implicated in TOR (Target of Rapamycin) signaling. Lipid kinases are in orange boxes (light color corresponds to yeast proteins, dark color to human proteins), phosphatases are in green, and the effector proteins corresponding to the different pathways are in blue boxes. From (Mayinger, 2012).

1.4.2. The phosphoinositide PI(3,5)P_2, a substrate of MTM1

In S. cerevisiae, **PI(3,5)P_2** is synthesized from the phosphorylation of the PI3*P* by the PI3*P* 5-kinase Fab1 (figure 26) (Dove et al, 1997). In yeast, the lipid kinase Fab1 governs vacuolar homeostasis by generating PI(3,5)P_2 on the vacuolar membrane. PI(3,5)P_2 is synthesized at the late endosomes and the vacuolar membrane and it represents only about 0.05-0.1% of total cellular PI (Hasegawa et al, 2017). In basal conditions, the PI(3,5)P_2 levels are 18-28 fold lower than the other phosphoinositides. Under osmotic stress or by overexpression of the two Fab1 regulators Vac7 and Vac14, the PI(3,5)P_2 levels increases 20-fold above the basal levels, and the vacuoles become fragmented (Bonangelino et al, 2002). Therefore, levels of PI(3,5)P_2 directly regulate the vacuolar morphology (figure 27). However the overexpression of only Fab1 has no effect on PI(3,5)P_2 levels. In the opposite, mutants defective in PI(3,5)P_2 synthesis as *fab1*Δ, *fig4*Δ, *vac7*Δ and *vac14*Δ, the class III non *vps* mutants (table 3), have remarkably enlarged vacuoles and are defective in vacuole fission. Vac7 and Vac14 are necessary for a correct vacuolar inheritance from mother to daughter cells and to maintain the vacuole morphology (Bonangelino et al, 2002). Fab1 is not able to produce PI(3,5)P_2 in the absence of either Vac7, Fig4 or Vac14 that assemble in a protein complex required for PI(3,5)P_2 synthesis (Duex et al, 2006b). Indeed, *vac14*Δ mutants have lower PI(3,5)P_2 levels than wild type cells, even when these mutants are exposed to hyperosmotic stress, showing that Vac14 is required for PI(3,5)P_2 production (Weisman, 2003).

Regarding to the turnover of PI(3,5)P_2, the PI 5-phosphatase Fig4 catalyzes the dephosphorylation reaction of PI(3,5)P_2 into PI3*P*. It is interesting to highlight that Fig4 plays a double role, as it also participates to the Fab1-Vac7-Vac14 complex required for PI(3,5)P_2 synthesis (Duex et al, 2006b; Jin et al, 2008). The production and turnover of PI(3,5)P_2 by the kinase Fab1 and the phosphatase Fig4 in the same protein complex ensure the transient and rapid adaptation of PI(3,5)P_2 levels to resist to the osmotic stress (Duex et al, 2006a; Jin et al, 2016). This type of regulation of a signaling molecule is a common mechanism used by cell to ensure fast and specific regulation of signaling pathways in time and space.

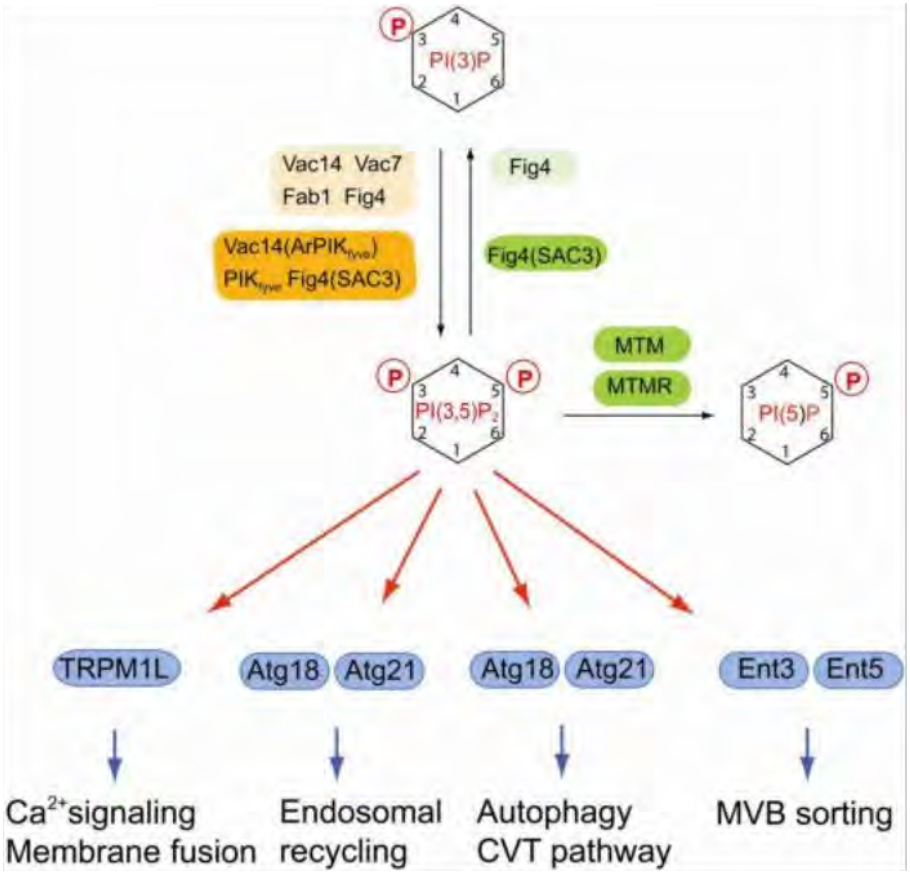

Figure 26: Regulation of PI(3,5)P_2 and its role in different pathways in mammal cells. PI(3,5)P_2 can be synthetized from dephosphorylation by the yeast protein Fab1, this lipid kinase needs to form a complex with Vac14, Vac7 and Fig 4 to develop its activity. The homologue in mammal cells is the PIKfyve kinase which forms a complex with Vac14 (also called ArPIKfyve) and Fig4 (also called SAC3). PI(3,5)P_2 is implicated in endosomal pathway, autophagy, MVB sorting and Ca^{2+} mediated membrane fusion. Effector proteins are in blue boxes. From (Mayinger, 2012).

Despite its low level, PI(3,5)P_2 is implicated in several processes in cell (figure 26) (Hasegawa et al, 2017; Mayinger, 2012). It is required for the membrane tubulation that occurs during formation of the vacuolar segregation structure. It is necessary for regulation of V-ATPase activity since *fab1*Δ mutant cells are defective in vacuolar acidification and vacuolar ion homeostasis, even though they have normal V-ATPase assembly (Weisman, 2003). In yeast an osmotic stress with NaCl results in a 20 times increase in PI(3,5)P_2 levels and in vacuolar fragmentation (Bonangelino et al, 2002). In these stress conditions, PI(3,5)P_2 interacts with the N-terminal of the Vo subunit of the V-ATPase in order to recruit it from the cytosol to the vacuolar membrane, and this recruitment stabilizes the V_0-V_1 assembly resulting in an increased activity of the V-ATPase (Li et al, 2014). The vacuolar acidification defects observed in *fab1*Δ mutant cells are the consequence of defects in V-ATPase activity.

In yeast cells, the cellular role of PI(3,5)P_2 were deciphered thanks to the phenotypes observed in the in *fab1*Δ mutant cells. The *fab1*Δ mutant strain is defective in endosomal protein sorting and vacuolar sorting of some carboxypeptidase, as the carboxypeptidase S CPS. Indeed, PI(3,5)P_2 is

required for the ubiquitin-dependent sorting of vacuolar protein cargo into the intraluminal vesicles of the multivesicular body (MVB), but not for the formation of the MVB compartment per se (Odorizzi et al, 1998).

Different proteins that bind PI(3,5)P_2 were identified but none of them is really specific (De Craene et al, 2017). Among them the yeast Ent3 and Ent5 epsins, which are required for ubiquitin-dependent MVB sorting of cargo, destined to the vacuolar lumen (Eugster et al, 2004; Friant et al, 2003). However, *in vitro* the PROPPIN proteins Atg18/Svp1 and Hsv2 proteins show the best binding to PI(3,5)P_2 (Baskaran et al, 2012; Dove et al, 2004). Atg18 acts in autophagy but this role is thought to be disconnected from its role in the PI(3,5)P_2 pathway. Atg18 regulates Fab1 by interacting with the regulatory protein Vac7 protein, which in turn is recruited by the scaffold protein Vac14 to form the Fab1-Vac7-Vac14 complex required for PI(3,5)P_2 synthesis (Efe et al, 2007).

In wild-type yeast cells grown in normal conditions, vacuoles have one or two lobes of intermediate size. However, an osmotic stress or overexpression of Vac14 or Vac7 results in increased PI(3,5)P_2 levels and in fragmentation of the vacuoles that are increased in number but decreased in their size. The *fab1*Δ yeast mutant cells present a very large vacuole filling almost the cell and an absence of PI(3,5)P_2 synthesis. During my PhD thesis, I have used the *ymr1*Δ mutant cells. The deletion of *YMR1* is no lethal for yeast and these mutant cells have a wild type level of PI(3,5)P_2, suggesting that contrary to mammalian cells, the yeast myotubularin Ymr1 does not dephosphorylate PI(3,5)P_2 in PI5*P* (Parrish et al, 2004; Taylor et al, 2000). However, *ymr1*Δ yeast cells show a fragmented vacuolar morphology and this phenotype is similar to the one observed for wild type yeast cells upon an osmotic stress with an increased level of PI(3,5)P_2 (figure 27) (Amoasii et al, 2012). This fragmented vacuole could be due to the increased PtdIns3P levels observed in *ymr1*Δ mutant cells, since PI3*P* is the precursor of PI(3,5)P_2. Indeed, yeast cells lacking Ymr1 have a 2-fold increase in the PI3*P* intracellular levels (Parrish et al, 2004). The human myotubularin MTM1 is the orthologue of the yeast ymr1 (**y**east **m**yotubularin **r**elated 1) protein. In yeast there is only one myotubularin termed Ymr1, which facilitated the study of human MTM1 in yeast. Interestingly, *ymr1*Δ cells expressing the human myotubularin MTM1 which dephosphorylates PI3*P* and PI(3,5)P_2 have an enlargement of the vacuoles, showing that the fragmented vacuolar phenotype of the yeast *ymr1*Δ mutant cells was indeed due to its aberrant levels of PI3*P* (figure 27) (Amoasii et al, 2012).

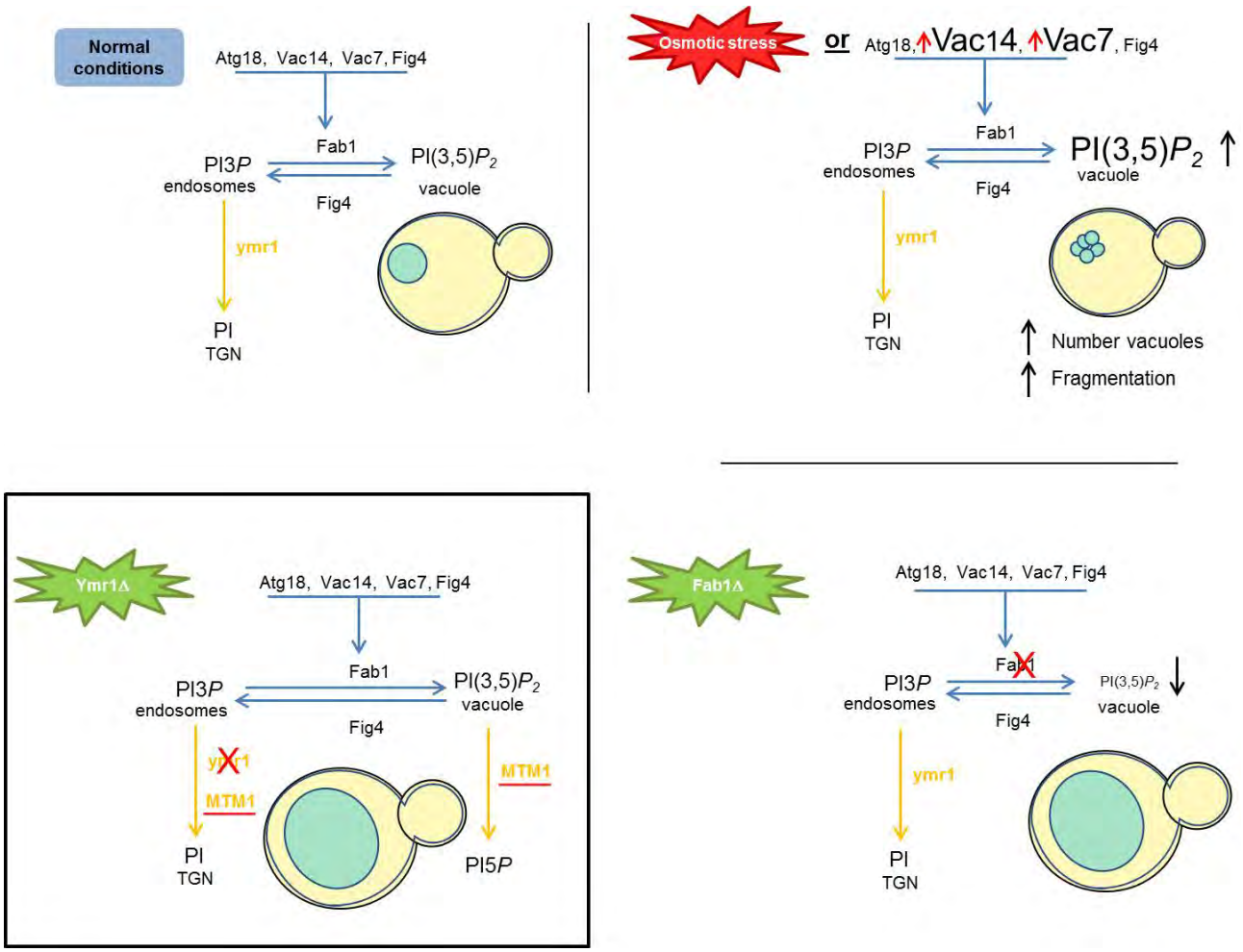

Figure 27: PI(3,5)P_2 levels and the vacuolar phenotypes in *S. cerevisiae* cells; in normal conditions, in osmotic stress or overexpression of Vac14 or Vac7, in *fab1*Δ or *ymr1*Δ deletion strains and in *ymr1*Δ cells bearing the human myotubularin MTM1.

In human cells, PI(3,5)P_2 synthesis and turnover are similar to yeast cells, and they are catalyzed by a protein complex composed of the sole PI3*P* 5-kinase PIKfyve, the phosphatase FIG4 and the protein VAC14 (Bissig et al, 2017; De Craene et al, 2017; Shisheva, 2008). The kinase PIKfyve is homologous to the yeast Fab1. As in yeast cells, VAC14/ArPIKfyve is an adaptor protein that interacts directly with PIKfyve, FIG4/SAC3 and VAC7 belong to the complex to regulate PI(3,5)P_2 synthesis in cells (Jin et al, 2008). Loss of VAC14 decreases PI(3,5)P_2 levels in fibroblast and neurons cultured from the Vac14 KO mice and provokes neurodegeneration (Zhang et al, 2007). Biallelic mutations in the *VAC14* gene are responsible for pediatric-onset neurological disease (Lenk et al, 2016). Mutations in the *FIG4* gene cause Charcot-Marie-Tooth neuropathy (CMT) type 4J, a severe autosomal recessive demyelinating neuropathy (Chow et al, 2007). It has been shown that FIG4 and MTMR2 interact in Schwann cells and neurons in a mice model and that imbalance in PI(3,5)P_2 levels are at the basis of the disease (Vaccari et al, 2011). Indeed, in this CMT disorder the loss of the myotubularin 3-phosphatase MTMR2 increases PI(3,5)P_2 levels and consequently alters longitudinal myelin growth and formation of myelin outfoldings. However, loss of *FIG4*

decreases PI(3,5)P_2 levels and rescues myelin outfoldings due to *MTMR2* deficiency (Vaccari et al, 2011).

At the endosomes, production of PI(3,5)P_2 regulates branched actin dynamics since it inhibits binding of actin filament to cortactin which is necessary for its stabilization and activity (Hong et al, 2015). At the central nervous system (CNS), PI(3,5)P_2 regulates oligodendrocytes differentiation by directing endosomal trafficking of plasma membrane-derived myelin-associated glycoprotein (MAG) (Mironova et al, 2016). It was shown that inhibition of the phosphoinositide kinase PIKfyve, which generates PI(3,5)P_2, increased exosome release and reduced autophagic degradation, possibly due to impaired fusion of lysosomes with MVBs and autophagosomes (Hessvik et al, 2016).

PI(3,5)P_2 production also seems to be necessary in the Ca^{2+} release in cytosol induced by hyperosmotic stress (Dong et al, 2010). This process is dependent on the vacuolar channel Yvc1p in yeast, which presents homology with the transient receptor protein (TRP) (Palmer et al, 2001). It was suggested that the homologous mammalian endolysosome-localized mucolipin transient receptor potential (TRPML) is a PI(3,5)P_2 effector that controls Ca^{2+}-dependent membrane dynamics in response to extracellular stimuli (Dong et al, 2010; Mayinger, 2012).

1.4.3. The phosphoinositide PI5*P*, a product of MTM1 phosphatase activity

In yeast cells, no PI5*P* production could be detected in basal conditions and by conventional HPLC techniques. The yeast Ymr1 myotubularin is described as an enzyme that does not dephosphorylate PI(3,5)P_2 to produce PI5*P* (Parrish et al, 2004; Taylor et al, 2000).

In human cells, PI5*P* was described as being synthesized by phosphorylation of PtdIns by the PIKfyve lipid kinase or by dephosphorylation of PI(3,5)P_2 by active myotubularin 3-phosphatases (Lecompte et al, 2008). *In vivo*, the MTM1 and the MTMR3 myotubularins were shown to produce PI5*P* from dephosphorylation of PI(3,5)P_2 (Tronchere et al, 2004; Walker et al, 2001). In normal mammalian cells culture conditions, PI5*P* represents less than 10% of monophosphorylated PI (Hasegawa et al, 2017; Payrastre et al, 2001).

PI5*P* is less studied compared to the other types of phosphoinositides. Even though, PI5*P* plays a role in membrane and actin rearrangement of host cells during the invasion process of some bacterial pathogens as *Shigella flexneri* that produce a high level of PI5*P* at the plasma membrane by dephosphorylation of PI(4,5)P_2 by the bacterial phosphatase IpgD (Niebuhr et al, 2002). In these infected cells, PI5*P* was identified as a regulator of the PI 3-kinase/Akt pathway by protecting Akt from dephosphorylation (Pendaries et al, 2006; Ramel et al, 2011).

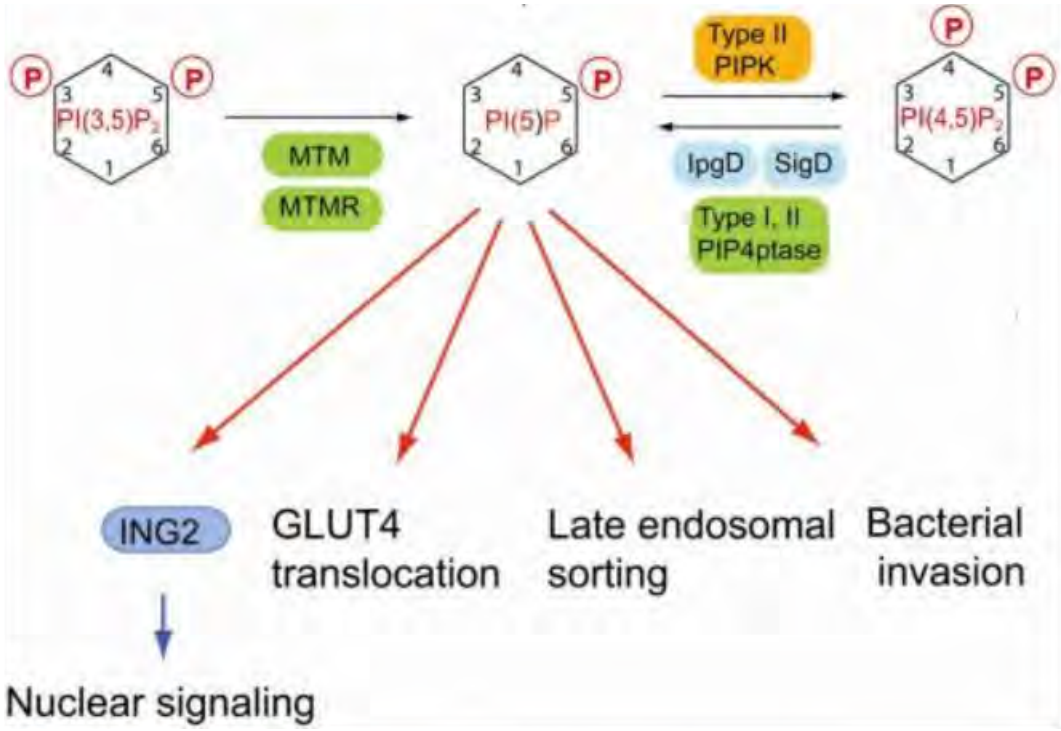

Figure 28: Regulation of PI5*P* and its role in different pathways in mammal cells. PI5*P* can be synthetized from dephosphorylation of PI(3,5)P_2 by myotubularins or of PI(4,5)P_2 by 4- phosphatases (indicated in green boxes). IpgD and SigD are bacterial phosphatases able to dephosphorylate PI(4,5)P_2 in PI5*P* inside host cell during invasion. It was the first time PI5*P* could be detected. PI5*P* is also implicated in endosomal trafficking, GLUT4 translocation and it binds to the nuclear adaptor ING2 that regulates chromatin rearrangement in response to stress. From (Mayinger, 2012).

PI5*P* also plays a regulatory role in the nucleus, where it is involved in stress response by modulating the transcriptional activity of the chromatin regulator ING2 (inhibitor of growth protein-2) that was shown to directly interact with PI5*P* (Gozani et al, 2003). Moreover, PI5*P* was also shown to be involved in actin and membrane dynamic through activation of Tiam1/Rac module. Tiam (T lymphoma invasion and metastasis) is a guanine nucleotide exchange factor (GEF). Indeed PI5*P* directly binds the C-terminus PH domain of Tiam1 at early endosomes, which in turn activates the Rho GTPase Rac1, then driving actin remodeling (Viaud et al, 2014). In relation with its role as effector regulating endosomal maturation, the PI5*P* recruits TOM1 on signaling endosomes, and this interaction delays the endosomal MVB internalization of the epidermal growth factor (EGF) receptor (Boal et al, 2015). PI5*P* also participates in autophagosome biogenesis via a non-canonical autophagy pathway, which is independent of PI3*P* synthesis by the VPS34-VPS15 complex (Vicinanza et al, 2015). Upon infection, *Shigella flexneri* alters the subcellular trafficking of the intercellular adhesion molecule-1 (ICAM-1), a key molecule in immune cell recruitment, and this depends on PI5*P* produced from plasma membrane PI(4,5)P_2 by the bacterial IpgD phosphatase (Boal et al, 2016).

Sbrissa and colleagues have shown that PI5*P* is involved in GLUT4 translocation at the plasma membrane in adipocytes. Concerning the response to insulin in muscle cells, the production of PI5*P* is necessary for PI(3,4,5)P_3 production and this latter is necessary for enhanced GLUT4 translocation in a PI 3-kinase dependent pathway (Grainger et al, 2011).

II. Objective of the PhD thesis and background

2.1. The Myotubularin MTM1 and its PH-GRAM domain

The objective was to study within a unicellular eukaryotic cell, the yeast *Saccharomyces cerevisiae*, the two main domains of the myotubularin MTM1 (figure 29): the phosphoinositides membrane binding domain termed PH/GRAM and the phosphatase domain.

Indeed, the results of Matthieu Raess, a former PhD student in the team of Sylvie Friant have shown that the N-terminal PH-GRAM is the key domain to differentiate the myotubularins MTM1 and MTMR2. His results show that a short MTMR2-S myotubularin produced by alternative splicing of the *MTMR2* gene displays membrane localization and catalytic activity in yeast cells *in vivo*. However, the long full-length isoform of MTMR2, termed MTMR2-L, is not localized to membranes but is cytosolic and has only a poor catalytic activity (Raess et al, 2017a). The difference between MTMR2-S and MTMR2-L lies in the N-terminal PH-GRAM domain that is shorter for MTMR2-S compared to MTMR2-L. Interestingly, the sequence alignment between the three MTM1, MTMR2-S and MTMR2-L proteins shows that the length of the PH-GRAM domain of MTM1 is shorter than that of MTMR2-L (figure 29). The yeast data show that MTM1 and MTMR2-S are localized on membranes and have a good catalytic activity *in vivo* with production of PI5*P*, contrary to MTMR2-L (Raess et al, 2017a).

These yeast results were confirmed in the *Mtm1* KO mice model, with the MTMR2-S construct showing a better rescue of the CNM phenotypes upon AAV-MTMR2-S injection in the tibialis anterior TA muscle of the Mtm1 KO mice, compared to MTMR2-L treatment (Raess et al, 2017a).

However, even though MTMR2-S shows good rescue properties of the CNM phenotypes in the *Mtm1* KO mice, this construct is less active than MTM1.

Overall, these data suggest that the PH-GRAM domain is important pour membrane localization and for catalytic activity of MTM1. Therefore, I studied the PH-GRAM and the catalytic domains of MTM1 in yeast cells.

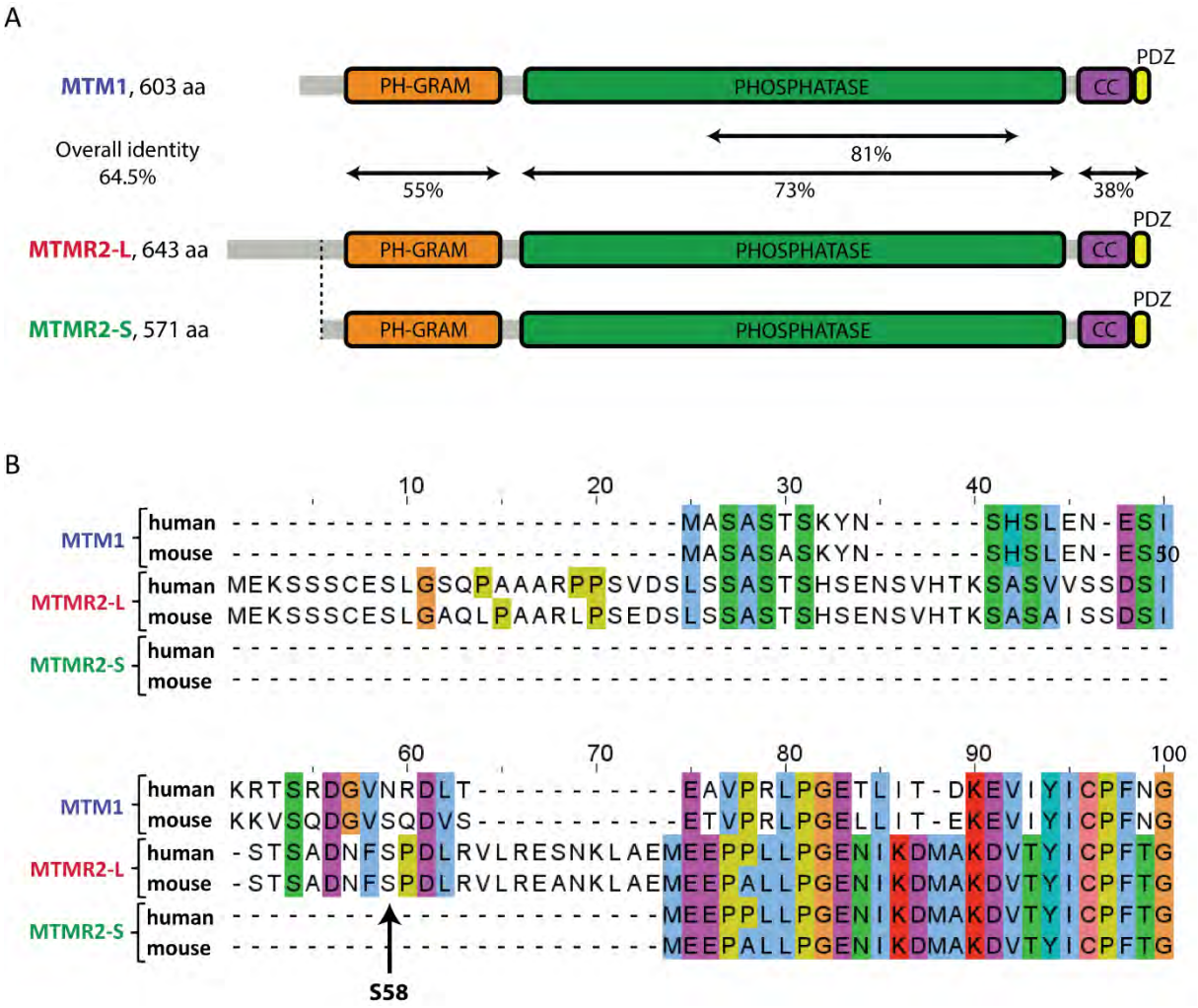

Figure 29: Comparison between MTM1, MTMR2-S and MTMR2-L myotubularins. (A) Myotubularins MTM1, MTMR2-L and MTMR2-S are indicated with their domain organization. Percentage of identity between MTM1 and MTMR2-L are indicated for each domain, except the coiled-coil (CC) and PDZ domains that are grouped. **(B)** Protein alignment of the first 100 amino acids of human and mouse MTM1, MTMR2-L and MTMR2-S. The Serine S58 of MTMR2-L that is subjected to phosphorylation in HeLa cells is indicated by an arrow. From M. Raess, PhD thesis, 2017.

2.2. The DNM2 dynamin and yeast mitochondria fusion

As already mentioned, there are 3 different dynamins in human cells, but only DNM2 is ubiquitously expressed, unlike DNM1 and DNM3. Recently, Jocelyn Laporte's team (I.G.B.M.C, Illkirch) identified a new hDNM2 isoform that was found in mice muscle biopsies and named DNM2 isoform 12b (Cowling et al, 2017). This isoform lacks the GEIL (glycin-aspartic-isoleucine-leucine) sequence but has a 10 amino acids extension at the end of the Middle domain. This motif, GEIL, is located in the c-terminal part of the middle domain (516-519 aa) of the ubiquitous hDNM2 (Durieux et al, 2010a). This motif allows its targeting to the Trans Golgi network (TGN). In this study I will name the ubiquitous isoform, DNM2 iso1 and the muscle isoform DNM2 iso12b.

2.2.1. Objectives of the hDNM2 study in yeast

The objectives of the human DNM2 study in yeast cells were :

- to find the correct dynamin deletion mutant yeast strain to humanize it with the human orthologue DNM2 iso1 or iso12b, to establish a genotype-phenotype correlation.
- to transform yeast cells with patient mutations in the *DNM2* gene in order to elucidate how these mutations affect the cellular role of the protein in a single eukaryote cell.

I have used two yeast strains bearing deletion of the *VPS1* or *DNM1* gene. Yeast Vps1 and Dnm1 are dynamin proteins that show the highest level of identity when compared to human dynamins (figure 30).

2.2.2. Preliminary data on the hDNM2 humanization of yeast cells

The Vps1 yeast protein (already been mentioned before in the introduction (table 2)) is a protein implicated in vacuolar sorting, required for Golgi-to-endosomes vesicular traffic (Vater et al, 1992). Vps1 belongs to the vesicles tethering/fusion machinery required for retrograde trafficking from endosomes to Trans Golgi Network TGN (Saimani et al, 2017). This protein encoded by the *VPS1* gene was also identified as a member of the GTPase family since it is able to bind and to hydrolyze

GTP, having a similar mechano-chemical GTPase activity as described for human hDNM1 and hDNM2 dynamins (Vater et al, 1992). As a dynamin, Vps1 is implicated in endocytosis, during which it interacts with the yeast amphiphysin Rvs167 (homologue of BIN1) (Feyder et al, 2015). During yeast endocytosis, actin cytoskeleton polymerization plays a crucial role, as it gives the driving force required for the vesicle formation and budding at the plasma membrane (Idrissi & Geli, 2014). In addition, *vps1*Δ mutants but not *dnm1*Δ mutants have marked actin cytoskeleton defects, suggesting a role of Vps1 in cortical actin organization (Yu & Cai, 2004). Yu and colleagues thought that the role of Vps1 in protein transport from TGN could be connected with its actin-related function (Yu & Cai, 2004). Vps1 is also involved in peroxisomes biogenesis, indeed *vps1*Δ mutants lacking the corresponding gene have reduced number of peroxisomes compared to wild type cells (Vizeacoumar et al, 2006). Indeed, as a dynamin protein, Vps1 could be implicated in a membrane fission process necessary for peroxisomes abundance and size. Peroxisomes are single-membrane organelles implicated in β-oxidation of fatty acids and in H_2O_2 metabolism. Peroxisomes are ubiquitous and colocalize with actin microfilaments in yeast. Interestingly, peroxisomes can proliferate by division of pre-existing peroxisomes and also from the ER (Hoepfner et al, 2005).

The yeast DNM1 gene encodes a dynamin-related protein linked to mitochondrial fission and peroxisome fission and proliferation (Kuravi et al, 2006). In mammalian cells, the homologue of the Dnm1 yeast protein is the DNM1L/DLP1, also involved in mitochondria and peroxisomes fission (Li & Gould, 2003). The yeast Dnm1 also displays the dynamin mechano-chemical GTPase activity (Kuravi et al, 2006).

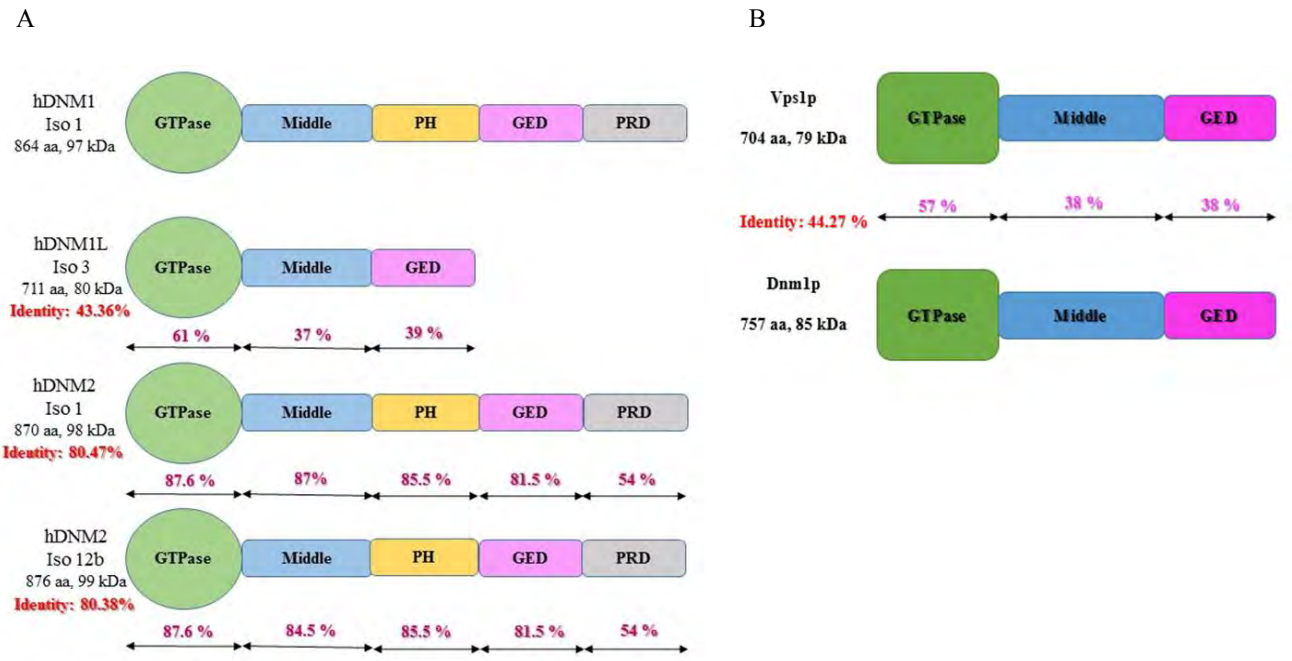

Figure 29: Protein domain and percentage of identity among them. (A) hDNM1L iso3, hDNM2 iso 1and hDNM2 iso 12b have different percentage of identity. hDNM1 iso 1was used as reference. Domain percentage of identity is also shown. (B) Protein and domain percentage of identity between yeast Vps1 and Dnm1.

As the human dynamin-related proteins (DRPs), Vps1 and Dnm1 lack the dynamin pleckstrin homology PH domain that binds membrane lipids, suggesting that other factors recruit them to mitochondria and peroxisome membranes. A protein complex with Fis1 and Mdv1/Caf4 proteins allows Dnm1 function at the level of the mitochondria and peroxisomes (Motley et al, 2008). Dnm1 plays an important role for mitochondria partition between the mother and daughter yeast cells during cell division. In addition, Dnm1 action on mitochondria fission enables mitophagy (Westermann, 2012).

Preliminary data obtained by the postdoctoral researcher Joëlle Morvan in the laboratory of Sylvie Friant showed that expression of the ubiquitous hDNM2 iso1 did not rescue the *vps1*Δ mutant yeast phenotypes of endocytosis, actin cytoskeleton morphology and vacuolar protein sorting (figure 30). Indeed a carboxypeptidase (CPY) secretion test was performed in order to establish a phenotype related to trafficking in the *vps1*Δ mutants yeast cells (table 2). In *vps1*Δ mutant cells the trafficking to vacuoles is impaired and consequently CPY is secreted outside the cells in the extracellular medium. Secreted CPY is observed by a colony blotting by immunodetection with anti-CPY antibodies (figure 30). The data show that the *vps1*Δ mutant cells secrete CPY as observed by the strong CPY staining on the colony, unfortunately the human hDNM2iso1 wild type protein did not rescue this defect (figure 30). Joëlle Morvan also tested the catalytic-dead GTPase mutant hDNM2-K44A. The results were the same for this hDNM2 mutant as the ones observed for hDNM2, with no rescue (figure 30). To determine whether trafficking to the vacuole of other vacuolar hydrolases

could be rescued a milk-plate assay was performed on *vps1*Δ mutant yeast cells expressing hDNM2 or hDNM2-K44A. Due to vacuolar trafficking impairment in mutant cells, the hydrolases are secreted into the milk plate and degrade the proteins of the milk resulting in a halo around the yeast colony. Again there is now rescue observed for the different hDNM2 constructs expressed in *vps1*Δ cells. This lack of rescue is not due to a lack of expression of hDNM2 since the different hDNM2 proteins were detected by anti-DNM2 western blot on yeast protein extracts (data not shown). These results suggest that the human DNM2 is not a functional orthologue of yeast Vps1 dynamin. The endocytosis and actin cytoskeleton morphology were also tested with no rescue, these data are not shown.

Jöelle Morvan has also carried out a mitochondrial staining experiment using the *dnm1*Δ yeast mutant cells (figure 30). Interestingly, the mitochondria network defects were ameliorated in the *dnm1*Δ mutant yeast cells upon hDNM2 iso1 expression (figure 30). This preliminary result supports a role of hDNM2 iso1 linked to mitochondria fission.

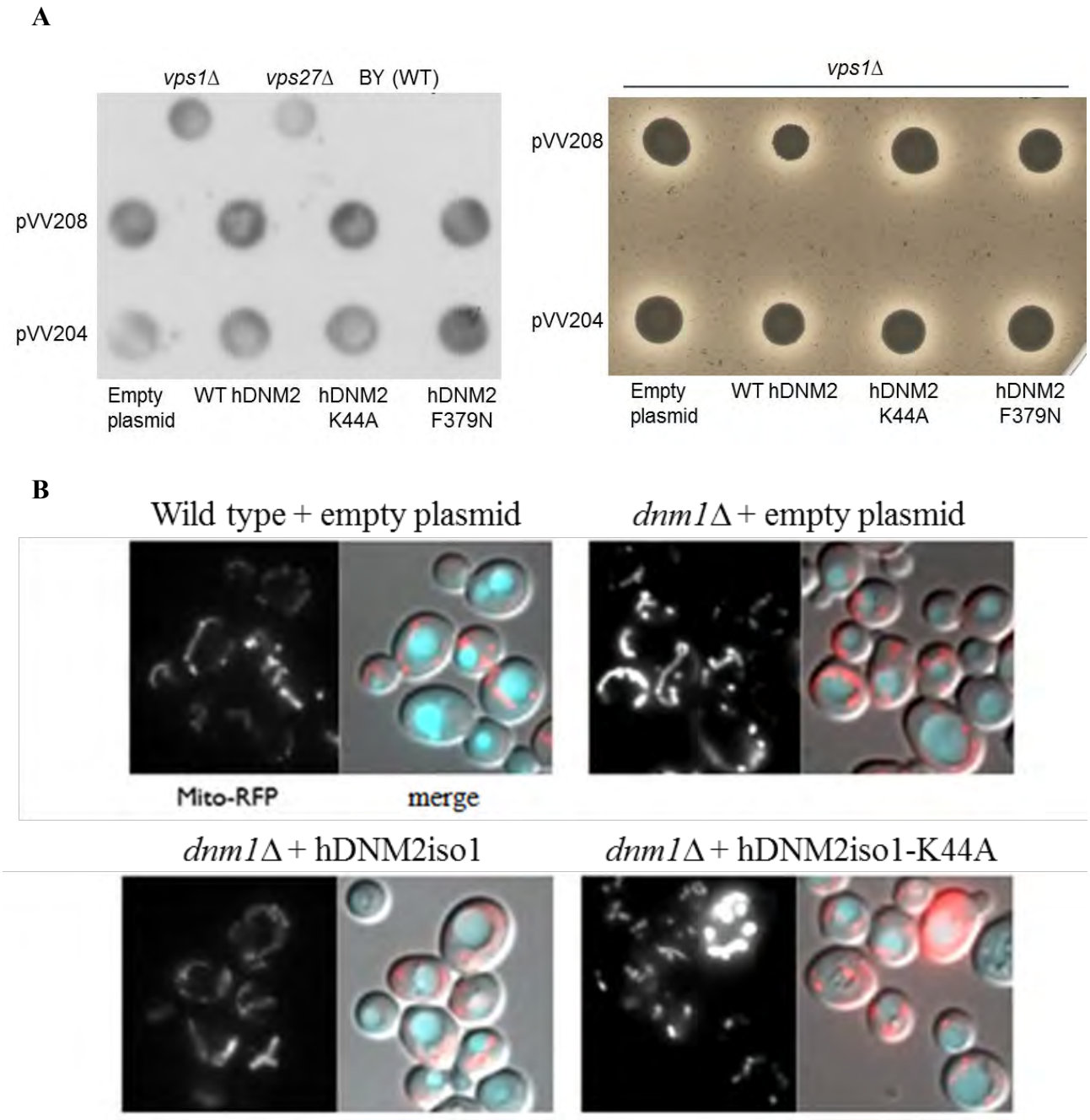

Figure 30: Humanization of yeast *vps1*Δ and *dnm1*Δ to study the human DNM2 protein. **A.** Wild type and catalytic dead mutation (K44A) hDNM2 iso1 were used in this yeast phenotypic analysis. Two types of vectors were used: a 2µ overexpression vector (pVV208) and a CEN expression vector (pVV214). CPY secretion assay and protease secretion assay in a milk-plate assay. **B.** Mitochondria staining was observed in a fluorescent microscopy assay (pVV214 plasmid) with the mito-RFP fluorescent reporter. Mitochondria fusion defect was observed in dnm1 mutant yeast. Fusion was recovered when transformed with wild type hDNM2 iso1 but not with K44A dead catalytic hDNM2 iso1 mutant. pVV is the empty plasmid

A study about metal toxicity in *Saccharomyces cerevisiae* was performed comprising more than 200 mutated genes (Ruotolo et al, 2008). This study revealed that different *vps* mutant strains

including the *vps1*Δ mutant were implicated in nickel and/or cadmium tolerance (figure 31). Therefore during my PhD thesis, I also studied the resistance to cadmium.

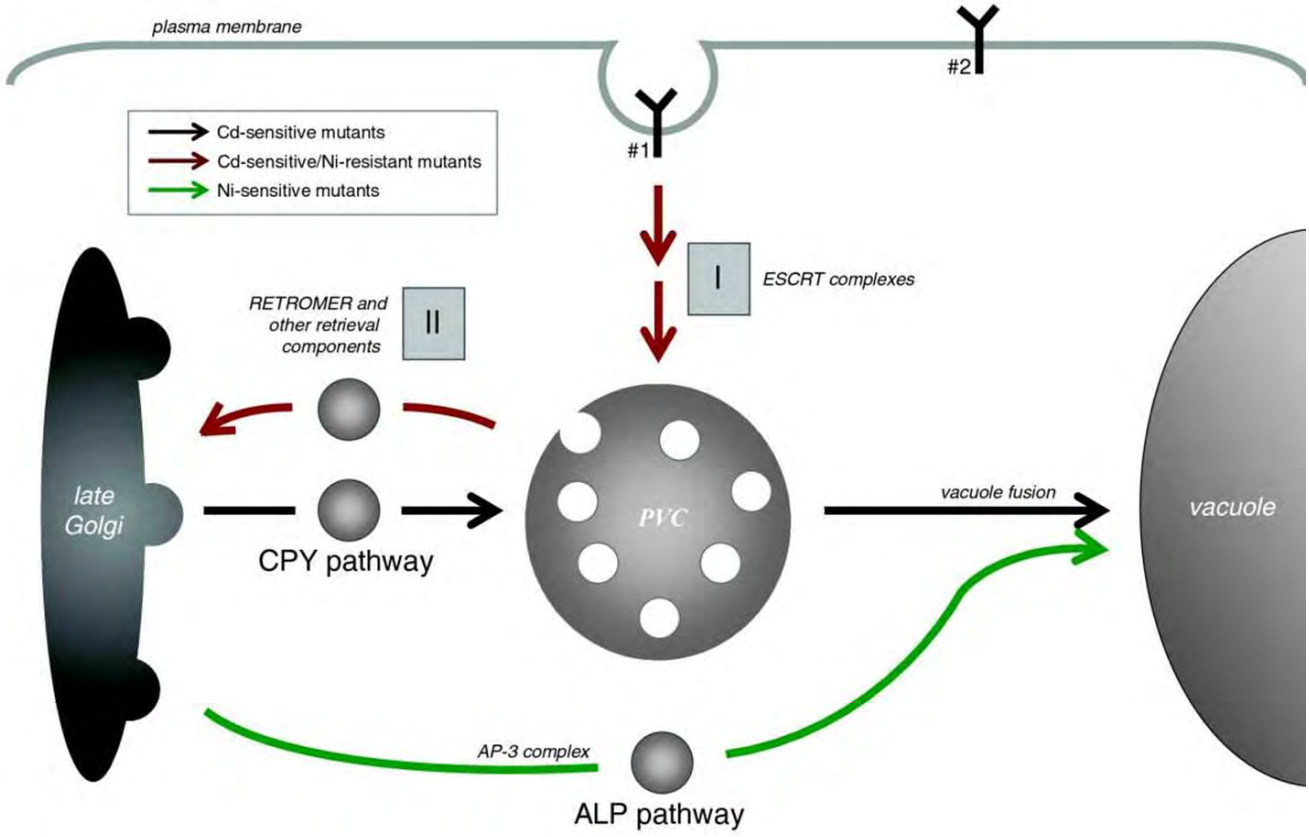

Figure 31: Cadmium sensitive/nickel resistant mutants and their link to vacuolar protein trafficking Schematic representation of endocytic pathway (in red) and the two possible pathways from Golgi to vacuole (known as ALP and CPY pathways). PVC is refers to prevacuolar compartment, also called multivesicular bodies (MVB). From (Ruotolo et al, 2008).

2.3. The oxydoreductase PYROXD1 and yeast oxidative stress

Congenital myopathies are a large group of human diseases with about ~50% of patients having a molecular diagnosis (Amburgey et al, 2011). The next-generation sequencing technologies have helped to identify new genes responsible for myopathies. Thanks to an international collaboration between laboratories in Australia, France, the United States and Turkey, the *PYROXD1* gene was identified as a new gene whose mutations are responsible for early-onset myopathy in 5 families (nine probands) (O'Grady et al, 2016). The PYROXD1 gene is located at 12p12.1 and encodes the

pyridine nucleotide-disulphide oxidoreductase domain-containing protein 1 also named PYROXD1; it is a 500 amino acid protein with no characterized role before this CNM-like patient driven study (O'Grady et al, 2016). The laboratory of our collaborator Jocelyn Laporte (IGBMC, Illkirch, France) participated to this PYROXD1 international study. As the redox activity of PYROXD1 was not known, Jocelyn Laporte contacted us in order to characterize the function of PYROXD1 in yeast cells by using humanization. As previously done for MTM1 (Amoasii et al, 2012), we used humanization of the yeast *S. cerevisiae* cells to study the disease-mutations in the human *PYROXD1* gene. I established a complementation assay in yeast to test the oxidoreductase activity of human PYROXD1 and the impact of the CNM-like patient missense mutations (O'Grady et al, 2016).

S. cerevisiae has two overlapping oxidoreductase systems, the cytoplasmic and mitochondrial redox systems where enzymes from GSH-glutaredoxin and thioredoxin systems cooperate tightly in order to maintain the redox homeostasis of the cell (figures 32 and 33) (Herrero et al, 2008; Trotter & Grant, 2005). Among the yeast oxidoreductase, the Glr1 glutathione reductase has two isoforms (due to alternate translation initiation sites), which localize to the cytoplasm and mitochondria and are required for survival under oxidative stress (Outten & Culotta, 2004). Glutathione GSH is a small antioxidant molecule essential for resistance in basal and stress conditions, it catalyzes cellular reduction reactions. Indeed Glr1 catalyzes the reduction reaction of GSSH in GSH in a NADH-dependent manner, thus maintaining the high intracellular GSH/GSSG ratio inside the cell (Trotter & Grant, 2005). I observed that PYROXD1-GFP protein was mainly localized in the cytoplasm in yeast cells. Therefore I used the *glr1*Δ mutant strain for PYROXD1 humanization studies, since the Glr1 oxidoreductase is also active in the cytoplasm. Moreover, the *glr1*Δ mutant strain has a strong phenotype of H_2O_2 resistance defect, which I can use to test the different PYROXD1 constructs.

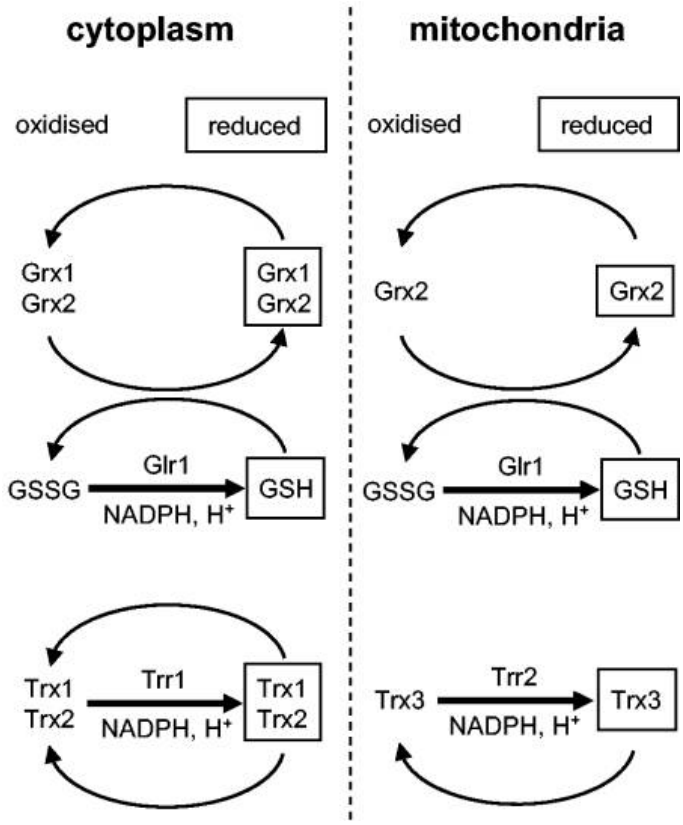

Figure 32: Overlapping oxidoreductase system in Saccharomyces cerevisiae. From (Trotter & Grant, 2005).

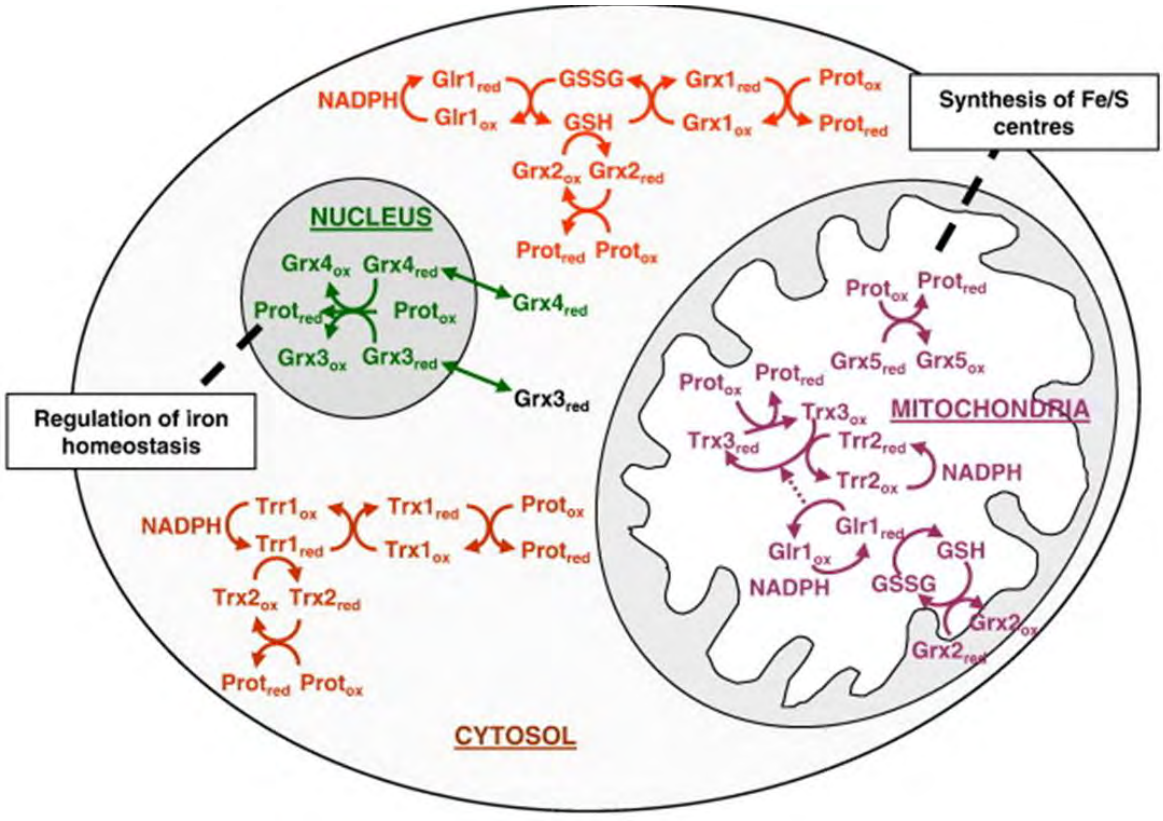

Figure 33: Cytoplasmic and mitochondria oxidorecductase system in yeast cell. From (Herrero et al, 2008).

Grx6 is one glutarexodin of the 8 GRXs found in *S. cerevisiae*. GRXs are small antioxidant proteins; they protect the cell against oxidative stress provoked by ROS (Herrero et al, 2008). Glutaredoxins catalyze the reduction of protein disulfide or glutathione-protein mixed disulfide bound using a system coupled with glutathione, NADPH and glutathione reductase (Glr). The reduced glutathione GSH acts as hydrogen donor and glutathione reductase uses electrons from NADPH to regenerate the oxidized glutathione (GSSG) (figures 32 and 33) (Herrero et al, 2008). The Grx6 protein is enriched at the ER and becomes up-regulated upon ER stress by tunicamycin (Izquierdo et al, 2008).

The expression of the *GRX6* gene is also induced by high-calcium and sodium stresses and by oxidative stress in a Crz1-dependent manner (Izquierdo et al, 2008). Moreover, the *grx6*Δ mutant cells show imbalance in Ca^{2+} homeostasis with Ca^{2+} accumulation in the cytosol and Ca^{2+} depletion at the ER lumen. This calcium stress activates the calcineurin-dependent pathway (Puigpinos et al, 2015). The calcineurin-dependent pathway triggers the transcription of genes required for survival cell during environment stress. Under calcium or sodium stresses, the Ca^{2+}/calmodulin complex activates the serine/threonine protein phosphatase calcineurin, which in turn activates the Crz1 transcription factor by dephosphorylation. This dephosphorylation allows the import of Crz1 from the cytosol into the nucleus and targets promoter elements with the CDRE motif (Calcineurin-dependent response element) (Tang & Liu, 2010). A schematic explanation of calcium control system in yeast cell is represented in figure 34.

This calcium phenotype linked to an oxidoreductase activity is very interesting since calcium is required for muscle function; therefore I also used the *grx6*Δ mutant strain for humanization studies with PYROXD1.

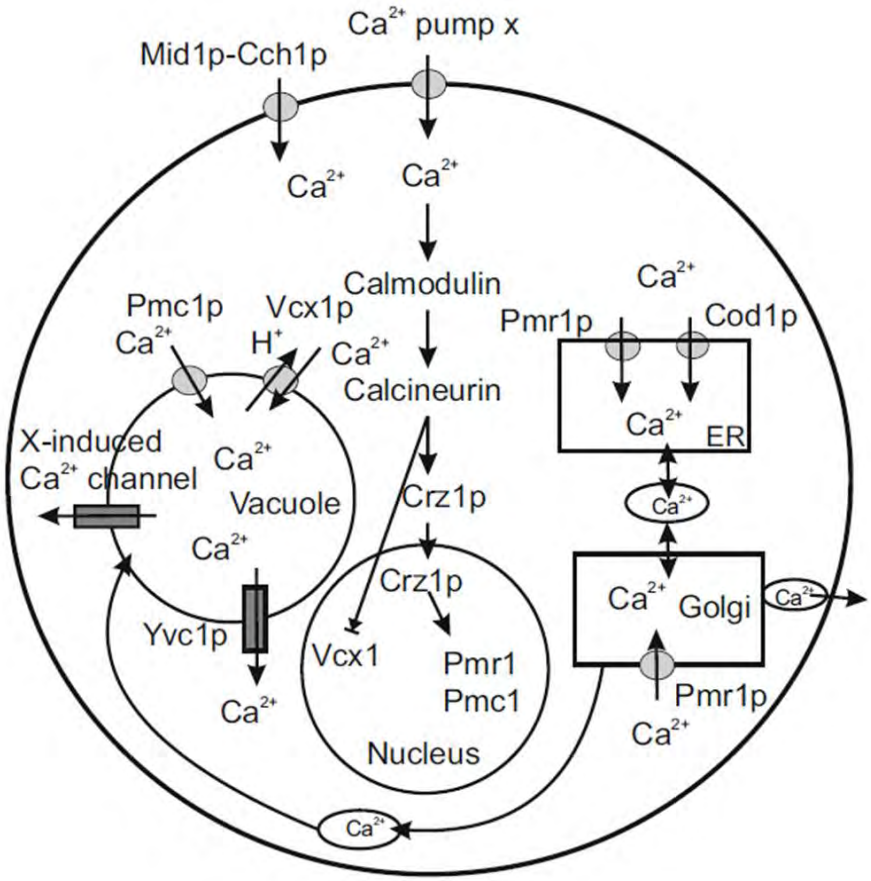

Figure 34: Schematic representation of calcium homeostasis in yeast cell. Yeast uptakes calcium from the environment via an unknown Ca^{2+} pump X in the normal conditions and Mid1p-Cch1p under some abnormal conditions such as depletion of secretory Ca^{2+}. Increased intracellular Ca^{2+} levels lead to the activation of calcium/calmodulin/calcineurin signaling pathway. The vacuole is the major Ca^{2+} storage compartment in yeast cells and plays an important role in maintaining a normal cytosolic Ca^{2+} level. In response to environmental osmotic pressure variation or cell cycle progression, the fission and fusion of vacuole changes and activates the channel Yvc1. This channel also increases the cytosolic calcium ions. From (Tang & Liu, 2010) and ("Introduction to modeling biological cellular control systems" Vol 6, by Weijiu Liu, Springer)

Recently, the laboratory of Marc Bitoun showed that mice model for DNM2 CNM presented an imbalance in calcium homeostasis (Fraysse et al, 2016). In addition, in yeast altered intracellular calcium homeostasis affects the redox state (Puigpinos et al, 2015). In addition, a connection between redox state and CNM like myopathy was shown in our article about PYROXD1 (O'Grady et al, 2016). Therefore, at the end of my PhD I have focused my research on the link between redox state and calcium homeostasis in a *dnm1*Δ yeast strain to establish a phenotype in *S. cerevisiae*, which I would use to study the effect of CNM patient mutations in DNM2.

III. Results

3.1. The Myotubularin MTM1 and its phosphatase activity in yeast

The objective was to study within a unicellular eukaryotic cell the two main domains of MTM1: the phosphoinositides membrane binding domain termed PH/GRAM and the catalytic domain phosphatase domain.

3.1.1. Interactions between the PH/GRAM and the catalytic domain reconstitute an active myotubularin MTM1 phosphoinositide phosphatase

These results will be submitted for publication.

Interactions between the PH/GRAM and the catalytic domain reconstitute an active myotubularin MTM1 phosphoinositide phosphatase

Sanjuan-Vazquez Myriam, Bertazzi Dimitri, Bruno Rinaldi and Sylvie Friant

Introduction

The myotubularin family encompasses 14 members in human, only some of them being catalytically active phosphatases: MTM1, MTMR1-4, MTMR6-8. They catalyze the dephosphorylation reaction of the phosphoinositides PI3*P* and PI(3,5)P_2 at the 3 position of the inositol ring (Raess et al, 2017b). Mutations in the *MTM1* gene lead to the development of X-linked centronuclear myopathy (XLCNM) (Laporte et al, 1996). This disease is characterized at the histological level by nuclei placed in the center of the myofibers, instead of being at the periphery.

The main symptoms of patients affected by XLCNM are muscle weakness and hypotonia. It is estimated that 1 of every 50,000 males in the world are affected by this disease (Staiano et al, 2015).

MTM1 study in human cells is complicated due to the presence of the 14 homologues (Raess et al, 2017b). Yeast is a good model to study human MTM1 and humanization of yeast cells is a powerful approach to better understand cellular functions of human proteins (Amoasii et al, 2012; Kachroo et al, 2015; Raess et al, 2017a). Thus, we used the unicellular eukaryotic yeast model *Saccharomyces cerevisiae* to study MTM1. Yeast has a similar organelle organization as human cells and encodes only 1 myotubularin, termed Ymr1 (yeast myotubularin related 1) (Parrish et al, 2004). Ymr1 is a phosphoinositide phosphatase like MTM1. In *S. cerevisiae*, PI3*P* and PI(3,5)P_2 intracellular levels directly control the vacuolar size (Jin et al, 2016). Low PI(3,5)P_2 levels are associated to vacuolar enlargement and high PI(3,5)P_2 levels as observed during hyperosmotic shock, induce fragmentation of the vacuoles (Mayinger, 2012). Accordingly, the yeast *ymr1*Δ deletion mutant cells have fragmented vacuoles. In previous studies, we have shown that expression of human MTM1 rescue *ymr1*Δ yeast cells phenotype by inducing an enlargement of the vacuole, associated with a decrease in PI3*P* levels and a production of PI5*P* resulting from the dephosphorylation of PI(3,5)P_2 (Amoasii et al, 2012; Raess et al, 2017a). This shows that the *ymr1*Δ mutant strain is a good model to study the enzymatic activity of the human myotubularin MTM1. Here, we used the *ymr1*Δ mutant cells to study domains of MTM1 protein.

The members of the myotubularin family share two domains: PH/GRAM (pleckstrin homology-glucosyltranferase, rab-like GTPase activator and myotubularin), and the protein tyrosine phosphatase (PTP) domain (Laporte et al, 2003). The PH/GRAM is a phosphoinositide binding domain that favors the membrane interaction of MTM1, thereby allowing the phosphatase to have access to its lipid substrates. The PTP catalytic domain contains the canonic CX5R motif, the conserved cysteine (Cys) and arginine (Arg) being key residues for the phosphatase activity. The catalytically-dead phosphatases MTMR5 and MTMR9-13 lack these conserved Cys and Arg residues. However, despite their lack of phosphatase activity these dead-myotubularins were shown to heterodimerize with active myotubularins, thereby regulating their activity (Lorenzo et al, 2005). Moreover, homo-oligomerization of MTM1 increases its phosphatase activity (Schaletzky et al, 2003). The XLCNM patient mutations are mainly localized in the PH-GRAM and in the phosphatase catalytic domains highlighting their important role for the cellular function of MTM1 (Cowling et al, 2012).

Here, we studied the expression of the PH-GRAM and the catalytic domains in yeast cells and our results show that interactions between these two domains are necessary for the phosphatase activity of MTM1.

Materials and Methods

Plasmids, yeast strains and media

The human MTM1 ORF, the PH/GRAM domain (1-160 aa) or the catalytic domain (161-603 aa) were cloned into pDONR207 plasmid (Invitrogen) to generate an entry clone. Gateway system (Invitrogen) was used to clone the different MTM1 constructs into the yeast expression vectors pAG424 and pAG426, which are tagged with GFP or DsRed proteins respectively. The C375S mutation was introduced into the hMTM1 by polymerase chain reaction (PCR) with Phusion High-Fidelity DNA polymerase (Thermo Scientific) on the pAG424 entry vector bearing hMTM1 (pSF143).

*S. cerevisiae ymr1*Δ (Matα ura3-52, leu2-3, 112, his3-Δ200, trp1-Δ901, lys2-801, suc2-Δ9, ymr1::HIS3) and WT (SEY6210 strain; MATα ura3-52, leu2-3, 112, his3-Δ200, trp1-Δ901, lys2-801, suc2-Δ9) cells were grown at 30°C in rich medium (YPD): 1% yeast extract, 2% peptone, 2% glucose or synthetic complete drop-out medium (SC): 0.67% yeast nitrogen base with ammonium sulfate, 2% glucose and the appropriate amino acids mixture to ensure plasmids maintenance. Yeast cells were transformed using the modified lithium acetate method (Gietz et al, 1992).

Western blot analysis

Yeast *ymr1*Δ transformed cells were grown at 30°C in selective medium until OD_{600nm}=0,5-0,8. A volume of culture corresponding to 1,5 OD_{600nm} was harvested by a 1600xg centrifugation for 5 min and resuspended in 0.5 mL of medium before lysis by addition of 50 µL of NaOH 1,85 M and incubation for 10 min on ice, followed by addition of 25 µL of TCA 100% and incubation for 10 min on ice. Total proteins were recovered by a centrifugation at 10000xg at 4°C for 15 min, and analyzed by SDS-PAGE after being solubilized in 50 µL of Laemmli buffer containing a volume of Tris-Base 1M and incubated at 37°C for 10 min. For western blot, proteins were transferred to nitrocellulose membranes (Protran), incubated with primary antibodies and secondary antibodies coupled to horseradish peroxidase (HRP) and revealed by ECL chemiluminescence, followed by acquisition of the images with the ChemidocTouch (BioRad) and use of the ImageLab software for

quantification. Rabbit anti-MTM1 (R1208) and mouse monoclonal anti-MTM1 (IG6) (kind gifts of J. Laporte, IGBMC, Illkirch, France), rabbit Anti-Vti1 (9424t) (kind gift of G. Fischer von Mollard, Germany), mouse monoclonal anti-PGK1 and mouse monoclonal anti-Vps10 antibodies (Invitrogen) were used.

The CPY secretion assay was done as previously described (Morvan et al, 2012).

Yeast vacuolar staining

Yeast cells were grown overnight at 30°C in 2 mL of SC selective medium and diluted in the morning in 10 mL of SC medium to obtain in the afternoon an OD_{600nm} about 0.8-1.5. Cells were centrifuged at room temperature, at 1600xg for 5 min and the pellet suspended with 0.6 mL of YPD medium containing 10 mM of CMAC (Invitrogen), before being incubated for 10 min at 30°C. Stained yeast cells were washed twice with 0.5 mL of YPD and the cell pellet was suspended with 100 µL of SC selective medium prior observation by fluorescence microscopy.

For vacuolar staining with FM4-64, yeast cells were grown as described for CMAC staining. After centrifugation, yeast cells were suspended with 50 µL of YPD containing 2 µL of FM4-64 200 µM, and incubated for 15 min at 30°C under gentle agitation (pulse) prior washing by addition of 0.5 mL of YPD and centrifugation at 1600xg for 2 min. Cells were suspended in 0.5 mL of YPD and incubated for 20 min at 30°C for FM4-64 chase, prior two steps of washing with 0.5 mL of YPD. The cell pellet was suspended with 100 µL of selective SC medium prior observation by fluorescence microscopy. The Zeiss AxioObserverD1 microscope with 100x objective was used for observation and the Axiovision software (Zeiss) for images acquisition. The ImageJ software (Rasband, W.S., ImageJ, U.S. National Institutes of Health, Bethesda, Maryland, USA, http://rsb.info.nih.gov/ij/,1997-2009) was used for the montage of microscopy images.

Subcellular fractionation

Yeast *ymr1Δ* transformed cells were grown in SC-Trp medium until OD_{600nm} =0.5-0.8. Cells were harvested by a 1600xg centrifugation for 5 min at 4ºC and washed once in PBS1X, sorbitol 0.3 M buffer. Pellets were suspended in 1 mL lysis buffer (PBS1X, sorbitol 0.3 M, Complete Mini EDTA-free protease inhibitor cocktail™ (Roche Diagnostics), PMSF 1mM) and after addition of 1mL of 0.45 mm acid-washed glass beads (Sigma), cells were broken at 4ºC using a FASTprep® (MP Biomedicals) with 5 runs of 30 sec under strong agitation (6.5 M/S) and cooled on ice for 1 min

between each run. Lysates were cleared by a 5 min centrifugation at 800xg, supernatants representing total yeast protein extracts were collected, and protein concentrations were determined by using the Biorad Protein Assay detection kit.

Yeast subcellular fractionation was performed by differential centrifugation on the total protein extracts as previously described (Bonangelino et al, 2002). The lysate was centrifuged at 13000xg for 10 min at 4ºC. The pellet (P13) was kept for analysis and the supernatant was subjected to centrifugation at 100000xg for 1h at 4ºC. The resulting pellet (P100) and supernatant (S100) were collected and S100 represents the cytoplasmic fraction. All pellets (P13 and P100) representing the membrane fractions were suspended in 200 µL of lysis buffer. All fractions were analyzed by SDS-PAGE and Western blot using ECL protocols (GE Healthcare). Mouse monoclonal 1G6 anti-MTM1 (1/1000), mouse monoclonal anti-PGK1 (1/1000) (Invitrogen), anti-Vps10 (1/200) (Invitrogen) and HRP-coupled anti-mouse Ig (1/10000) (GE Healthcare) antibodies were used.

Interaction assays by co-immunoprecipitation

For one co-immunoprecipitation assay, protein A-Sepharose, protein G-Sepharose and γ-bind-Sepharose beads (GE Healthcare) were mixed, before being washed twice in cold PBS1X buffer. Mouse monoclonal anti-MTM1 1G6 (specific for N-term of MTM1; (Laporte et al, 2001)) antibodies (5 µL) were bound to the beads by incubation under gentle agitation on a wheel at 4ºC for 90 min in 500 µL of PBS 1X, BSA 2%, NP40 0.5% buffer. The coated beads were washed twice, before addition of 5 mg of total yeast protein extract and incubation under gentle agitation on a wheel at 4ºC for 15 h. Beads were then washed 5 times in cold PBS1X, Complete Mini EDTA-free protease inhibitor cocktail™ (Roche Diagnostics), PMSF 1mM buffer. The proteins fixed on the beads were eluted by incubation at 37°C for 10 min in 100 µL of Laemmli buffer, and analyzed by SDS-PAGE followed by western blot using anti-MTM1 rabbit polyclonal (R1208; (Laporte et al, 2001)) and anti-Sla2 (H. Riezman) antibodies.

Results

The N-terminal domain PH/GRAM domain and the catalytic domain are membrane localized

The yeast *S. cerevisiae* is a good model to study the human MTM1 myotubularin (Amoasii et al, 2012; Raess et al, 2017a). Indeed expression of MTM1 rescues the fragmented vacuoles phenotype displayed by the *ymr1*Δ deletion mutant cells and size of the vacuole directly correlates with the *in*

vivo phosphatase activity of MTM1. To determine the intracellular localization of MTM1 in yeast cells, the cDNA encoding MTM1 was cloned into yeast expression vectors bearing a GFP tag either at the N- or the C-terminus of MTM1. The *ymr1*Δ yeast cells were transformed with plasmids expressing GFP (used as control), GFP-MTM1 or MTM1-GFP. Vacuolar membranes were stained with FM4-64 dye (red fluorescence) that enters into the cells by endocytosis and is transported to the vacuolar membrane (Vida & Emr, 1995). Living yeast cells were observed by fluorescence microscopy (Fig. 1A). MTM1-GFP produces an enlargement of vacuoles whereas cells expressing GFP-MTM1 and catalytic dead MTM1-C375S-GFP present fragmented vacuoles, as the control (empty vector, pAG-GFP). This shows that addition of a GFP tag at the N-terminus of MTM1 impaired its 3-phosphatase activity *in vivo* in yeast cells. MTM1-GFP is localized to a large punctuate structure adjacent to the vacuolar membrane while GFP-MTM1 is dispersed in the cytoplasm. The MTM1 protein has two main domains: the PH-GRAM membrane binding domain and the catalytic phosphatase domain (Fig. 1A). Analysis of the PH/GRAM domain localization upon GFP tagging at the N- or C-terminus shows that membrane localization was observed only for the PH-GRAM-GFP construct (Fig. 1A). To determine, the role of the PH-GRAM domain for membrane localization, we tagged with GFP an MTM1 construct lacking the PH/GRAM domain and here termed as catalytic domain (Fig. 1A). The catalytic-GFP is observed in punctuate structures next to the fragmented vacuolar membranes, indicating that this MTM1 construct lacking only the PH-GRAM domain shows no phosphatase activity *in vivo*. These results show that the N-terminal PH-GRAM is essential for the phosphatase activity of MTM1 *in vivo* in yeast cells and that this domain has to be free at its N-terminus for proper membrane localization.

A subcellular fractionation of yeast cells expressing MTM1 wild-type, the catalytic-dead phosphatase mutant MTM1-C375S and the catalytic domain was done to determine the membrane localization of non-tagged MTM1 constructs. The cell extracts were sequentially centrifuged at 13,000x*g* and 100,000x*g* yielding a soluble fraction (S100) and two membrane fractions (P13 and P100). All fractions were tested for the presence of MTM1 (polyclonal rabbit serum), the 100 kDa vacuolar ATPase subunit (Vph1), and the cytosolic marker phosphoglycerate kinase (Pgk1), using specific antibodies. The vacuolar membranes, identified by the presence of Vph1 are found predominantly in P13 and P100 fractions and the cytosol in the S100 fraction as indicated by the detection of the Pgk1 marker. The majority of MTM1 is detected in the fraction P13 and also for some extent into the P100 fraction. MTM1 is enriched in fractions that contain vacuolar membranes, in good agreement with the intracellular localization of MTM1-GFP observed by fluorescent microscopy (Fig. 1A). The MTM1-C375S phosphatase mutant is also enriched in the P13 and P100 membrane fractions, showing that this membrane localization does not depend on the catalytic activity.

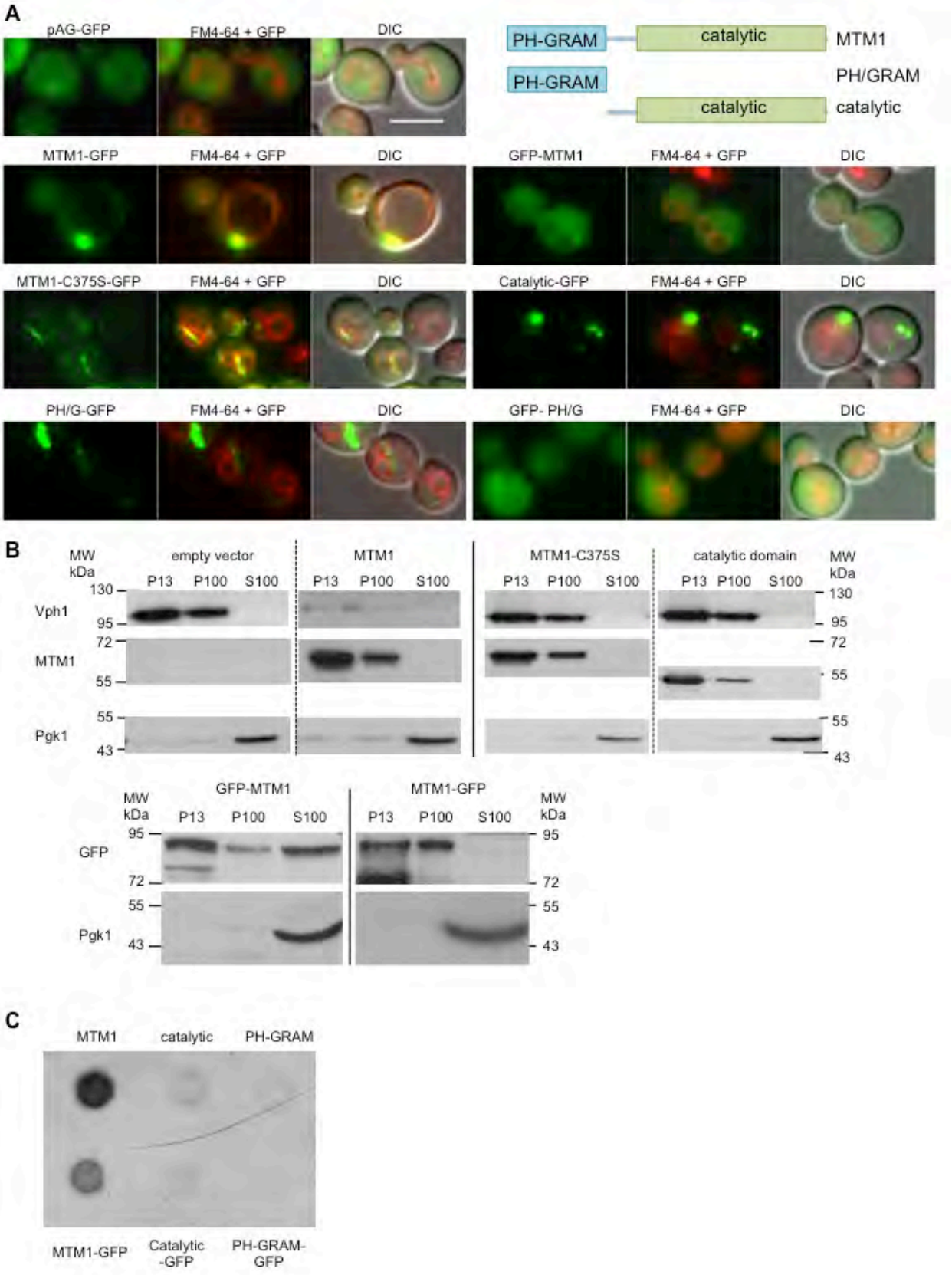

Figure 1. Intracellular localization of the different constructions of MTM1 in *ymr1*Δ yeast cells. A. Epifluorescence microscopy of yeast cells transformed with the following vectors: MTM1 WT, MTM1-C375S, catalytic domain or PH/GRAM (PH/G) domain tagged with GFP in N- or C-terminus as indicated. Vacuoles were labeled using FM4-64 fluorescent dye (red). Tagging of MTM1 at the N-terminus results in localization of the protein into the cytoplasm and a lack of phosphatase activity (fragmented vacuoles). Scale bar 5μm. **B**. Subcellular

fractionation of total protein extracts by differential centrifugation, the different fractions (pellet 13000g=P13, pellet 100000g=P100, supernatant 100000g=S100) were analyzed by western blot. Anti-Vph1 was used to localize the vacuolar ATPase Vph1 as a control of the vacuolar membrane (P13, P100), anti-PGK was used to detect the cytoplasmic phosphoglycerate kinase Pgk1 (S100). Anti-MTM1 R2827 polyclonal antibodies were used to identify non-tagged MTM1, the catalytic dead MTM1-C375S and the catalytic domain. **C**. CPY secretion assay of yeast cells transformed with the following vectors: MTM1 WT, MTM1GFP, catalytic domain or PH/GRAM (PH/G) domain tagged with GFP in C-terminus or not tagged as indicated.

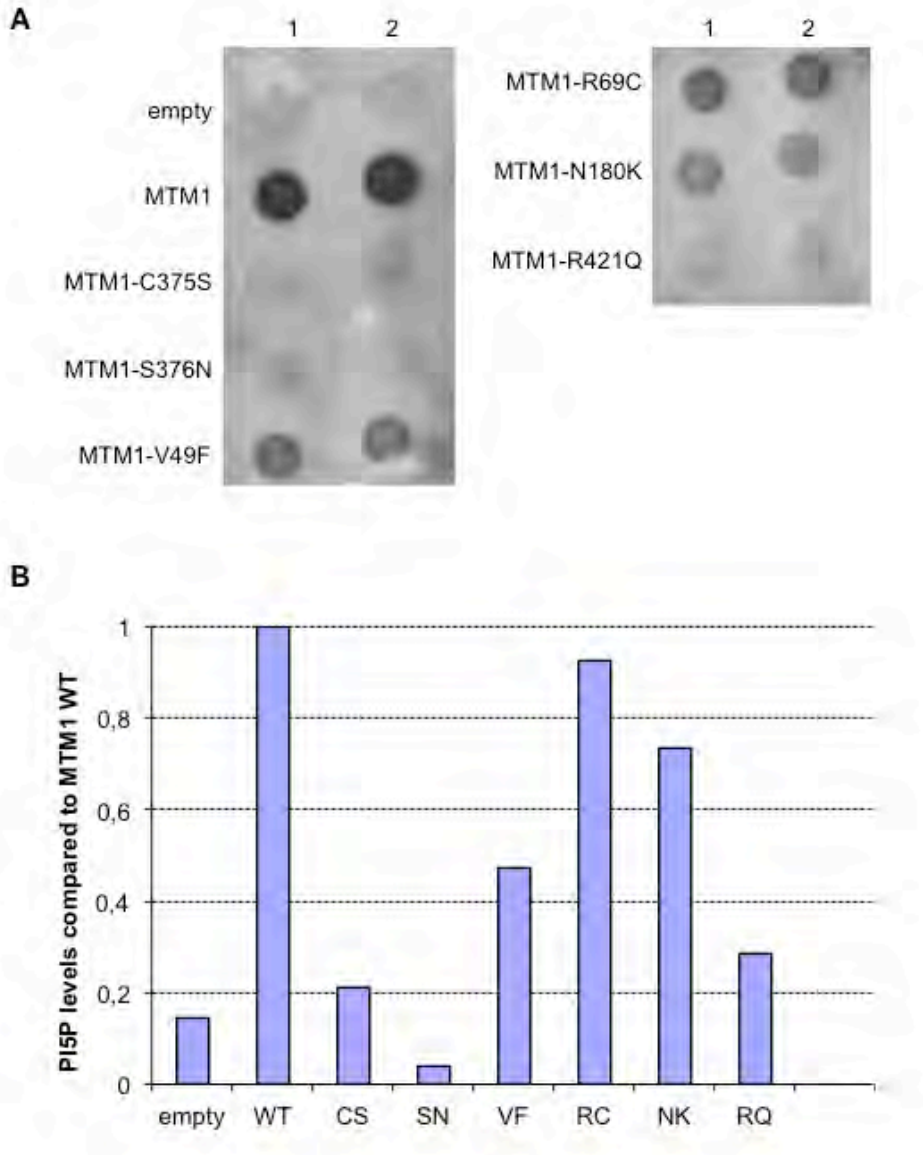

Supplementary Figure 1. CPY secretion and the MTM1 catalytic activity in yeast cells. A. CPY secretion assay of yeast cells transformed with the following vectors: MTM1 WT, MTM1-C375S and the CNM patient mutations MTM1-S376N, MTM1-V49F, MTM1-R69C, MTM1-N180K and MTM1-R421Q. B. Relative production of PI5*P* compared to the wild-type MTM1 by the myotubularin phosphatase activity due to dephosphorylation of PI(3,5)P_2 in yeast cells.

The catalytic domain is enriched in the membrane fractions P13 and P100 (Fig. 1B), but despite this membrane localization, it does not display phosphatase activity, as the vacuoles remain fragmented (Fig. 1A). MTM1-GFP is detected in the P13 and P100 fractions as the non-tagged MTM1, and

contrary to the N-terminal tagged GFP-MTM1 that is also present in the S100 cytosolic fraction (Fig. 1B), as observed by fluorescent microscopy (Fig. 1A). This shows that the N-terminal domain of MTM1 is important for its membrane association.

The MTM1 phosphatase activity is detected *in vivo* in yeast cells via the vacuolar morphology, with enlarged vacuoles being the sign of MTM1 catalytic activity (Amoasii et al, 2012; Raess et al, 2017a). In yeast, PI3*P* and PI(3,5)P_2 are required for vacuolar protein sorting, and in their absence, the carboxypeptidase Y, CPY, is secreted into the extracellular medium, instead of being addressed of the vacuolar lumen (Mayinger, 2012). CPY secretion was analyzed in the yeast cells expressing different MTM1 constructs bearing CNM patient mutations in either the PH-GRAM or the catalytic domain and having different catalytic activity (Supplementary Fig. 1). The rate of CPY secretion (Supplementary Fig. 1A) depends on the MTM1 catalytic activity as revealed by the production of PI5*P* ((Supplementary Fig. 1B), with the MTM1 wild type showing the higher level of CPY secretion and MTM1-C375S and MTM1-S376N catalytic defective phosphatases displaying no CPY secretion (Supplementary Fig. 1). Therefore, the CPY secretion assay was used to monitor the catalytic activity of the different MTM1 domains constructions. The CPY secretion assay shows that MTM1-GFP is catalytically active, albeit to a lesser extent than the non-tagged MTM1 (Fig. 1C). This CPY assay also confirms that the neither the PH-GRAM, nor the catalytic domain is catalytically active (Fig. 1C).

The MTM1 PH/GRAM and catalytic domains interact and reconstitute an active phosphatase

The *ymr1*Δ yeast mutant cells were transformed with vectors bearing PH/GRAM-DsRed and/or the catalytic-GFP domain to observe their localization within the cells (Fig. 2A). The vacuolar lumen was stained in blue with the CMAC (7-amino-4-chloromethyl-coumarin) dye to visualize the vacuolar phenotype. Between 600-800 cells from each transformation were analyzed in order to classify the vacuoles in 3 types: 1-large 2- fragmented vacuoles and 3- small, intermediate, one or two lobes (Fig. 2B). The MTM1 and MTM1-C375S catalytic-dead myotubularins were used as controls (Fig. 2B). The enlarged vacuolar phenotype is due to MTM1 catalytic activity (Amoasii et al, 2012; Raess et al, 2017a). The percentage of large vacuoles between cells expressing MTM1 and the catalytic dead MTM1-C375S are significantly different (Fig. 2B), showing a direct correlation between the size of the vacuole and the phosphatase activity of MTM1 *in vivo*. As previously observed, based on the CPY secretion assay, neither the PH/GRAM nor the catalytic domain are catalytically active, as their percentage of large vacuoles is similar to the one observed for MTM1-C375S. However, in yeast cells co-expressing the PH-GRAM and the catalytic domain, these two domains are co-localized in a dot-like structure, adjacent to the vacuole, and the vacuoles are

enlarged. Only, the yeast cells having the two domains colocalized next to the vacuole have enlarged vacuoles, whereas the other cells have fragmented vacuoles (white stars, Fig. 2A). Quantification of the vacuolar phenotype shows that yeast cells co-expressing the PH-GRAM and the catalytic domain have an increased percentage of enlarged vacuoles (Fig. 2B). This suggests that these two domains interact and reconstitute a catalytic active MTM1 phosphatase.

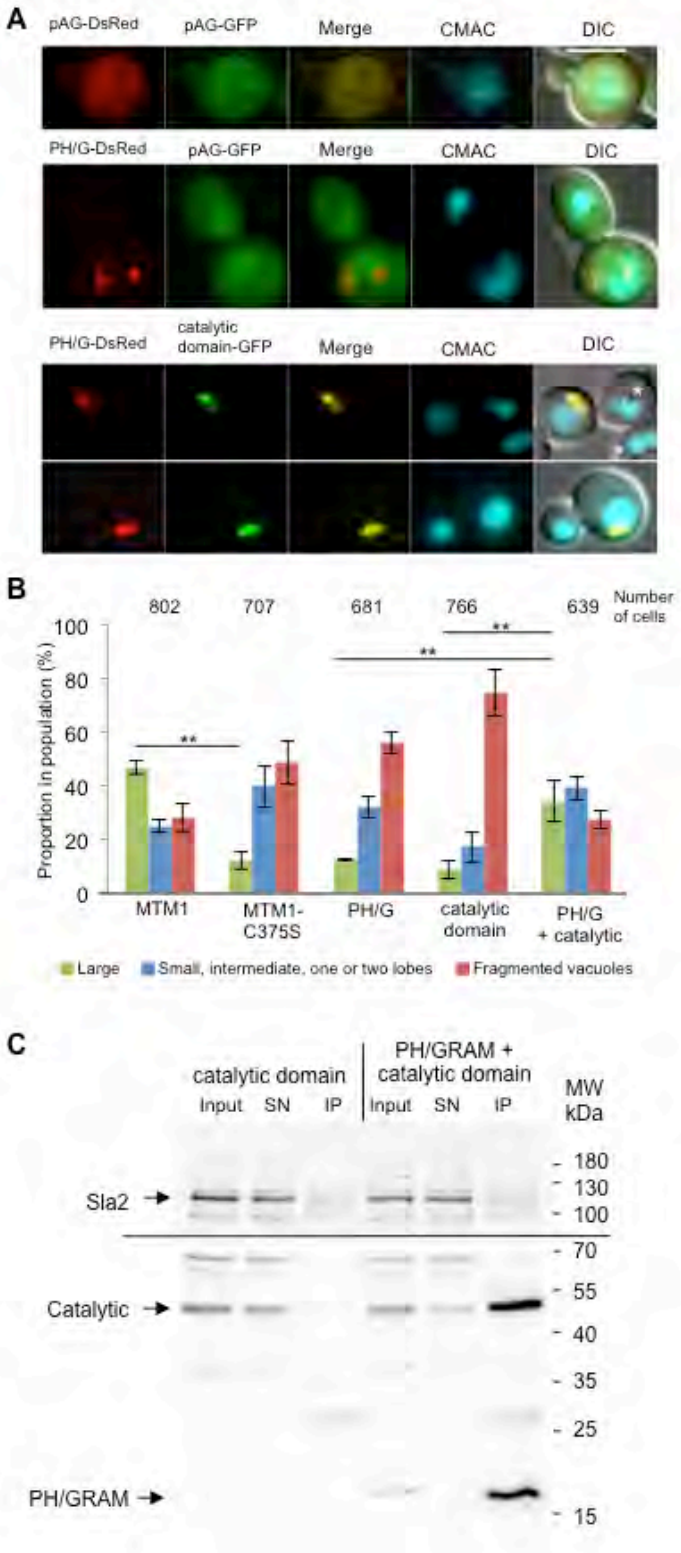

Figure 2. Analysis of MTM1 phosphatase activity in yeast cells with PH/GRAM and catalytic domains. A. Epifluorescence microscopy. On the upon, pAG-DsRed and pAG-GFP empty plasmids were used as controls for locating the GFP and DsRed proteins in the cells and for describing a vacuolar phenotype (fragmented vacuoles), on the middle PH/GRAM domain (red) is placed on the vacuolar membrane which is fragmented, on the bottom PH/GRAM(red) and catalytic domains (green) colocalize on the vacuolar membrane (merge in yellow) leading to large vacuoles. Scale bar 5μm. **B**. Total number of counted cells at the microscopy is indicated on the top of every graph. Green bars indicate the percentage of large vacuoles, blue bars indicate the percentage of small one, intermediate or two lobes and red bars indicate the percentage of fragmented vacuoles. Colocalization of PH/GRAM and catalytic domains produces a similar effect those MTM1 wt. *= $p<0.05$ and **= $p<0.01$ **C**. Co-immunoprecipitation Rabbit anti-MTM1 antibody (R1208) was used to identify PH/GRAM domain (17 kDa), and catalytic domain (50 kDa). Anti-Sla2 was used as a control.

To determine whether the PH-GRAM and the catalytic domains interact, the PH-GRAM domain was immunoprecipitated and co-immunoprecipitation (coIP) of the catalytic domain was assessed by western blot (Fig. 2C). The catalytic domain was detected in the input of the control (no PH-GRAM) but not in the immunoprecipitated fraction (IP) indicating that it did not bind on the beads and was not recognized by the monoclonal 1G6 antibodies specific for the MTM1 N-terminus. The catalytic domain interacted with the PH-GRAM since it was detected in the IP fraction only in presence of the PH-GRAM domain (Fig. 2C). This shows that these two domains via their interaction can reconstitute a functional and active phosphatase leading to the enlargement of the yeast vacuoles (Fig. 2B).

The PH/GRAM or the catalytic domain rescues GFP-MTM1 or MTM1-C375S inactive phosphatases

To determine whether the PH-GRAM domain rescues the loss of activity of non-functional MTM1 phosphatase, GFP-MTM1 was co-expressed with PH-GRAM-DsRed, and MTM1-GFP was used as control (Fig. 3A). Expression of the PH/GRAM domain allows GFP-MTM1 to be associated to multiple dotty structures adjacent to the vacuole (yellow dots in merge) and yeast cells develop large vacuoles (Fig. 3A), contrary to cells transformed only with GFP-MTM1 (Fig. 1A).

In a second experiment, cells co-transformed with the catalytic-DsRed domain and the empty GFP, MTM1-GFP or MTM1-C375S-GFP plasmids were observed by fluorescent microscopy after staining of the vacuolar lumen with CMAC (blue, Fig. 3B). The catalytic domain of MTM1 allows the catalytic dead MTM1-C375S-GFP phosphatase to develop large vacuoles (Fig. 3B), contrary to yeast cells expressing only MTM1-C375S-GFP (Fig. 1A). About 700-800 cells from each

transformation were analyzed to classify their vacuoles according to their morphology (1-large, 2-fragmented vacuoles and 3- small, intermediate, one or two lobes) (Fig. 3C). The percentage of large vacuoles of cells co-expressing MTM1-C375S and the catalytic domain is significantly different from cells expressing only MTM1-C375S (Fig. 3C). This increased percentage of large vacuoles indicates a catalytic phosphatase activity, and this shows that the catalytic domain restores activity of the catalytic dead MTM1-C375S.

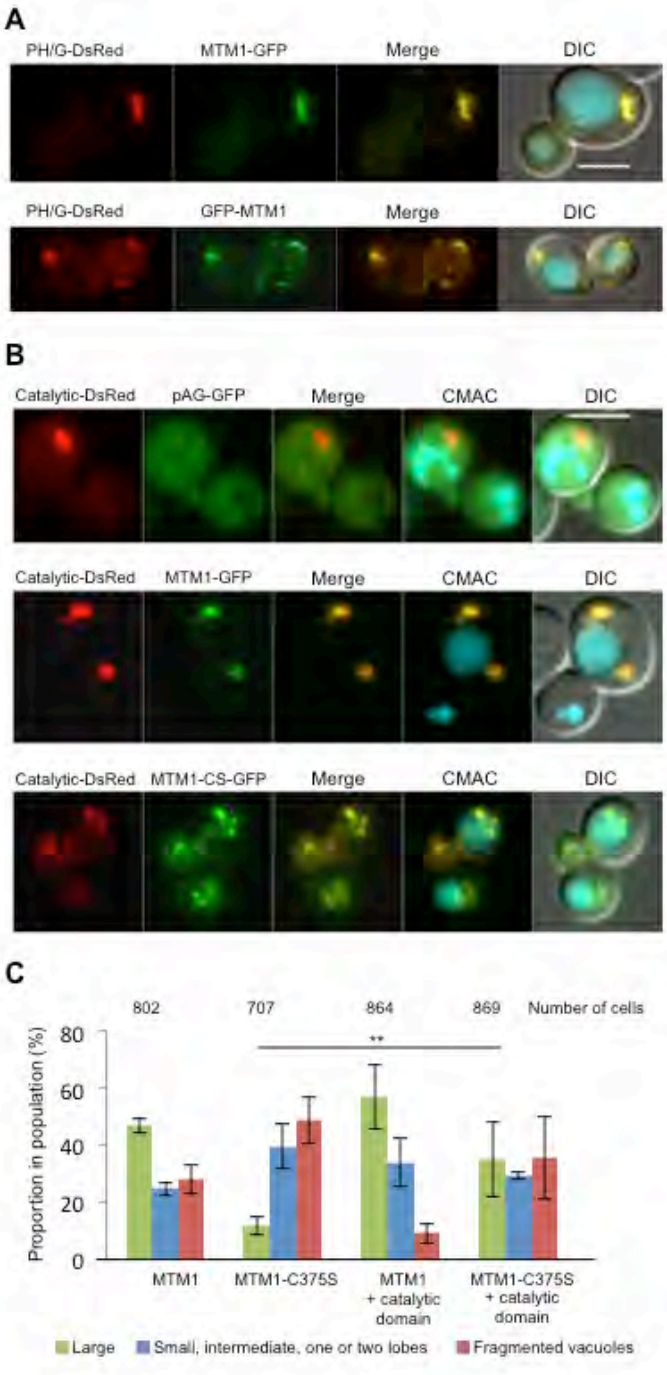

Figure 3. Complementation of GFP-MTM1 and MTM1C375S with PH/GRAM and catalytic domains respectively. A. Epifluorescence microscopy of cotransformed yeast cells expressing PH/GRAM-DsRed and C-terminus GFP tagged MTM1 (upon) or PH/GRAM-DsRed and N-terminus GFP tagged MTM1 (bottom). PH/GRAM domain expression leads to GFP-MTM1 to localize at the membrane and to a vacuolar enlargement. Vacuoles were labeled using CMAC fluorescent dye (blue) **B**. pAG-GFP empty plasmid was used as control, catalytic domain is shown in red. (upon). Cotransformation of yeasts cells with catalytic domain and MTM1-GFP was the other control and the merge in yellow shows colocalization of both proteins (middle). Cotransformation with catalytic domain (red) and the catalytic-dead MTM1-C375S protein (green) restores large vacuoles, indicating phosphatase activity. Scales bar 5μm. **C**. Total number of counted cells at the microscopy are indicated on the top of every graph. Green bars indicate the percentage of large vacuoles, blue bars indicate the percentage of small one, intermediate or two lobes and red bars indicate the percentage of fragmented vacuoles. Cotransformation of the yeast cells with catalytic domain and the catalytic-dead myotubularin MTM1-C375S increases the percentage of large vacuoles. Indicating phosphatase activity. Statistical analysis with the t-Test *= $p<0.05$.

Discussion

Our results show that the N-terminal PH-GRAM domain of MTM1 is important to target it to membranes and to develop its phosphoinositide phosphatase activity. The PH-GRAM domain is present in the different myotubularins, the active and the inactive ones and is conserved along the evolution from the yeast Ymr1 to the human myotubularins (Lecompte et al, 2008; Raess et al, 2017b). The N-terminal PH-GRAM has to be free to allows its association to membranes, indeed tagging it with GFP (Fig. 1) or having a 73 amino acids extension as in the human MTMR2-L long isoform impairs its binding to membranes (Raess et al, 2017a). Indeed, the *MTMR2* gene whose mutations are implicated in Charcot-Marie-Tooth neuropathy, presents two isoforms, MTMR2-S lacking 73 amino acids at its N-terminal and MTMR2-L. The MTMR2-S isoform was shown to be more similar to MTM1 *in vivo* in yeast cells and in mice muscles (Raess et al, 2017a). The PH-GRAM domain of MTMR3 is required for the *in vitro* phosphatase activity of this myotubularin-related protein (Lorenzo et al, 2005). Our results show that addition of the GFP tag at the N-terminus of MTM1, or deletion of the PH-GRAM domain renders the MTM1 phosphatase inactive *in vivo* in yeast cells. Deletion of the PH-GRAM domain decreased MTMR2 binding to phosphoinositides (Berger et al, 2003). The PH-GRAM domain of MTM1 binds to phosphoinositides *in vitro*, with the highest affinity towards PI(3,5)P_2 (Tsujita et al, 2004). This could explain its association to membranes adjacent to the vacuole upon expression in yeast cells (Fig. 1), since the late endosomes and the vacuolar membranes are enriched in PI(3,5)P_2, which is synthesized from PI3*P* by the Fab1 kinase (Gillooly et al, 2000; Odorizzi et al, 1998). A mutation in

the PH-GRAM or in the coil-coiled domain of MTMR2 abolishes its binding to membranes in COS transfected cells, contrary to mutations in the catalytic domain (Berger et al, 2003). In yeast cells, the MTM1 phosphatase construct (termed the catalytic domain) lacking the PH-GRAM but bearing the coil-coiled domain is associated to P13 and P100 membrane fractions (Fig. 1B). This shows that the PH-GRAM domain is important for the catalytic activity of the myotubularins, rather than for their membrane association.

In this study, we show that an active phosphatase can be reconstituted by interaction between the PH-GRAM and the catalytic domain of MTM1 (Fig. 2), and that it is possible to rescue the catalytic activity of MTM1-C375S via expression of its catalytic domain (Fig. 3). Indeed, the PH-GRAM and the catalytic domain of MTM1 interact. Myotubularins have been shown to hetero- , homo- or oligomerize. The myotubularin MTM1 was shown to oligomerize, this oligomerization being associated to its catalytic activity with an allosteric activation by its PtdIns5P product (Schaletzky et al, 2003). MTMR2 was also shown to form dimers *in vitro* and the coil-coiled domain is required for this dimerization (Berger et al, 2003). Moreover, heterodimer are formed between an active and an inactive myotubularin as for example MTM1 with MTMR12 (Lorenzo et al, 2006; Raess et al, 2017b). Interestingly, the activity of MTM1 increases by adding the catalytic dead MTM1-C375S mutant (Schaletzky et al, 2003).

This study has advanced our understanding of the mode of action of the myotubularin MTM1. We have demonstrated that intermolecular interactions are necessary for the activity of this phosphatase enzyme. On one hand, the PH/GRAM domain needs to be accessible for a link with the membranes while on the other hand, the catalytic domain needs the PH/GRAM to enable its phosphatase activity. Interestingly, many XLCNM patient mutations are found in these two domains (Cowling et al, 2012). Our data show that these MTM1 mutant forms could be rescued by expression of the wild type version of the domain bearing the mutation via these intermolecular interactions. These findings help clarify how the MTM1 phosphatase functions *in vivo*. These results obtained in the yeast model have now to be tested in other models of the XLCNM disease.

3.1.2. Perspectives on the MTM1 study in yeast cells

Centronuclear myopathies have been related to autophagy (Jungbluth & Gautel, 2014). Autophagy is fundamental for removing defective proteins and organelles. Mutations in *MTM1* provoke X-linked centronuclear myopathy, it would not be very surprising that MTM1 might be implicated in autophagy since it is a lipid 3-phosphatase whose substrates are PI3*P* and PI(3,5)P_2. Indeed, PI3*P* is

enriched at the autophagosomal membranes, the PI(3,5)P_2 effector Atg18 is required for autophagosome maturation, and the product of 3-dephosphorylation reaction of PI(3,5)P_2, the PI5*P* is needed for autophagosome biogenesis (Mayinger, 2012). In order to continue the researches for understanding the molecular level of myotubularin MTM1 and its implication within the yeast cell; it would be really interesting to perform experiments concerning autophagy. Indeed, autophagy was first described in yeast *S. cerevisiae* by Y. Ohsumi, Nobel Prize in Physiology and Medicine 2016. The yeast *ymr1*Δ mutant cells bearing either wild-type MTM1, the catalytic-dead MTM1-C375S mutant or different patient mutations (Supplementary Figure 1, article Sanjuan et al.) will be tested for survival upon autophagy and autophagy will be analyzed by following the intracellular trafficking of the Atg8 reporter.

3.2. The human DNM2 and its study in yeast cells

During my PhD thesis, I co-supervised an Erasmus Master student Roberto Silva Rojas during his Master internship in the team of Sylvie Friant. Some of the data presented in this chapter about the yeast DNM2 humanization project were done by Roberto and me.

3.2.1. The human DNM1L is the closest homologue of the yeast Vps1 and Dnm1 proteins

In this study, I studied the different types of human dynamins: hDNM1, hDNM1L, hDNM2 iso1 (ubiquitously isoform) and hDNM2 iso 12b (muscle isoform). Indeed, the aim was to find a phenotypic rescue that was specific for the hDNM2 and not a rescue that depended only on the GTPase activity of the dynamin. In this study, I also hoped to find a different phenotypic rescue for the hDNM2 muscle isoform compared with the ubiquitous isoform. For hDNM1, I used the isoform 1 that is the best described in the literature and required for endocytosis. For hDNM1L, also termed DLP1 or DRP1, I used the DNM1L isoform 3, for which we had the cDNA.

Alignments between the four human dynamins used in this study were done, that is, hDNM1, hDNM1L, hDNM2 iso1 (ubiquitously isoform) and hDNM2 iso 12b (muscle isoform). hDNM1 was taken as reference for the alignment. It has the 5 specific domains of dynamins: GTPase,

middle, PH, GED and PRD domains. The sequence comparison between hDNM1 and hDNM1L, shows an identity of about 43.36%, but it must be taken into account that hDNM1L lacks the PH and PRD domains (figure 35A). hDNM1 iso1 is highly similar in amino acid sequence with the two hDNM2 (isoforms 1 and isoform 12b), the identity between them is around 80%; there is just an exception for the PRD domains where their identity is only 54% (figure 35A).

Both yeast proteins used in this study, Vps1 and Dnm1, are dynamin-related proteins and they lack the PH and PRD domains (figure 35B). However the alignment of both sequences revealed a low percentage of identity of only 44%. This difference in sequence could be due to their different cellular roles in yeast cells. Next, protein sequences between the yeast Vps1 and Dnm1 proteins and the human dynamins were compared. The percentages of identity range from 41% to 48% between them (figure 35C). On one hand, as expected the GTPase domain was the most similar domain between yeast and human dynamins; on the other hand Middle and GED domains were more divergent. The human DNML1 middle and GED domains were more similar to their yeast counterparts.

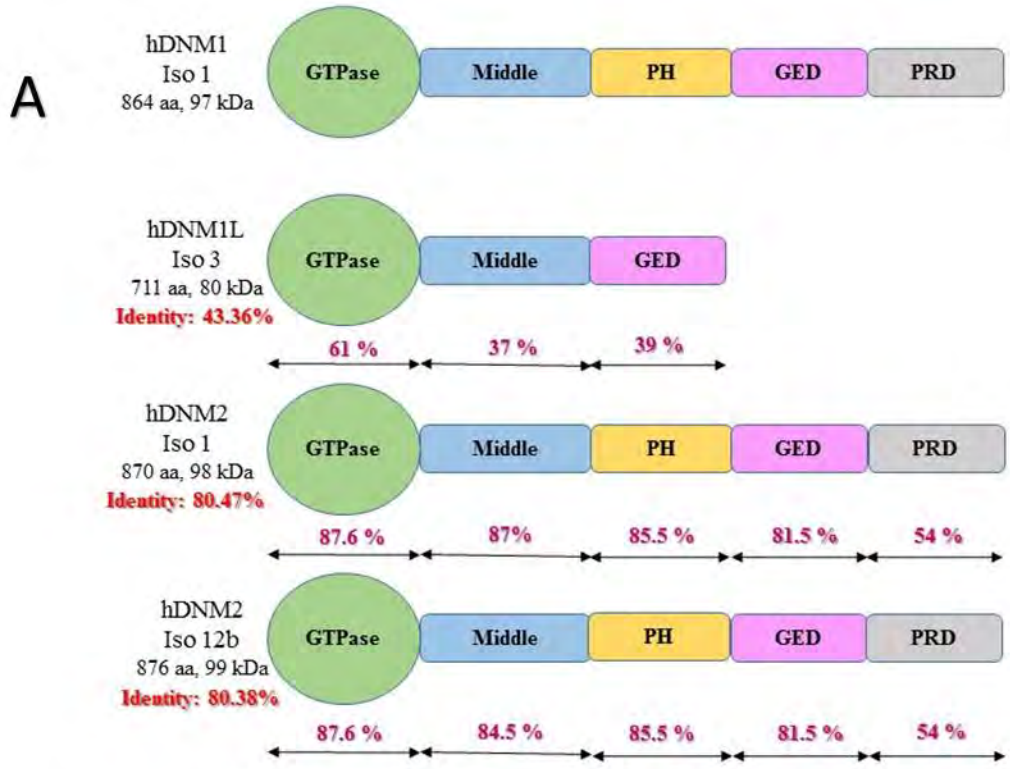

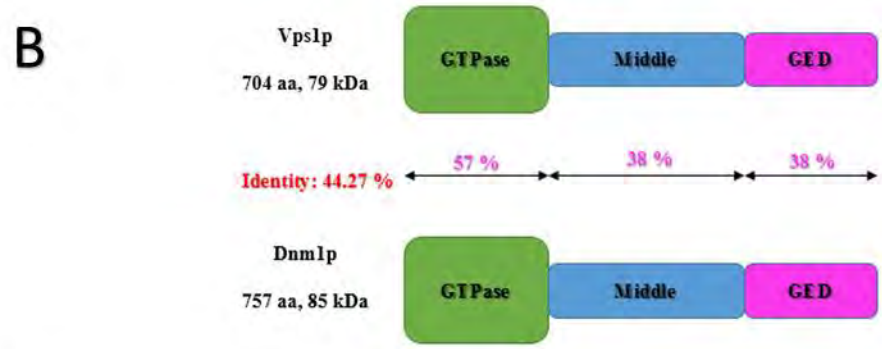

C

Full length	Vps1p	Dnm1p
hDNM1 iso 1	44%	42%
hDNM1L iso 3	45%	48%
hDNM2 iso 1	45%	42%
hDNM2 iso 12b	44%	41%

GTPase	Vps1p	Dnm1p
hDNM1 iso 1	72%	69%
hDNM1L iso 3	59%	62%
hDNM2 iso 1	72%	69%
hDNM2 iso 12b	72%	69%

Middle	Vps1p	Dnm1p
hDNM1 iso 1	35%	36%
hDNM1L iso 3	41%	54%
hDNM2 iso 1	36%	35%
hDNM2 iso 12b	35%	35%

GED	Vps1p	Dnm1p
hDNM1 iso 1	35%	28%
hDNM1L iso 3	40%	47%
hDNM2 iso 1	32%	30%
hDNM2 iso 12b	32%	30%

Figure 35: Protein domain structures and percentage of identity among the human and the yeast dynamins. (A) hDNM1L iso 3, hDNM2 iso 1 and hDNM2 iso 12b have different percentage of identity. hDNM1 iso 1 was used as reference. Domain percentage of identity is also shown. (B) Protein and domain percentage of identity between yeast VPS1 and DNM1. (C) Protein and domain identity between hDNM1 iso 1, hDNM1L iso 3, hDNM2 iso 1 and hDNM2 iso 12b and yeast VPS1 and DNM1. Percentage of identity is the percentage of amino acids that are similar.

Note: GTPase for GTPase domain; Middle for Middle domain; PH for Pleckstrin homology domain; GED for GTPase effector domain; and PRD for Proline rich domain. Exon 12b (10 extra amino acids) differentiates hDNM2 iso 1 and iso 12b.

3.2.2. Yeast expression plasmids bearing human dynamins cDNAs

The four studied human dynamins hDNM1 iso1, hDNM1L iso3, hDNM2 iso1 (ubiquitously isoform) and hDNM2 iso 12b (muscle isoform), were cloned by the Gateway technology (Invitrogen) in yeasts expression plasmids with the Gateway attB recombination sites flanking the dynamin cDNA sequences. Yeast dynamin *vps1*Δ and *dnm1*Δ mutant strains were transformed with these expression plasmids.

In order to detect the human dynamin expression in yeast cells, total yeast extracts of *vps1*Δ and *dnm1*Δ strains transformed with either the empty expression plasmid (control) or the plasmids bearing the different human dynamins were analyzed by western-blot. The polyacrylamide gels used for this purpose contain 2,2,2-Trichloroethanol (TCE). This compound TCE labels the tryptophan residues of the proteins that become fluorescent after UV activation (ChemidocTouch machine, BioRad), allowing total proteins to be observed by stain free imaging. This stain-free was used as loading control for the western blot experiments (figure 36, right). After immunoblotting with specific antibodies for the different human dynamins (hDNM1L, hDNM1 and hDNM2), bands corresponding to the full-length proteins were observed (figure 36). hDNM2 iso1 and iso12b were expressed in both *vps1*Δ and *dnm1*Δ yeast strains as one band is clearly observed at 98 kDa, the expected size of hDNM2, and this band is absent in the control strains bearing the empty expression plasmid (figure 36a, left). hDNM1 iso1 is also expressed in both yeast strains, indeed, one band at 97 kDa corresponding to the size of hDNM1 is observed (figure 36b, left). Finally, hDNM1L iso3 was also expressed in the two strains and detected as a band of 80 kDa (figure 36c, left).

Expression of the human EGFP tagged dynamins was also observed in the two *vps1*Δ and *dnm1*Δ yeast strains by western blot. Indeed, bands of about 130 kDa corresponding to the size of the tagged proteins were specifically observed in yeast cells bearing the human hDNM2 iso1-EGFP, hDNM2 iso12b-EGFP, hDNM1 iso1-EGFP and hDNM1L iso3-EGFP expression vectors (data not shown).

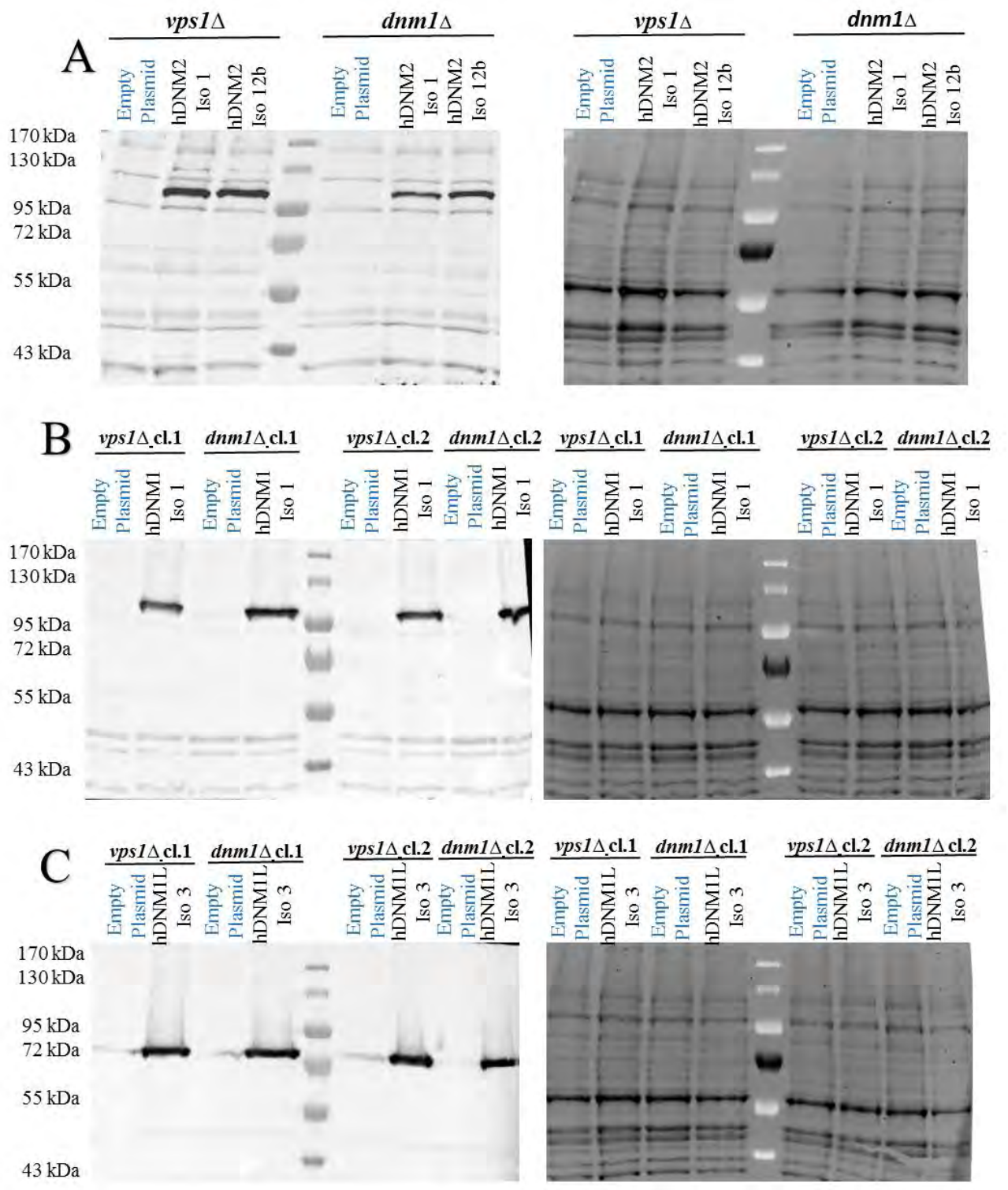

Figure 36: Expression of human dynamins by *vps1*Δ and *dnm1*Δ mutant yeasts was confirmed. Western blots are placed on the left side and the stain free on the right side. (A) hDNM2 iso 1 and hDNM2 iso 12b were clearly expressed as observed by Western Blot. (B) hDNM1 iso 1 was also expressed in both mutants. (C) hDNM1L iso 3 was also detected in vps1 and dnm1 mutants. Empty vector means that yeas t were transformed with the Gateway ® backbone vector used for Gateway ® LR cloning reaction. Antibodies used were protein specific and are described in Material and Methods

3.2.3. The yeast vps1Δ mutant phenotypes are not rescued by hDNM2 isoforms

3.2.3.1. Drop tests phenotyping assays on vps1Δ mutant strain

As explained in the Introduction chapter, the yeast *vps1*Δ mutant strain was described as being sensitive to cadmium and/or nickel stresses in a large-scale screening study. Indeed, the *vps1*Δ mutant strain was described as being affected in the retention of late Golgi proteins required for vesicle trafficking and is cadmium sensitive and nickel resistant (Ruotolo et al, 2008). In order to establish a complementation assay, growth test were performed by drop tests with wild type (BY4742), *dnm1*Δ and *vps1*Δ yeast strains either on rich medium (YPD) or on rich medium containing Cadmium ($CdCl_2$) or Nickel ($NiCl_2$) (figure 37a). The *vps1*Δ strain was sensitive to $CdCl_2$ concentrations ranging from 10 to 60 µM (data not shown). The nickel stress resistance of the *vps1*Δ strain was clearly observed on YPD medium containing 5 mM $NiCl_2$ 48 hours after the incubation of the plates at 30°C (figure 37a). These results show that *vps1*Δ was indeed sensitive to cadmium and resistant to nickel, whereas the yeast *dnm1*Δ strain was similar to wild-type strain (figure 37a). The *vps1*Δ yeast strains transformed with expression plasmids bearing the different human dynamins (DNM1, DNM1L, DNM2 iso1 and iso12b) did not show any rescue of the cadmium sensitivity. This was observed even at the low concentration of 20 µM $CdCl_2$, after 48 hours of growth at 30ºC (figure 37b). There was no recovery of the sensitivity of *vps1*Δ cells to cadmium even upon expression of hDNM1 iso1, which was suggested in databases as being the human functional homolog of yeast Vps1 dynamin (SGD database).

Other drop tests were performed but this time under osmotic stress (NaCl). In the laboratory of Sylvie Friant it was shown that the yeast amphiphysin *rvs167*Δ mutant strain displays sensitivity to NaCl osmotic stress (data not shown) (Youn et al, 2010). Since in yeast and in human cells, DNM2 dynamin interacts with BIN1 amphiphysin and both are involved in CNMs, we hypothesized that *vps1*Δ could also display a sensitivity to NaCl. However, we tested an osmotic NaCl 0.5 M stress on *vps1*Δ mutant cells, and the drop test assays showed no difference between wild type (BY4742) cells and *vps1*Δ mutants (data not shown). Thus, only $CdCl_2$ sensitivity was validated as a specific *vps1*Δ mutant phenotype.

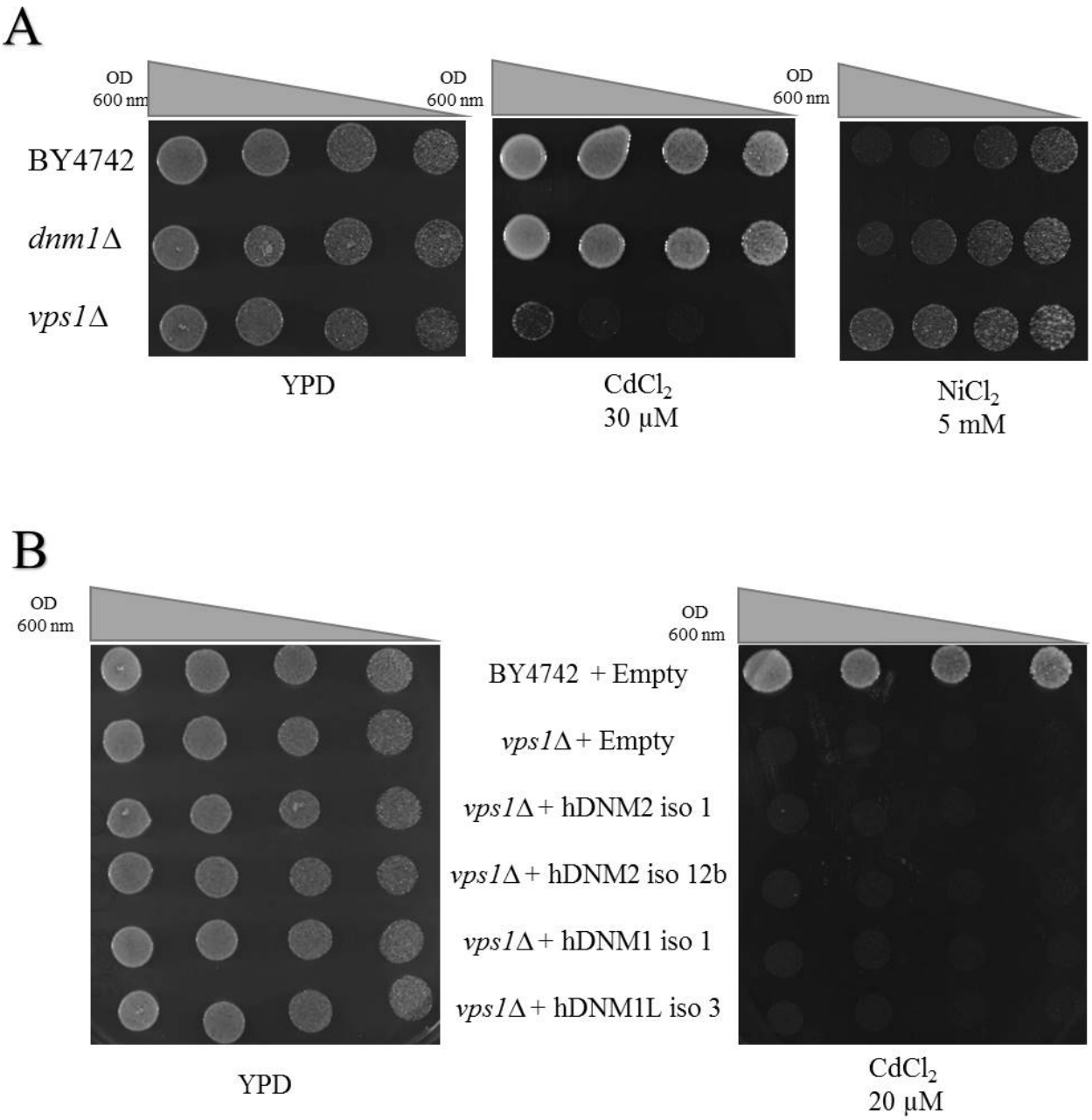

Figure 37: (A) Drop test assays carried out on different yeast strains: wild-type BY4742, *vps1*Δ and *dnm1*Δ on 5 mM $NiCl_2$ and 30 µM $CdCl_2$ plates. (B) Drop test assays with human dynamin expression plasmids transformed yeast strains are shown. YPD and 20 µM $CdCl_2$ cultures were carried out in this case. Yeast cultures at OD 600nm used in the drop tests were 0.5, 0.25, 0.1 and 0.05. YPD images were acquired 24 hours after the start of the culture while $NiCl_2$ and $CdCl_2$ images were acquired 48 hours after the start of the culture

3.2.3.2. Peroxisome fission defect of vps1Δ mutant strain

Peroxisomes are organelles of eukaryotic cells surrounding by only a single membrane. Among other functions, they are involved in degradation of very long chain fatty acids by oxidation.

Peroxisomes have no genome, so they need to import all their proteins from the cytosol. The yeast *vps1*Δ mutant strain is affected in the peroxisome number, size and distribution (Kuravi et al, 2006). For these experiments, the wild-type (BY4742), *pex14*Δ (control, no peroxisome import) and *vps1*Δ yeast cells transformed or not by human dynamin (hDNM1, hDNM1L, hDNM2 iso1 or iso12b) expression plasmids were co-transformed with the SKL-GFP reporter allowing staining of the peroxisomes. Indeed, the SKL peptide is a yeast peroxisomal import sequence. The transformed cells were observed by fluorescent microscopy after growth overnight on oleic acid medium, which induces peroxisome biogenesis and SKL-GFP import into peroxisomes (figure 38a) (Lockshon et al, 2007). No differences were observed between non-transformed *vps1*Δ cells and *vps1*Δ cells expressing human dynamin, indeed 1 to 2 peroxisomes per cell are predominantly observed in both cases (figure 38b and table 4). Wild type yeast (BY4742) carried significantly higher numbers of peroxisomes per cell when grown in oleic-containing medium (figure 38b and table 4). These results show that there is no functional rescue of the peroxisome phenotype displayed by the yeast *vps1*Δ mutant cells with the tested human dynamins. This allows us to show that none of the tested human dynamin hDNM1 iso1, hDNM2 iso1 and iso12b and even hDNM1L iso3, that shares a similar organization in domains with Vps1, are functional homologues for peroxisome function of the yeast Vps1 dynamin-related protein.

By analyzing the *vps1*Δ peroxisome phenotype, DIC images revealed dots in all yeast strains. We hypothesized that these dots could be lipid droplets, as lipid droplets accumulate in lipid rich medium and appear as dots in DIC observation (Fukumoto & Fujimoto, 2002). To check this, Nile Red staining of lipid droplets was performed on the different yeast transformed cells. Nile red stained lipid droplets colocalized with the dots detected in DIC microscopy but no difference was observed between the different transformants, showing that the expression of human dynamins did not modify the accumulation of lipid droplets in the yeast *vps1*Δ cells (figure 38a). Another observation was that peroxisomes were close to the lipid droplets. This position fits with the fact that peroxisomes are responsible for a part of fatty acid β-oxidation. A relevant result of this experiment was that *vps1*Δ yeast cells transformed with hDNM2 iso12b displayed a unique and large vacuole (DIC image figure 38a). It was described in the literature that *vps1*Δ mutant cells have fragmented vacuoles (table 2). This result suggests that hDNM2 iso12b could have a rescue effect on the vacuolar morphology of the *vps1*Δ mutant cells. This hypothesis will be tested in future experiments.

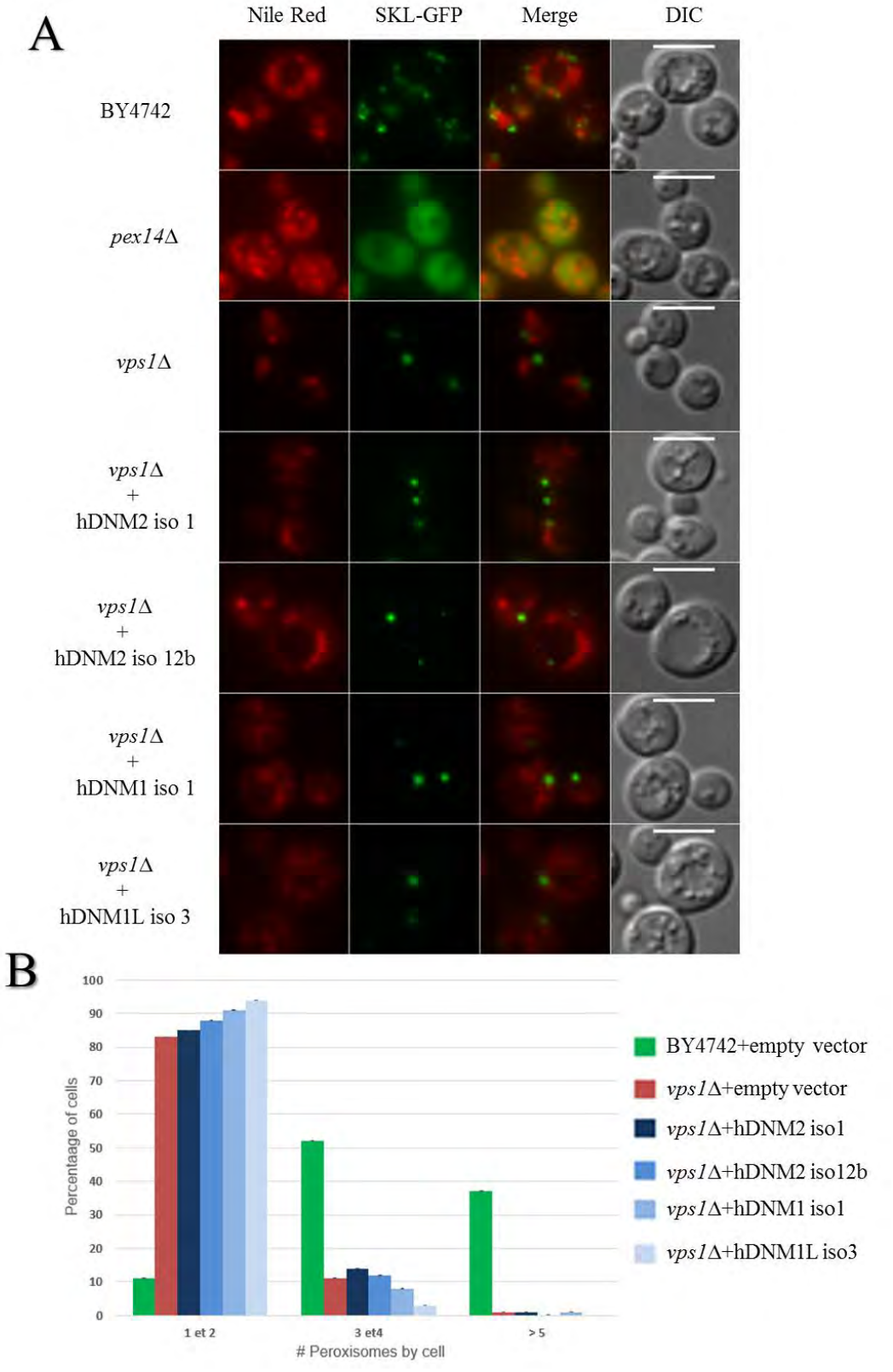

Figure 38 : Difference in number of peroxisomes was evident between wild type BY4742 yeast and *vps1*Δ mutant yeast. No difference between mutant *vps1*Δ yeast and transformed *vps1*Δ yeast was observed. (A) Co-transformed yeast cells with SKL-GFP plasmid and plasmids expressing human dynamins. Nile red shows the presence of lipid droplets, which were not different in number among all the samples shown. hDNM2 iso 12b transformed cells present bigger and non fragmented vacuoles. (B) Percentage of cells carrying 1-2, 3-4 or more than 5 peroxisomes by cell. For each sample, peroxisomes were counted in 100 cells from 2 independent cultures and 2 different clones at each time. Cells were grown in 0.1 % oleic-containing medium. Error bars represent the s.e.m.

	Average	s.e.m
BY4742 + Empty + pFL47	4,21	0,17
***vps1*Δ + Empty + pFL47**	1,51	0,08
***vps1*Δ + hDNM2 iso1 + pFL47**	1,65	0,08
***vps1*Δ + hDNM2 iso12b + pFL47**	1,56	0,08
***vps1*Δ + hDNM1 iso1 + pFL47**	1,48	0,08
***vps1*Δ + hDNM1 L iso3 + pFL47**	1,25	0,05

Table 4: Peroxisome average per cell of 100 cells counted for each transformant. Empty, empty vector; s.e.m, standard error of the mean done on three independent experiments.

3.2.4. hDNM2 iso1 expression ameliorates *dnm1*Δ H_2O_2 sensitivity but not mitochondria net-like shape

3.2.4.1. Drop test phenotyping assays on the dnm1Δ strain

Heat shock sensitivity to stresses from 30°C to 50ºC is a phenotype referred for the *dnm1*Δ mutant strain (SGD database). However, a temperature adaptation of the *dnm1*Δ strain by 1 hour incubation at 37ºC overcomes this heat-sensitivity phenotype (Gibney et al, 2013). Therefore, we performed an experiment where exponential phase growing yeast cells were treated by a heat shock at 50ºC for different times (3 to 15 minutes), with or without a 1 hour adaptation at 37ºC. However with this assay we did not observe any difference in growth for the wild type (BY4742) and the *dnm1*Δ strain (figure 39). In both cases, similar sensitivity to heat shock was observed between the wild type (BY4742) and the *dnm1*Δ strain (figure 39), as well as an acquired resistance to the heat shock upon adaptation at 37ºC. In conclusion, this phenotype cannot be used for screening human dynamin rescue in *dnm1*Δ yeast cells.

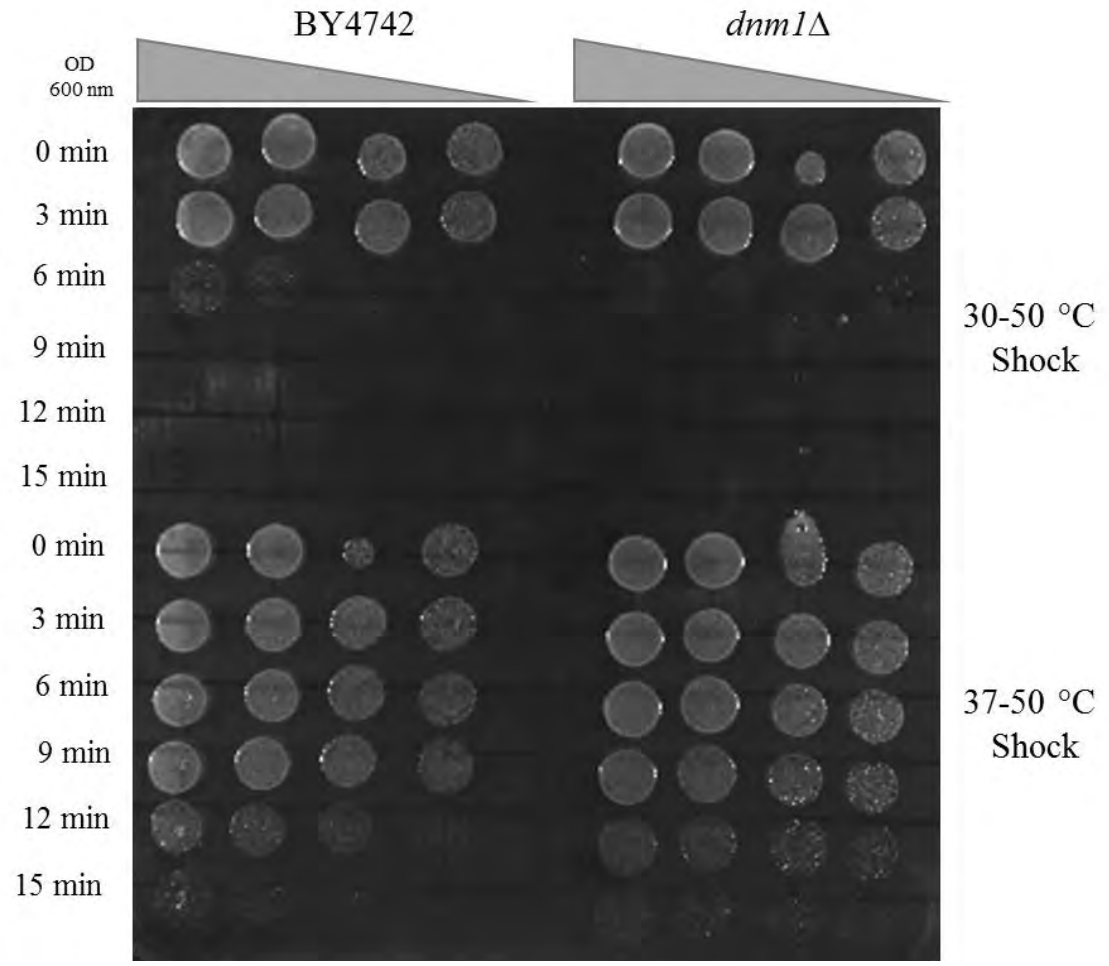

Figure 39: Yeast cultures were incubated at 50 ºC for the indicated time and drops were deposited on a YPD plate. 37-50ºC means that these drops consisted of yeast cells that were adapted one hour in a 37ºC YPD culture with agitation. The OD 600 nm of the cultures used to make the drops was 0.5, 0.25, 0.01 and 0.05.

The *dnm1*Δ strain is sensitive to oxidative stress due to the mitochondrial fission defect (Scheckhuber et al, 2007). The reasons for this are not very clear, but lipid peroxidation could be the culprit of such sensitivity. This modification leads to mitochondrial membrane permeability and loss of membrane potential that triggers mitophagy. This autophagy is started by mitochondrial fission, which is impaired in *dnm1*Δ strain (Scheckhuber et al, 2007). Thus, we carried out a first experiment with wild-type (BY4742), *dnm1*Δ and *vps1*Δ strains grown on YPD plates with H_2O_2 to induce an oxidative stress. A difference in growth was observed between wild-type (BY4742) and the *dnm1*Δ strain in presence of 3 mM H_2O_2 (figure 40). Thus we used this phenotype to screen the *dnm1*Δ mutant strain transformed with the plasmids allowing expression of the four different human dynamins. In some assays, hDNM2 iso1 seems to perform a rescue of the oxidative stress sensitivity (figure 40). However, in other plate assays wild-type yeast cells did not grew homogeneously and thus the results could not be analyzed since the control experiment was not

reproducible (data not shown). Therefore, since the drop assay was not sensitive and reproducible enough, I used another protocol with liquid cultures and measure of the growth rate.

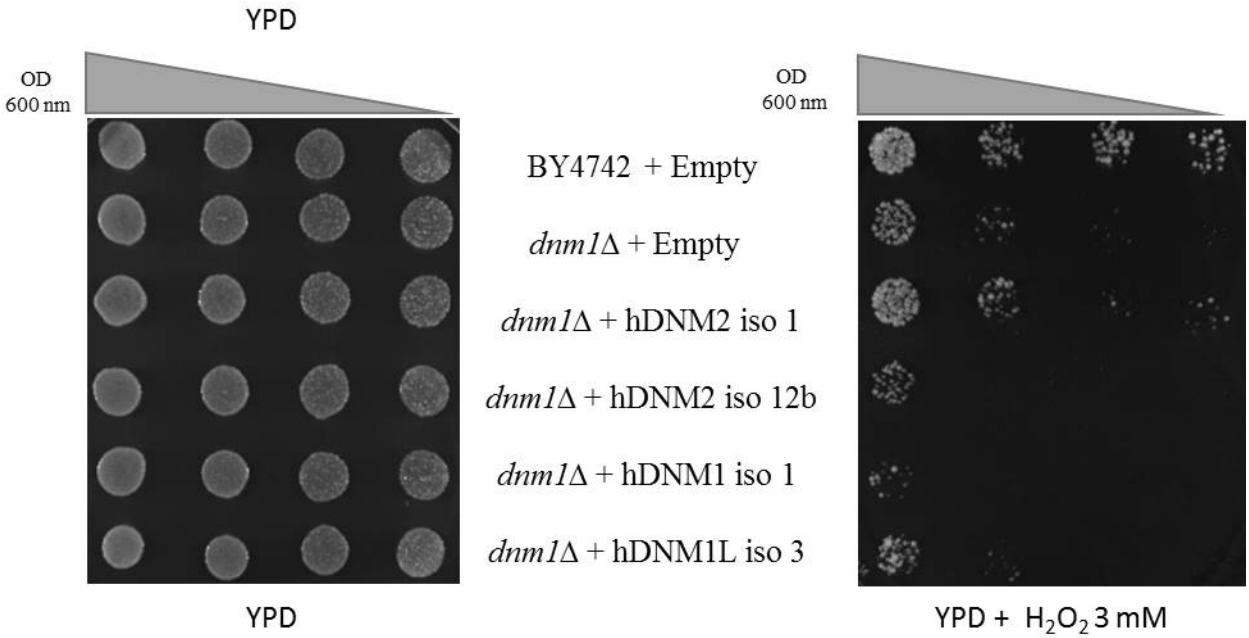

Figure 40: Drop tests with H_2O_2 oxidative stress revealed *dnm1*Δ sensitivity and hDNM2 iso1 rescue was observed. Yeast cultures OD 600 nm used in the drop tests were 0.5, 0.25, 0.1 and 0.05. YPD images were acquired after 24 hours of incubation at 30°C while H_2O_2 images were acquired after 72 hours of incubation.

3.2.4.2 Growth curves in oxidative stress conditions for phenotyping of dnm1Δ strain

Oxidative stress sensitivity was observed for the *dnm1*Δ yeast strain during drop tests assays as described above. The growth curves were done using a spectrofluorimeter. This instrument measures the OD 600 nm of the cultures under continuous agitation and at the desired temperature in liquid medium. In our case, we used it to determine the oxidative stress phenotype of the *dnm1*Δ strain expressing the different types of human dynamins hDNM1, hDNM1L, hDNM2 iso1 or hDNM2 iso12b. Yeast strains were grown at 30ºC under continuous agitation in 96 well plates and every ten minutes the OD_{600} was acquired in order to record the growth over time. Different concentrations of H_2O_2 were tested in YPD liquid cultures ranging from 2 to 4 mM, with a clear phenotype observed at 4 mM of H_2O_2 (data not shown and figure 41). In presence of 4 mM H_2O_2 *dnm1*Δ mutant cells had a clear increase in the latency phase compared to wild-type strain (figure 41). Indeed, growth curves show an increased latency phase but they maintain a similar slope. This experiment shows that only hDNM2 iso1 could rescue the sensitivity to H_2O_2 of the yeast *dnm1*Δ strain, as these cells grew with a wild-type pattern (figure 41). The *dnm1*Δ strain expressing

hDNM2 iso12b, hDNM1 iso1 and hDNM1L iso3 displayed no rescue (figure 41). Growth curves were performed in YPD as a control, and it was clear that all the transformants grew properly in this rich medium (figure 41).

To validate this hDNM2 iso1 rescue phenotype, three different clones of *dnm1*Δ strain expressing hDNM2 iso1 and hDNM1L iso3 were tested. This experiment shows that the *dnm1*Δ sensitivity was rescued by hDNM2 iso1 for the 3 clones, in contrast *dnm1*Δ expressing hDNM1L iso3 grew as the *dnm1*Δ strain (figure 42). YPD control cultures showed no difference in growth of the different human dynamin expressing yeast strains (figure 42).

In order to reproduce the rescue of *dnm1*Δ by hDNM2 iso1 observed in oxidative stress conditions, I have performed several experiments to measure growth curves with different concentrations of H_2O_2 (figure 43). Unfortunately, these assays using a different batch of H_2O_2 were no reproducible, despite different attempt.

I also tested another oxidative reagent, Paraquat. This reagent is referred as producer of reactive oxygen species (ROS). We hypothesized that since *dnm1*Δ strain was sensitive to H_2O_2, this strain could also be sensitive to other oxidative stresses. However, Paraquat growth test did not show differences between wild type and *dnm1*Δ strains (data not shown).

Due to these technical issues, I decided to focus on the other phenotypes observed for the *dnm1*Δ strain.

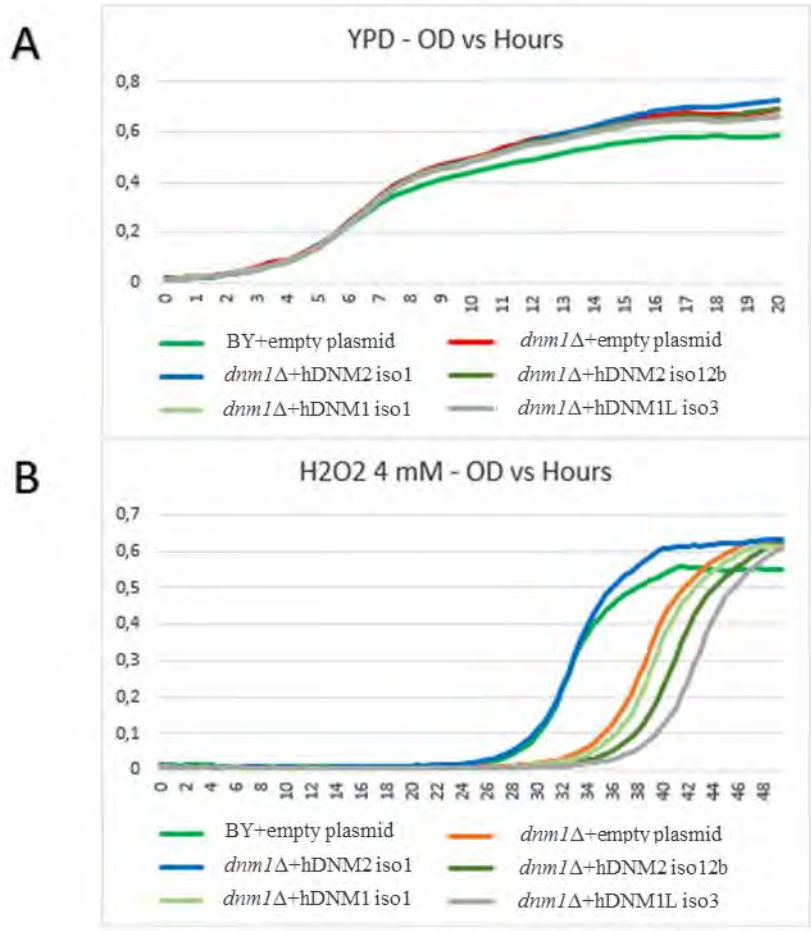

Figure 41: Growth curves of the BY4742, *dnm1*Δ and *dnm1*Δ transformed yeast. (A) YPD liquid culture was carried out as growth control. All the strains grew equally. (B) Yeast grew in YPD + H_2O_2 4 mM. Latency phase was prolonged in all strains but hDNM2 iso 1 transformed dnm1 yeast. The mentioned yeast display a growth pattern similar to wild type (BY4742) strain. X axe represents time in hours while Y axe is optical density.

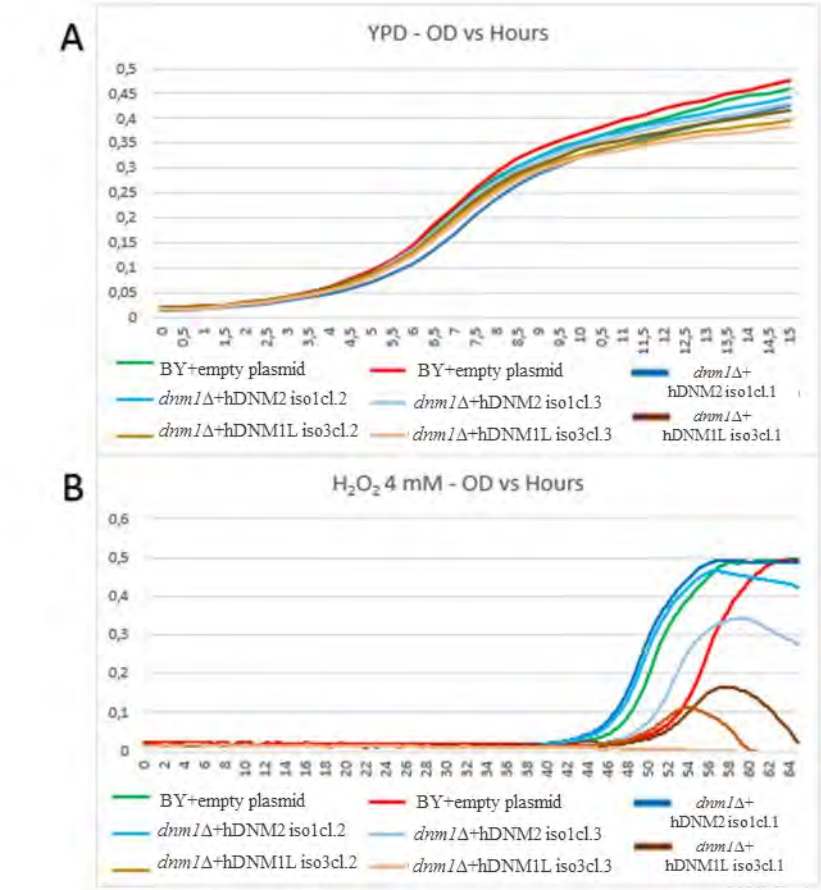

Figure 42: Growth curves of the BY4742, *dnm1*Δ mutant and transformed yeast. 3 clones of *dnm1*Δ yeast expressing hDNM2 iso 1 and hDNM1L iso 3 were used in this experiment. (A) YPD liquid culture was carried out as growth control. All the strains grew equally. (B) Yeast grew in YPD + H_2O_2 4 mM. Latency phase was prolonged in all yeast. hDNM2 iso 1 expressing *dnm1*Δ yeast displayed the same growth pattern that wild type yeast (BY4742). hDNM1L iso 3 displayed mutant dnm1Δ growth pattern.

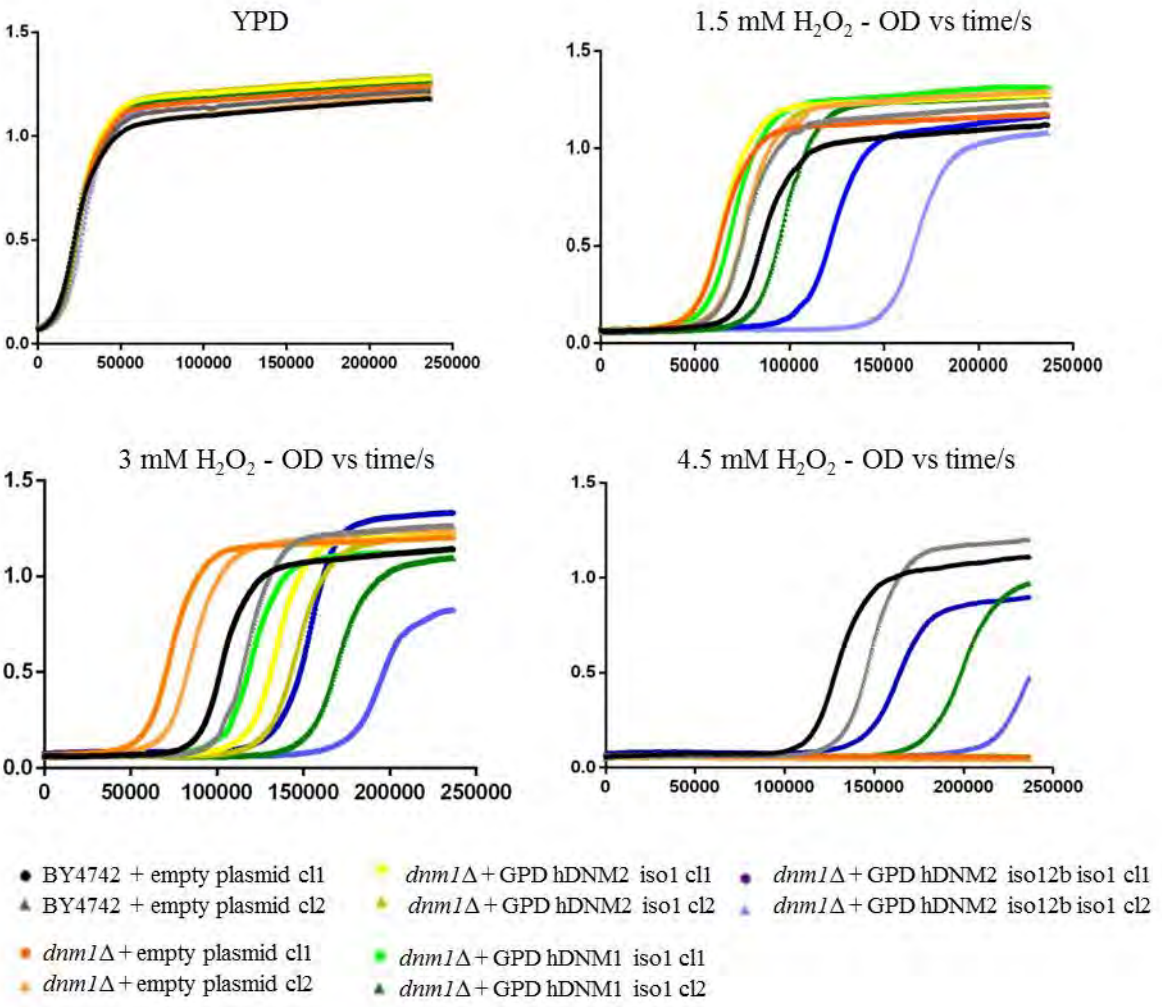

Figure 43: Growth curves of the BY4742, *dnm1*Δ yeast strains expressing different types of dynamin with different H_2O_2 concentrations.

3.2.4.3. Analysis of the mitochondria fission defect of the dnm1Δ strain

The yeast *dnm1*Δ strain is referred as having an abnormal mitochondria network (figure 44). This is the result of the defect in the fission of the mitochondria. If no fission can take place, the wild type mitochondria branched shape turns into a net-like morphology. This effect is only visible if the mitochondria are not repressed. Glucose and mannose-containing media lead to fermentation and repress mitochondria. Galactose-containing medium does not repress mitochondria even though the yeast cells are in fermentation. Ethanol and glycerol-containing media are mitochondria dependent respiration carbon sources (Fendt & Sauer, 2010). To study, mitochondria fission, I used Galactose-containing medium to observe branched mitochondria.

Young cells

Strain	Tubular	Fragmented	Linear	Nets	Large spots
WT BY	65	25	6	1	2
dnm1Δ BY	1	4	16	46	32

Old cells

Strain	Tubular	Fragmented	Linear	Nets	Large spot
WT BY	35	58	0	0	6
dnm1Δ BY	8	1	4	57	31

Figure 44: Schematic representation of mitochondrial morphology in WT and *dnm1*Δ yeast strains. Numbers represent the percentage of a total. Interestingly, the experiment was performed by Scheckhuber and colleagues in order to establish a relation between mitochondria shape and biological ageing. From (Scheckhuber et al, 2007).

Mito-RFP consisted of a fusion protein between RFP (red fluorescent protein) and a mitochondria targeting signal (MTS) in N-terminal. This allows the import of the fluorescent protein into the mitochondria matrix and the staining of the mitochondria network. The *dnm1*Δ strain was transformed with a plasmid bearing the different human dynamins hDNM2 iso1, hDNM2 iso12b, hDNM1 iso1 or hDNM1L iso3 and the mito-RFP plasmid. Yeast cells grown in an YPGal were directly observed under the fluorescence microscope. Wild type strain displayed branched mitochondria while *dnm1*Δ mutant cells had mitochondria net-like structures (figure 45). Expression of the different human dynamins did not rescue *dnm1*Δ mitochondria network organization defect (figure 45). However, the mito-RFP staining was not homogeneous. This could be due to the overexpression of this mito-RFP construct.

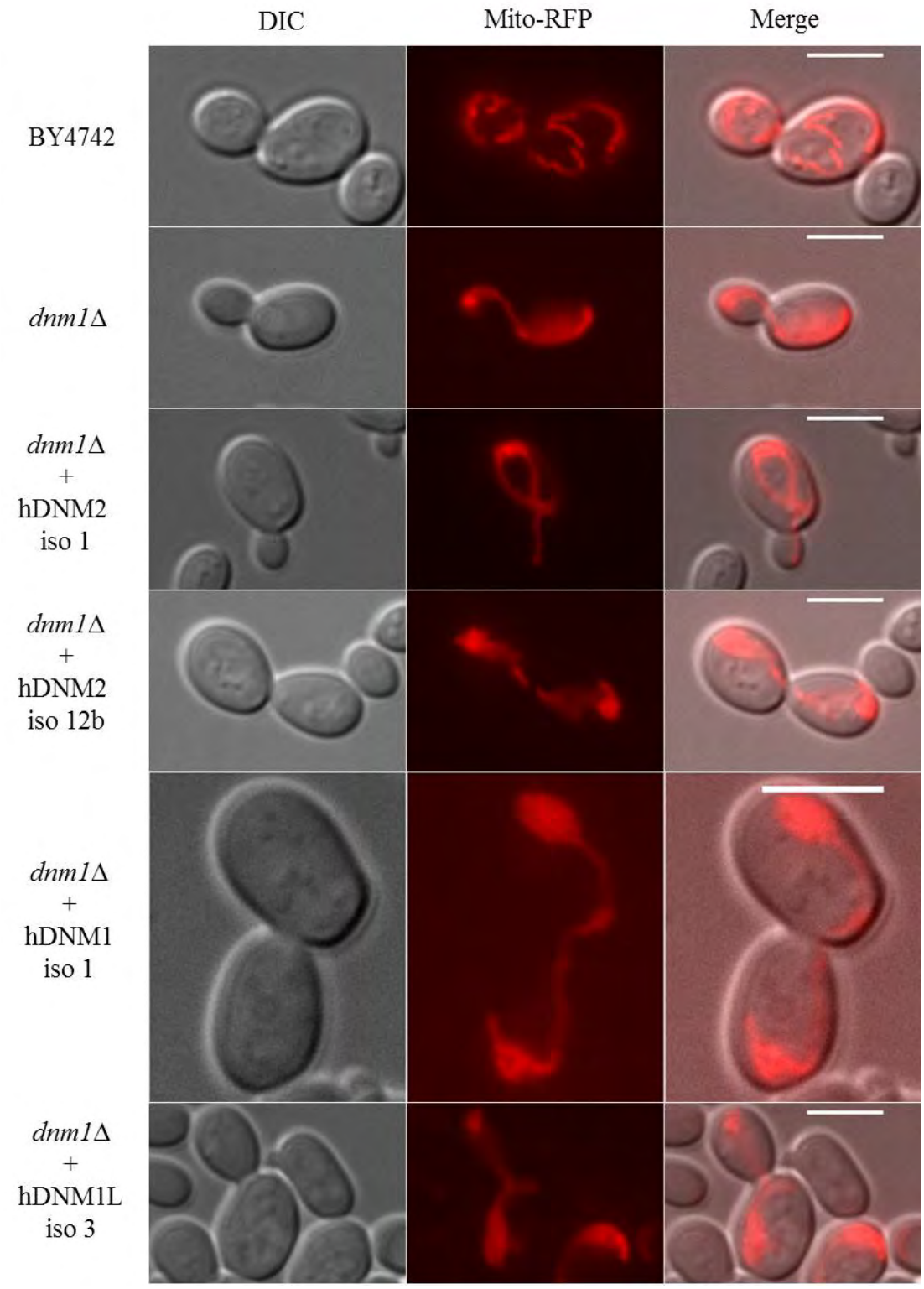

Figure 45: Mitochondria shape highlighted with mito-RFP. Branched mitochondrion was observed in wild type (BY4742) yeast while net-like structures were stated in *dnm1*Δ mutant cells. No mitochondria shape rescue was shown in this experiment as all the transformed yeast shared the same mitochondria net like structure. Yeast was cultured in 2% galactose-containing medium.

As we observed non-homogenous and low rate staining of cells by mito-RFP, we decided to use another technic for mitochondria staining. So we performed the Mitotracker® Red dye staining on

the different yeast cells grown in galactose-containing media. This dye remains in mitochondria membranes with membrane potential.

I analyzed the mitochondria network of *dnm1*Δ strain expressing the different human dynamins under the control of the strong constitutive GPD (glyceraldehyde 3-phosphate dehydrogenase) promoter and compared to the plasmid expressing hDNM2 iso1 under the control of the inducible tetO promoter. This plasmid was constructed by Joelle Morvan, a former postdoctoral in the laboratory, as mentioned in the DNM2 background.

Wild type cells displayed a branched mitochondria network and *dnm1*Δ cells had a net-like phenotype (figure 46). Interestingly, hDNM2 iso1 expressed under the control of the GPD promoter did not rescue the mitochondria phenotype, but hDNM2 iso1 expression regulated by tetO promoter led to the appearance of two populations. One of them displayed partially branched mitochondria while the other displayed a net-like morphology of mitochondria (figure 46, left). For hDNM2 iso12b, no rescue was observed, but hDNM1L iso3 expression led also to two populations. One of them displayed partially branched mitochondria while the other had a dnm1Δ net-like morphology (figure 46, right). It remained clear that hDNM2 iso1 and hDNM1L iso3 expressed under the control of the strong constitutive yeast GPD promoter rescued partially the *dnm1*Δ mitochondria defect. For the hDNM2 iso1 construct, this rescue effect was only observed for the inducible tetO promoter.

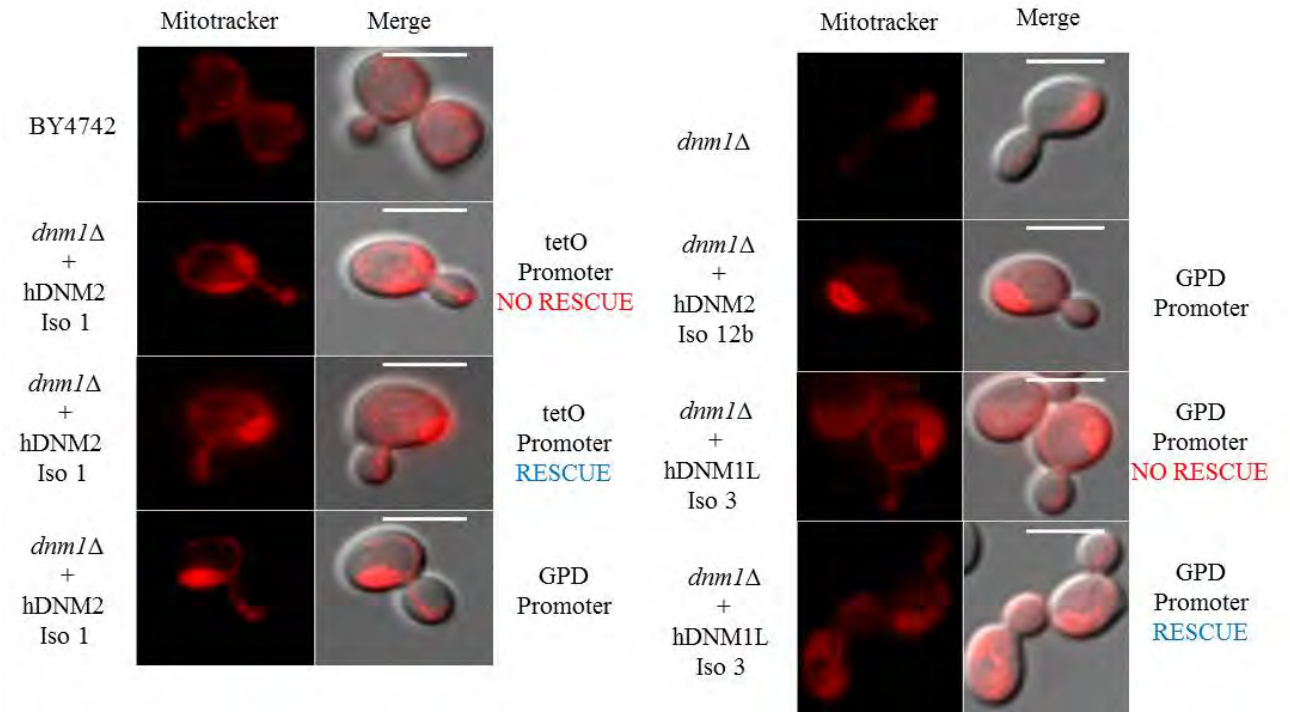

Figure 46: Mitochondria shape determined upon Mitotracker staining. Scale bars represent 5 µm. Merge was carried out with Mitotracker staining and DIC imaging.

In previous researches about hDNM2, the tetO promoter was used for protein expression (figure 29 and 30 in Objectives-Background chapter). Here, I performed all the experiments with plasmids expressing the different human dynamins under the control of a GPD promoter. As shown above, hDNM2 iso1 expression regulated by tetO promoter led to partial rescue of the mitochondria network of *dnm1*Δ strain compared to the results obtained under GPD promoter. Thus, we compared the level of hDNM2 iso1 expression between the plasmids bearing the tetO promoter constructed by J. Morvan and my constructions. I compared the level of expression by analyzing the protein levels with an anti-DNM2 western blot. The results show that the expression level of hDNM2 iso1 is higher for the GPD promoter compared to the tetO promoter (figure 47). Therefore, the expression level of the human dynamins in yeast could be a key point for the phenotyping assays and a low rate level of expression is necessary to study hDNM2 iso1 in yeast cells.

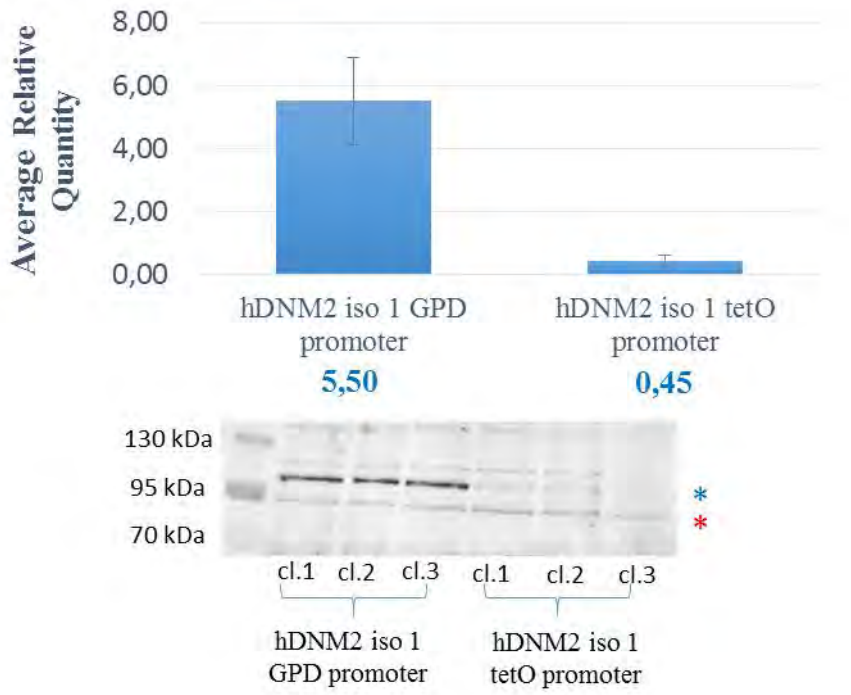

Figure 47: Difference in protein expression between hDNM2 iso1 when using tetO promoter or GPD promoter. Relative protein quantity was determined by a ratio of detected protein (*)/ unspecific band (*) for all the clones used. Average of the relative protein amount of three clones of each construction. GPD promoter clearly increased protein expression. Error bars are standard deviation.

3.2.5. Study of hDNM2 iso1-EGFP localization in yeast cells

Control of the human dynamin expression level is a key factor for the study of hDNM2 iso1 in yeast. Thus, I performed an experiment to analyze the localization of EGFP (enhanced green fluorescent protein) tagged human dynamins in yeast cells. I also co-stained the mitochondria

network of wild type (BY4742), *dnm1*Δ and *vps1*Δ expressing the EGFP tagged human dynamins. The transformed yeast cells were grown in galactose-containing media and Mitotracker® Red staining was carried out, prior observation under the microscope.

In the 3 different yeast strains, EGFP tagged hDNM2 iso1 and iso12b were localized in one or two dots at the top of mitochondria network. The hDNM1 iso1 and hDNM1L iso3 human dynamins were mainly detected in the cytosol, with some rare dots (figures 48, 49 and 50). The mitochondria staining show that expression of hDNM1L-EGFP in wild type (BY4742) and *vps1*Δ yeast induced a *dnm1*Δ mutant like defect in the mitochondria network. This mitochondrion phenotype was not observed for hDNM2 iso1, hDNM2 iso12b and hDNM1 iso1 human dynamins (figure 48, 49 and 50). hDNM1L iso3-EGFP displayed a probable dominant negative effect on wild type and *vps1*Δ cells.

The *dnm1*Δ mitochondria phenotype was not rescued by expression of hDNM2 iso1-EGFP, hDNM2 iso12b-EGFP or hDNM1 iso1-EGFP, but a partial recovery was observed for hDNM1L iso3-EGFP (figure 49).

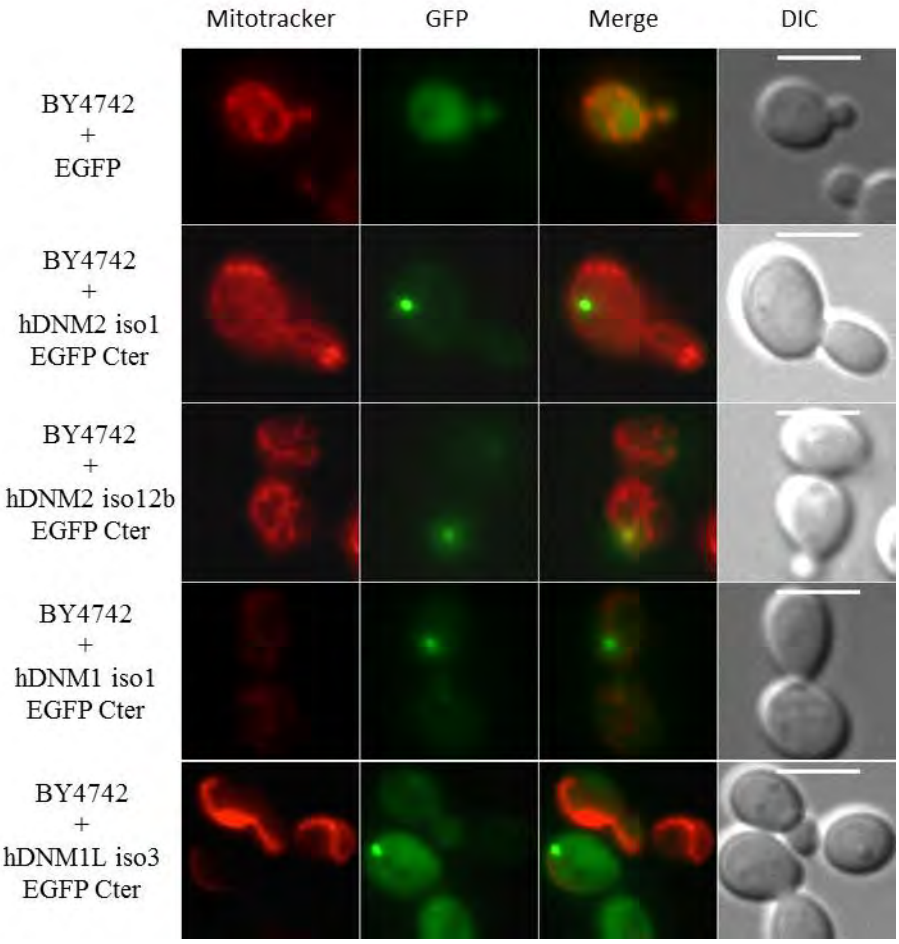

Figure 48: Wild type mitochondria shape is shown in all wild type transformants but not hDNM1L iso 3 - EGFP transformants. These transformants display a *dnm1*Δ mutant like mitochondria. Merged images show a colocalization between mitochondria and EGFP tagged proteins. Cells were grown in 2% galactose-containing medium. Scale bar represents 5 µm.

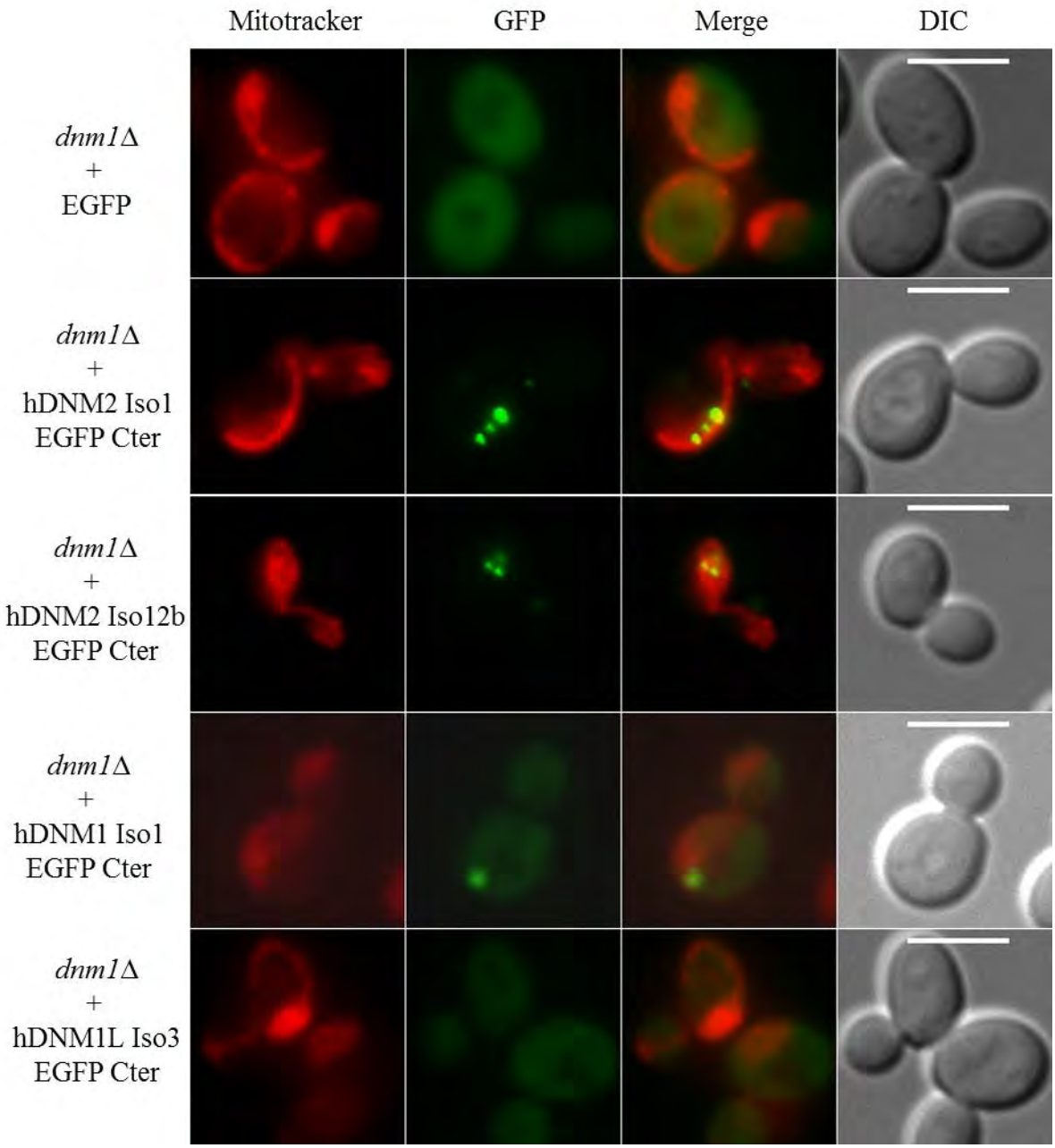

Figure 49: *dnm1*Δ net like mitochondria shape is also present in transformed cells. No recovery is observed with exception of a part of hDNM1L iso 3- EGFP transformed cells. Only the cells expressing significantly a higher rate of hDNM1L iso 3- EGFP display the wild type mitochondrion shape. Cells were grown in 2% galactose-containing medium. Scale bar represents 5 µm.

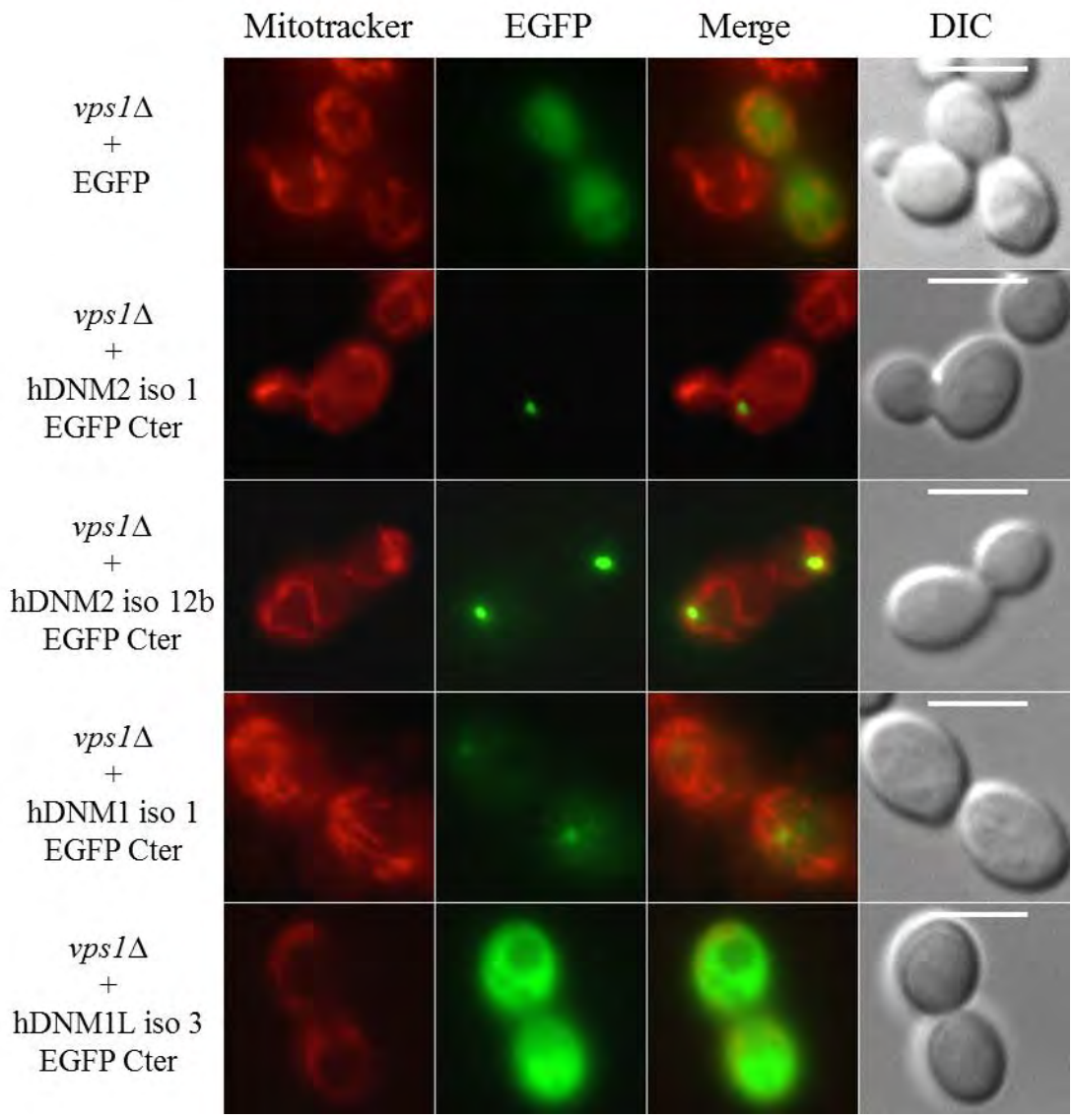

Figure 50: Mitochondria morphology is observed with Mitotracker ® Red staining. *vps1*Δ yeast displayed a wild type mitochondria shape. Only *vps1*Δ transformed with hDNM1L iso 3- EGFP displayed a *dnm1*Δ-like mitochondrion. hDNM2 iso 1 and iso 12b were present in a dot while hDNM1 iso 1 and hDNM1L iso 3 remained mainly cytosolic. hDNM2 dots colocalized with mitochondria. Scale bars represent 5 µm.

3.2.6. Conclusion about the different phenotypic rescue experiments

Before proceeding further, I think it is better to clarify the reasons of our experiments. Until here, we have tried several experiments to establish the phenotype of the *vps1*Δ or *dnm1*Δ mutant yeast cells, in order to find a phenotypic rescue upon expression of the human dynamins. In the literature Vps1 is associated with trafficking and Dnm1 with mitochondria dynamics. We have performed several experiments, such as mitochondria and peroxisomes observation by microscopy, membrane

trafficking analyses by CPY secretion, milk plate halo assays or metal toxicity tests and growth in different carbon sources or upon an oxidative stress.

In view of the disappointing results with no rescue, or a rescue that could not be reproduced once the H_2O_2 batch was changed (even with 2 different batches of H_20_2 from different suppliers), I had two options:

- First abandon the study of the human dynamins by humanization of yeast cells and conclude that yeast is not a good model for this specific project. This would have been an easy and tempting option…but not very rewarding.
- Second, keep thinking that yeast is a good model to study human dynamins, but question what was possible to study and what was not. At the same time, I also realized that the possibilities in yeast are huge and the problem is not yeast but us who perhaps do not have all the necessary knowledge or the vision to use it in the best way to study the human DNM2 dynamin.

So, in my opinion, this second option was more interesting and it allowed me to look for other alternatives. Therefore, I tried new experiments and even though I did not expect them to give only positive results, at least they will enlarge our knowledge about yeast and dynamins; what in my opinion was exciting and fascinating, so worse tenting. Therefore, this second option was for me the only way to open new horizons in my researches. On this basis, I am going to explain the last experiments, I did concerning this project of humanization of yeast cells with human dynamins.

3.2.7. Connecting Dnm1 dynamin with oxidative stress and calcium signaling in yeast

Mutations in *DNM2* are also associated to impairment of calcium homeostasis. Indeed, the CNM Dnm2-R465W KI model mice had a higher cytosolic concentration of Ca^{2+} in EDL muscle, an increase of the sarcolemmal permeability to Ca^{2+} and a higher sarcoplasmic reticulum Ca^{2+} content in EDL contrary to the soleus muscle fibers (Fraysse et al, 2016). Interestingly, no differences in calcium homeostasis were observed between the soleus muscle from Dnm2-R465W KI and wild type mice. Fraysse and colleagues suggested that the plasma membrane permeability could be at the origin of these calcium alterations observed in the Dnm2-R465W KI mice, and that sarcoplasmic reticulum SR would compensate the increase calcium concentration in cell by taking calcium from cytosol (Fraysse et al, 2016). In conclusion, CNM mutations in *DNM2* could be associated to

impaired endocytosis of the calcium channels and consequently result in increased calcium uptake in cell.

Oxidative misregulation is a common feature observed in several myopathies. For example, the CNM-like early-onset myopathy, which I also studied, was due to mutations in the *PYROXD1* gene that encodes an oxidoreductase (O'Grady et al, 2016). The SEPN1-related myopathy involving the Selenoprotein N (SelN) is also linked to oxidation-reduction reactions and a calcium homeostasis imbalance was also detected in this myopathy (Castets et al, 2012).

In yeast *Saccharomyces cerevisiae*, the absence of the glutaredoxin Grx6 causes constitutive calcium stress (figure 33 and 34) (Puigpinos et al, 2015). Grx6 is a thiol oxidoreductase found at the ER membrane and the calcineurin pathway is activated in response to alterations in intracellular Ca^{2+} and to high environmental concentrations of cations such as Ca^{2+} or Na^{2+}. As shown in figure 34 in introduction, the calmodulin/Ca^{2+} complex activates the phosphatase calcineurin, which in turns dephosphorylates the Crz1 transcription factor, allowing its import to the nucleus. Crz1 targets promoter elements with the CDRE motif (calcineurin-dependent response element). Puigpinos and colleagues observed that expression from a Crz1-dependent promoter was constitutively up-regulated in the absence of Grx6 (figure 51) (Puigpinos et al, 2015). For this experiment they used two lacZ reporter plasmids containing either wild-type CDRE promoter (pAMS366) or mutated CDRE promoter (pAMS364).

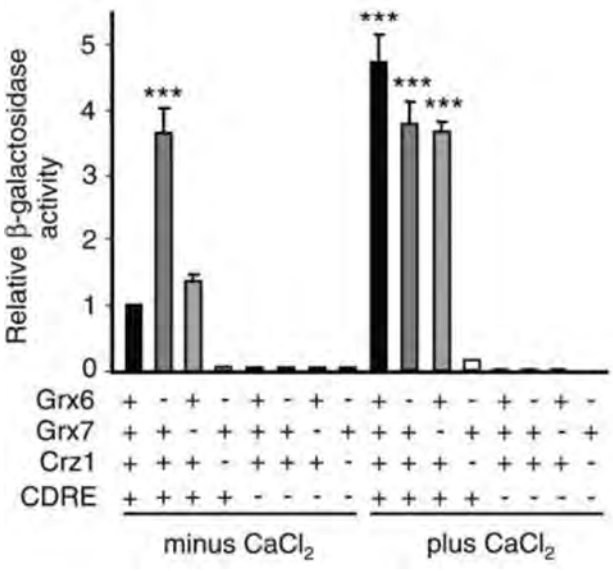

Figure 51: Calcineurin pathway–dependent gene expression in strains lacking Grx6 or Grx7. (A) Wild-type (W303-1A), *grx6Δ*, *grx7Δ*, and *grx6Δ crz1Δ* cells were transformed with the *lacZ* reporter plasmid bearing a functional (+) or nonfunctional (–) CDRE motifs. Yeast cells were exponentially grown in SC medium without or with added (0.2 M, 60 min) $CaCl_2$. β-Galactosidase activity was determined in three independent experiments. Bars indicate the mean ± SD, made relative to the unit value corresponding to pAMS366 transformed with type cells from SC medium without added $CaCl_2$. These conditions were used as reference for statistical analyses with the Mann–Whitney *U* test. From (Puigpinos et al, 2015).

The idea for the new experiments was to establish a phenotype for *dnm1*Δ cells related to calcium homeostasis under oxidative stress as observe in the figure 51. For that, I asked for plasmids pAMS364 and pAMS366, which were gently provided by Enrique Herrero.

The calcineurin signaling pathway as tested by using the CDRE-dependent β-galactosidase assay on wild type BY4742, the *grx6*Δ and the *dnm1*Δ mutant strains (figure 52). No oxidative stress was applied for the moment, since the first objective was to establish whether there were phenotypic differences between these 3 strains in normal conditions. The β-galactosidase was performed on these 3 strains expressing the functional or non-functional CDRE motif and β-galactosidase activity was calculated by the Miller's formula.

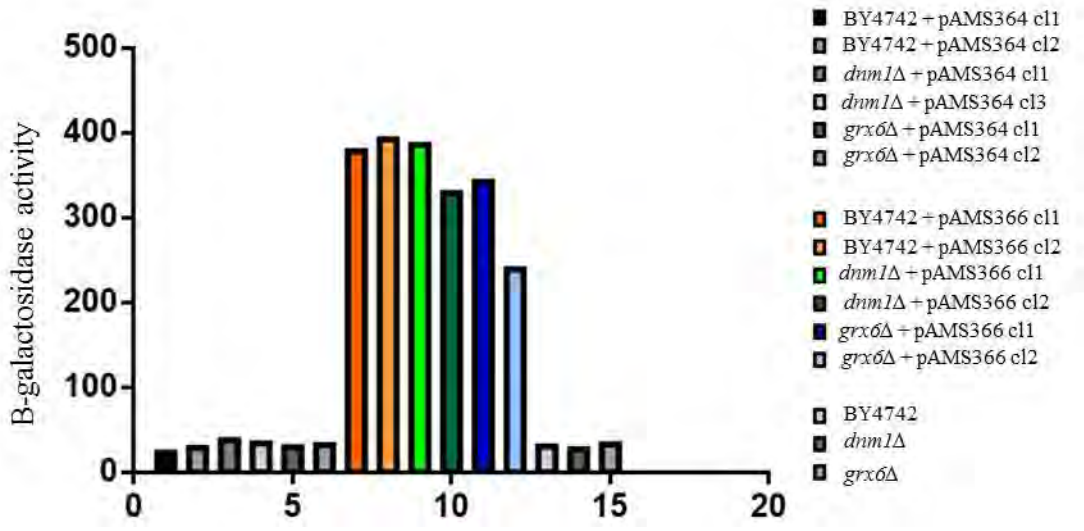

Figure 52 : Calcineurin pathway–dependent gene expression in Wild-type (BY4742), *grx6*Δ and *dnm1*Δ cells were transformed with the *lacZ* reporter plasmid bearing a functional (pAMS366) or nonfunctional (pAMS364) CDRE motifs. Yeast cells were exponentially grown in YPD rich medium. β-Galactosidase activity was determined in two different clones.

Unfortunately, in my assay, I could not reproduce the results of Puigpinos and colleagues showing an upregulation of the CDRE pathway in the absence of Grx6 (figure 51 and 52) (Puigpinos et al, 2015). Therefore, I tested whether the *grx6*Δ mutant strain was sensitive to oxidative stress to validate my mutant strain. The growth test assays show that the *grx6*Δ mutant strain did not grow in presence of an H_2O_2 oxidative stress (as described in the PYROXD1 chapter). Therefore, the *grx6*Δ mutant strain that I used and that is in the BY4742 background is validated, and the reason for this different phenotype could be the culture conditions. Indeed, I grew my cells in rich YPD medium, whereas Puigpinos and colleagues used minimal synthetic medium.

Another reason to explain these different results could be that Puigpinos and colleagues have used as wild type another strain than the BY4742 yeast strains. I used BY4742 because it is the wild-type reference for the *dnm1*Δ mutant strain. Indeed, they have used the *grx6*Δ strain constructed in the W303-1A background. This W303-1A strain has a mutation in the *YBP1* gene, which abolishes its function required for oxidation of specific cysteine residues of Yap1 transcription factor, increasing

its sensitivity to oxidative stress (SGD database). Therefore, I should also analyze the oxidative stress response in the *grx6*Δ and the *dnm1*Δ deletion mutant strains constructed into the W303-1A background.

Unfortunately, due to time constraint, I could not continue this analysis by doing different assays with different strains and in different medium

3.2.8. Discussion on DNM2 humanization of yeast cells

A summary of the experiments performed during this DNM2 project is indicated in table 5. We have used two yeast strains: *vps1*Δ and *dnm1*Δ. Vps1 and Dnm1 are two yeast dynamin-related proteins, orthologues of human dynamins. Specifically, Vps1 was described as being the homologue of hDNM1 and Dnm1 as homologous to hDNML1 (also called DRP1 or DLP1). However, our results complementation assays suggest these yeast proteins are not functional homologues of the human dynamins. This result was unexpected since Vps1 and Dnm1 fulfill similar roles in yeast to that of human dynamins. For example, Dnm1 is involved in mitochondria fission as does hDNM2 in human cells (Lee et al, 2016). However, based on the mitochondria staining of *dnm1*Δ expressing or not the human hDNM2 iso1, hDNM2 iso 12b, hDNM1 iso1, or hDNM1L iso3, human dynamins do not rescue the characteristic branched/tubular mitochondrial phenotype of wild type yeast cells. Even though, the mitotracker staining of mitochondria done on *dnm1*Δ cells transformed with hDNM1L iso3 under GPD promoter presented two phenotypes in population, one of them showing complementation. Interestingly, mitotracker staining done on *dnm1*Δ cells expressing hDNM2 iso1 under TetO promoter, also showed some rescue. Unfortunately, this complementation is not strong enough to be used for screening CNM patient mutations phenotypes. These experiments were carried out on cells transformed with plasmids bearing the human dynamin cDNA under the control of two different promoters, so not under the control of a dynamin promoter nor integrated into the genome. GPD is a strong constitutive yeast promoter, whereas TetO promoter is a regulatable promoter (Blazeck et al, 2012; Yen et al, 2003). Indeed, the expression level of hDNM2 iso1 in *dnm1*Δ cells was 12 times higher for the GPD promoter compared to the TetO promoter. This high level expression of hDNM2 could affect to its cellular function in cells. Indeed, the expression level of hDNM2 iso1 is highly controlled in human cells and the *Mtm1* KO mice are rescued by lowering the expression level of hDNM2 (Tasfaout et al, 2017). Further experiments should be carried out with TetO promoter in order to have lower levels of expression of human dynamins or with plasmids allowing the human dynamin cDNA to be

integrated into the yeast genome at the *DNM1* or *VPS1* locus for a endogenous expression of human dynamins in yeast cells.

The mitochondrion morphology analysis done on *vps1*Δ strain show that these mutant cells have a wild type phenotype. Interestingly, wild type and *vps1*Δ mutant cells expressing high levels of GFP tagged hDNM1L iso3, under the control of the GPD promoter had an abnormal mitochondria network, with a dnm1Δ-like mitochondria phenotype. This suggests a probable dominant effect of hDNM1L iso3 these yeast cells.

Interestingly, the intracellular localization of the 3 analyzed human dynamins tagged with GFP and observed in the three *vps1*Δ, *dnm1*Δ and BY4742 yeast strains presented almost the similar pattern, that is, some dots on mitochondria, even though there were some differences. In *dnm1*Δ cells, GFP tagged hDNM2 iso1 and iso 12b presented several dots on mitochondria whereas hDNM1 iso1 showed less number of dots at mitochondria and hDNM1L iso3 was mainly cytosolic. In *vps1*Δ cells there was a big difference between hDNM1L iso3 expression and the other three dynamins; specifically hDNM1L iso3 displayed a clearly cytosolic pattern whereas hDNM1, hDNM2 iso1 and hDNM2 iso 12b showed single dots located at mitochondria. This is really surprising since hDNM1L iso3 is supposed to be the counterpart of Vps1 and its expression induced a dominant mitochondria defect in the *vps1*Δ cells. The question is how the hDNM1L protein that is mainly cytosolic and not present at the mitochondrial membrane, is able to accomplish its role at the mitochondria to induce a dnm1-like abnormal mitochondria phenotype? It would be interesting to perform subcellular fractionation experiments in order to identify and quantify the hDNM1L dynamin present in membrane (mitochondria membrane) and cytosolic fractions.

The *dnm1*Δ strain is characterized by a mitochondria fission defect, leading to an abnormal mitochondrial network while grown in galactose-containing medium. Defects in mitochondria morphology can result in mitochondrial dysfunction, leading to a pathological accumulation of ROS and consequently the dissipation of the mitochondrial membrane potential (Muller et al, 2015). Increase of oxidative stress and loss of membrane potential favor mitophagy.

vps1Δ strain							
		transformed with					BY4742 (WT)
Experiments	No transformed	Empty plasmid	hDNM2 iso1	hDNM2 iso 12b	hDNM1 iso 1	hDNM1L iso3	
Metal toxicity (drop test)							
CdCl2 20 - 30 µM	sensitive	sensitive	sensitive	sensitive	sensitive	sensitive	resistant
NiCl2 5mM	resistant						sensitive?
Peroxisome fission defect (microscopy)		1- 2/cell	1- 2/cell	1- 2/cell	1- 2/cell	1- 2/cell	3 - 5/cell
lipid droplets		no changes	no changes	no changes	no changes	no changes	no changes
Respiration (drop tests)							
Glycerol	sensitive						sensitive
Ethanol 6%	no sensitive						no sensitive
Mitochondria morphology (microscopy)							
Mitotracker	as WT	as WT	as WT	as WT	as WT	dnm1Δ-like mitochondrion	branched/ tubular
GFP tagged protein		cytosolic	dots at mitochondria	dots at mitochondria	mainly cytosolic	cytosolic	(info figure 15)

dnm1Δ strain							
		transformed with					BY4742 (WT)
Experiments	No transformed	Empty plasmid	hDNM2 iso1	hDNM2 iso 12b	hDNM1 iso 1	hDNM1L iso3	
Metal toxicity (drop test)							
CdCl2 30 µM	resistant						resistant
NiCl2 5mM	sensitive ?						sensitive?
Respiration (drop tests)							
Glycerol	sensitive						sensitive
Ethanol 6%	no sensitive						no sensitive
Shock temperature (drop test)							
30 - 50 °C	as WT						
37 - 50 °C	as WT						
Mitochondria morphology (microscopy)							
Mito-RFP	net-like and spots	net-like and spots	net-like and spots	net-like and spots	net-like and spots	net-like and spots	branched/ tubular
Mitotracker	net-like	net-like	Some cells rescue when TetO prom.	net-like	net-like	Some cells rescue when GPD prom.	branched/ tubular
GFP tagged protein		cytosolic	dots at mitochondria	dots at mitochondria	dots and cytosolic	cytosolic	(info figure 15)
Oxidative stress H2O2							
Drop tests	6 mM H2O2 sensitive	3 mM H2O2 sensitive	3 mM H2O2 perhaps rescue	3 mM H2O2 no rescue	3 mM H2O2 no rescue	3 mM H2O2 no rescue	3 - 6 mM H2O2 sensitive
Growth curves			4mM H2O2 similar to wt	Latency time longer than wt	Latency time longer than wt	Latency time longer than wt	
			1.5 mM to 4.5 mM H2O2 no reproductibility figs 9, 10	1.5 mM to 4.5 mM H2O2 no reproductibility figs 9, 10	1.5 mM to 4.5 mM H2O2 no reproductibility figs 9, 10	1.5 mM to 4.5 mM H2O2 no reproductibility figs 9, 10	

Table 5 : Summary of experiments done in DNM2 project using *S. cerevisiae* yeast. The experiments about β-galactosidase activity are not included, neither the experiments done before my PhD thesis by the postdoctoral Jöelle Morvan.

We have performed H_2O_2 stress assays using the *dnm1*Δ cells expressing or not the human dynamins to observe the sensitivity of this mutant strain to oxidative stress. Interestingly, in normal conditions (YPD media) both wild type and *dnm1*Δ transformed or not with human dynamins expression plasmids, displayed similar growth curves. In the oxidative stress conditions, there is an extension of the latency phase for the *dnm1*Δ mutant cells, but the slopes of the curves are the same. This suggests that *dnm1*Δ mutant cells have a delay in adaptation to stress conditions. This could be due to a delay in the cytosol and mitochondria redox pathways mediated by the glutathione-NADH oxidoreductase in the *dnm1*Δ cells. It would be interesting to do the same experiment but with adding the H_2O_2 in media when cells are in the exponential phase to see whether the *dnm1*Δ cells respond differently to oxidative stress. Another interesting experiment would be the visualization of H_2O_2 by staining the cells with dihydro-rhodamine, an uncharged and non-fluorescent reactive oxygen species (ROS) indicator (Scheckhuber et al, 2007); the mitochondrial membrane potential could also be stained by using $DiOC_6$. These two dyes are selective for the mitochondria and measuring their signal intensity would allow to study the *dnm1*Δ expressing or not with the human dynamins. Interestingly, we could observe a rescue of the *dnm1*Δ cells expressing hDNM2 iso1 in presence of 4 mM H_2O_2, on plate and with the spectrofluorimeter. Unfortunately, since these results were no reproducible, I cannot conclude on this.

The *vps1*Δ mutant cells have membrane trafficking defects, with a delayed vacuolar protein sorting pathway leading to cadmium sensitivity as observed in drop tests (Ruotolo et al, 2008). However, there was no rescue of the *vps* phenotype by human dynamins. The other assays related to membrane trafficking were performed by the postdoctoral Joelle Morvan before I have started with this project during my PhD thesis. These tests consisted in CPY test and milk assays and there was no rescue by the human DNM2 iso1, even so its expression was under the regulatable TetO promoter, so without a strong overexpression.

The peroxisome number defect observed in the *vps1*Δ cells was not complemented by the expression of the tested human dynamins, not even the hDNM1L, which plays a key role in peroxisome biogenesis in human cells. This absence of rescue could be due because the human peroxisomal division requires Mff protein for hDNM1L targeting to the peroxisomes, while yeast cells do not have Mff homologues and use other adaptors (Schrader et al, 2016).

Interestingly, by analyzing the results of the peroxisome staining we have realized that hDNM2 iso12b seemed to have an effect on the vacuolar size and form. The *vps1*Δ mutant cells have abnormal fragmented vacuoles, even though the mechanisms remain poorly understood. In order to further characterize this vacuolar phenotype, vacuolar staining should be done by using FM4-64® or CellTracker™ blue CMAC dyes that specifically stain the vacuoles and were used to study the

human MTM1 induced vacuolar phenotype in yeast cells. A possible vacuole rescue would show that the differences in amino acids sequences between hDNM2 isoforms 1 and 12b can led to their implication in different pathways.

3.3. PYROXD1 is an oxidoreductase implicated in a CNM-like myopathy

PYROXD1 (pyridine nucleotide-disulphide oxidoreductase [PNDR] domain-containing protein 1) is a new causative gene implicated in early-onset myopathies characterized by nuclei located at the centre of muscle cells instead at the periphery. It has been identified by exome sequencing in nine probants from five families by an international laboratory consortium between Australia, France, Turkey and United States; coordinated by Sandra T. Cooper (Australia) and Jocelyn Laporte (France). Two missenses mutations were detected as the cause of the disorder, namely Gln372His and Asn155Ser. However the activity of this protein had not been tested before. Therefore, Jocelyn Laporte contacted Sylvie Friant to participate in this project and my role was:

- First, to define the activity of this new protein using as a model the yeast *Saccharomyces cerevisiae*
- Second, to test the impact of these two patient mutations in the protein activity.

My yeast data were included in an article that I have signed as second co-author and that was published in 2016 in the American Journal of Human Genetics.

3.3.1. Humanizing yeast with human PYROXD1

In order to test the redox activity of the human PYROXD1 in yeast, I had to consider the redox system in *Saccharomyces cerevisiae.* As mentioned in the Introduction, the glutaredoxins (GRX) and thioredoxin (TRX) systems are two overlapping oxidoreductase pathways sharing some enzymes in yeast. They work to maintain the redox balance catalyzing the reduction of oxidized proteins in cell (see figures 32 and 33 in Introduction).

In the first experiments, I have established a complementation assay in the yeast strain lacking the *GLR1* gene. Yeast has two isoforms of the glutathione reductase Glr1, one at the cytosol and other at the mitochondria. Glr1 participates to the GRX system activity by reducing the glutathione GSSG

in GSH. During my experiments, the *glr1*Δ mutant cells were transformed with yeast plasmids expressing GFP-tagged or non-tagged human PYROXD1 cDNA, either wild type, or bearing the patient mutations: Q372H or N155S. First, their expression in yeast was verified by western blot with a specific antibody for PYROXD1. The figure 3 of the article includes the western blot of the non-tagged plasmids and the drop test of GFP-tagged plasmids. Second, in order to determine the localization of human PYROXD1 in yeast cells, I have observed the transformed yeast cells expressing the different the GFP-tagged PYROXD1 constructions (Fig. 3D, article). The PYROXD1-GFP wild type and the patient mutant forms PYROXD1-Q372H and PYROXD1-N155S have a similar localization with a cytoplasmic staining and also a lower signal in the nucleus, as observed for PYROXD1 staining in COS7 cell cultures (Fig. 6). I also did a western-blot to verify the expression of the GFP tagged PYROXD1 constructs, this western blot is shown after the publication (figure 53). The wild type PYROXD1 and the two patient mutant forms are all detected in the yeast protein extracts, showing that the patient mutations do not impair the expression of the PYROXD1 cDNA, or result in protein instability (figure 53).

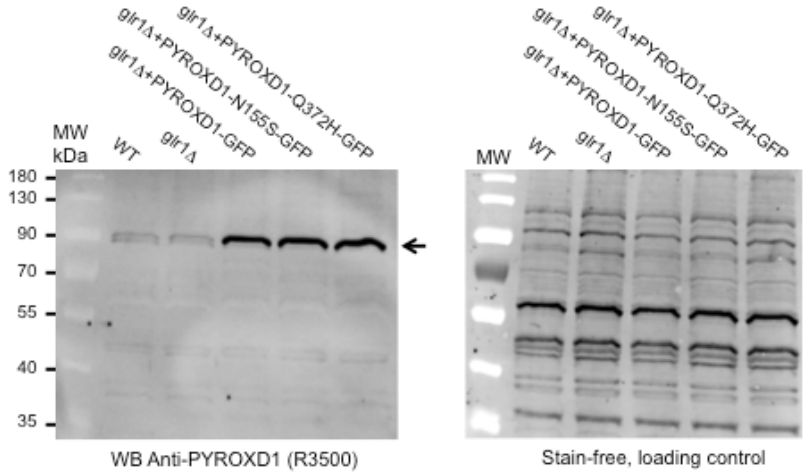

Figure 53: Western blot of non-transformed wild-type (WT) and *glr1*Δ, as well as *glr1*Δ yeast transformed with PYROXD1 GFP tagged expression vectors. The black arrow indicates the PYROXD1-GFP and the stain-free total protein staining is used as loading control.

Grx6 is a yeast glutarexodin that protects the cell against oxidative stress due to ROS (Herrero et al, 2008). Grx6 catalyzes the reduction of protein disulfide or glutathione-protein mixed disulfide bound using a system coupled with glutathione, NADPH and glutathione reductase such as Glr1. The reduced glutathione GSH acts as hydrogen donor and glutathione reductase uses electrons from NADPH to regenerate the oxidized glutathione (GSSG) (figures 32 and 33) (Herrero et al, 2008).

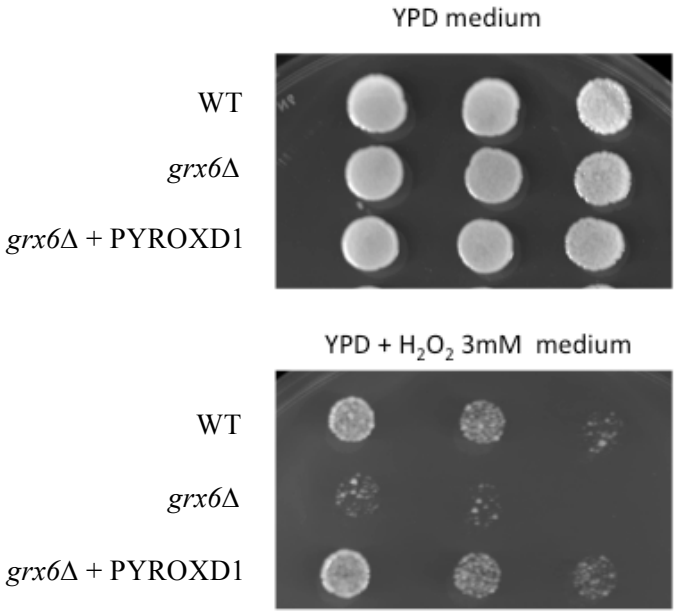

Figure 54: Drop-test assays of wild-type (WT) and *grx6*Δ, as well as *grx6*Δ yeast transformed with PYROXD1 expression vector. The strains were grown in rich YPD medium and in presence of an H_20_2 oxidative stress.

The *grx6*Δ mutant cells show imbalance in Ca^{2+} homeostasis with Ca^{2+} accumulation in the cytosol and Ca^{2+} depletion at the ER lumen (Puigpinos et al, 2015). This calcium phenotype linked to an oxidoreductase activity is very interesting since calcium is required for muscle function; therefore I also used the *grx6*Δ mutant strain for humanization studies with PYROXD1. Since, I could not reproduce the results of Puigpinos and colleagues showing an upregulation of the CDRE pathway in the absence of Grx6 (Puigpinos et al, 2015), I tested whether the *grx6*Δ mutant strain was sensitive to oxidative stress to validate my mutant strain. The growth test assays show that the *grx6*Δ mutant strain did not grow in presence of an H_2O_2 oxidative stress (figure 54). Interestingly, expression of the human PYROXD1 complemented this H_2O_2 sensitivity, showing that human PYROXD1 acts as an oxidative stress protective protein in yeast cells (figure 54).

Future experiments will be done using yeast cells to test a new PYROXD1 patient mutation that was identified in the laboratory of Sandra Cooper (Australia). Other yeast strains bearing deletions in the yeast redox pathway (grx, trx, trr strains, figure 32 and 33) will be tested for complementation by PYROXD1, to determine which pathways can be rescued, and what are the rescuing limits of the human enzyme expressed in yeast cells. These yeast studies will help to better understand the cellular and molecular functions of the human PYROXD1 enzyme.

ARTICLE

Variants in the Oxidoreductase PYROXD1 Cause Early-Onset Myopathy with Internalized Nuclei and Myofibrillar Disorganization

Gina L. O'Grady,[1,2,3,25] Heather A. Best,[1,2,25] Tamar E. Sztal,[4,25] Vanessa Schartner,[5,26] Myriam Sanjuan-Vazquez,[6,26] Sandra Donkervoort,[7,26] Osorio Abath Neto,[5] Roger Bryan Sutton,[8] Biljana Ilkovski,[1] Norma Beatriz Romero,[9,10] Tanya Stojkovic,[10] Jahannaz Dastgir,[7] Leigh B. Waddell,[1] Anne Boland,[11] Ying Hu,[7] Caitlin Williams,[4] Avnika A. Ruparelia,[4] Thierry Maisonobe,[10] Anthony J. Peduto,[12] Stephen W. Reddel,[13] Monkol Lek,[14,15] Taru Tukiainen,[14,15] Beryl B. Cummings,[14,15] Himanshu Joshi,[1] Juliette Nectoux,[16,17] Susan Brammah,[18] Jean-François Deleuze,[11] Viola Oorschot Ing,[19] Georg Ramm,[19,20] Didem Ardicli,[21] Kristen J. Nowak,[22] Beril Talim,[21] Haluk Topaloglu,[21] Nigel G. Laing,[22] Kathryn N. North,[1,23] Daniel G. MacArthur,[14,15] Sylvie Friant,[6] Nigel F. Clarke,[1,2] Robert J. Bryson-Richardson,[4] Carsten G. Bönnemann,[7] Jocelyn Laporte,[5,24,27] and Sandra T. Cooper[1,2,27,*]

This study establishes *PYROXD1* variants as a cause of early-onset myopathy and uses biospecimens and cell lines, yeast, and zebrafish models to elucidate the fundamental role of *PYROXD1* in skeletal muscle. Exome sequencing identified recessive variants in *PYROXD1* in nine probands from five families. Affected individuals presented in infancy or childhood with slowly progressive proximal and distal weakness, facial weakness, nasal speech, swallowing difficulties, and normal to moderately elevated creatine kinase. Distinctive histopathology showed abundant internalized nuclei, myofibrillar disorganization, desmin-positive inclusions, and thickened Z-bands. PYROXD1 is a nuclear-cytoplasmic pyridine nucleotide-disulphide reductase (PNDR). PNDRs are flavoproteins (FAD-binding) and catalyze pyridine-nucleotide-dependent (NAD/NADH) reduction of thiol residues in other proteins. Complementation experiments in yeast lacking glutathione reductase *glr1* show that human PYROXD1 has reductase activity that is strongly impaired by the disease-associated missense mutations. Immunolocalization studies in human muscle and zebrafish myofibers demonstrate that PYROXD1 localizes to the nucleus and to striated sarcomeric compartments. Zebrafish with *ryroxD1* knock-down recapitulate features of PYROXD1 myopathy with sarcomeric disorganization, myofibrillar aggregates, and marked swimming defect. We characterize variants in the oxidoreductase *PYROXD1* as a cause of early-onset myopathy with distinctive histopathology and introduce altered redox regulation as a primary cause of congenital muscle disease.

Introduction

Myopathies are a group of genetically heterogeneous conditions characterized by muscle weakness, with overlap in the clinical presentation and histopathological features of different genetic subtypes.[1] Within this group, congenital myopathies are most commonly characterized by hypotonia and weakness, often from birth, commonly with the presence of facial weakness, with or without ptosis and ophthalmoplegia. There are 25 recognized genetic causes of congenital myopathy (see GeneTable in Web Resources); currently a genetic diagnosis is achieved in only ~50% of

[1]Institute for Neuroscience and Muscle Research, Kid's Research Institute, Children's Hospital at Westmead, Sydney, NSW 2145, Australia; [2]Discipline of Paediatrics and Child Health, Faculty of Medicine, University of Sydney, Sydney, NSW 2006, Australia; [3]Paediatric Neurology Service, Starship Children's Health, Auckland 1023, New Zealand; [4]School of Biological Sciences, Monash University, Melbourne, VIC 3800, Australia; [5]Institut de Génétique et de Biologie Moléculaire et Cellulaire (IGBMC), 67400 Illkirch, France; [6]Department of Molecular and Cellular Genetics, UMR7156, Université de Strasbourg, CNRS, Strasbourg 67081, France; [7]National Institute of Neurological Disorders and Stroke Neurogenetics Branch, Neuromuscular and Neurogenetic Disorders of Childhood Section, NIH, Bethesda, MD 20892-1477, USA; [8]Department of Cell Physiology and Molecular Biophysics, and Center for Membrane Protein Research, Texas Tech University Health Sciences Center, Lubbock, TX 79430, USA; [9]Sorbonne Universités, UPMC Univ Paris 06, INSERM UMRS974, CNRS FRE3617, Center for Research in Myology, GH Pitié-Salpêtrière, 47 Boulevard de l'hôpital, 75013 Paris, France; [10]Centre de Référence de Pathologie Neuromusculaire Paris-Est, Institut de Myologie, GHU La Pitié-Salpêtrière, Assistance Publique-Hôpitaux de Paris, 7503 Paris, France; [11]Centre National de Génotypage, Institut de Génomique, CEA, CP5721, 91057 Evry, France; [12]Department of Radiology, Westmead Hospital, Western Clinical School, University of Sydney, Sydney, NSW 1024, Australia; [13]Department of Neurology, Concord Clinical School, University of Sydney, Sydney, NSW 2139, Australia; [14]Analytic and Translational Genetics Unit, Massachusetts General Hospital, Boston, MA 02114, USA; [15]Broad Institute of Harvard and Massachusetts Institute of Technology, Cambridge, MA 02142, USA; [16]Service de Biochimie et Génétique Moléculaire, HUPC Hôpital Cochin, Paris 75014, France; [17]INSERM, U1016, Institut Cochin, CNRS UMR8104, Université Paris Descartes, Paris 75014, France; [18]Electron Microscope Unit, Concord Repatriation General Hospital, Concord, NSW 2139, Australia; [19]The Clive and Vera Ramaciotti Centre for Structural Cryo-Electron Microscopy, Monash University, Melbourne, VIC 3800, Australia; [20]Department of Biochemistry and Molecular Biology, Monash University, Melbourne, VIC 3800, Australia; [21]Department of Pediatric Neurology, Hacettepe University Children's Hospital, 06100 Ankara, Turkey; [22]Centre for Medical Research, The University of Western Australia & the Harry Perkins Institute of Medical Research, Perth, WA 6009, Australia; [23]Murdoch Children's Research Institute, The Royal Children's Hospital, Flemington Road, Parkville, VIC 3052, Australia; [24]Université de Strasbourg, 67081 Illkirch, France
[25]These authors contributed equally to this work
[26]These authors contributed equally to this work
[27]These authors contributed equally to this work
*Correspondence: sandra.cooper@sydney.edu.au
http://dx.doi.org/10.1016/j.ajhg.2016.09.005.

patients,[2,3] driving ongoing gene discovery. The introduction of next-generation sequencing technologies has seen a rapid acceleration in the identification of new genetic causes of neuromuscular disorders.[4,5]

Through international whole-exome sequencing programs in Australia, France, the United States, and Turkey, we identified five families (nine probands) with four different recessive variants (missense and splicing variants) in *PYROXD1*. *PYROXD1* is located at 12p12.1 and encodes pyridine nucleotide-disulfide oxidoreductase domain-containing protein 1, a 500 amino acid protein previously undescribed in published literature. Pyridine nucleotide-disulphide reductases (PNDRs) are flavoproteins (FAD-binding) and catalyze the pyridine nucleotide (NAD/NADH)-dependent reduction of cysteine residues in their substrates.[6] PNDRs catalyze complex reduction reactions and use several steps of electron transfer via their enzymatic co-factors FAD and NAD. Although functionally uncharacterized, PYROXD1 is classified as a class 1 oxidoreductase and bears two putative enzymatic domains: a pyridine nucleotide-disulphide oxidoreductase domain (amino acids 39–361) and a NADH-dependent nitrite reductase domain (amino acids 447–494) (see Figure 3).

Herein we establish PYROXD1 as a nuclear-cytoplasmic oxidoreductase that underlies an early-onset myopathy characterized by generalized weakness with multiple internalized nuclei and myofibrillar aggregates on biopsy.

Subjects and Methods

Genetic Analysis

Family A was the index family identified through whole-exome sequencing of a large cohort of undiagnosed myopathy and dystrophy patients (367 individuals from 193 families) recruited from The Institute for Neuroscience and Muscle Research (Sydney, Australia). No further families were identified in this cohort with PYROXD1-related disease. Exome sequencing was performed on gDNA from both brothers and their unaffected parents at the Broad Institute using the XBrowse bioinformatics platform as described previously.[7] Family B was identified through the French Myocapture project (1,000 exomes from 397 families with myopathies or dystrophies). Exome sequencing was performed for both affected brothers and their parents at Centre National de Génotypage (CNG, Evry, France). Common variants (>1%) found in dbSNP, 1000 Genomes, Exome Variant Server, and an internal database of 1,550 exomes including ethnically matched individuals were filtered out. The Varank pipeline was used for variants scoring and ranking.[8] Data were filtered for homozygous recessive variants based on the known consanguinity of the family. Family B was the only family identified with recessive *PYROXD1* variants in the Myocapture cohort. For family C, exome sequencing was performed through the NIH Intramural Sequencing Center (NISC) on genomic DNA obtained from both affected siblings. Data were analyzed using a custom analysis program, MPG (Most Probable Genotype) based on a probabilistic Bayesian algorithm.[9] For families D and E, exome sequencing was performed on gDNA from both siblings and unaffected parents at the Theragen Etex Bio Institute. ANNOVAR was used to functionally annotate genetic variants.[10] Table S1 provides a list of recessive variants shown to segregate with disease for each family.

Phylogenetic Analysis and Calculation of the PYROXD1 Homology Model

PYROXD1 sequence alignments were performed using CLUSTAL.[11] Identity and similarity were calculated using Sequence Manipulation Suite.[12,13] Modeler[14] was used to compare the primary sequence of PYROXD1 with homologous proteins in the PDB database. The primary sequence of PYROXD1 was aligned with eight of the most similar protein sequences determined from Modeler using Promals3D:[15] *Shewanella* PV-4 NADH-dependent persulfide reductase (PDB: 3NTD), *Staphylococcus* Coenzyme A-disulfide reductase (PDB: 1YQZ), *Bacillus* Coenzyme A-disulfide reductase (PDB: 3CGC), *Novosphingobium* ferredoxin reductase (PDB: 3LXD), *Rhodopseudomonas* ferredoxin reductase (PDB: 3FG2), *Pseudomonas p.* putidaredoxin reductase (PDB: 1Q1R), *Pseudomonas sp.* ferredoxin reductase (PDB: 2GQW), and *Enterococcus* NADH peroxidase (PDB: 1NHQ). Modeler was used to compute the homology model of human PYROXD1 using information from all eight homologous crystal structures. The resulting model with the lowest energy was further refined using Modrefiner.[16] FAD binding residues were determined via the 3DLigandSite server.[17] Figures were generated with Pymol (The PyMOL Molecular Graphics System, v.1.8, Schrödinger, LLC).

Western Blot

Western blot of skeletal muscle and skin fibroblasts was carried out as described in Yuen et al.[18] Primary antibodies used were anti-PYROXD1 (1:1,000; Abcam cat# ab122458; RRID: AB_11129858), β-tubulin (1:1,000; E7, Developmental Studies Hybridoma bank), GAPDH (1:10,000; Millipore cat# MAB374; RRID: AB_2107445), Emerin (NCL 1:300, Novocastra), and sarcomeric alpha-actinin (EA-53 1:2,500, Sigma-Aldrich). For zebrafish, embryos were deyolked and protein extracted as described.[19] 13 μL of protein sample was reduced using NuPAGE Reducing Agent (Thermo Fisher) and equal amounts loaded onto a NuPAGE 4%–12% Bis-Tris Gel using MES SDS running buffer (Thermo Fisher). Membranes were blocked and probed with antibodies diluted in 1× phosphate-buffered saline, 0.1% Tween20 (Sigma-Aldrich), and 5% skim milk. Primary antibodies used were 1:1,000 anti-Ryroxd1-C (Abmart), 1:1,000 anti-GFP (Abcam cat# ab137827), and 1:2,000 α-tubulin (Sigma-Aldrich cat# T6074; RRID: AB_477582). The secondary antibody used was 1:10,000 HRP-conjugated mouse IgG (Southern Biotech) and developed using chemiluminescent detection (GE Life Sciences). For yeast, total yeast extracts were obtained by NaOH lysis followed by TCA precipitation. The equivalent of 1.5 OD_{600nm} unit of yeast cells were resuspended in 50 μL of 2× Laemmli buffer plus Tris Base. Samples were incubated 5 min at 37°C and analyzed by 10% SDS-PAGE followed by immunoblotting with anti-PYROXD1 (1:500), polyclonal R3500 produced in rabbit with human PYROXD1 immunogen amino acid 488–500 (Cys Leu Leu Asp Pro Asn Ile Asp Ile Glu Asp Tyr Phe Asp). Images were acquired with the ChemiDoc Touch Imaging System (Bio-Rad).

Immunostaining and Microscopy

For skeletal muscle, 8 μm muscle cryosections were fixed in 3% paraformaldehyde for 15 min, extracted with cold methanol for

10 min, and probed with primary antibodies diluted in 2% BSA/PBS for 16 hr at 4°C: PYROXD1 (1:50; Abcam cat# ab122458 or ab204560; RRID: AB_11129858), desmin (1:50; NCL-Des, Novacastra), myosin (1:20; RS034, Novacastra), and lamin A/C (1:80; NCL-LAM-A/C, Novacastra). After washing in PBS, samples were incubated with secondary antibody for 1 hr at room temperature, washed, and mounted with ProLong Gold with DAPI antifade reagent (Life Technologies). Goat anti-rabbit $IgG^{Alexa555}$ goat anti-mouse $IgG^{Alexa488}$ (H+L) (1:200, A21428 and A110018, Life Technologies). Specimens were imaged on a Leica SP5 confocal microscope. For zebrafish, 4% paraformaldehyde (PFA)-fixed 2 dpf whole-mount or 4 dpf whole-mount and vibratome-sectioned embryos were stained as described.[19] Antibodies used were α-actinin2 (Sigma clone A7811, 1:100) and an AlexaFluor-labeled-488 secondary antibody (Molecular Probes, 1:200) and rhodamine-Phalloidin (Molecular Probes, 1:200). Imaging was performed with an LSM 710 confocal microscope (Zeiss), using a 20× 1.0 numerical aperture water-dipping objective.

For yeast, living cells expressing EGFP C-terminal-tagged PYROXD1, PYROXD1-Asn155Ser, or -Gln372His were imaged on a fluorescence Axio Observer D1 microscope (Zeiss) using GFP filter and DIC optics with 100×/1.45 oil objective (Zeiss). Images were captured with a CoolSnap HQ2 photometrix camera (Roper Scientific).

Cell Culture, Constructs, cDNA Synthesis, and Transfections

HEK293 cells were cultured and transfected as described.[20] Cos-7 cells and primary human fibroblasts were cultured in DMEM/F12 with 10% FBS and 1:200 gentamycin (all from Life Technologies). Cos7 cells were transfected with Lipofectamine LTX (15338-100, Life Technologies) as per the manufacturer's instructions in 10 cm^2 dishes. Human *PYROXD1* cDNA (GenBank: NM_024854) was cloned into pEGFP-CI (Genscript) via BspE1/Sal1. GFP was then removed via AgeI/BspEI. RNA extraction of primary human fibroblasts was carried out using TRIzol (Invitrogen) and alcohol precipitation. cDNA was synthesized using random primers $p(dn)_6$ (Roche 11043921) or $Oligo(dt)_{20}$ primers (Invitrogen 55063) and Superscript III reverse transcriptase (Invitrogen 56575) according to the manufacturer's instructions. Primers used for PCR of *PYROXD1* cDNA were exon 1 F: 5′-AGGGAAGTTCGTGGTGGTC-3′; exon 6 R: 5′-TGGCCCAAATCACTTCACAG-3′; exon 12 R: 5′-AGGACGAGAATACATCAAAGTCG-3′.

Plasmids, Strains, Media, and Methods for Yeast Cells

The PYROXD1 and missense mutants p.Asn155Ser or p.Gln372His cDNA sequences were cloned into pDONR221 entry vector (Invitrogen) and then into yeast destination vectors (Addgene) via the Gateway (Invitrogen) method to obtain the pAG415-promGPD-PYROXD1, p.Asn155Ser or p.Gln372His (pSF371 to pSF373) and pAG415-promGPD-PYROXD1-EGFP, p.Asn155Ser or p.Gln372His (pSF374 to pSF376) plasmids. Plasmid sequences were verified (GATC Biotech). *S. cerevisiae* strains used were BY4742 WT (*MATα leu2Δ0 ura3Δ0 his3Δ0 lys2Δ0*) and *glr1Δ* (BY4742 *glr1:kanMX*). Yeast were grown in YPD-rich medium (1% yeast extract, 2% peptone, 2% glucose) or in Synthetic Medium (SD): 0.67% yeast nitrogen base (YNB) without amino acids, 2% glucose, and the appropriate –Leu dropout mix to maintain the plasmid. Yeast cells were transformed using the modified lithium acetate method.[21]

Zebrafish

Production of Transgenic Constructs, Morpholino Injections, and RNA Rescue Experiments

Zebrafish were maintained according to standard protocols.[22] Transgenic constructs were assembled with the modular tol2 kit. N-terminal eGFP-tagged wild-type or mutant PYROXD1 constructs were created using p5E-actc1b,[23] p5E-SP6-CMV,[24] p3E-pA, and pDEST-Tol2-pA2. Transgenic constructs used were actc1b-h2afv-mCherry[24] and actc1b-actinin3-mCherry.[25] For morpholino injections, ryroxd1 morpholinos (splice MO: 5′-TCGATGGTTTCTTACCTGTTCTGCA-3′, 0.25 mM and ATG MO: 5′-CCATTGAACTTCAGCACATGGAGAT-3′, 0.25 mM) and GFP morpholino (5′-GTTCTTCTCCTTTACTCAGGATC-3′, 0.5 mM) were diluted in distilled water and co-injected with Cascade Blue-labeled dextran (Molecular Probes) into one-cell embryos. For RNA rescue experiments, wild-type PYROXD1-eGFP RNA, lacking the morpholino binding site, was synthesized using the mMessage mMachine SP6 Transcription Kit (Ambion). RNA was co-injected at a concentration of either 0.5 or 1 ng/μL into one-cell stage embryos with Cascade Blue. Injected embryos were sorted for Cascade Blue labeling prior to analysis.

In Situ Hybridization

Whole-mount in situ hybridization was carried out as described previously.[26] Probes were constructed using specific gene primers (F: 5′-AGAAACCGAAGATGGTCAGAGA-3′ and R: 5′-GAGCGAAGACGCTTCTCTTCTA-3′). Imaging was performed with an Olympus SZX16 stereomicroscope.

cDNA Synthesis and Quantitative PCR

Total RNA was extracted using TRIzol reagent (Invitrogen Life Technologies) and cDNA was synthesized using Protoscript first strand cDNA synthesis kit (New England Biosciences). Quantitative PCR (qPCR) was performed on a Roche Lightcycler instrument using β-actin as a reference gene. Primers for qPCR are β-actin (F: 5′-GCATTGCTGACCGTATGCAG-3′ and R: 5′-GATCCACATCTGCTGGAAGGTGG-3′) and ryroxd1 (F: 5′-TCAATGGCTTCAGAGAAACAAG-3′ and R: 5′-CTGTTCTGCACAAGTGACACC-3′).

Swimming Assays

Touch-evoked response assays and analysis were performed on 48 hr post fertilization zebrafish as per Sztal et al.[19]

Electron Microscopy

Zebrafish were fixed in 2.5% gluteraldehyde, 2% paraformaldehyde in 0.1 M sodium cacodylate buffer, with post-fixation in 1% OsO_4 1.5% K3Fe(III)(CN)6 in 0.065 M sodium cacodylate buffer. Samples were dehydrated through an ethanol series and embedded in Epon 812. 80 nm sections were stained with Uranyl acetate and lead citrate before imaging using a Hitachi H-7500. Muscle biopsies were fixed in 2.5% glutaraldehyde in 0.1 M sodium cacodylate buffer and processed routinely for electron microscopy. Ultrathin sections were examined in an FEI Tecnai Spirit Biotwin.

Study Approval

Ethical approval for this research was obtained from the Human Research Ethics Committees of the Children's Hospital at Westmead, Australia (10/CHW/45), The University of Western Australia, the Comité de Protection des Personnes Est IV (DC-2012-1693), France, the Institutional Review Board of the National Institute of Neurological Disorders and Stroke, NIH (12-N-0095), and Ethical Committee of Hacettepe University, Faculty of Medicine. Written informed consent was obtained from participants for genetic testing, biobanking of DNA, muscle, and fibroblasts,

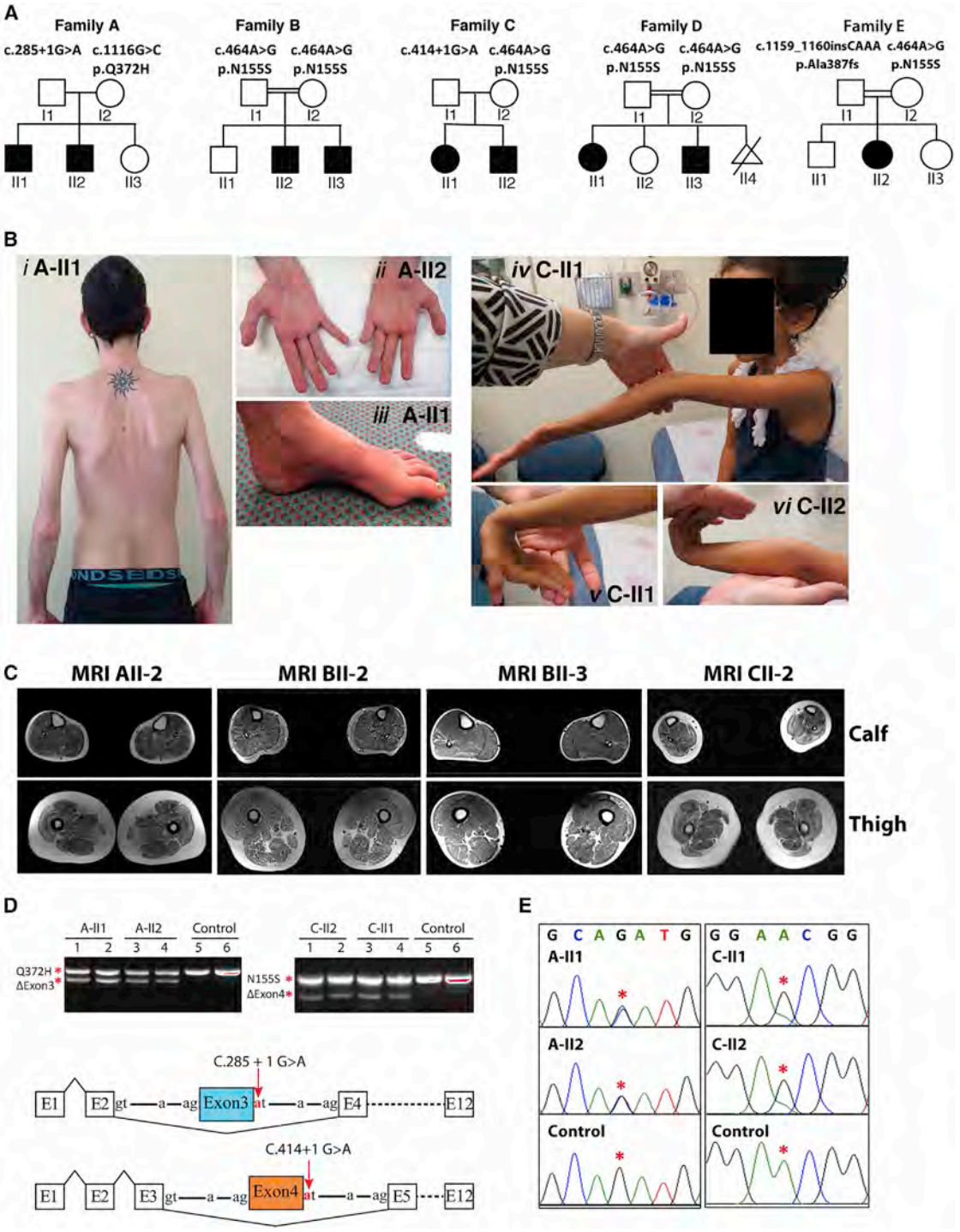

Figure 1. Clinical Features of *PYROXD1*-Related Myopathy

(A) Pedigrees of the five affected families.

(B) Posterior view of A-II1 (*i*) demonstrating generalized reduction of muscle bulk and prominent scapulae. Hands of A-II2 (*ii*) demonstrating marked wasting of the thenar and hypothenar eminence. Foot of A-II1 (*iii*) showing pes cavus and skin discoloration. C-II1 (*iv*) demonstrating hyperextension of the elbow and reduced muscle bulk. C-II1 (*v*) wrist hyperextension. C-II2 (*vi*) hand and wrist hyperextension.

(C) Axial T1 muscle MRI of calf and thigh of individuals A-II2, B-II2, B-II3, and C-II2. In all individuals, the thigh shows generalized reduction in muscle, atrophy, and fatty marbling. There is relative sparing of rectus femoris relative to vastus lateralis. The calf of individuals in family B is more mildly affected.

(D) Top: Agarose gel of PCR products of fibroblast cDNA from two affected siblings from family A (left) and family C (right). For both families, sequencing of the lower band established in-frame skipping of exon 3 in family A and exon 4 in family C. Sequencing of the upper band in family A identified only transcripts bearing the maternal c.1116 G>C (p.Gln372His) missense variant. Sequencing

(legend continued on next page)

and publishing of photographs of affected individuals. Fish maintenance and handling were carried out as per standard operating procedures approved by the Monash Animal Services Ethics Committee.

Results

Recessive *PYROXD1* Variants Cause Early-Onset Myopathy with Combined Histopathology of Multiple Internalized Nuclei and Myofibrillar Disorganization

Clinical Features of PYROXD1 Myopathy

Nine affected individuals from five families presented with childhood-onset muscle weakness (infancy to 8 years) (Figure 1A; Table 1). Perinatal history and early gross motor milestones were largely within normal limits. All affected individuals walked between 9 and 20 months of age. Two probands had poor head control in infancy (family C, II1 and II2). Weakness was slowly progressive. All affected individuals were still ambulant at 7–31 years but had difficulty with running and stairs. A-II1 required a cane for support and was unable to climb stairs from 24 years. All individuals had generalized reduction in muscle bulk (Figure 1B) and displayed symmetrical proximal weakness of the upper and lower limbs. Triceps brachii power was disproportionally reduced in three affected individuals. Distal weakness of the upper and lower limbs was also present in families A, B, C, and E. A-II1 and A-II2 showed marked wasting of distal musculature, in particular the thenar and hypothenar muscles (Figure 1B, *ii*), with abductor digiti minimi strength graded 3/5 and abductor pollicus brevis 0/5 in A-II2.

Neck weakness and mild scapular winging (5/9) were present (Figure 1B, *i*). Deep tendon reflexes were reduced or absent. Moderate joint laxity was present in families A and C (Figure 1B, *iv*–*vi*) but had resolved in family A by adulthood. Joint contractures did not occur, with the exception of mild tendoachilles contractures in A-II1. Mild scoliosis was seen in 2/9, pectus excavatum in 2/9, and thoracolumbar rigidity in family C. All affected individuals had mild to moderate facial weakness and mild ptosis was present in 3/9. A high arched palate and dental malocclusion were present in 7/9. Nasal speech was present in all individuals, swallowing difficulties in 6/9, fatigue with chewing in 2/9, and A-II2 required surgery for velopharyngeal incompetence. Ophthalmoplegia was not present.

Cognition was normal, except A-II1 who had mild, specific learning difficulties. Mild restrictive lung disease was present in the teenage years, but no individual had nocturnal hypoventilation. Frequent respiratory infections were seen in 4/9. Cardiac evaluations were normal, except for A-II1 who had developed abnormal septal wall motion and a low normal ejection fraction (50%) on his most recent assessment at 27 years of age.

Creatine kinase levels ranged from normal to moderately elevated (up to 1,051 IU/L). Electromyography (EMG) was myopathic in all individuals tested. Electrophysiological studies are summarized in Table S2. Nerve conduction studies in A-II1 and A-II2, the oldest affected individuals (26 and 29 years of age), found compound muscle action potential (CMAP) amplitudes reduced to 1%–10% of normal, absent peroneal CMAPs, reduced sural sensory potentials, but normal upper limb sensory amplitudes, suggestive of a mild length-dependent axonal neuropathy. Muscle MRI imaging of family A showed diffuse muscle atrophy and fatty marbling with relative sparing of rectus femoris relative to vastus lateralis in the thigh. In family B, only mild changes were seen, with vastus lateralis most affected in the upper leg and gastrocnemius in the lower leg (Figure 1C).

Histopathological Features of PYROXD1 Myopathy

Muscle biopsies were available from five affected individuals (Table 1). Haemotoxylin and eosin staining showed marked variation in fiber size and multiple internalized nuclei, commonly occurring in clusters (Figure 2A, *i*, *v*, *ix*, and see EM in Figure 2B, *i* and *vi*). Occasional degenerating and regenerating fibers were seen, with a moderate increase in interstitial connective tissue. Oxidative stains showed large central core-like zones devoid of mitochondrial activity (Figure 2A, *ii*, *vi*, *x* NADH). Immunohistochemical staining of skeletal muscle demonstrated large myofibrillar inclusions positive for desmin (Figure 2A, *iii*, *vii*, and *xi*), myotilin (Figure 2A, *iv* and *viii*), alpha-actin (Figure 2A, *xii*), and αB crystallin (not shown). Electron microscopy showed extensive sarcomeric disorganization, with small atrophied fibers showing complete loss of sarcomeric architecture, absence of aligned thick filaments, and accumulation of thin filaments (Figure 2B, *i*, *iii*, *iv*, *vi*, *vii*, *viii*). In some small fibers, electron-dense thickened z-line remnants or small nemaline rods were also present (Figure 2B, *iv* and *vii*). Large fibers showed multiple areas of Z-band streaming and large, focal zones of sarcomeric disorganization (Figure 2B, *ii*), devoid of mitochondria and organelles (Figure 2B, *v*). Thus, PYROXD1 myopathy

of the upper band in family C identified only transcripts bearing the maternal c.464A>G (p.Asn155Ser) variant. Bottom: Schematic of *PYROXD1* exon skipping events in family A and family C (not to scale).
(E) Sequencing chromatogram of the total PCR mixture using exon 1 forward and exon 12 reverse primers. Family A shows equal peak heights for the paternal wild-type and maternal missense variant c.1116 G>C (p.Gln372His) (red asterisks), suggesting approximately equal abundance of exon 3 skipped transcripts and missense c.1116 G>C (p.Gln372His) transcripts among the total mRNA pool. In contrast, family C shows evidence for maternal allele bias, with a lower peak height of the paternal c.464A relative to maternal c.464G variant (red asterisks).
Collective data (D, right and E, right) suggest that the paternal exon 4-skipped transcripts are less abundant than the maternal c.464A>G (p.Asn155Ser) among the total mRNA pool.

Table 1. Clinical Characteristics of Affected Individuals with PYROXD1 Variants

ID	Family A-II1	Family A-II2	Family B-II2	Family B-II3	Family C-II1	Family C-II2	Family D-II1	Family D-II3	Family E-II2
Gender, current age	male, 29 y	male, 26 y	male, 31 y	male, 21 y	female, 9 y	male, 7 y	female, 22 y	male, 17 y	female, 15 y
Ethnicity; consanguinity	European descent; no	European descent; no	Turkish; yes	Turkish; yes	Persian Jewish; no	Persian Jewish; no	Turkish; yes	Turkish; yes	Turkish; yes
PYROXD1 variants	c.285+1G>A (chr12: g.21598401G>A), c.116G>C (p.Gln372His, chr12: g.21615796G>C)	c.285+1G>A (chr12: g.21598401G>A), c. 0.116G>C (p.Gln372His, chr12: g.21615796G>C)	Hom. c.464A>G (p.Asn155Ser, chr12: g.21605064A>G)	Hom. c.464A>G (p.Asn155Ser, chr12: g.21605064A>G)	c.414+1G>A (chr12: g.21602626G>A), c.464A>G (p.Asn155Ser, chr12: g.21605064A>G)	c.414+1G>A (chr12: g.21602626G>A), c.464A>G (p.Asn155Ser, chr12: g.21605064A>G)	Hom. c.464A>G (p.Asn155Ser, chr12: g.21605064A>G)	Hom. c.464A>G (p.Asn155Ser, chr12: g.21605064A>G)	c.464A>G (p.Asn155Ser, chr12: g.21605064A>G), c.1159_1160insCAAA, chr12: g.21620457_21620458insCAAA)
Onset/progression	onset 5 y, difficulty running; slowly progressive weakness from 20 y; unable to climb stairs from 24 y; slow walk with a cane	onset 8 y; stable in childhood; mild progression from teenage years; increasing difficulty with stairs	onset 10 y; ambulant with difficulty ascending stairs	onset 10 y; ambulant	congenital onset; hypotonia; mild gross motor delay; walked age 20 mo; weakness from 6 y; increasing difficulty with stairs	infantile onset with hypotonia; walked age 13 mo; stable strength; difficulty with stairs	onset 2 y; ambulant; difficulty running and climbing; frequent falls; slowly progressive weakness from 20 y	onset 2.5 y; ambulant; difficulty climbing; stable in childhood	onset 4 y; easy fatigue; frequent falls; difficulty on stairs; slowly progressive; increasing difficulty with stairs
Pattern of limb weakness (HP:0001324)	symmetrical; UL, LL, axial; P, D	symmetrical; UL, LL, axial; P, D	symmetrical; UL, LL, axial; P UL, D LL	symmetrical; UL, LL, axial; P	symmetrical; UL, LL, axial	symmetrical; UL, LL, axial	symmetrical; UL, LL, axial; P	symmetrical; UL, LL, axial; P	symmetrical: UL, LL; P, D
Severity of limb weakness	all 4− and 4/5, except deltoid 2/5, shoulder abduction 1/5	all 4+ and 5/5, except deltoid 2/5, ADM 3/5, APB 0/5; lower limbs 4/5 except hip flex 3/5	–	–	all 4+ and 4−/5, except shoulder abd. 3/5, wrist flex 3+/5, neck flex 2/5, hip abduction 3/5	all 4 and 4−/5, except deltoid 3+/5, finger spread 3+/5, neck flex 2/5; hip extension 5−/5	proximal 4−, distal 4+/5, lower limbs more affected	proximal 4+ and 5−/5, distal 5/5	proximal 4− and 4+/5; hip flexion 3/5; thenar wasting
Hyporeflexia (HP:0001265)	reduced or absent	reduced or absent	reduced or absent	reduced or absent	reduced or absent	reduced or absent	reduced or absent	reduced or absent	reduced or absent
Achilles contractures (HP:0001771)	yes	no	no	no	yes	no	no	no	no
Joint contracture 5th finger (HP:0009183)	yes	no	no	no	yes	no	no	no	no
Joint hypermobility (HP:0001382)	distal laxity, resolved with age	distal laxity, partial patella subluxations	no	no	elbow and MCP joints	mild at elbow, wrist, and MCP joints	no	no	no
Facial weakness (HP:0002058)	yes	yes	yes	yes	yes	yes	yes	yes	yes
Ptosis (HP:0000508)	no	no	no	mild	no	no	mild	mild	no

(*Continued on next page*)

Table 1. ***Continued***

ID	Family A-II1	Family A-II2	Family B-II2	Family B-II3	Family C-II1	Family C-II2	Family D-II1	Family D-II3	Family E-II2
Ophthalmoplegia (HP:0000602)	no	no	no	no	no	no	no	no	no
High arched palate (HP:0000218)	yes	yes	no	no	yes	yes	yes	yes	yes
Additional facial features	dental malocclusion (HP:0000689), elongated face	dental malocclusion (HP:0000689), elongated face	no	micrognathia and retrognathia (HP:0000308)	int. exotropia, surgical correction (HP:0000577)	no	elongated face (HP:0000276)	elongated face (HP:0000276)	no
Dysphagia (HP:0002015)	present from 12 y; improved	yes, plus nasal regurgitation from 9 y; surgery for VPI	yes	no	no	no	yes	yes	yes
Chewing difficulties (HP:0030193)	no	no	no	no	yes	yes	no	no	no
Nasal speech (HP:0001611)	yes	yes	yes	yes	yes	yes	yes	yes	yes
Scoliosis (HP:0002650)	mild thoracic scoliosis from 20 y	no	no	no	mild scoliosis from 7 y	no	no	no	no
Spinal rigidity (HP:0003306)	no	no	no	no	thoracolumbar rigidity	thoracolumbar rigidity	no	no	no
Pectus excavatum (HP:0000767)	yes	no	no	no	yes	no	no	no	no
Scapular winging (HP:0003691)	yes	no	mild	mild	mild	mild, asymmetric	no	no	no
Pes cavus (HP:0001761)	yes	no	no	no	no	no	no	no	no
Pes planus (HP:0001763)	no	yes	yes	yes	no	no	yes	yes	no
Restrictive lung disease (HP:0002091)	yes, from 15 y	no	no	yes	no	no	no	no	no
Recurrent infections (HP:0002783)	no	no	no	no	yes	yes	yes	no	yes
Cardiac disease	abnormal septal motion and low normal ejection fraction at 27 y	no	no	no	mild to moderate pulmonic insufficiency	no	no	no	mild mitral and tricuspid insufficiency (HP:0001653)
Elevated CK (IU/L) (HP:0040081)	no (148–262)	yes (118–1,051)	yes (500–700)	yes (700–800)	no	no	yes (400–700)	no (290–376)	no

(*Continued on next page*)

Table 1. *Continued*

ID	Family A-II1	Family A-II2	Family B-II2	Family B-II3	Family C-II1	Family C-II2	Family D-II1	Family D-II3	Family E-II2
Histology	11 y	not performed	not performed	16 y	not performed	4 y	not performed	13 y	10 y
Internalized nuclei	yes	–	–	yes	–	yes	–	yes (>50% of fibers)	yes
Central cores	yes	–	–	yes	–	yes	–	yes on NADH and SDH stains	yes
Myofibrillar inclusions[a]	yes	–	–	yes	–	yes	–	EM not performed	EM not performed
Sarcomeric disorganization	yes	–	–	yes	–	yes	–	–	–
Thin filament accumulations	yes	–	–	yes	–	–	–	–	–
Nemaline rods	yes	–	–	yes	–	–	–	–	–

Abbreviations are as follows: UL, upper limb; LL, lower limb; P, proximal; D, distal; ADM, abductor digiti minimi; APB, abductor pollicus brevis; MCP, metocarpophalyngeal; VPI, velopharyngeal insufficiency; CMAP, compound muscle action potential; EMG, electromyography; NCS, nerve conduction studies; NCV, nerve conduction velocity; y, year; mo, month.
[a]Myofibrillar inclusions were positive to desmin, myotilin, alpha-actin, and αB crystallin.

has a distinctive histopathology that combines features seen in central and minicore disease, centronuclear, myofibrillar, and nemaline myopathies.

Genetic Analyses

Exome sequencing in five unrelated families identified compound heterozygous variants in *PYROXD1* (GenBank: NM_024854.3) in families A, C, and E and the same homozygous recessive missense variant in consanguineous Turkish families B and D (Figures 1A and 3). Sanger sequencing confirmed all variants and familial segregation was consistent with autosomal-recessive inheritance. DNA was not available for D-II2 or D-II4.

In family A, a paternally inherited essential splice site variant, c.285+1G>A (chr12: g.21598401G>A), was identified. The variant is found at low frequency in the heterozygous state in the Exome Aggregation Consortium (ExAC) database (allele frequency 4.295×10^{-5}).[27] cDNA analysis performed on muscle from A-II1 (not shown) and fibroblasts from A-II1 and A-II2 (Figure 1D) confirmed disruption of the donor splice site, with in-frame skipping of exon 3 a common consequence of the splice variant (Figure 1D, left gel, approximately equal levels of normal splicing [upper band] and exon 3 skipping [lower band]). PCR using exon 1 forward and intron 3 reverse primers did not provide evidence for increased frequency of exon 3 extension in family A relative to control fibroblasts (not shown). A second maternally inherited missense variant, c.1116G>C (p.Gln372His; chr12: g.21615796G>C), was not found in the ExAC database.[27] In silico predictions support pathogenicity (PolyPhen-2 score 1.0 = probably damaging;[28] Provean score −4.68 = deleterious;[29] MutationTaster score 0.999 = disease causing[30]). c.1116 G>C is the terminal 3′ base of exon 10, but cDNA analyses revealed no obvious consequence for splicing (Figures 1D and 1E) and approximately equal levels of the c.1116 G>C (p.Gln372His) variant on cDNA (Figure 1E, family A; equal peak heights at position c.1116G>C are asterisked).

In families B and D, exome sequencing identified a homozygous missense variant c.464A>G (p.Asn155Ser; chr12: g.21605064A>G) in the affected siblings (B-II2 and B-II3 and D-II1 and D-II3, Figure 1A). The variant was found at very low frequency in the ExAC database and always in the heterozygous state (allele frequency 7.157×10^{-5}).[27] In silico predictions support pathogenicity (PolyPhen-2 score 1.0 = probably damaging;[28] SIFT score 0.74 = tolerated; Provean score −4.97 = deleterious;[29] MutationTaster score 0.999 = disease causing[30]).

Families C and E (Figure 1A) had compound heterozygous variants including the c.464A>G (p.Asn155Ser; chr12: g.21605064A>G) missense variant described in family B and D. In family C an essential splice site variant c.414+1G>A (chr12: g.21602626G>A) was paternally inherited. The c.414+1G>A variant is present in the heterozygous state at very low frequency in ExAC (allele frequency 4.295×10^{-5}).[27] The c.414+1G>A (chr12: g.21602626G>A) variant is predicted to disrupt the donor splice site of exon 4.[30] cDNA analysis on skin fibroblasts

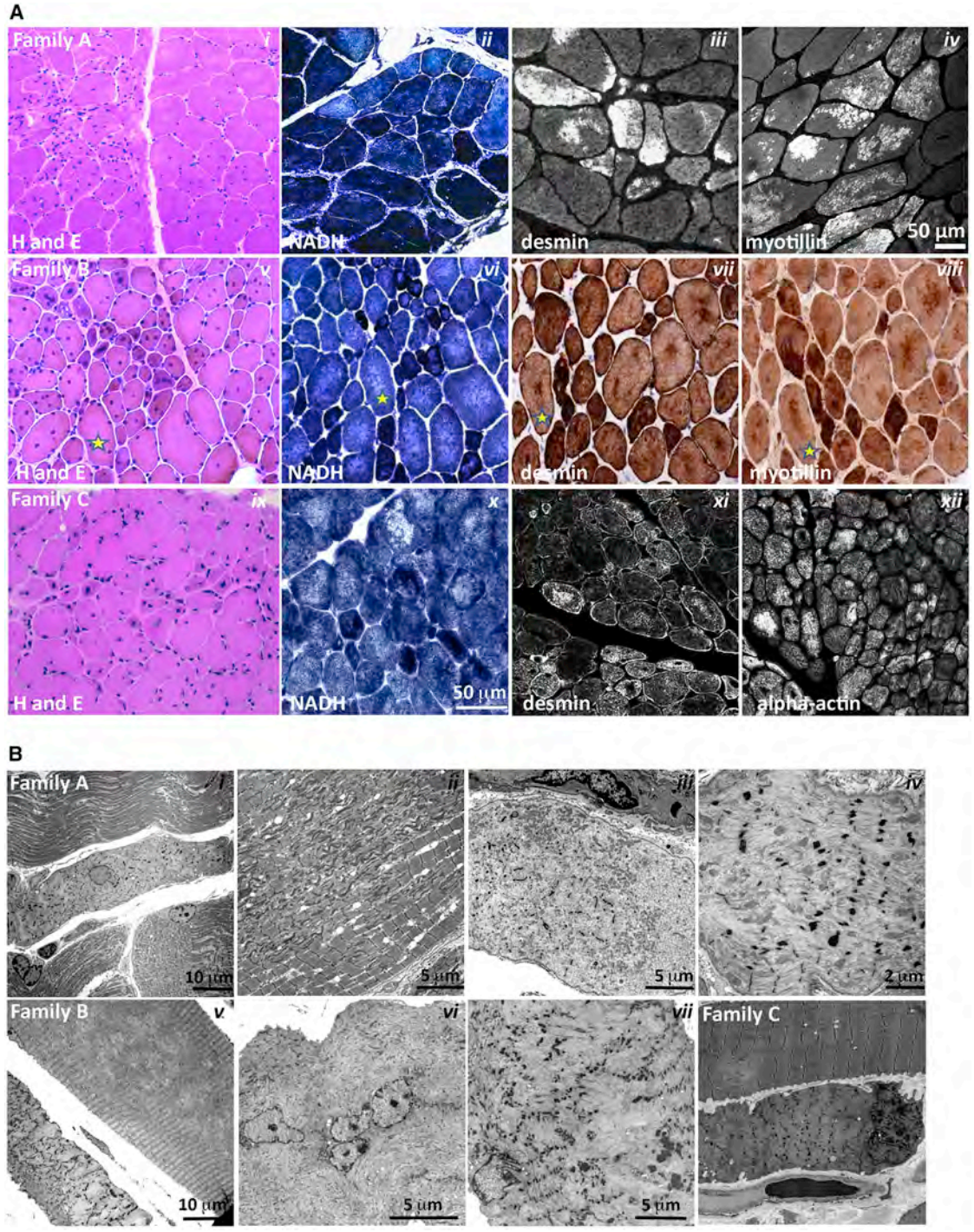

Figure 2. Histopathological Findings in PYROXD1 Myopathy

(A) Histopathological findings in skeletal muscle sections from family A (A-II1, quadriceps biopsy at 11 years of age), family B (B-II3, quadriceps biopsy at 16 years of age), and family C (C-II2, quadriceps biopsy at 4 years of age). Haemotoxylin and eosin (H&E) staining of muscle biopsy specimens from each family shows variation in fiber size, multiple internalized nuclei, and increased fibrous connective tissue. Immunofluorescent staining of skeletal muscle from A-II1 and C-II2 and immunoperoxidase staining from B-II3 demonstrate inclusions highly immunoreactive to desmin, myotillin, and alpha-actin (and αB-crystallin, not shown). H&E and immunoperoxidase images are provided via Hospital Pathology without a scale bar. Fibers in sequential sections of B-II3 are marked with a yellow star.

(B) Electron microscopy of muscle biopsy specimens. Family A: (*i*) small atrophic fiber with a central nucleus and loss of sarcomeric organization; (*ii*) large region of Z-band streaming with only occasional areas of normal sarcomeric register; and (*iii*, *iv*) atrophic fibers showing total loss of sarcomeric register, loss of thick filaments, and prominent Z-bands sometimes forming small nemaline bodies. Family B: (*v*) Large fibers show large central minicore-like regions devoid of normal myofibrillar structure and lacking mitochondria and organelles, with adjacent small fibers showing total loss of sarcomeric structure, accumulations of thin filaments, and loss of thick

(legend continued on next page)

from C-II1 and C-II2 confirmed that the c.414+1G>A splice site variant disrupts normal splicing, effecting in-frame skipping of exon 4 in a subset of transcripts (Figure 1D, right gel: normal splicing [upper gel], exon 4 skipping [lower gel]). PCR was also performed with exon 1 forward and intron 3 or intron 4 reverse primers. Family C fibroblast cDNA showed higher levels of exon 3 extension, relative to controls; no evidence for exon 4 extension was observed (not shown). Sanger sequencing of cDNA across the c.464A>G (chr12: g.21605064A>G) maternal variant showed some evidence for maternal allele bias (Figure 1E, family C, note lower peak height of the paternal c.464A relative to maternal c.464G variant, red asterisks). Collectively, our data suggest at least two outcomes from the c.414+1G>A donor splice variant; in-frame skipping of exon 4 and ectopic inclusion of intron 3 sequences that create a premature stop codon after 97 amino acids and may be subject to nonsense-mediated decay.

In family E the second variant was a heterozygous 4 bp insertion, c.1159_1160insCAAA (p.Ala387fs*13; chr12: g.21620457_21620458insCAAA), which was paternally inherited. This frameshift variant will encode a truncated protein lacking the conserved NADH-nitrile reductase domain and bearing 13 ectopic amino acids downstream of Ala387 before an early termination codon.

Families B, D, and E are Turkish. SNP markers in the region of the c.464A>G (chr12: g.21605064A>G) variant are consistent with a shared minimal confirmed haplotype between the three families of at least 348 Kb, from chr12: 21,331,987 to 21,680,609 (Table S3).

PYROXD1 Belongs to an Ancient Family of Oxidoreductases

PYROXD1 (pyridine nucleotide-disulphide oxidoreductase [PNDR] domain-containing protein 1) is classified as a class I pyridine nucleotide-disulphide oxidoreductase by neXtprot and UniProtKB. PNDRs are an ancient family of enzymes that regulate the redox state of other proteins. Unlike the five other human class I PNDRs—dihydrolipoamide dehydrogenase (DLD [MIM: 238331]), glutathione reductase (GSR [MIM: 138300]), and thioredoxin reductases 1, 2, and 3 (TXNRD1 [MIM: 601112], TXNRD2 [MIM: 606448], TXNRD3 [MIM: 606235])—PYROXD1 does not bear a consensus redox active site within the oxidoreductase domain (Gly Gly Thr Cys Val Asn Val Gly Cys in GSR and thioredoxin reductases, Gly Gly Thr Cys Leu Asn Val Gly Cys in DLD; reactive cysteine disulphide underlined). Moreover, PYROXD1 does not bear a conserved C-terminal dimerization domain identified in all other class I PNDRs, and instead bears a highly evolutionarily conserved nitrile reductase domain (69% identity and 85% similar in *Dictyostelium*). Though apparently divergent to other class I PNDRs, PYROXD1 is highly evolutionarily conserved, with 63% identity (78% similarity) of human PYROXD1 to zebrafish PYROXD1 and 39% identity (54% similarity) to *Dictyostelium* PYROXD1 (slime mold). Structural modeling of PYROXD1 using eight homologous solved crystal structures derived from other PNDRs support a predicted FAD-binding site (Figure 3B) that is vital for oxidoreductase activity of the PNDR family.[6]

The amino acids affected by the p.Gln372His and p.Asn155Ser substitutions are both highly evolutionarily conserved (Figure 3C), and removal of amino acids encoded by exon 3 (family A) or exon 4 (family C) (see Figures 3A and 3B) appears likely to significantly impact tertiary folding and abolish FAD binding and enzymatic function.

Missense Variants in Human PYROXD1 Impair Reductase Activity in Yeast

Redox activity of PYROXD1 was not previously reported, so we established a complementation assay in yeast to test the reductase activity of human PYROXD1 and the impact of identified missense variants. Replacing the yeast gene by its human counterpart is a powerful approach to help decipher the role of the human protein.[31,32] *Saccharomyces cerevisiae* has two overlapping oxidoreductase pathways, a cytoplasmic and a mitochondrial thioredoxin system, sharing some enzymes. To determine the localization of exogenous human PYROXD1 in yeast, GFP-tagged constructs were expressed in wild-type (WT) *S. cerevisiae* (Figure 3D). Fluorescent imaging of GFP-tagged PYROXD1 revealed widespread cytosolic localization, with wild-type, p.Asn155Ser, and p.Gln372His missense mutants showing similar, high expression in transformed *S. cerevisiae* by western blot (Figure 3F). Among the cytoplasmic yeast oxidoreductases, the Grl1 glutathione reductase localizes to the cytoplasm and mitochondria and is required for survival under oxidative stress.[33] Expression of non-tagged human PYROXD1 in *glr1Δ* mutant yeast that are hypersensitive to H_2O_2 due to lack of oxidoreductase activity rescued the growth defect of the *glr1Δ* mutant strain (Figure 3E), with wild-type and missense mutants showing similar, high protein levels in transformed *S. cerevisiae* by western blot (Figure 3F). Conversely, p.Asn155Ser and p.Gln372His PYROXD1 mutants failed to complement *glr1Δ* (Figure 3F). These data show that human PYROXD1 has a reductase activity that is strongly impaired by both identified missense variants.

Individuals with *PYROXD1* Variants Show Near-Normal or Reduced Levels of PYROXD1 Protein in Muscle, Fibroblasts, or Myoblasts

Western blot analysis of PYROXD1 protein levels showed a marked reduction in primary skin fibroblasts of A-II1 and

filaments; (*vi*) many large fibers have multiple internalized nuclei, often in clusters; and (*vii*) fibers show thin filament accumulations with electron-dense aggregates that resemble thickened z-lines and small nemaline bodies. Family C: (*viii*) Small atrophic fiber with loss of sarcomeric register. A large fiber shows multiple areas of Z-band streaming and a minicore-like region with absence of normal myofibrillar structure.

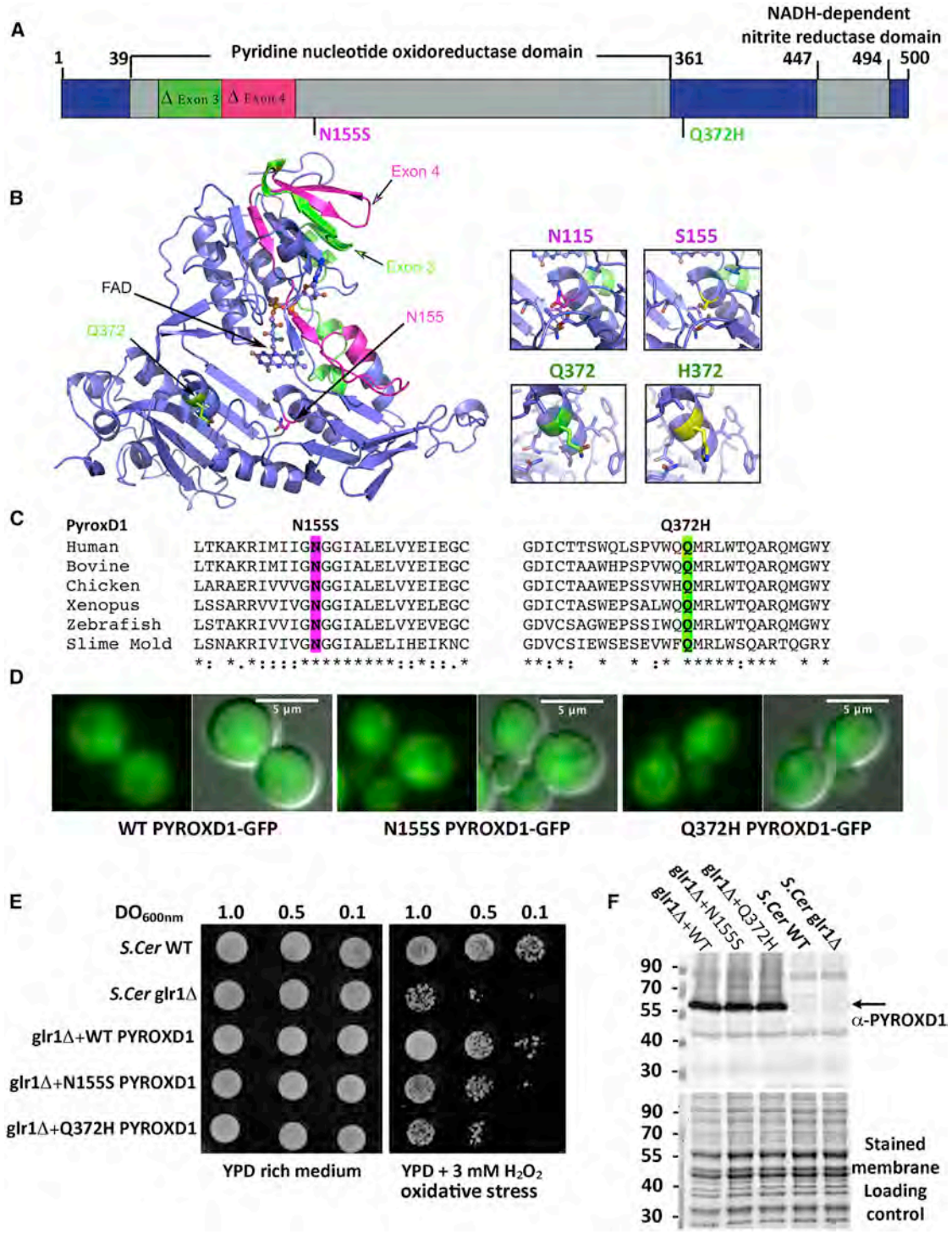

Figure 3. PYROXD1 Is an Oxidoreductase

(A) A schematic of PYROXD1 with functional domains and identified missense variants created using DOG 2.0.[35] Family A, Δexon3 and p.Gln372His (Q372H, green); families B and D, p.Asn155Ser (N155S); family C, Δexon4 and p.Asn155Ser (N155S, red).

(B) PYROXD1 homology model derived from eight homologous crystal structures (see Subjects and Methods). A co-ordinated FAD co-factor and the position of each identified variant on the crystal structure of PYROXD1 are highlighted in green (family A, Δexon3 and Q372H) and pink (family C: Δexon4 and N155S) as in (A).

(C) The identified missense variants p.Asn155Ser and p.Gln372His are evolutionarily conserved to primitive eukaryotes (Uniprot identifiers): human (Q8WU10), bovine (A7YVH9), chicken (F1NPI8), *Xenopus* (B1WAU8), *Danio rerio* (Q6PBT5), *Dictyostelium* (Q54H36).

(D) Living wild-type (WT, BY4742) yeast cells expressing human PYROXD1-GFP, PYROXD1-N155S-GFP, or PYROXD1-Q372H-GFP were observed by fluorescence microscopy with GFP filters and DIC optics. The merge represents the merge between the GFP and DIC images.

(legend continued on next page)

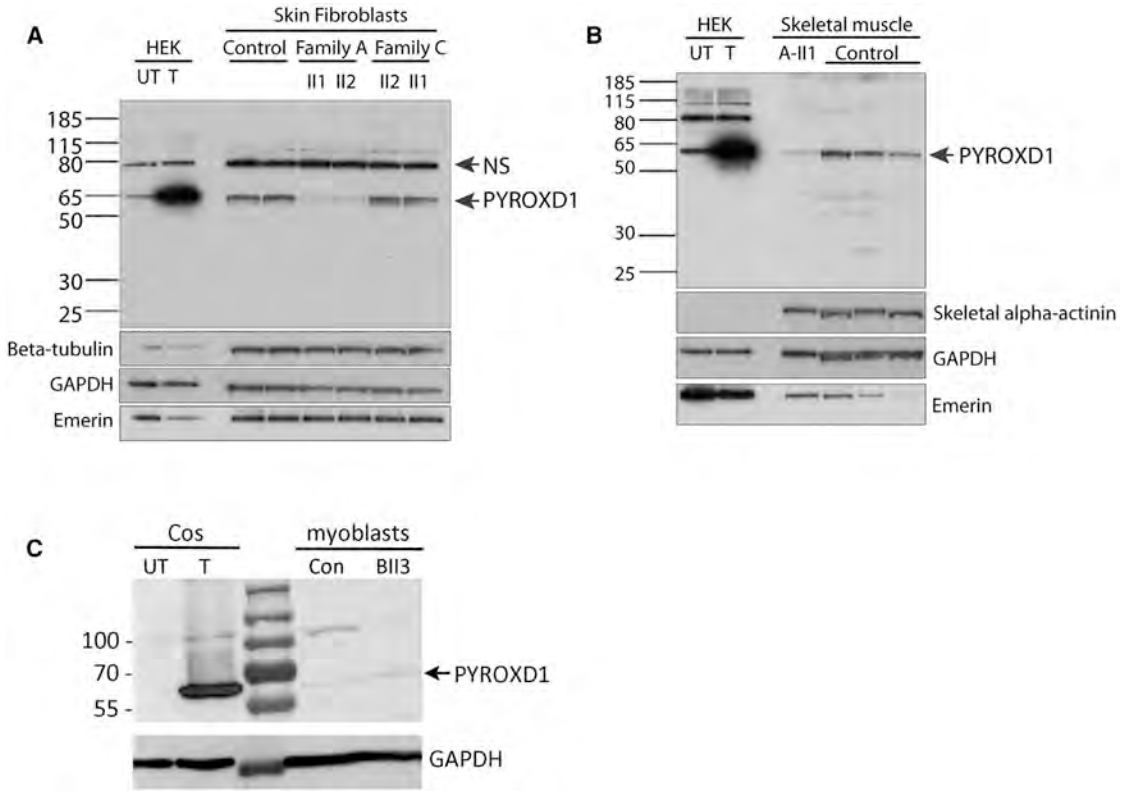

Figure 4. Affected Individuals with *PYROXD1* Variants Show Reduced or Near-Normal Levels of PYROXD1
(A) Western blot of skin fibroblasts from two controls (42 and 46 years of age) and affected siblings from family A (29 and 26 years) and family C (6 and 8 years). HEK293 cells transfected with a plasmid encoding human PYROXD1 establishes the apparent molecular weight of PYROXD1 at ~60 kDa (UT, untransfected; T, transfected). A non-specific (NS) band is indicated by an arrow. Levels of PYROXD1 are reduced in family A but not different to control levels in family C.
(B) Western blot of A-II1 triceps (11 years) (Abcam cat# ab122458; RRID: AB_11129858) shows reduced levels of PYROXD1 relative to three age-matched control biopsy specimens (quadriceps 11 years, 10 years, 15 years). Loading controls: β-tubulin and GAPDH control for overall protein content, with one cytoskeletal and one cytoplasmic marker; emerin controls for the number of nuclei; skeletal α-actinin controls for myofibrillar content.
(C) Western blot of myoblasts extracts from control subject and B-II3. Extracts from COS-1 cells transfected with the 500 aa human PYROXD1 cDNA (GenBank: NM_024854.3) was used as size control.

A-II2 (collected at 29 and 26 years of age) (Figure 4A, family A: ΔExon 3 and p.Gln372His), with no significant change in PYROXD1 levels in skin fibroblasts from C-II1 or C-II2 (8 and 6 years) (family C ΔExon 4 and p.Asn155Ser). In-frame deletion of exon 3 or exon 4 is predicted to remove 4.4 kDa or 4.7 kDa, respectively. Using two different anti-PYROXD1 antibodies (Abcam cat# ab122458 or ab204560; RRID: AB_11129858), we were unable to detect evidence for a lower molecular weight species, even with long exposures. Thus, our results suggest that in-frame deletions of exon 3 or exon 4 do not produce a stable protein. Western blot analyses of skeletal muscle specimens from A-II1 (collected at 11 years of age) similarly demonstrate reduced levels of PYROXD1 (Figure 4B), consistent with results in skin fibroblasts. Western blot analysis of family B (B-II3) cultured myoblasts detected low levels of PYROXD1 that did not appear altered compared to control (Figure 4C). Together, our data indicate that the splice variants lead to unstable proteins that are not detected by western blot, PYROXD1-Asn155Ser appears to have normal stability and protein levels (family B and C), whereas PYROXD1-Gln372His is detected at reduced levels (family A).

PYROXD1 Is a Nuclear-Cytoplasmic Oxidoreductase

Figure 5A demonstrates the localization of PYROXD1 in control human skeletal muscle longitudinal sections, lightly stretched (10% passive stretch) prior to fixation to facilitate resolution of thin and thick filaments. PYROXD1 protein shows a distinct nuclear localization and also

(E) Cultures of non-transformed wild-type (WT) or *glr1*Δ yeast, or *glr1*Δ yeast transformed with expression plasmids bearing wild-type, N155S-, or Q372H-PYROXD1 were spotted at the indicated concentration (OD_{600nm}) on rich (YPD) or on solid medium containing 3 mM H_2O_2. Plates were incubated at 30°C and observed after 48 hr.
(F) Western blot of non-transformed wild-type (WT) and *glr1*Δ, as well as *glr1*Δ yeast transformed with PYROXD1 expression vectors. The black arrow indicates PYROXD1 and the lower panel shows the protein-stained membrane used as loading control.

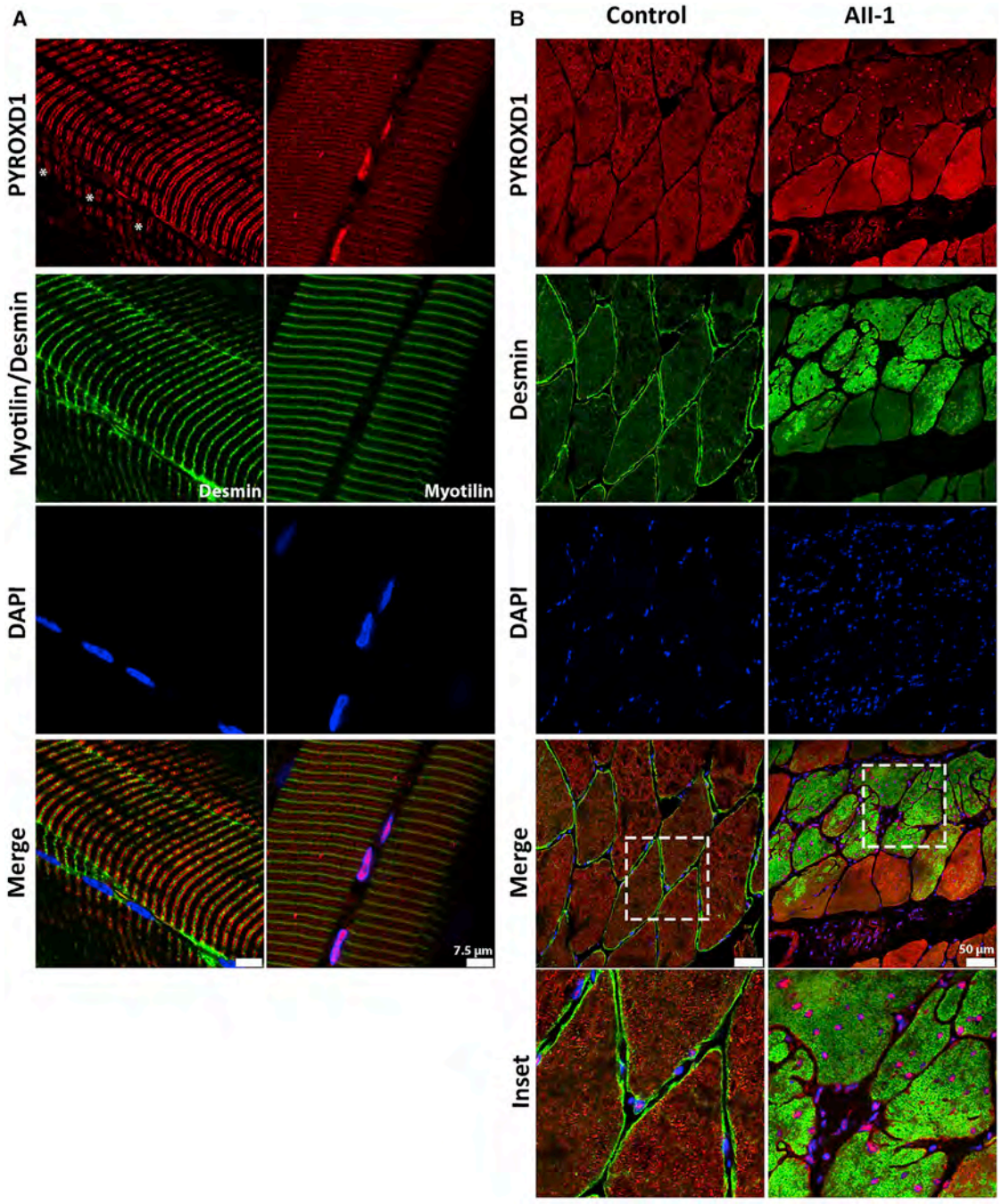

Figure 5. PYROXD1 Shows Both Nuclear and Striated Immunolocalization in Human Muscle
(A) Control stretched human skeletal (quadriceps) muscle co-stained with α-PYROXD1 (red), myotilin or desmin (green), and DAPI (blue). PYROXD1 intensely labels peripheral myonuclei, as well as showing two different patterns of striated labeling. Right: In this fiber, PYROXD1 brightly labels consecutive myonuclei and shows cytoplasmic striated labeling that aligns with desmin (Z-band region) and interdigitates between Z-bands (M-line region). Left: PYROXD1 does not brightly label myonuclei (asterisks show the position of DAPI-labeled nuclei) and shows a broader banding of striated labeling spanning the breadth of the I-band.
(B) Control and AII-1 tricep cross-sectioned human skeletal muscle co-stained with α-PYROXD1 (red), α-desmin (green), and DAPI (blue). The triceps muscle from AII-1 bears large inclusions that positively label for desmin, split fibers, and multiple internalized nuclei that brightly label for PYROXD1. Coverslips were imaged on a Leica SP5 confocal and single Z-planes are presented.

striated labeling (Figure 5A). PYROXD1 labels some peripheral nuclei more intensely than other nuclei (Figure 5A, left, asterisks show nuclei negative for PYROXD1). The sarcomeric compartment labeled by anti-PYROXD1 antibodies varied in different muscle specimens. Images presented show the two main types of striated labeling observed. The right panel of Figure 5A shows striations aligning both with the Z-band *and* interdigitating between Z-lines (near the M-band). The left panel shows a broader band of PYROXD1 labeling spanning the breadth of the

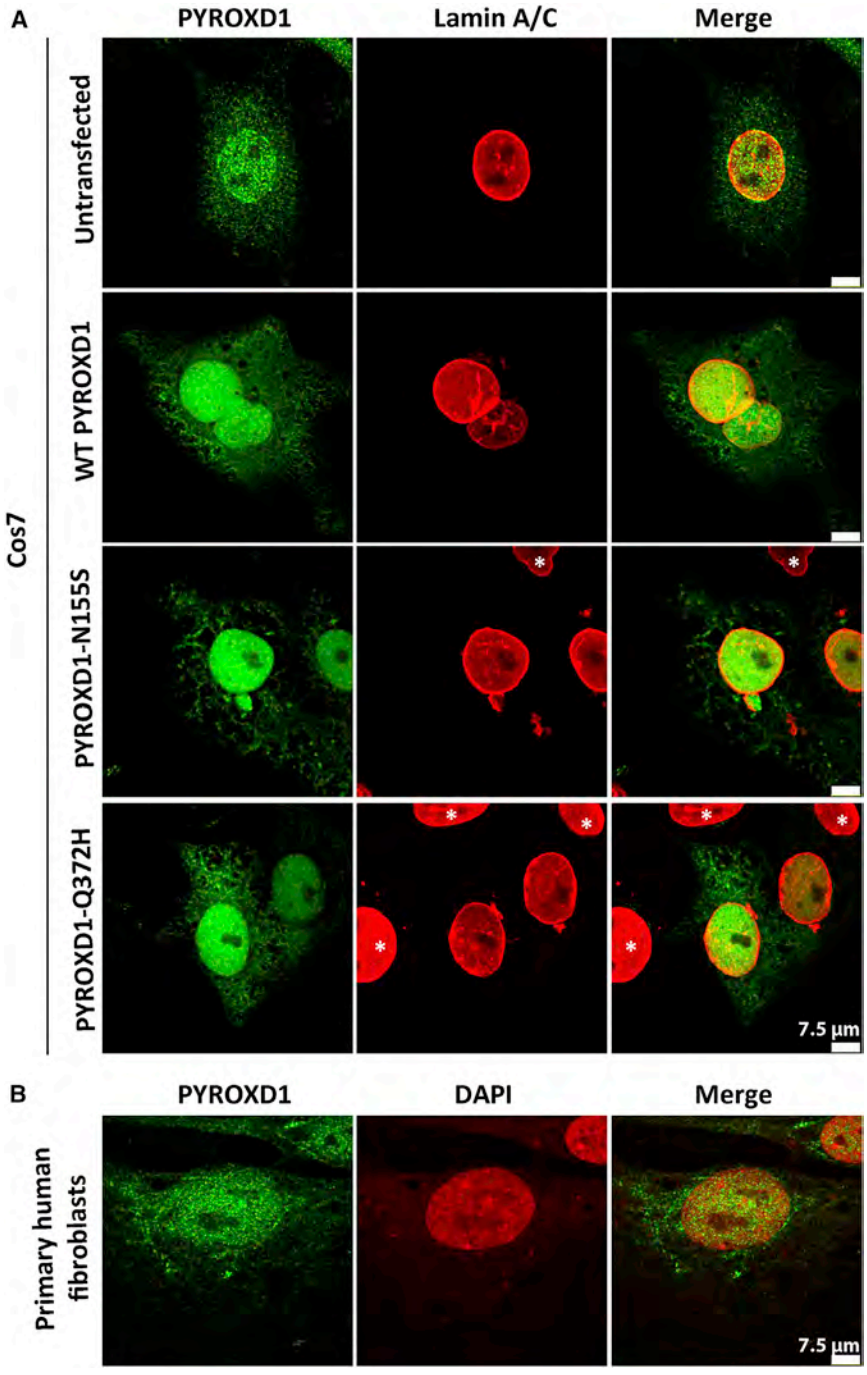

Figure 6. PYROXD1 Shows Nuclear Localization in Human Skin Fibroblasts and Transfected Cos-7 Cells

(A) Untransfected Cos-7 cells (top row) and Cos-7 cells transfected with human wild-type, p.Asn155Ser (N155S)-, or p.Gln372His (Q372H)-PYROXD1 expression constructs co-stained for PYROXD1 (green) and lamin A/C (red) shows enriched labeling for PYROXD1 within the nucleus, as well as labeling of cytoplasmic networks. For transfected Cos-7 cells (bottom three rows), asterisks demark untransfected cells within the field, with much lower levels of PyroxD1, that show very weak labeling under optimum capture conditions for transfected cells.

(B) Nuclear-cytoplasmic labeling is observed for endogenous PYROXD1 in primary human fibroblasts.

I-band. These data establish that PYROXD1 localizes to the nucleus and to sarcomeric/sarcoplasmic compartments.

Immunohistochemistry of control human skeletal muscle in cross section similarly shows dual localization of PYROXD1 in peripheral myonuclei as well as intramyofibrillar labeling throughout the contractile apparatus (Figure 5B). Levels of PYROXD1 in the triceps of A-II1 were lower relative to control muscle, and higher capture conditions are presented in order to portray key findings. As observed in the quadriceps of A-II1 (Figure 2A, *i*), the triceps muscle has large inclusions that label positively for desmin (Figure 5B, desmin, green) and multiple internalized nuclei (Figure 5B, DAPI, blue) that label positively for PYROXD1-Gln372His (Figure 5B, PYROXD1, red). Levels of cytoplasmic PYROXD1 appear brighter in myofibers *without* myofibrillar aggregates (Figure 5B, PYROXD1, red, enlarged inset). Thus, our results suggest that the equilibrium of cytoplasmic versus nuclear PYROXD1 is shifted to more predominant nuclear localization in muscle fibers burdened with myofibrillar aggregates.

Dual nuclear-cytoplasmic localization of PYROXD1 is supported by immunostaining of untransfected and transfected Cos-7 fibroblasts and primary human fibroblasts (Figure 6). Heterologous transfection of expression constructs encoding wild-type, p.Asn155Ser, or p.Gln372His PYROXD1 into Cos-7 fibroblasts showed a similar distribution of nuclear and cytoplasmic localization (Figure 6); similar patterns of staining for wild-type and PYROXD1 missense variants were also observed in transfected C2C12 myoblasts and immortalized human myoblasts (not shown). Moreover, no overt changes in PYROXD1 localization were observed in primary fibroblasts from two siblings from family A or two siblings from family C relative to fibroblasts from two age-matched controls (not shown).

PYROXD1 Shows Nuclear-Cytoplasmic Localization in Mature Zebrafish Myofibers, with Evidence for Aggregates Induced by Expression of p.Asn155Ser and p.Gln372His Mutant Constructs

To determine the localization of PYROXD1 within the skeletal muscle, we overexpressed eGFP-tagged wild-type and mutant (p.Asn155Ser and p.Gln372His) human PYROXD1 within zebrafish muscle using the muscle-specific *actc1b*

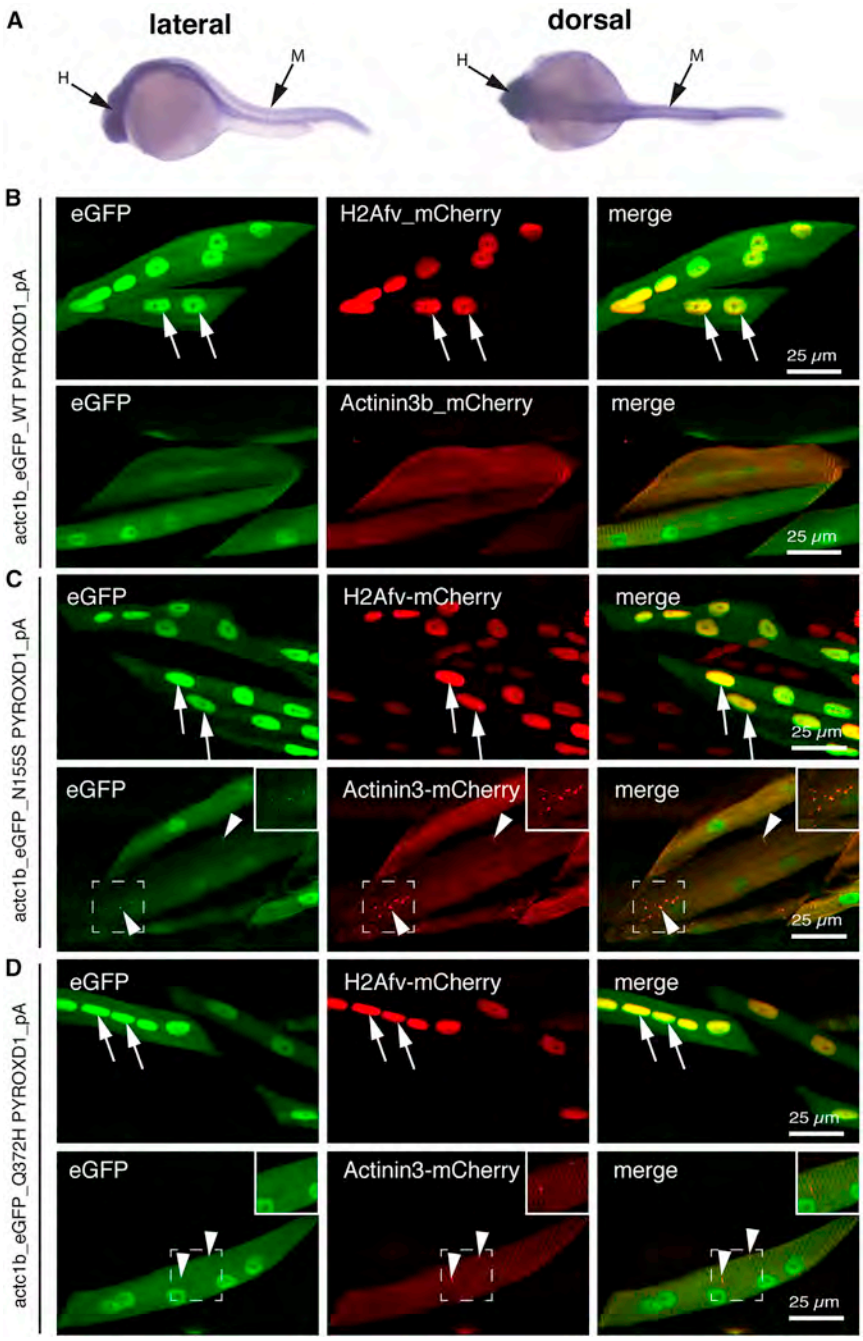

Figure 7. PYROXD1 Shows Nuclear-Cytoplasmic Localization in Zebrafish Myofibers, with Aggregates Induced by Expression of Asn155Ser and Gln372His Variants

(A) In situ hybridization on 24 hpf zebrafish shows widespread *ryroxd1* expression including the trunk musculature (M) in both lateral and dorsal views.

(B–D) Immunolabeling of vibratome-sectioned embryos 4 days post fertilization (dpf) expressing eGFP-conjugated human PYROXD1, either wild-type (B), p.Asn155Ser (C; N155S), or p.Gln372His (D; Q372H) via a muscle-specific actin promoter (*actc1b*) together with the Z-disk marker Actinin3-mCherry or nuclear marker histone H2A-mCherry. PYROXD1 localizes to myonuclei and shows striated labeling of sarcomeres. Small regions of thickening and sarcomeric disruption (arrowheads and inset) were observed after heterologous expression of N155S- or Q372H-PYROXD1, but not with wild-type PYROXD1.

promoter. All PYROXD1 constructs show dual nuclear and striated labeling aligning with the Z-disk, as evidenced by co-localization with actc1b:actinin3-mCherry and actc1b:H2Av-mCherry (Figure 7B, arrows). We also observed an occasional thickening of the Z-disk at 48 hpf when p.Asn155Ser and p.Gln372His PYROXD1 isoforms were overexpressed (Figures 7C and 7D, actinin3-mCherry arrowheads).

Zebrafish with Knockdown of RyroxD1 Show Sarcomeric Disorganization, Myofibrillar Aggregates, and a Defect in Swimming

We identified a single *PYROXD1* ortholog in zebrafish, *ryroxd1*, which is expressed throughout the developing embryo, including the skeletal muscle (Figure 7A). To study the function of Ryroxd1, we analyzed the effects of *ryroxd1* knockdown during early embryogenesis (Figure 8). Both quantitative PCR (qPCR) and western blot analyses confirm reduction of Ryroxd1 when *ryroxd1* ATG and exon2 splice morpholinos were used singularly and in combination (Figures 8A–8C).

To determine the effect of Ryroxd1 knockdown, we examined the swimming performance of the morpholino-injected embryos. Ryroxd1 single (ATG) and double (ATG and splice) morphants show a significant reduction in maximum acceleration in a touch-evoke response assay at 2 dpf compared to GFP morpholino-injected control zebrafish (Figure 8C). Co-injection of eGFP-tagged human wild-type PYROXD1 mRNA (wtPYROXD1-eGFP) with both Ryroxd1 morpholinos rescued the reduction in swim performance, demonstrating that the effect was due specifically to reduction of Ryroxd1 (Figure 9D).

Examination of zebrafish muscle through antibody labeling for Actinin2 and phalloidin shows no obvious defects in Ryroxd1 splice and ATG single morphants (Figure S1), but disrupted sarcomeric structure is evident in Ryroxd1 double morphants (Figure 8D). By 96 hpf, Actinin2 and phalloidin-positive aggregates are observed in Ryroxd1 ATG morphants (Figure S1). However, RyroxD1 double morphants show severe disruption of the musculature

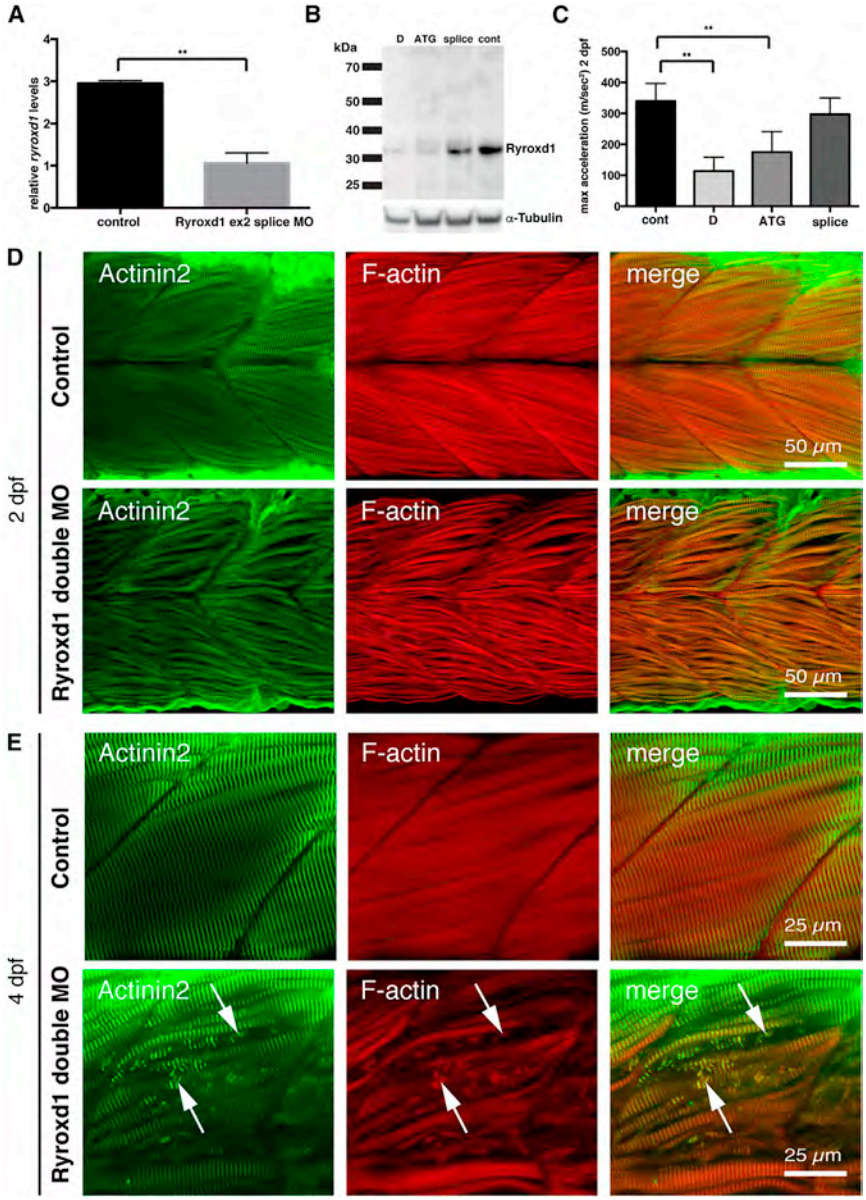

Figure 8. Zebrafish Deficient for RyroxD1 Show Sarcomeric Disorganization, Myofibrillar Aggregates, and a Defect in Swimming

(A) Quantitative PCR for *ryroxd1* mRNA levels in control (uninjected) and Ryroxd1 morpholino-injected (Ryroxd1 ex2 splice MO) zebrafish at 2 dpf.

(B) Western blot for Ryroxd1 protein and α-tubulin loading control in control (uninjected) and Ryroxd1 morpholino-injected zebrafish (D = Ryroxd1 double morpholino, ATG = Ryroxd1 ATG morpholino, and splice = Ryroxd1 splice-site targeting morpholino) at 48 hpf demonstrates effective reduction of Ryroxd1.

(C) Ryroxd1 ATG-single and ATG/splice double morphants show a significant reduction, of 48% and 73% respectively, in maximum acceleration in a touch-evoke response assay at 2 dpf compared to control zebrafish injected with a GFP targeting morpholino (Cont).

(D and E) Antibody labeling of Ryroxd1 double morphants at 48 hpf (D) and 96 hpf (E) for Actinin2 and phalloidin show disruption of muscle structure compared to uninjected controls.

(E) At 96 hpf, Ryroxd1 double morphants show severe disruption of the musculature with remnants of fragmented muscle fibers evident (arrows).

For (A) and (C), error bars represent SEM for three independent replicate experiments comprising 15 fish in each, $^{**}p < 0.01$.

with fragmentation of the muscle fibers (Figure 8E) and, in some cases, loss of fiber integrity and accumulation of actin at the myosepta (Figure 9A). Consistent with the improvement in muscle performance, the severity of structural muscle defects was significantly reduced by co-injection of Ryroxd1 double morphants with wtPYROXD1-eGFP mRNA (Figure 9A), demonstrating that the phenotype is due to reduction of Ryroxd1.

To further investigate the muscle phenotype observed in the morphant embryos, we examined the muscle structure using electron microscopy. In morphant embryos, but not uninjected controls, we observed disintegration of the myofibrils with mitochondrial infiltration of the resulting space, loss of Z-disk structures, and the formation of electron dense, nemaline-like, bodies reminiscent of those observed in the human muscle biopsies (Figure 9E).

Discussion

This publication describes the oxidoreductase function of *PYROXD1* and identifies recessive variants in *PYROXD1* as a cause of early-onset myopathy characterized histologically by a combination of multiple internalized nuclei, with large zones of sarcomeric disorganization—often devoid of mitochondria and organelles, accumulations of thin filaments, thickened Z-bands, and desmin-positive inclusions (Figure 2). All affected individuals presented in infancy or early childhood (1–8 years) with slowly progressive symmetrical weakness affecting both proximal and distal muscles, with normal to moderately elevated creatine kinase. Mild facial weakness, a high palate, nasal speech, and swallowing difficulties were typical features, mild restrictive lung disease was common, and evidence of cardiac involvement was present in the eldest individual, now aged 27. Thus, we emphasize the need for respiratory and cardiac surveillance in individuals with PYROXD1 myopathy. Nerve conduction studies in family A in the third decade showed a mild length-dependent axonal sensory neuropathy. These findings were present only in family A, so the significance is uncertain, but raises the possibility that different

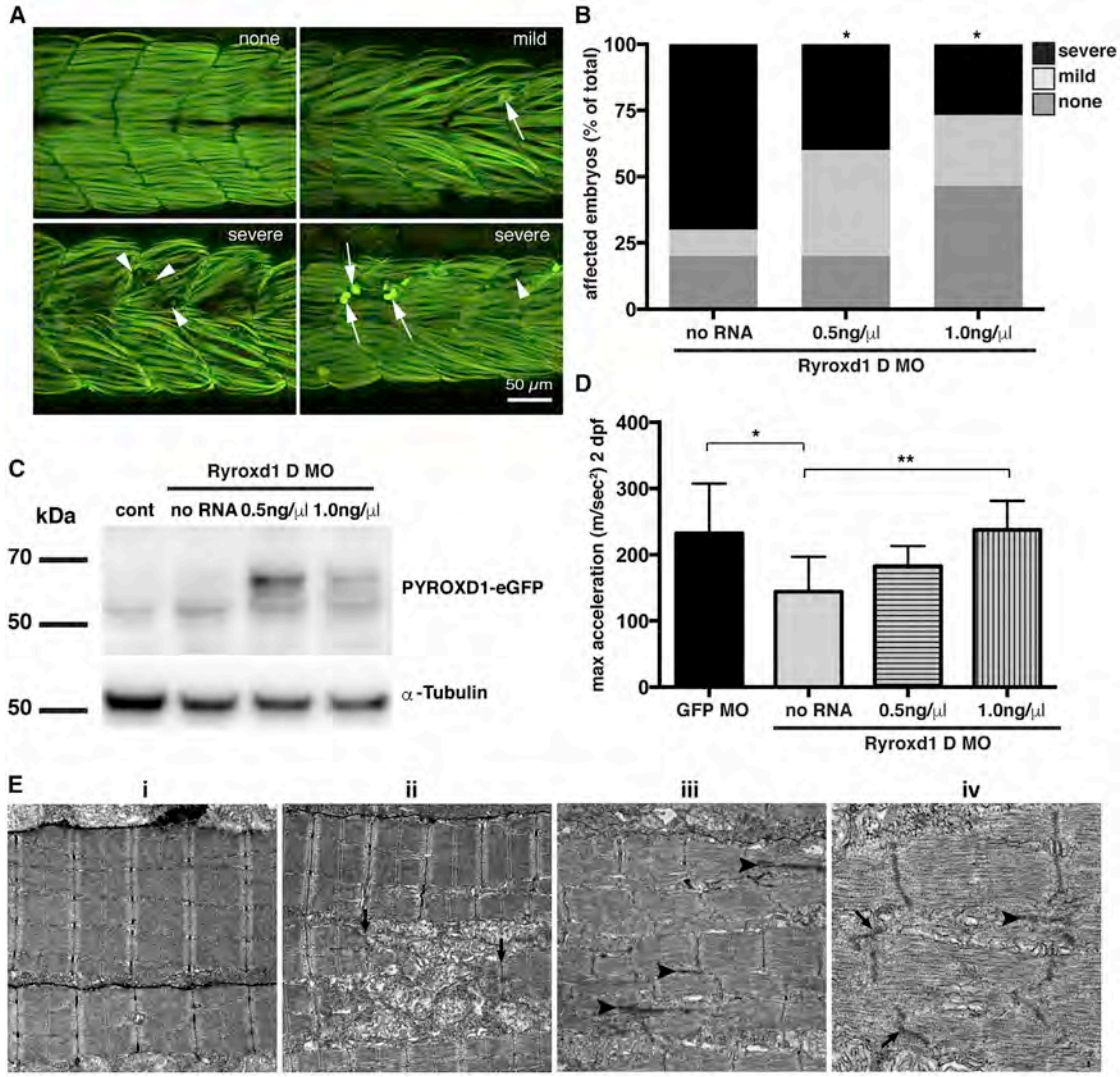

Figure 9. Human PYROXD1 Rescues Muscle Pathology and Swimming Defects in Ryroxd1 Morphants and EM of Zebrafish Muscle Pathology

(A) Representative images depicting the range of severity of muscle defects in Ryroxd1 double morphants. No obvious phenotype (none), embryos displaying occasional broken fibers and actin accumulation (mild, arrows), severe fragmentation of muscle fibers (severe, arrowheads), severe loss of fiber integrity and accumulation of actin at the myosepta (severe, arrows).

(B) Quantification of phenotypes (as in A) observed in Ryroxd1 double morphants (Ryroxd1 D MO) injected with either 0.5 ng/μL or 1.0 ng/μL wild-type (wt) wtPYROXD1-eGFP RNA compared to Ryroxd1 double morpholino injection alone (no RNA). 15–20 animals were scored per condition, *$p < 0.05$.

(C) Western blot for GFP and α-tubulin in GFP morpholino-injected control embryos (cont), Ryroxd1 double morpholino-injected zebrafish (no RNA), and Ryroxd1 double morpholino-injected zebrafish co-injected with either 0.5 ng/μL or 1.0 ng/μL wtPYROXD1-eGFP RNA, demonstrating translation of the injected mRNA.

(D) Ryroxd1 double morphants injected with human wtPYROXD1-eGFP mRNA show dose-dependent rescue in a touch-evoke response assay at 2 dpf. Ryroxd1 double morphants injected with 1.0 ng/μL human wtPYROXD1-eGFP show a 61% increase in maximum acceleration compared to Ryroxd1 double morphants (no RNA), achieving similar levels of maximum acceleration to wild-type embryos injected with a control GFP targeting morpholino (GFP MO).

(E) Electron micrograph of muscle (*i*) in a wild-type uninjected 96 hpf zebrafish embryo; examination of Ryroxd1 double morphant embryos (*ii–iv*) demonstrates myofibrillar fragmentation (*ii*, arrows) with mitochondrial infiltration, small nemaline-like bodies (*iii*, black arrowheads), and Z-disk fragmentation and loss (*iii–iv*; black arrowheads).

Scale bar represents 1 μm. Error bars represent SEM for three independent replicate experiments comprising 15 animals in each replicate experiment, *$p < 0.05$, **$p < 0.01$.

PYROXD1 variants may eventually predispose to the development of a neuropathy with increasing age.

All families identified in this study for which muscle, myoblasts, or fibroblasts were available exhibited either normal levels or reduced levels of PYROXD1; no individual showed absence of PYROXD1. Analysis of splice variants identified in *PYROXD1* in family A and family C revealed a subset of transcripts with in-frame deletion of amino acid sequences encoded by exon 3 (family A) or exon 4 (family C). However, we could not find evidence for

expression of truncated proteins, suggesting that the resulting protein products are unstable and degraded. The two substitutions p.Asn155Ser and p.Gln372His strongly impair the oxidoreductase activity of PYROXD1 in a yeast heterologous expression system. Importantly, no affected individuals described to date possess two predicted loss-of-function variants or exhibited complete loss of PYROXD1 in skin fibroblasts or skeletal muscle specimens. Thus, our findings suggest that myopathy results from partial loss of PYROXD1 function. Of note, targeted deletion of *PYROXD1* in murine models results in embryonic lethality (our own studies and confirmed by the International Mouse Phenotyping Consortium). This suggests that recessive loss-of-function variants in *PYROXD1* may result in a severe-lethal presentation in humans. Our current studies are defining the tissue-specific and developmental expression of PYROXD1, together with determination of the consequences of PYROXD1 deficiency, using a PYROXD1 conditional knock-out and LacZ reporter mouse-model.

PYROXD1 mRNA is ubiquitously expressed at low levels (GTex Portal). *PYROXD1* is highly evolutionarily conserved to unicellular eukaryotes, with functional FAD-dependent oxidoreductase and NADH-dependent nitrile reductase domains present in prokaryotic enzymes. Thus, PYROXD1 has an ancient biology not yet understood. In contrast to PYROXD1, the five other class I PNDRs are well characterized and play significant roles in regulation of cellular redox: glutathione reductase (*GSR*), thioredoxin reductases 1, 2, and 3 (*TXNRD1*, *TXNRD2*, and *TXNRD3*), and mitochondrial dihydrolipoyl dehydrogenase (*DLD*).[6] Recessive variants in *DLD* cause dihydrolipoamide dehydrogenase deficiency (DLDD [MIM: 246900]), a metabolic disorder characterized by lactic acidosis and neurological dysfunction. Dihydrolipoamide dehydrogenase is the E3 component of several vital mitochondrial enzyme complexes, including pyruvate dehydrogenase and ketoglutarate dehydrogenase, affecting oxidative metabolism via both the citric acid cycle and fatty acid biosynthesis.[6]

In addition to the reducing capabilities of their enzyme co-factors (FAD and NAD), PNDRs typically bear an intrinsic "redox active site" that catalyzes the final step to reduce their substrate, most commonly a conserved redox-reactive disulphide motif. Many PNDRs form enzymatic homodimers via a C-terminal conserved motif and are grouped into two classes (class 1 and class 2), according to characteristics related to nucleotide and flavin binding sites, the type of non-flavin redox active site, and the structural features of their dimer interface.[34] Although PYROXD1 is classified as a class 1 PNDR, it does not contain a conserved redox active disulphide within the oxidoreductase domain, nor a classical C-terminal dimerization motif, and thus appears a divergent member of the class I PNDR family.

Importantly, using a heterologous complementation assay in yeast, we showed that human PYROXD1 exhibits a reductase activity that can rescue the H_2O_2 sensitivity of yeast cells lacking the glutathione reductase *glr1*. As the two missense variants impair this activity, it supports that the myopathy observed in affected individuals arises, at least in part, from a defect in oxidoreductase activity. Future work will need to identify what are the substrate(s) of PYROXD1 to better understand the pathophysiology.

Immunolocalization studies in human skeletal muscle, skin fibroblasts, and zebrafish myofibers show that PYROXD1 localizes to both the nucleus and cytoplasmic/sarcomeric compartments. Knockdown of the zebrafish ortholog Ryroxd1 produced embryos with abnormal musculature and marked sarcomeric disorganization within individual myofibrils, including Z-disk loss and fragmentation and the presence of electron-dense bodies, reminiscent of findings observed in human muscle biopsies. In addition to the pathological features observed, Ryroxd1 morphants also performed poorly in a touch-evoked swim assay, consistent with impaired muscle function.

In summary, we describe PYROXD1 as a nuclear-cytoplasmic oxidoreductase conserved through evolution and important for human skeletal muscle biology. Recessive variants in *PYROXD1* cause an early-onset myopathy characterized by slowly progressive limb and facial weakness, nasal speech, and swallowing difficulties. PYROXD1 myopathy histopathology is distinctive in that it combines multiple pathological hallmarks characteristic of different myopathies: central core and minicore disease, centronuclear, myofibrillar, and nemaline myopathies. Although one or two of these histopathological features can often exist in combination, it is rare to observe core-like zones, multiple internal nuclei, extensive myofibrillar disorganization, myofibrillar accumulations, and small nemaline-like bodies all within a single biopsy specimen. Thus, our discovery of PYROXD1 myopathy introduces altered redox regulation as a primary disease mechanism in congenital myopathy and raises the provocative possibility that several pathological endpoints in the myopathies may be linked ultimately to altered cellular redox.

Supplemental Data

Supplemental Data include five case reports, one figure, and three tables and can be found with this article online at http://dx.doi.org/10.1016/j.ajhg.2016.09.005.

Acknowledgments

This study was supported by the following funding: The Australian National Health and Medical Research Council (NHMRC) 1080587 (S.T.C., N.F.C., D.G.M., K.N.N., R.B.R., K.J.N., N.G.L.), 1022707 and 1031893 (K.N.N., N.F.C., and N.G.L.), 1048816 (S.T.C.), and 1056285 (G.L.O.), Muscular Dystrophy New South Wales (G.L.O.), Royal Australasian College of Physicians (G.L.O.), Australian Research Council FT100100734 (K.J.N.), National Human Genome Research Institute of the NIH (D.G.M., Medical Sequencing Program grant U54 HG003067 to the Broad Institute principal investigator, Lander), Division of Intramural

Research of the National Institutes of Neurological Disorders and Stroke, France Génomique National infrastructure grant Investissements d'Avenir and Agence Nationale pour la Recherche (ANR-10-INBS-09 and ANR-11-BSV1-026), Fondation Maladies Rares "Myocapture" sequencing project, Association Française contre les Myopathies (AFM-15352 and AFM-16551), Muscular Dystrophy Association (MDA-186985), Myotubular Trust and IDEX-Université de Strasbourg PhD fellowship (M.S.-V.), and intramural funds of the NINDS/NIH (C.G.B. and S.D.).

We thank Sarah Sandaradura for recruitment and consent of family A, Meganne E. Leach for clinical review of family C, Goknur Haliloglu for clinical review of family D, Xavière Lornage and Christine Kretz for help with experiments for family B, Pierre Bouche and Gisèle Bonne for sequence analysis in family B, Roberto Silva Rojas for help with yeast experiments, and Maud Beuvin, Guy Brochier, and Dr. Edoardo Malfatti from the Morphological Unit of the Myology Institute (Paris).

Received: April 27, 2016
Accepted: September 7, 2016
Published: October 13, 2016

Web Resources

Clustal Omega, http://www.ebi.ac.uk/Tools/msa/clustalo/
dbSNP, http://www.ncbi.nlm.nih.gov/projects/SNP/
ExAC Browser, http://exac.broadinstitute.org/
GenBank, http://www.ncbi.nlm.nih.gov/genbank/
GeneTable of Neuromuscular Disorders, http://www.musclegenetable.fr/
GTEx Portal, http://www.gtexportal.org/home/gene/PYROXD1
Human Phenotype Ontology (HPO), http://www.human-phenotype-ontology.org/
International Mouse Phenotyping Consortium, http://www.mousephenotype.org/data/genes/MGI:2676395#section-associations
Knockout Mouse Project (KOMP) Repository, https://www.komp.org/
neXtprot, https://www.nextprot.org/term/FA-00613/
NHLBI Exome Sequencing Project (ESP) Exome Variant Server, http://evs.gs.washington.edu/EVS/
OMIM, http://www.omim.org/
RCSB Protein Data Bank, http://www.rcsb.org/pdb/home/home.do
RRID, https://scicrunch.org/resources
seqr, https://seqr.broadinstitute.org/
Sequence Manipulation Suite, http://www.bioinformatics.org/sms2/ident_sim.html
UniProt, http://www.uniprot.org/

References

1. Nance, J.R., Dowling, J.J., Gibbs, E.M., and Bönnemann, C.G. (2012). Congenital myopathies: an update. Curr. Neurol. Neurosci. Rep. *12*, 165–174.
2. Amburgey, K., McNamara, N., Bennett, L.R., McCormick, M.E., Acsadi, G., and Dowling, J.J. (2011). Prevalence of congenital myopathies in a representative pediatric united states population. Ann. Neurol. *70*, 662–665.
3. Chae, J.H., Vasta, V., Cho, A., Lim, B.C., Zhang, Q., Eun, S.H., and Hahn, S.H. (2015). Utility of next generation sequencing in genetic diagnosis of early onset neuromuscular disorders. J. Med. Genet. *52*, 208–216.
4. Ng, S.B., Buckingham, K.J., Lee, C., Bigham, A.W., Tabor, H.K., Dent, K.M., Huff, C.D., Shannon, P.T., Jabs, E.W., Nickerson, D.A., et al. (2010). Exome sequencing identifies the cause of a mendelian disorder. Nat. Genet. *42*, 30–35.
5. Ng, S.B., Nickerson, D.A., Bamshad, M.J., and Shendure, J. (2010). Massively parallel sequencing and rare disease. Hum. Mol. Genet. *19* (R2), R119–R124.
6. Argyrou, A., and Blanchard, J.S. (2004). Flavoprotein disulfide reductases: advances in chemistry and function. In Progress in Nucleic Acid Research and Molecular Biology (Academic Press), pp. 89–142.
7. Ghaoui, R., Cooper, S.T., Lek, M., Jones, K., Corbett, A., Reddel, S.W., Needham, M., Liang, C., Waddell, L.B., Nicholson, G., et al. (2015). Use of whole-exome sequencing for diagnosis of limb-girdle muscular dystrophy: outcomes and lessons learned. JAMA Neurol. *72*, 1424–1432.
8. Geoffroy, V., Pizot, C., Redin, C., Piton, A., Vasli, N., Stoetzel, C., Blavier, A., Laporte, J., and Muller, J. (2015). VaRank: a simple and powerful tool for ranking genetic variants. PeerJ *3*, e796.
9. Teer, J.K., Bonnycastle, L.L., Chines, P.S., Hansen, N.F., Aoyama, N., Swift, A.J., Abaan, H.O., Albert, T.J., Margulies, E.H., Green, E.D., et al.; NISC Comparative Sequencing Program (2010). Systematic comparison of three genomic enrichment methods for massively parallel DNA sequencing. Genome Res. *20*, 1420–1431.
10. Wang, K., Li, M., and Hakonarson, H. (2010). ANNOVAR: functional annotation of genetic variants from high-throughput sequencing data. Nucleic Acids Res. *38*, e164.
11. Thompson, J.D., Higgins, D.G., and Gibson, T.J. (1994). CLUSTAL W: improving the sensitivity of progressive multiple sequence alignment through sequence weighting, position-specific gap penalties and weight matrix choice. Nucleic Acids Res. *22*, 4673–4680.
12. Dereeper, A., Audic, S., Claverie, J.-M., and Blanc, G. (2010). BLAST-EXPLORER helps you building datasets for phylogenetic analysis. BMC Evol. Biol. *10*, 8.
13. Dereeper, A., Guignon, V., Blanc, G., Audic, S., Buffet, S., Chevenet, F., Dufayard, J.-F., Guindon, S., Lefort, V., Lescot, M., et al. (2008). Phylogeny.fr: robust phylogenetic analysis for the non-specialist. Nucleic Acids Res. *36*, W465-9.
14. Webb, B., and Sali, A. (2002). Comparative protein structure modeling using MODELLER. In Current Protocols in Bioinformatics (John Wiley & Sons, Inc.).
15. Pei, J., Kim, B.-H., and Grishin, N.V. (2008). PROMALS3D: a tool for multiple protein sequence and structure alignments. Nucleic Acids Res. *36*, 2295–2300.
16. Xu, D., and Zhang, Y. (2011). Improving the physical realism and structural accuracy of protein models by a two-step atomic-level energy minimization. Biophys. J. *101*, 2525–2534.
17. Wass, M.N., Kelley, L.A., and Sternberg, M.J.E. (2010). 3DLigandSite: predicting ligand-binding sites using similar structures. Nucleic Acids Res. *38*, W469-73.
18. Yuen, M., Sandaradura, S.A., Dowling, J.J., Kostyukova, A.S., Moroz, N., Quinlan, K.G., Lehtokari, V.-L., Ravenscroft, G., Todd, E.J., Ceyhan-Birsoy, O., et al. (2014). Leiomodin-3 dysfunction results in thin filament disorganization and nemaline myopathy. J. Clin. Invest. *124*, 4693–4708.
19. Sztal, T.E., Zhao, M., Williams, C., Oorschot, V., Parslow, A.C., Giousoh, A., Yuen, M., Hall, T.E., Costin, A., Ramm, G., et al.

(2015). Zebrafish models for nemaline myopathy reveal a spectrum of nemaline bodies contributing to reduced muscle function. Acta Neuropathol. *130*, 389–406.
20. Redpath, G.M.I., Sophocleous, R.A., Turnbull, L., Whitchurch, C.B., and Cooper, S.T. (2016). Ferlins show tissue-specific expression and segregate as plasma membrane/late endosomal or trans-Golgi/recycling ferlins. Traffic *17*, 245–266.
21. Gietz, D., St Jean, A., Woods, R.A., and Schiestl, R.H. (1992). Improved method for high efficiency transformation of intact yeast cells. Nucleic Acids Res. *20*, 1425.
22. Westerfield, M. (2007). The Zebrafish Book. A Guide for the Laboratory Use of Zebrafish (*Danio rerio*), Fifth Edition (Eugene: University of Oregon Press).
23. Higashijima, S., Okamoto, H., Ueno, N., Hotta, Y., and Eguchi, G. (1997). High-frequency generation of transgenic zebrafish which reliably express GFP in whole muscles or the whole body by using promoters of zebrafish origin. Dev. Biol. *192*, 289–299.
24. Sztal, T.E., Sonntag, C., Hall, T.E., and Currie, P.D. (2012). Epistatic dissection of laminin-receptor interactions in dystrophic zebrafish muscle. Hum. Mol. Genet. *21*, 4718–4731.
25. Ruparelia, A.A., Oorschot, V., Ramm, G., and Bryson-Richardson, R.J. (2016). FLNC myofibrillar myopathy results from impaired autophagy and protein insufficiency. Hum. Mol. Genet., ddw080.
26. Ruparelia, A.A., Zhao, M., Currie, P.D., and Bryson-Richardson, R.J. (2012). Characterization and investigation of zebrafish models of filamin-related myofibrillar myopathy. Hum. Mol. Genet. *21*, 4073–4083.
27. Lek, M., Karczewski, K., Minikel, E., Samocha, K., Banks, E., Fennell, T., O'Donnell-Luria, A., Ware, J., Hill, A., Cummings, B., et al. (2015). Analysis of protein-coding genetic variation in 60,706 humans. bioRxiv http://dx.doi.org/10.1038/nature19057.
28. Adzhubei, I.A., Schmidt, S., Peshkin, L., Ramensky, V.E., Gerasimova, A., Bork, P., Kondrashov, A.S., and Sunyaev, S.R. (2010). A method and server for predicting damaging missense mutations. Nat. Methods *7*, 248–249.
29. Kumar, P., Henikoff, S., and Ng, P.C. (2009). Predicting the effects of coding non-synonymous variants on protein function using the SIFT algorithm. Nat. Protoc. *4*, 1073–1081.
30. Schwarz, J.M., Rödelsperger, C., Schuelke, M., and Seelow, D. (2010). MutationTaster evaluates disease-causing potential of sequence alterations. Nat. Methods *7*, 575–576.
31. Amoasii, L., Bertazzi, D.L., Tronchère, H., Hnia, K., Chicanne, G., Rinaldi, B., Cowling, B.S., Ferry, A., Klaholz, B., Payrastre, B., et al. (2012). Phosphatase-dead myotubularin ameliorates X-linked centronuclear myopathy phenotypes in mice. PLoS Genet. *8*, e1002965.
32. Kachroo, A.H., Laurent, J.M., Yellman, C.M., Meyer, A.G., Wilke, C.O., and Marcotte, E.M. (2015). Evolution. Systematic humanization of yeast genes reveals conserved functions and genetic modularity. Science *348*, 921–925.
33. Trotter, E.W., and Grant, C.M. (2005). Overlapping roles of the cytoplasmic and mitochondrial redox regulatory systems in the yeast *Saccharomyces cerevisiae*. Eukaryot. Cell *4*, 392–400.
34. Kuriyan, J., Krishna, T.S.R., Wong, L., Guenther, B., Pahler, A., Williams, C.H., Jr., and Model, P. (1991). Convergent evolution of similar function in two structurally divergent enzymes. Nature *352*, 172–174.
35. Liu, W., Xie, Y., Ma, J., Luo, X., Nie, P., Zuo, Z., Lahrmann, U., Zhao, Q., Zheng, Y., Zhao, Y., et al. (2015). IBS: an illustrator for the presentation and visualization of biological sequences. Bioinformatics *31*, 3359–3361.

IV. Final thoughts and conclusion

4.1. Humanization of yeast cells and background of the yeast strains

4.1.1. Background of yeast strains, a parameter to be considered

In the project about the myotubularin MTM1, the SEY6210 yeast strain was used as wild type. This strain was constructed by Scott Emr by crossing strains from 5 different laboratories (Gerry Fink, Ron Davis, David Botstein, Fred Sherman, Randy Schekman). Scott Emr used this strain in studies about autophagy and protein sorting. The mutant *ymr1*Δ that I have used during my thesis is a derivative from this SEY6210 strain. This *ymr1*Δ has a fragmented vacuole with several small lobes, unlike the SEY6210 wild type, which has one unilobed vacuole. This vacuolar phenotype was central for the experiments performed on myotubularin MTM1 throughout my thesis. Noteworthy, the *ymr1*Δ from the systematic yeast deletion collection provided by Euroscarf for the scientific community has a different background. This *ymr1*Δ is a derivative mutant of the laboratory strain BY4742. It was shown by Dimitri Bertazzi during his thesis that this *ymr1*Δ mutant strain in the BY4742 background does not present fragmented vacuoles, a characteristic of the increased level of PtdIns3P observed in the *ymr1*Δ with the SEY6210 background. Therefore to study MTM1 and other myotubularins, only the *ymr1*Δ strain in the SEY6210 background was used.

In the project about the dynamin DNM2, I have used 3 strains from the yeast deletion collection, the BY4742, *vps1*Δ and *dnm1*Δ. These strains are derived from S288C. I have tried to establish a phenotype between wild type and mutant strains in order to study the human DNM2. However, the deficiencies of yeast cells lacking Vps1 or lacking Dnm1 have not been restored by the human DNM2 despite performing different experiments. I have not validated yet a rescue phenotype that would allow carrying out experiments about CNM patient mutations in DNM2. Considering these results and the need to find a phenotype in order to humanize yeast with human dynamin, it would be interesting to use other yeast strain. It would be possible to create the mutant *vps1*Δ in the SEY6210 background. Since SEY6210 has been used by Scott Emr for protein sorting studies and

the Vps1 (vacuolar protein sorting 1) is a yeast protein implicated in trafficking, it would be interesting to establish the phenotype in *vps1*Δ cells with the SEY6210 background and to humanize them with hDNM2. Moreover the DNM2 was suggested to play a role in membrane trafficking (Ishida et al, 2011). Similarly, it would be possible to create the *dnm1*Δ deletion mutant in the SEY6210 background. The SEY6210 strain was used in autophagy studies and DNM2 is important for the autophagy of cytosolic lipid droplets, as explained in Introduction. It would be interesting to perform experiments about autophagy with the dynamin DNM2, as for the myotubularin MTM1.

I could not reproduce the *grx6*Δ strain redox defect observed by Puigpinos and colleagues (Puigpinos et al, 2015). One possible explanation would be that they have used the *grx6*Δ strain constructed in the W303-1A background. This W303-1A strain has a mutation in the *YBP1* gene, which abolishes its function required for oxidation, increasing its sensitivity to oxidative stress (SGD database). Therefore, I should also analyze the oxidative stress response in the *grx6*Δ and the *dnm1*Δ deletion mutant strains constructed into the W303-1A background.

4.1.2. Studying human proteins in yeast cells

Throughout the history of molecular biology, yeast has been widely used as a model in different laboratories to study different pathways in eukaryotic cells. Several discoveries made in yeast were later extrapolated to human cells, allowing acquisition of new knowledge. However, humanization of yeast cells is a recent approach used in research to gain access to cellular functions of human proteins. Even if this approach is really powerful, it is also complex, and does not always work out as observed for the study of human dynamins in yeast cells. Indeed, in a systematic study only about 50% of the yeast genes were successfully humanized (Kachroo et al, 2015).

In a recent study, different CMT patient mutations such as DNM2-G358R were mimicked in the Vps1 yeast protein orthologue and analyzed, as the vps1-G397R mutant for example, in order to study the effect of these mutations in the molecular and cellular function of the yeast Vps1 dynamin (Moustaq et al, 2016). This approach by generating equivalent DNM2 patient mutations in the yeast Vps1 protein was effective and demonstrated that some of these CMT patient mutations disrupt Vps1 oligomerization, endocytosis or lipid binding (Moustaq et al, 2016). However, based on my studies showing that the human *DNM2* does not rescue the trafficking defects of yeast *vps1*Δ mutant cells, maybe these yeast results do not reproduce the CNM patient defects of the human DNM2. Moreover, this approach by introducing the patient mutations in the yeast protein is also limited by

the poor conservation in amino acids between the yeast and the human proteins, as shown by my protein alignments and conservation studies (figure 29 and 35).

In view of the results I have obtained in the DNM2 project, it would be possible to imagine a difference in evolution between yeast and human dynamin proteins. For that it is necessary to take into account that the dynamin-related proteins Vps1 and Dnm1 yeast proteins are lacking the PH and PRD domains, unlike the human dynamins hDNM1, hDNM2 iso1 and hDNM2 iso 12b. The human dynamin domain organization could be the result of evolution via sequence re-arrangements such as domain-wise evolution, the fusion of small peptide fragments or the "chimeric" recombination of fragments (Sikosek & Chan, 2014).

4.2. Centronuclear myopathies

Centronuclear myopathies linked to mutations in *MTM1*, *DNM2* and *PYROXD1* genes provoke hypotonia and muscle weakness. The most severe cases suffer respiratory failure; other patients need ventilation respiratory or a wheelchair. Various causes can lead to alterations in excitation-contraction coupling in muscles; and several factors, as organelles or intracellular pathways are in play. We can consider neuromuscular disorders as resulting from problems in energy production where mitochondria could be implicated, or in an electrochemical potential imbalance where Golgi could be involved. The patients affected by centronuclear myopathies are not able to contract their muscles or to maintain their tonicity. Symptoms are the consequences of macromolecular deficiencies in cells and/or between cells. To better understand centronuclear myopathies, it is important to better characterize the dysfunctions of the muscles at the molecular level. In my opinion, we could use the knowledge about the molecular dysfunctions present in these diseases and link them to the symptoms observed in patients by doctors, since this integrated approach could help to discover new symptoms which may have not been considered and this could also help fundamental research to go further and to develop new lines of researches based on the diagnosis of the doctors.

The muscle type I fibers are the main fibers affected in these centronuclear myopathies. These type I fibers are characterized by a higher concentration of mitochondria, which is coherent with the mitochondria defects observed in the muscles of patients affected of centronuclear myopathies. In addition, mitochondria are the main organelles producing the energy in form of ATP, and muscles and neurons need a lot of energy to correctly fulfill their functions. Therefore, type I fibers also

have the highest concentration of oxidative enzymes. Interestingly, they also have a high concentration in lipids, and lipids are oxidized by β-oxidation in the mitochondria and peroxisomes; two organelles affected in neuromuscular diseases. The pattern of motor neuron activity is a key determinant of muscle fiber specification: slow fibers, as fibers type I, experience more frequent neuronal stimulation than fast fibers, and this results in higher levels of $[Ca^{2+}]_{cyt}$ present in slow fibers compared to fast fibers. Interestingly, *in vitro*, fast fibers can be converted to slow fibers by exposing them to frequent electrical stimulation that mimics the neuronal activity pattern of a slow fiber (Cyert, 2003).

Taking into account these properties of type I fibers and the organization of sarcomeres in muscle, I have tried to connect different cellular functions observed in muscles: reactive oxygen species (ROS), β-oxidation of lipids and lipid peroxidation, membrane curvature and dynamics concerning the lipid composition of membranes, the flow of calcium which triggers muscle contraction through the action potential and also for example favors GLUT4 translocation but inhibits myosinV mobility during contraction; and finally, the endoplasmic reticulum stress and the unfolded protein response, linked to autophagy, problems in trafficking and ionic imbalance as it is the case of calcium in RYR- or STIM- related CNM. If we think that action potential is an electrochemical potential and patients have deficiencies in muscle contraction because of deficiencies in energy demanding; I think it is important to ask: where does this energy come from and which players are implicated? This is a general question that opens a huge diversity of possibilities, which could be studied in further researches.

"Because PhD means Philosophiæ Doctor"

I apologize from now if in the next paragraphs, I make mistakes about symptoms in patients, since I am not a medical doctor and my idea is rather to connect fundamental research in science with medicine, by asking questions whose answers could help unraveling molecular and cellular dysfunctions linked to the CNM diseases.

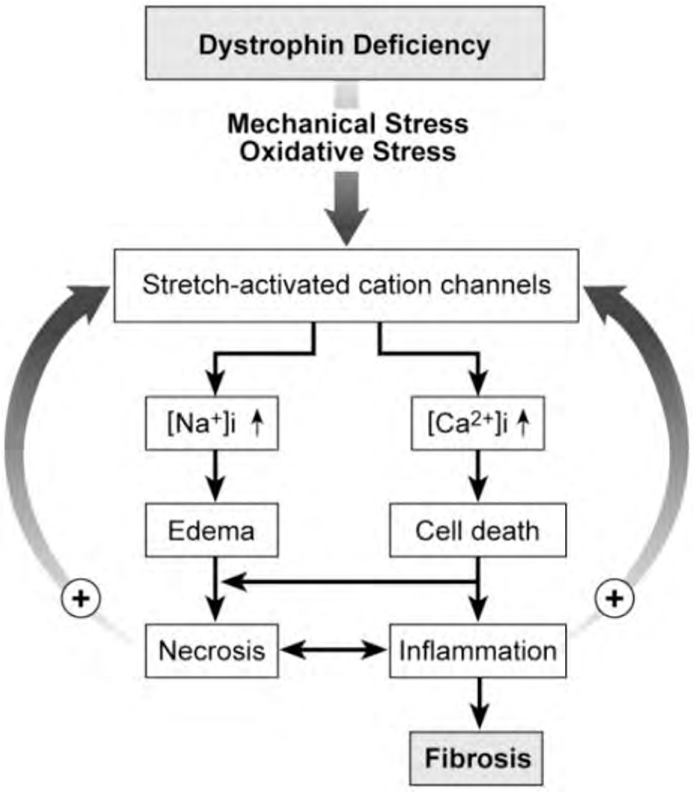

Figure 55: From dystrophin deficiency to fibrosis in Duchenne muscular dystrophy. Fibrosis is the formation of excess fibrous connective tissue in an organ or tissue in a reparative or reactive process.

Do the patients affected by CNM present symptoms linked to oxidative stress? Is fibrosis observed in CNM patients muscle histology as observed for Duchenne muscular dystrophy (figure 55), and could this be the consequence of an oxidative stress (figure 55)?

Do patients have a problem with calcium in bones and in teeth and could this be progressive?

Are there reports of electrochemical problems in patients? Has the action potential of neurons been measured? And in neuromuscular junction?

4.3. Muscle disorders with oxidative stress features.

It has been shown that DNM2 interacts with endothelial nitric oxide synthase, eNOS or NOS3 (Su, 2014), as well as with the nNOS in collecting ducts in rat (neuronal isoform or NOS1) (Hyndman et al, 2016). Both isoforms constitutively synthesize nitric oxide from L-arginine in a calcium-

calmodulin dependent manner. Nitric oxide (NO) is a free radical, which in biology is called reactive nitrogen specie (RNS). The nNOS isoform is located at the nervous tissue (central and peripheral nervous system) and skeletal muscle type II. The eNOS isoform is located at the endothelium and generates NO in blood vessels and is involved in regulating vascularization. Interestingly, eNOS is located on the Golgi complex and in the caveolae of endothelial cells (Liu et al, 1997).

Do CNM patients have problems in kidney functions?

Do CNM patients have problems in the formation of blood vessels and capillaries in some specific tissues? What about vascularization in skeletal muscle?

In mammalian cells, it is known that the actin cytoskeleton network is required for the morphology and cellular positioning of the Golgi apparatus, and disruption of the actin cytoskeleton network causes a concomitant collapse of the Golgi complex (figure 56) (Valderrama et al, 1998; Valderrama et al, 2000). In yeast *Saccharomyces cerevisiae*, Vps1 was identified as a new factor at the TGN required for normal actin organization (Yu & Cai, 2004). These data further support the connection between protein transport and actin cytoskeleton organization. New experiments could be performed with the *vps1*Δ strain concerning the link between the Golgi complex and the actin cytoskeleton in order to find a phenotype that could be rescued by hDNM2.

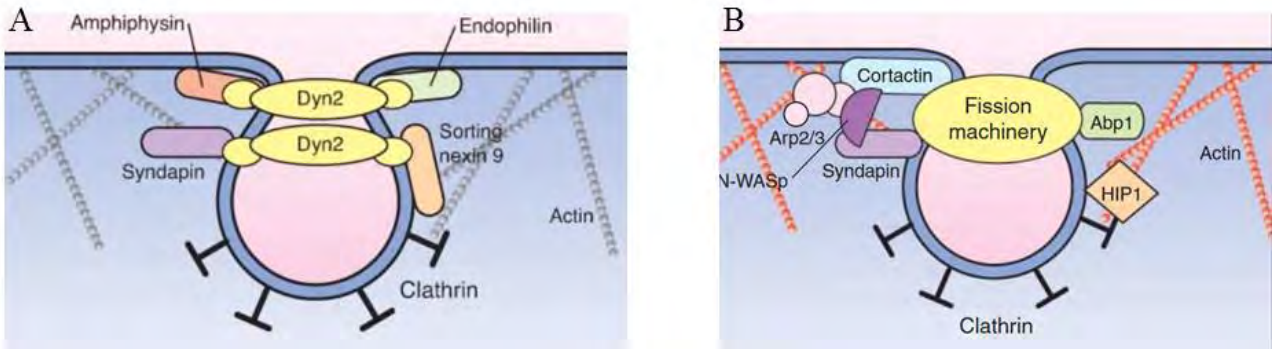

Figure 56: Membrane tubulation mechanism at the plasma membrane PM and TGN. Similar protein players are used to bind and deform lipids at both the PM and TGN. Along with conventional clathrin coats and adaptors, amphiphysins having BAR domain bind and deform membranes into tubules, in concert with Dynamin 2 (Dyn2) and the actin cytoskeleton (A). The vesicle fission machinery associated to actin cytoskeleton organization liberates the nascent vesicles from both the PM and TGN. A complex actin cytoskeletal network centered around proteins involved in

membrane fission functions together with the clathrin-based sorting and budding machinery to complete the process of cargo sequestration, vesicle formation, and membrane scission (B). From (McNiven & Thompson, 2006).

4.4. Oxidative stress and neuropathies.

Other genes than *DNM2* linked to oxidation-reaction system have been shown to be involved in Charcot-Marie disorders, as for example *GDAP1*. The *GDAP1* gene encodes a protein belonging to the glutathione S-transferase (GST) enzyme subfamily. Autosomal recessive mutations in this *GDAP1* gene cause the axonal, intermediate and demyelinating forms of the disease. Even if the GST enzymatic activity of this protein has to be demonstrated, the GDAP1 protein plays a role in peroxisome fission, regulation of mitochondrial dynamics and calcium homeostasis (Sivera et al, 2017). Indeed, in mammalian cells the mechanism of growth and division of peroxisomes is initiated by a membrane remodeling process similarly to mitochondria and regulated by peroxisomal morphology proteins such as Pex11, DLP1/Drp1, Fis1, Mff, and GDAP1, which with the exception of Pex11, are partially shared with mitochondria (Schrader et al, 2016).

The calcium/calmodulin-dependent phosphatase calcineurin may dephoshorylate endocytic proteins such as dynamin (Sun et al, 2010). Calcineurin could play a role in rapid and slow endocytosis observed at synapses. It is noteworthy that modulation of intracellular Ca^{2+} homeostasis through thiol redox regulation of transporters may be evolutionary conserved in eukaryotes (Oka & Bulleid, 2013; Puigpinos et al, 2015). Therefore, it would be interesting to conduct new experiments linking calcium and redox regulation in yeast in the *dnm1*Δ strain.

PIKFyve participates in the translocation of GLUT4 to the membrane in mammalian cells and DNM2 plays also a role in GLUT4 translocation. Fab1 is the yeast homologue of PIKFyve and the Gap1 protein in yeast is the homologue of GLUT4. Gap1 interacts with the GSH1 that catalyzes the first step of GSH synthesis and with Pis1 (phosphatidylinositol synthase) (Shewan et al, 2013). It would be interesting to analyze the Gap1 trafficking in the *dnm1*Δ or *vps1*Δ strains.

Interestingly in yeast cells, stress triggers triacylglycerol accumulation in lipid droplets. Lipid droplets are physically connected to the different organelles such as endoplasmic reticulum, mitochondria, and peroxisomes (Yadav et al, 2017). However, the physiological relevance of these physical interactions needs to be further study. Anyway, it has been shown that alterations in DNM2 function lead to an accumulation of lipid droplet in hepatocytes (Schulze & McNiven, 2014).

Has the translocation of Glut4 at the membranes been measured in patients and if yes is it effective? What about the accumulation of lipid droplets in hepatocytes in patients?

There could be a relation between the percentage of fat in membranes and problems in the curvature of membranes in CNM patients. Interestingly, recently studies in the laboratory of Fanny Pilot-Storck have shown abnormalities in the synthesis of very long fatty acids are linked to myoblast fusion and to abnormalities in the mitochondria crista (Blondelle et al, 2015). Related studies have been performed in yeast by Ludovic Pineau during his doctoral thesis where deficiency of unsaturated fatty acid and ergosterol provoked a stress in membrane curvature, decreasing membrane curvature and affecting membrane trafficking from the Golgi to the vacuole (Pineau et al, 2008).

Have problems in the fat metabolism been observed in patients?

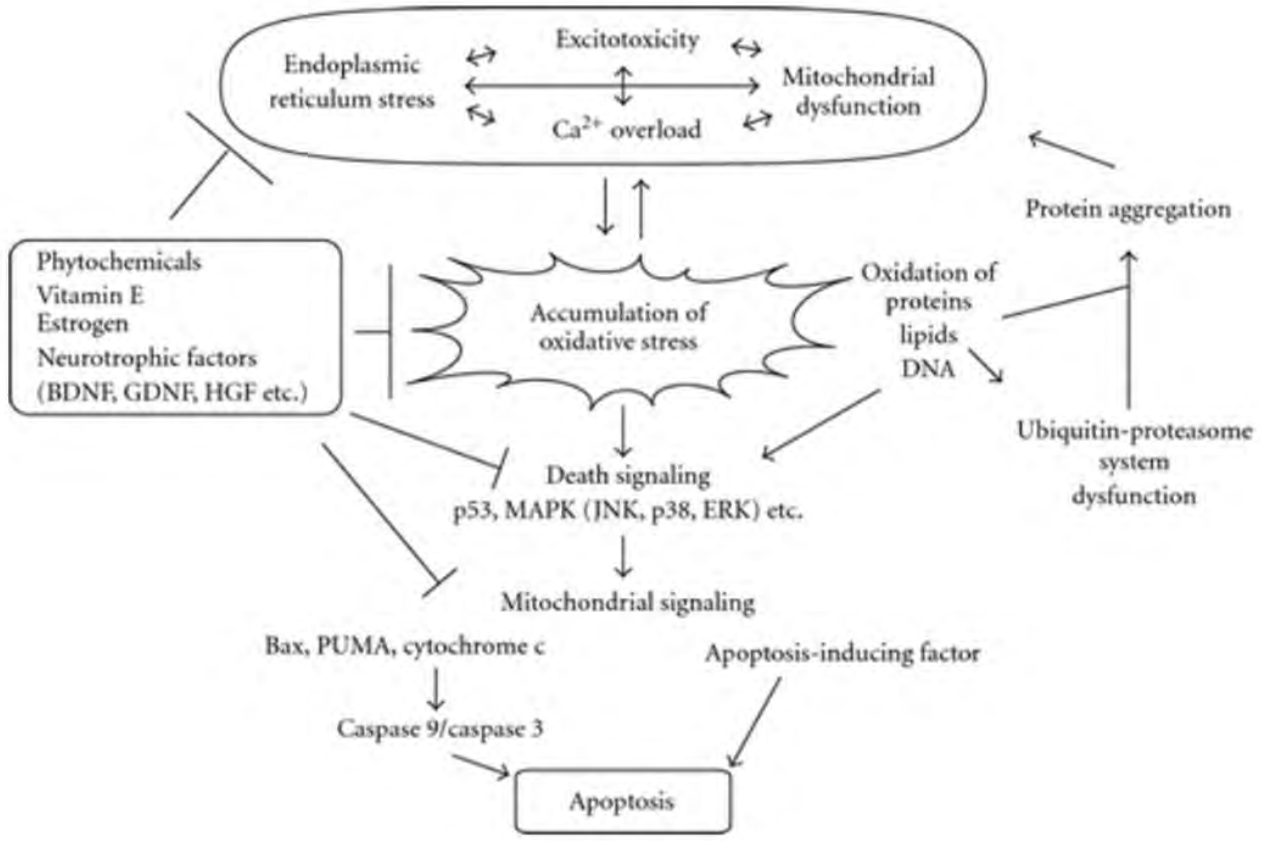

Figure 57: Mechanisms underlying oxidative stress-mediated neuronal apoptosis. Effects of oxidative stress in neurodegenerative diseases. Events such as excitotoxicity, mitochondrial dysfunction, Ca^{2+} overload, and endoplasmic reticulum stress are associated with excess reactive oxygen species (ROS) and reactive nitrogen species (RNS) generation. From (Numakawa et al, 2011).

4.5. Conclusion

As a general conclusion, centronuclear myopathies are complex genetic diseases with several features being altered in skeletal muscle. What is the most surprising in these genetic diseases is that the genes bearing the mutations are ubiquitously expressed, since their expression is not restricted to nervous tissues and skeletal muscles. However, the nervous system and the skeletal muscles are the tissues affected by the disease. The MTM1 myotubularin is a phosphoinositide 3-phosphatase and mutations in the *MTM1* gene are responsible for X-linked centronuclear myopathy. Myotubularins from the same family as MTM1 and some being very similar is amino acids sequences such as MTMR2 are associated with a Charcot-Marie Tooth neuropathy (Raess et al, 2017b). The centronuclear myopathy due to mutations in the *DNM2* gene is also surprising since mutations in the same gene lead either to a myopathy or to a neuropathy, with the missense mutations being sometimes only distant from few amino acids (figure 13). Moreover, there is no correlation between the position of the mutations in a specific domain of the DNM2 protein and the resulting type of disease CNM or CMT (figure 13). For the moment, there are no molecular explanations allowing us to understand why some mutations lead to myopathy and others to neuropathy. Maybe there is a specific tissue feature due to association with a specific protein, or due to some specific splice variants as the muscular DNM2 isoform 12b, recently identified by Belinda Cowling in the laboratory of Jocelyn Laporte (Cowling et al, 2017). Indeed, DNM2 could interact with different partners depending on the tissue, as it was observed for MTM1 that interacted with Desmin, a specific muscle protein (Hnia et al, 2011). There could also be some specific conformation changes depending on the environment conditions. For example, different pH could provoke changes in the protein folding allowing interaction with a specific protein, or changing the localization of the protein. The oxidative stress has a different effect on the different phosphoinositide 3-phosphatases, since ROS have a strong impact on PTEN phosphatase activity compared to myotubularins that are poorly affected by ROS (Ross et al, 2007). An ionic imbalance could also lead to changes in electrical charges, which in turn modify the capacity of interaction between enzymes and their substrates or between two interacting proteins. Taking into account the symptoms of the CNM patients it could be possible to design new experiments using yeast cells or other mammalian model organism in order to highlight molecular features implicated in these human diseases.

V. MATERIALS AND METHODS

Bioinformatic tools

Human dynamin protein sequences and isoform informations were consulted on ncbi, Ensembl genome browser 84 and Uniprot databases. Regarding protein size information, Expasy Translator Tool and Expasy Protparam were used. Multiple sequence alignments were performed with EMBL-EBI Clustal Omega software.

Saccharomyces Genome Database (SGD) was used as support for yeast phenotypic informations. In addition, BioGRID 3.4 was used for yeast protein interactors while STRING was used for human protein-protein interactions. A plasmid Editor (ApE) v2.0.49 was used for PCR and cloning design.

Plasmids and vectors constructs

The human MTM1 ORF, the PH/GRAM domain (1-160 aa) or the catalytic domain (161-603 aa) were cloned into pDONR207 plasmid (Invitrogen) to generate an entry clone. Gateway system (Invitrogen) was used to clone the different MTM1 constructs into the yeast expression vectors pAG424 and pAG426, which are tagged with GFP or DsRed proteins respectively. The C375S mutation was introduced into the hMTM1 by polymerase chain reaction (PCR) with Phusion High-Fidelity DNA polymerase (Thermo Scientific) on the pAG424 entry vector bearing hMTM1. (table1)

Name	Antibiotic Resistance	Yeast Replication	Auxotrophy Marker	Reference
pDONR207 Entry vector Gateway®	Gentamycin	-	-	Invitrogen
pAG424GPD_**EGFP**-ccdB GFP in N-terminus position	Ampicillin	2µ	TRP1	S.Lindquist
pAG424GPD_ccdB-**EGFP** GFP in C-terminus position	Ampicillin	2µ	TRP1	S.Lindquist
pAG426-GPD-ccdB-**Dsred**	Ampicillin	2µ	URA3	S.Lindquist
pDONR207-catalytic domain (MTM1) - No Stop	Gentamycin	-	-	D. Bertazzi
pAG424 - catalytic domain **- GFP**	Ampicillin	2µ	TRP1	This study
pAG426 - catalytic domain **-DsRed**	Ampicillin	2µ	URA3	This study
pDONR207 - MTM1 WT Full length - No Stop	Gentamycin	-	-	D. Bertazzi
pAG424 - MTM1**-GFP**	Ampicillin	2µ	TRP1	D. Bertazzi
pDONR207 - MTM1WT Full length - Stop	Gentamycin	-	-	This study
pAG424- **GFP-**MTM1 (GFP N-ter)	Ampicillin	2µ	TRP1	D. Bertazzi
pDONR207 - PH/GRAM (MTM1) - No stop	Gentamycin	-	-	This study
PH/GRAM-**DsRed**, Backbone pAG426	Ampicillin	2µ	URA3	This study

pAG424 - PH/GRAM-**GFP**	Ampicillin	2µ	TRP1	This study
pAG424 - **GFP**-PH/GRAM (GFP N-ter)	Ampicillin	2µ	TRP1	This study
pAG424 - MTM1-C375S-**GFP**	Ampicillin	2µ	TRP1	This study
pGEN		2µ	TRP1	Gari et al., 1997
pCM185		CEN-ARS	TRP1	Gari et al., 1997
pCM189		CEN-ARS	URA3	
pMD2		2µ	URA3	
pVV200 promPGK1-catalytic domain	Ampicillin	2µ	TRP1	D. Bertazzi
pVV200 promPGK1 PH/GRAM	Ampicillin	2µ	TRP1	D. Bertazzi
pVV214 promPGK1 hMTM1	Ampicillin	2µ	URA3	D. Bertazzi
pVV214 promPGK1 hMTM1 C375S,	Ampicillin	2µ	URA3	D. Bertazzi
pVV214 promPGK1 hMTMR12	Ampicillin	2µ	URA3	D. Bertazzi
pVV208 hMTM1	Ampicillin	CEN-ARS	URA3	D. Bertazzi
pVV208 hMTM1-C375S	Ampicillin	CEN-ARS	URA3	D. Bertazzi
pVV204 promTetON MTMR12	Ampicillin	CEN-ARS	TRP1	D. Bertazzi
pVV200 MTMR12	Ampicillin	2µ	TRP1	D. Bertazzi

Table 1: Plasmids used during the Myotubularin project

All the plasmids bearing dynamin genes were constructed by Gateway® Cloning technology (table 2). In a first step, PCR reactions were carried out for cloning the different cDNA of human dynamins: hDNM2 iso1, hDNM2 iso12b, hDNM1 iso1 and hDMN1L iso3. All these cDNAs were cloned in order to give the full-length proteins with or without an EGFP Tag in C-terminal. In case of EGFP tagged constructs, the reverse primer was designed in order to remove STOP codon

The cDNA of hDNM2 iso1 was amplified from a plasmid kindly provided by Jocelyn Laporte´s Team (IGBMC, Ilkirch). PCR was carried out with primers (Eurofin Genomics) (forward, GGGGACAAGTTTGTACAAAAAAGCAGGCTTCatgggcaaccgcgggatgg; reverse with STOP, GGGGACCACTTTGTACAAGAAAGCTGGGTCctagtcgagcagggatggc; reverse without STOP, GGGGACCACTTTGTACAAGAAAGCTGGGTCgtcgagcagggatggctcggc).

hDNM2 iso12b PCR was performed using a plasmid kindly provided by Jocelyn Laporte´s Team (IGBMC, Ilkirch). The same primers as the ones used for the amplification of hDNM2 iso1 were used. The PCR reaction composition: 1 µl of 10 µg/ml of plasmid, 1 µl of dNTP 10 mM (Thermo Fisher Scientific), 2.5 µl of forward (10 µM), 2.5 µl of reverse primer (10 µM), 0.5 µl of Phusion High-Fidelity DNA Polymerase 2 U/ µl (Thermo Fisher Scientific), 10 µl HF Buffer 10X (Thermo Fisher Scientific) and 30.5 µl of H_2O. The program: 98ºC 30”, (98ºC 30”, 48ºC 30”, 72ºC 3´) X 30, 72ºC 5´, and hold at 16 º C or store at 4 º C.

Amplification of hDNM1 iso1 was carried out using the pEGFPN1-human dynamin 1 plasmid delivered by addgene. PCR was performed with primers (forward, GGGGACAAGTTTGTACAAAAAAGCAGGCTTCatgggcaaccgcggcatggaag; reverse without STOP, GGGGACCACTTTGTACAAGAAAGCTGGGTCgaggtcgaaggggggcctggggctctc; reverse with STOP, GGGGACCACTTTGTACAAGAAAGCTGGGTCttagaggtcgaaggggggcctggggctctc). The reaction mix consisted of 0.5 µl of 5000U/ml Recombinant Taq DNA Polymerase (GE Healthcare Life Sciences), 1 µl of Forward primer (10 µM), 1 µl of Reverse primer (10 µM), 1 µl of Plasmid (10 µg/ml), 1.5 µl of DMSO 100% (GE Healthcare Life Sciences), 1 µl of dNTP 10 mM (Thermo Fisher Scientific), 5 µl of PCR Buffer 10X (GE Healthcare Life Sciences) and 39 µl of H_2O. The use of 3% of DMSO was based on the fact that secondary structures (self-dimers) are easily formed between these oligos as predicted (Oligo Analyzer 3.1 Software, Integrated DNA Technologies). The PCR was done as follows: 98ºC 30", (95ºC 30", 52ºC 30", 72ºC 3´) X 30, 72ºC 5´, hold at 16ºC or store at 4ºC.

A pDONR vector bearing the cDNA of hDNM1L iso3 was purchased from DNASU and used directly in a LR Reaction carried out by Bruno Rinaldi before I joined the team.

The forward and reverse primers used for the different PCR reactions shown above are designed to contain sequences that hybridize the human dynamin protein coding sequence (lower case letters) starting at the ATG initiation codon (forward primer) or stopping at the STOP codon or before the STOP codon for EGFP tagging (reverse primer) and sequences required for recombination step in Gateway® BP reaction (capital letters).

Type	Name	Antibiotic Resistance	Yeast Replication	Auxotrophy Marker
pDONR Backbone	pDONR221 (addgene)	Kanamycin	-	-
pDONR Backbone	pDONR207 (addgene)	Gentamycin	-	-
pDEST Backbone	pAG413GPD-ccdB (addgene)	Ampicillin	CEN-ARS	HIS3
pDEST Backbone	pAG413GPD-ccdB-EGFP (addgene)	Ampicillin	CEN-ARS	HIS3
BP Product	pDONR207-hDNM2 iso1	Gentamycin	-	-
BP Product	pDONR207-hDNM2 iso1-NO STOP	Gentamycin	-	-
BP Product	pDONR221-hDNM2 iso12b	Kanamycin	-	-
BP Product	pDONR221-hDNM2 iso12b-NO STOP	Kanamycin	-	-
BP Product	pDONR221-hDNM1 iso1	Kanamycin	-	-
BP Product	pDONR221-hDNM1 iso1-NO STOP	Kanamycin	-	-
BP Product	pDONR221-hDNM1L iso3	Kanamycin	-	-
BP Product	pDONR221-hDNM1L iso3-NO STOP	Kanamycin	-	-
LR Product	pAG413GPD-hDNM2 iso 1	Ampicillin	CEN-ARS	HIS3
LR Product	pAG413GPD-hDNM2 iso 1-EGFP	Ampicillin	CEN-ARS	HIS3

LR Product	pAG413GPD-hDNM2 iso 12b	Ampicillin	CEN-ARS	HIS3
LR Product	pAG413GPD-hDNM2 iso 12b-EGFP	Ampicillin	CEN-ARS	HIS3
LR Product	pAG413GPD-hDNM1 iso 1	Ampicillin	CEN-ARS	HIS3
LR Product	pAG413GPD-hDNM1 iso 1-EGFP	Ampicillin	CEN-ARS	HIS3
LR Product	pAG413GPD-hDNM1L iso 3	Ampicillin	CEN-ARS	HIS3
LR Product	pAG413GPD-hDNM1L iso 3-EGFP	Ampicillin	CEN-ARS	HIS3

Table 2: Vectors constructed and used during the Dynamin project. Gateway ® backbone vectors, as well as the products of BP and LR reactions are shown. Antibiotic resistance was used for the amplification of plasmid in *E.coli* DH5α.Yeast replication shows that plasmids used were low copy ones. Auxotrophy HIS3 enabled the work with the same marker for all plasmids

Plasmids maps of either PYROXD1 gene wild type, or with Q375H or N155S mutations were received from IGBMC and analyzed with the software "A plasmid editor" ApE. A problem in reading frame was detected, in order to synthesize the correct plasmids (table 3) I ordered new primers. New produced plasmids were verified by enzymatic digestion and then sanger sequencing (GATC company). A first simple digestion was made with PstI and a second double digestion with BglII and DraIII enzymes. Primers used for PCR and gateway cloning were: forward, GGGGACAAGTTTGTACAAAAAAGCAGGCTTCATGGAGGCAGCGCGCCCTCC; reverse with STOP, GGGGACCACTTTGTACAAGAAAGCTGGGTCTTAGTCAAAATAATCTTC; and reverse without STOP GGGGACCACTTTGTACAAGAAAGCTGGGTCGTCAAAATAATCTTC

Type	Description	Antibiotic Resistance	Yeast Replication	Auxotrophy Marker
BP Product	pDONR221-pyroxd1 WT Stop	Kanamycin	-	-
BP Product	pDONR221-pyroxd1 Q372 **No Stop**	Kanamycin	-	-
BP Product	pDONR221-pyroxd1 N155S Stop	Kanamycin	-	-
BP Product	pDONR221-pyroxd1 WT **No Stop**	Kanamycin	-	-
BP Product	pDONR221-pyroxd1 Q372H Stop	Kanamycin	-	-
BP Product	pDONR221-pyroxd1 N155S **No Stop**	Kanamycin	-	-
LR Product	pAG415 GPDprom – Pyroxd1 WT STOP	Ampicillin	CEN-ARS	LEU2
LR Product	pAG415 GPDprom – Pyroxd1 N155S STOP	Ampicillin	CEN-ARS	LEU2
LR Product	pAG415 GPDprom – Pyroxd1 Q372H STOP	Ampicillin	CEN-ARS	LEU2
LR Product	pAG415 GPDprom – Pyroxd1 WT **EGFP** c-term	Ampicillin	CEN-ARS	LEU2
LR Product	pAG415 GPDprom – Pyroxd1 N155S **EGFP** c-term	Ampicillin	CEN-ARS	LEU2
LR Product	pAG415 GPDprom – Pyroxd1 Q372H **EGFP** c-term	Ampicillin	CEN-ARS	LEU2

Table 3: Vectors constructed and used during the Pyrod1 project

Bacteria strains, culture conditions and transformation protocol

Two different *E. coli* bacteria strains were used for this study:

- **DH5 alpha** was used for amplification of plasmids without the *ccdB* gene. Genotype: *fhuA2 lac(del)U169 phoA glnV44 Φ80' lacZ(del)M15 gyrA96 recA1 relA1 endA1 thi-1 hsdR17*
- **DB3.1** was used for amplification of plasmids containing the *ccdB* gene which is important for Gateway cloning. This strain is ccdB resistant. Genotype: *gyrA462 endA1 Δ(sr1-recA) mcrB mrr hsdS20 glnV44 (=supE44) ara14 galK2 lacY1 proA2 rpsL20 xyl5 leuB6 mtl1*.

For liquid cultures, bacteria were grown at 37°C under agitation in LB (Lysogeny Broth, Yeast Extract 5 g/L ; Tryptone 10 g/L , NaCl 10 g/L) supplemented with the adapted antibiotic (Amp 1/1000 in general).

For culture in Petri dishes, agar-agar (20 g/L, Euromedex) was added to the LB medium, and bacteria were grown at 37°C.

Bacterial transformation protocol consisted of using chimiocompetent DH5α *E.coli*. 100 µl Aliquots were thawed on ice. 5 µl of plasmid (300-500 µg/ml) were added to the thawed out bacteria and kept for 30 minutes. After 45 seconds heat shock (42ºC), 200 µl of LB media were added. The tube was incubated for 1 hour at 37ºC except for Ampicillin selection. Afterwards, bacteria were spread on an antibiotic-LB plate and incubated over-night at 37ºC until the appearance of clones. The day after, some clones were selected and grown in an over-night liquid culture of 2 ml of LB + antibiotic at 37ºC and 200 rpm agitation (INFORS).

Plasmid isolation was performed with GeneJET Plasmid Miniprep Kit (Thermo Fisher Scientific). Plasmid isolation products were analyzed by restriction enzyme digestion with Thermo Scientific™ FastDigest™ enzymes. 300 ng of plasmid, 1 µl of Green Buffer 10X (Thermo Fisher Scientific), 1 µl of restriction enzyme (if two enzymes 0.5 µl each) and QS to 10 µl with H2OmilliQ. After 15 minutes of incubation at 37ºC, the reaction was loaded on a 1% agarose gel. BP products were sequenced before LR reaction. 30 µl of 100 ng/ µl of plasmid were sequenced by GATC Biotech. M13 forward primer (TGTAAAACGACGGCCAGT) and M13 reverse primer (CAGGAAACAGCTATGACC) were used.

LR reaction mix consisted of 150 ng of pENTR plasmid as entry vector, 150 ng of pDEST plasmid as destination vector, and 2µl of LR Buffer 5 X (Thermo Fisher Scientific), 1 µl of Gateway® LR Clonase® Enzyme mix (Thermo Fisher Scientific) and QS to 10 µl with H2OmilliQ. After

one hour at 25ºC the transformation followed the same protocol as described above for bacterial transformation and for plasmid isolation. Plasmids were verified by enzymatic restriction analyses.

Yeast Strains and media

S. cerevisiae *ymr1*Δ (Matα ura3-52, leu2-3, 112, his3-Δ200, trp1-Δ901, lys2-801, suc2-Δ9, ymr1::HIS3) and wild-type SEY6210 strain (genotype MATα ura3-52, leu2-3, 112, his3-Δ200, trp1-Δ901, lys2-801, suc2-Δ9) cells were grown at 30°C in rich medium (YPD): 1% yeast extract, 2% peptone, 2% glucose or synthetic drop-out medium (SC): 0.67% yeast nitrogen base with ammonium sulphate , 2% glucose and the appropriate amino acids mixture to ensure plasmids maintenance.

S. cerevisiae wild-type BY4742 (genotype MATα his3Δ1 leu2Δ0 lys2Δ0 ura3Δ0), *vps1*Δ (MATα his3Δ1 leu2Δ0 lys2Δ0 ura3Δ0 *vps1*::kanMX) and *dnm1*Δ (MATα his3Δ1 leu2Δ0 lys2Δ0 ura3Δ0 *dnm1*::KanMX) strains were used in the experiments.
*S. cerevisiae pex14*Δ (UTL7A MATa ura3-52 trp1 leu2-3/112 *pex14*::LEU2) strain was used as control for the peroxisome numbering experiments.

YPD-Agar media consisted of 1 % (m/v) yeast extract (EUROMEDEX), 2% (m/v) peptone (EUROMEDEX), 2% (m/v) D-Glucose (EUROMEDEX) and 2 % (m/v) Agar-Agar (EUROMEDEX).
SC auxotrophic selection medium plates consisted of 0.67% (m/v) YNB with ammonium sulfate (MP), 2 % (m/v) D-Glucose (EUROMEDEX), 0.128 % (m/v) of CSM-aa (MP) and 1 % (m/v) Agar-Agar (MP).
Liquid medium composition were the same as the described above with exception of agar-agar.
The media were autoclaved at 120°C for 20 min for sterilization.

Yeast Transformations

Yeast cells from YPD-Agar plate were diluted in 1ml of sterile water and centrifuged. After the centrifugation, the pellet was suspended in 20 µl of sterile water. 5 µl of DNA from salmon sperm 10 mg/ml were added and then mixed. 2 µl of plasmid (0.5-1 µg) were added and mixed again. Finally, addition of 500 µl of Polyethylene glycol (PEG) 4000/Lithium Acetate buffer was required. This buffer consisted of 40 % (m/v) PEG4000, 0.1 M Lithium Acetate, 10 mM Tris HCl pH 7.5 and EDTA 1 mM. After 15 minutes of incubation at room temperature and 15 minutes at 42ºC, a centrifugation of 30 seconds at 3000 rpm was done. One washing step was done with 1 ml of

sterile H_2O. The suspended pellet (100 µl of sterile water) was spread on a selective medium plate and incubated at 30ºC for 3-4 days until the clones appeared.

Protein Extraction and Western Blots

Yeast transformations were grown in an over-night YPD preculture (2 ml) at 30ºC and 200 rpm (INFORS). A dilution was done in the morning in selective media (SC-aa). The protein extraction protocol started when the OD_{600} reached 1. The equivalent volume to OD_{600} 1.5 was centrifuged 2 min at 5000 rpm (Eppendorf centrifuge 5418). Enough supernatant was removed in order to have 500 µl of remaining volume. 50 µl of NaOH 1.85 M were added and mixed gently and remained 10 minutes in ice. Then, 50 µl of 100 % trichloroacetic acid (TCA) was added and mixed again, 10 additional minutes incubation on ice were done. Afterwards, centrifugation at 13200 rpm for 5 minutes was performed. Supernatant was completely removed. Finally, 50 µl of Protein Extraction Buffer were added and the samples were incubated at 37ºC for 10 minutes. The mentioned buffer consisted of 2 volumes of 100 mM Tris-HCl pH 6.8, 4 mM EDTA, 4% SDS, 20% Glycerol and bromophenol blue, 1 volume of Tris Base 1 M pH 7.5 and 2% β-mercaptoethanol. Protein extractions were stocked at -20ºC until migration in gel.

10% acrylamide resolving gel consisted of 1.625 ml water, 1 ml Tris pH 8.8 SDS 4%, 1.333 ml acrylamide 30 %, 40 µl ammonium persulfate (APS) 10% and 2 µl TEMED.

8 % acrylamide resolving gel consisted of 1.891 ml water, 1 ml Tris pH 8.8 SDS 4%, 1.067 ml acrylamide 30 %, 40 µl APS 10% and 2 µl Temed.

5% stacking gel was a mixture of 1.145 ml water, 500 µl Tris pH 6.8 SDS 4%, 333 µl acrylamide 30%, 20 µl APS 10% and 2 µl Temed.

Acrylamid/bisacrylamid (37.5/1) Rotiphorese® was purchased from Carl ROTH (1 litre) and 5 ml of TCE (2,2,2-trichloroethanol) from SIGMA-ALDRICH were added in order to detect the proteins after UV activation. Temed (N, N, N´,N´-Tetramethylethylenediamine) was purchased in EUROMEDEX.

10 µl of the total protein extracts were loaded on the SDS-polyacrylamide gels and electrophoresis was done at 200 V until the 25 kDa band of Protein Ladder (Pageruler Thermo Fisher Scientific) went out from the gel. The running buffer was 10X TG-SDS (Tris 0,25 M - Glycine 1,92 M - SDS 0,1% pH 8.5, EUROMEDEX) diluted ten times. Before the transfer, proteins were stained by 45 seconds of UV activation with the stain-free system (ChemidocTouch, BioRad). Proteins were transferred from gel to nitrocellulose membrane at 100 V for 1 hour in the cold room (4ºC). Ice is required in order to avoid the increase of temperature. Transfer buffer consisted of 10X TG-SDS (EUROMEDEX) diluted ten times and 20 % (v/v) ethanol. The nitrocellulose Blotting membrane

used was Amersham ™ Protran™ 0.45 µm NC GE Healthcare. Afterwards, nitrocellulose membrane was incubated in the blocking buffer PBS-Tween-Milk buffer for 30 minutes under agitation. This buffer consisted of 1X PBS (10.6 mM KH2PO4 30.0 mM Na2HPO4, 2H_2O 1.54 M NaCl pH 7.4, EUROMEDEX), 0.1 % Tween 20 (EUROMEDEX) and 4 % (m/v) of skimmed milk in powder. Nitrocellulose membranes were incubated over-night at 4ºC in 10 ml of PBS-Tween containing the primary antibody at the indicated dilution (as described below). The next day, nitrocellulose membrane was incubated for 10 minutes in PBS-Tween-Milk buffer under agitation. Thereafter, 2 additional steps of 10 minutes washing with PBS-Tween were done before 2 hours of incubation in 10 ml of PBS-Tween containing the HRP-conjugated secondary antibody at the indicated dilution (as described below). Afterwards, 3 washing steps of 10 minutes under gentle agitation with PBS-Tween were done. Then, the Enhanced chemiluminiscence (ECL) detection was performed by addition of 3 ml of ECL buffer to each blotted membrane. Peroxidase linked to the secondary antibody led to oxidation of the luminol triggering to the emission of luminescence. 10 ml of ECL buffer was composed of 10 ml Tris HCl 0.1M pH 8.5, 3 µL H_2O_2 30 % (Carl ROTH), 50 µL 250 mM Luminol (5-amino-2,3-dihydrophthalazine-1,4-dione) and 25 µL of 90 mM p-Coumaric acid.

Rabbit anti-DNM2 antibody used was gently provided by Jocelyn Laporte´s Team (IGBMC, Ilkirch), bleed number 2680, 1/1000 dilution was used. Secondary antibody was ECL™ Anti-rabbit IgG, Horseradish Peroxidase (HRP)-Linked Whole antibody from donkey (GE Healthcare), 1/10000 dilution was used. Rabbit polyclonal Anti-dynamin 1 anbibody (ab55397, abcam ®) was used with a 1/1000 dilution to detect hDNM1. Secondary antibody was the same as for hDNM2. Mouse monoclonal anti-DRP1 antibody (ab56788, abcam ®) at 1/500 dilution was used to detect hDNM1L. Anti-mouse IgG, horseradish peroxidase linked whole antibody from sheep (GE Healthcare) was used as the secondary antibody with a 1/10000 dilution. Mouse monoclonal Anti-GFP antibody (Roche) was used to detect EGFP tagged proteins with a 1/1000 dilution.

After ECL incubation, the luminescent signal on the membrane was detected and recorded with the Chemidoc™ Touch Imaging System (BioRad). Images were treated and analyzed with Image Lab software (Bio-Rad).

Subcellular fractionation

Yeast *ymr1*Δ transformed cells were grown in SC-Trp medium until OD_{600nm} =0.5-0.8. Cells were harvested by a 1600xg centrifugation for 5 min at 4ºC and washed once in PBS1X, sorbitol 0.3 M buffer. Pellets were suspended in 1 mL lysis buffer (PBS1X, sorbitol 0.3 M, Complete Mini EDTA-free protease inhibitor cocktail™ (Roche Diagnostics), PMSF 1mM) and after addition of 1mL of

0.45 mm acid-washed glass beads (Sigma), cells were broken at 4ºC using a FASTprep® (MP Biomedicals) with 5 runs of 30 sec under strong agitation (6.5 M/S) and cooled on ice for 1 min between each run. Lysates were cleared by a 5 min centrifugation at 800xg, supernatants representing total yeast protein extracts were collected, and protein concentrations were determined by using the Biorad Protein Assay detection kit.

Yeast subcellular fractionation was performed by differential centrifugation on the total protein extracts as previously described (Bonangelino et al, 2002). The lysate was centrifuged at 13000xg for 10 min at 4ºC. The pellet (P13) was kept for analysis and the supernatant was subjected to centrifugation at 100000xg for 1h at 4ºC. The resulting pellet (P100) and supernatant (S100) were collected and S100 represents the cytoplasmic fraction. All pellets (P13 and P100) representing the membrane fractions were suspended in 200 µL of lysis buffer. All fractions were analyzed by SDS-PAGE and Western blot using ECL protocols (GE Healthcare). Mouse monoclonal 1G6 anti-MTM1 (1/1000), mouse monoclonal anti-PGK1 (1/1000) (Invitrogen), anti-Vps10 (1/200) (Invitrogen) and HRP-coupled anti-mouse Ig (1/10000) (GE Healthcare) antibodies were used.

Drop test growth assays

Yeast precultures were done in YPD medium or selective medium SC-aa for the transformed yeast strains (2 ml) and incubated over-night at 30ºC under agitation (INFORS 200 rpm). In the morning, this preculture was diluted ten times in 2 ml YPD and incubated for 3 hours at 30°C under agitation (INFORS 200 rpm). Then, OD_{600} was measured and dilutions in H2O milliQ were done to obtain OD_{600} of 0.5, 0.25, 0.1 and 0.05. Drops of 5 µl of the mentioned dilutions were spotted on different plates depending on the phenotype tested; the plates were incubated at 30ºC until the appearance of the clones. Plates were scanned with the Chemidoc™ Touch Imaging System (Bio-Rad). Images were analyzed with Image Lab software (Bio-Rad).

The different media tested were: YPD-$NiCl_2$ (2.5-12.5 mM), YPD-$CdCl_2$ (10-60 µM), YPD containing 0.5 or 0.6 M NaCl, YPD+ethanol 6%, YPGly (10 g/L Yeast extract, 20 g/L bacto peptone and 25.4 g/L glycerol), YPD+ H_2O_2 at concentrations ranging from 1.5 to 7.5 mM.

Heat shock experiment was as follows: BY4742 and dnm1Δ yeast were grown in 20 ml of YPD (over-night preculture, 30ºC) and diluted ten times in the morning for another 20 ml YPD culture during 3 hours at 30ºC under agitation. 1.5 ml of OD_{600} 0.5 aliquots were done in order to perform the heat shock. Two heat shocks were done: first, cells were directly warmed at 50ºC for 0, 3, 5, 7, 9, 12 or 15 minutes. second, cells were grown 1 hour at 37ºC under agitation before doing the above mentioned heat shock.

Yeast growth curves done with a spectrofluorimeter

Yeast transformations were grown in SC-His (2ml) for an over-night preculture, before being diluted ten times in the morning for a culture in YPD (2ml) until yeasts were in exponential phase (OD_{600} 03-0.6). Then, 20 µl of cultures were diluted in 80 µl of media containing the indicated product. These media were: YPD, YPD+H_2O_2 (2-4 mM), YPD+Paraquat 10 mM (Methyl Viologen hydrate, 98%, ACROS Organics™, Fisher Scientific) and YPD+Sodium(meta)arsenite 3 mM (SIGMA-ALDRICH). 96 well plates were used for this experiment.

Continuous agitation growth at 30°C was done with the spectrofluorimeter (Xenius XM, SAFAS Monaco). Agitation parameters were: continual shacking, orbital movement, 2 mm of shacking amplitude and 10 Hz shacking frequency. OD_{600} was measured every 10 minutes. Data were acquired by SP2000 V7 Spectroscopy Application (SAFAS Monaco). Graphics and analyses were performed by using Microsoft Excel and Graphpad.

Epifluorescence microscopy analyses

Microscopy analyses were performed with 100X/1.45 oil objective (Zeiss) on a fluorescence Axio Observer D1 microscope (Zeiss) using GFP, DsRED filter and DIC optics. Images were captured with a CoolSnap HQ2 photometrix camera (Roper Scientific) and treated by ImageJ (Rasband W.S., ImageJ, U. S. National Institutes of Health, Bethesda, Maryland, USAhttp://imagej.nih.gov/ij/).

Yeast vacuolar staining

CMAC (Invitrogen) staining was performed as detailed below. Yeast cells were grown over-night (ON) at 30°C in 2 mL of SD selective medium and diluted in the morning in 10 mL of selective medium to obtain in the afternoon a DO_{600nm} around 1-1,5. Cells were centrifuged at 4000 rpm and the pellet suspended with 600 µl YPD plus 2µl of CMAC 10mM, and then incubated for 10min at 30°C. Two washes with 500µl of YPD and suspend the cell pellet with 50µl of SD selective medium for doing fluorescent microscopy analysis.

For vacuolar staining with FM4-64 yeast cells were grown over-night at 30°C and diluted in the morning to obtain in the afternoon a DO_{600nm} around 0,8-1,5. Cells were centrifuged at 4000 rpm for 1min and suspended with 50µl YPD and 2µl FM4-64 200µM. Cells were incubated for 15 min at 30°C under agitation. Then washed by adding 500µl of YPD and centrifuged at 4000rpm, 1min. Cells suspended in 300µl of YPD were incubated again at 30°C, then centrifuged and washed with

500µl of YPD. The cell pellet was suspended with 50µl of selective medium or YPD for going for fluorescent microscopy analysis. Zeiss microscope with its 100x objective and the axiovision software were used to register the photos.

Peroxisomes number determination

Yeast cells were transformed with the SKL-GFP plasmid. SKL is a serine-lysine-leucine C-terminal peptide composing the PTS1 peroxisome import signal sequence fused to GFP and that is imported inside the peroxisome.

A yeast over-night culture was done in 2 ml of M1 medium : 6.7% YNB With Ammonium sulphate, 20 g/L D-glucose, 1 g/L Yeast Extract (EUROMEDEX), 1.5 g/L CSM-URA-HIS (MP). In the morning, a dilution was done in M2 medium in order to have an OD_{600} of 4 in the evening. M2 was composed of 6.7 g/L YNB with ammonium sulphate, 20 g/L D-glucose (EUROMEDEX), 1.5 g/L CSM-HIS-URA (MP). In the evening, M2 cultures were used and diluted in M3 medium. The starting OD_{600} of this over-night M3 culture was 0.2. M3 medium consisted of 1 g/L oleic acid (SIGMA), 0.2% (v/v) Tween 20, 0.5 % (w/v) potassium phosphate pH=6 , 0.3 g/L yeast extract and 5 g/L peptone. All the cultures were done at 30ºC under continuous agitation 200 rpm, INFORS). After the M3 incubation, samples were directly observed by fluorescent microscopy (with the GFP filter).

Nile Red staining was done on 500 µl of M3 over-night yeast cultures (OD_{600} 1-2) by addition of 50 µl of Nile Red (50 µg/ml) diluted in DMSO. After 15 minutes of incubation at room temperature in the dark, 1 centrifugation at 3000 rpm during 2 minutes (eppendorf 5418), and 3 washing steps with PBS, samples were observed by fluorescent microscopy (with the DsRED filter).

Mitochondria network observation

A plasmid encoding MTS-RFP fusion protein with a mitochondrial targeting sequence (MTS) fused in N-terminal with RFP (red fluorescent protein) allowing import into the mitochondria was used for mitochondria network staining.

An over-night preculture in 2 ml YPGal (20 g/L D-galactose, 20 g/L peptone, 10 g/L yeast extract, 10 g/L bacto-agar, EUROMEDEX) was required to activate the mitochondria. In the morning, a dilution was done in 2 ml SC-His-Ura Galactose (6.7 g/L YNB with ammonium sulphate, 20 g/L D-galactose, 0.69 g/L CSM-His-Ura). Samples were directly observed by fluorescent microscopy.

Mitotracker staining experiments were done on overnight preculture and culture done in YPGal and SC-His Galactose, respectively. 2-3 µl of 200 µM Mitotracker® Red CMXRos (Molecular Probes) were added to a 0.5-1 OD_{600} culture and incubated 15 minutes at 30ºC and 200 rpm of agitation

(INFORS). 3 washing steps with SC-His Galactose were done before observation by fluorescent microscopy (DsRED filter).

Determination of β-galactosidase activity in Miller Units

Yeast cells expressing the lacZ reporter (pAMS366 or pAMS364 plasmids) were incubated at 30°C until the exponential growth phase. Duplicate samples were prepared. A volume corresponding to 0.7 OD600 of culture were harvested and pelleted by centrifugation (4000 rpm, 3 min), then the cell pellet was washed with Z buffer and taken up in 200 µl of buffer Z + β-mercaptoethanol: 0.05M; pH 7. One control tube was made with 150 µl of buffer Z.

Z buffer: Na2HPO4, 7H2O: 0.04M; NaH2PO4, H2O: 0.06M; KCl: 0.01M; MgSO4, 7H2O: 0.001M

10 µl of 0.1% SDS and 1 drop of chloroform were added (this latter compound was added under the hood). This promotes partial disruption of cell membranes and allows small molecules such as ONPG to diffuse into the cytoplasm that contains ß-galactosidase. Vortex for 10 seconds

Tubes were opened under the hood for about 40 minutes. This step allows the evaporation of chloroform. 40 µl of ONPG solution were added (4 mg / ml in PBS1X phosphate buffer) and a stopwatch was started for timing, then the tubes were placed immediately in a water bath at 28 ° C.

As soon as it appeared a yellow color in tubes, these were removed from the water bath, and the reaction was stopped with 100 µl of 1M Na2CO3 (the reaction time was recorded). After 1 hour of reaction, the reactions in all tubes that have not turned yellow were stopped.

The β-galactosidase activity measured according to Miller is proportional to the absorbance at 420 nm resulting from the absorbance of ONP and is inversely proportional to the reaction time, the sample volume used to make the reaction and the cell concentration of the sample (given by the absorbance of the cells at 600 nm).
The β-galactosidase activity in Miller units is therefore given by the formula:
(OD420nm x 1000) / (OD600nm x t x v).
with t: reaction time in min v: volume of culture used to make the reaction in ml
Ref: Miller, J. H. 1972. Experiments in Molecular Genetics. Cold Spring Harbor Laboratory Press: 352-355.)

VI. References

Abath Neto O, Martins Cde A, Carvalho M, Chadi G, Seitz KW, Oliveira AS, Reed UC, Laporte J, Zanoteli E (2015) DNM2 mutations in a cohort of sporadic patients with centronuclear myopathy. *Genet Mol Biol* **38:** 147-151

Abath Neto O, Silva MR, Martins Cde A, Oliveira Ade S, Reed UC, Biancalana V, Pesquero JB, Laporte J, Zanoteli E (2016) A Study of a Cohort of X-Linked Myotubular Myopathy at the Clinical, Histologic, and Genetic Levels. *Pediatr Neurol* **58:** 107-112

Amburgey K, McNamara N, Bennett LR, McCormick ME, Acsadi G, Dowling JJ (2011) Prevalence of congenital myopathies in a representative pediatric united states population. *Ann Neurol* **70:** 662-665

Amoasii L, Bertazzi DL, Tronchere H, Hnia K, Chicanne G, Rinaldi B, Cowling BS, Ferry A, Klaholz B, Payrastre B, Laporte J, Friant S (2012) Phosphatase-dead myotubularin ameliorates X-linked centronuclear myopathy phenotypes in mice. *PLoS Genet* **8:** e1002965

Antonny B, Burd C, De Camilli P, Chen E, Daumke O, Faelber K, Ford M, Frolov VA, Frost A, Hinshaw JE, Kirchhausen T, Kozlov MM, Lenz M, Low HH, McMahon H, Merrifield C, Pollard TD, Robinson PJ, Roux A, Schmid S (2016) Membrane fission by dynamin: what we know and what we need to know. *EMBO J* **35:** 2270-2284

Azzedine H, Bolino A, Taieb T, Birouk N, Di Duca M, Bouhouche A, Benamou S, Mrabet A, Hammadouche T, Chkili T, Gouider R, Ravazzolo R, Brice A, Laporte J, LeGuern E (2003) Mutations in MTMR13, a new pseudophosphatase homologue of MTMR2 and Sbf1, in two families with an autosomal recessive demyelinating form of Charcot-Marie-Tooth disease associated with early-onset glaucoma. *Am J Hum Genet* **72:** 1141-1153

Baskaran S, Ragusa MJ, Boura E, Hurley JH (2012) Two-site recognition of phosphatidylinositol 3-phosphate by PROPPINs in autophagy. *Mol Cell* **47:** 339-348

Beggs AH, Byrne BJ, de Chastonay S, Haselkorn T, Hughes I, James ES, Kuntz NL, Simon J, Swanson LC, Yang ML, Yu ZF, Yum SW, Prasad S (2017) A Multicenter, Retrospective Medical Record Review of X-Linked Myotubular Myopathy: The RECENSUS Study. *Muscle Nerve*

Begley MJ, Dixon JE (2005) The structure and regulation of myotubularin phosphatases. *Curr Opin Struct Biol* **15:** 614-620

Begley MJ, Taylor GS, Brock MA, Ghosh P, Woods VL, Dixon JE (2006) Molecular basis for substrate recognition by MTMR2, a myotubularin family phosphoinositide phosphatase. *Proc Natl Acad Sci U S A* **103:** 927-932

Begley MJ, Taylor GS, Kim SA, Veine DM, Dixon JE, Stuckey JA (2003) Crystal structure of a phosphoinositide phosphatase, MTMR2: insights into myotubular myopathy and Charcot-Marie-Tooth syndrome. *Mol Cell* **12:** 1391-1402

Berger P, Niemann A, Suter U (2006) Schwann cells and the pathogenesis of inherited motor and sensory neuropathies (Charcot-Marie-Tooth disease). *Glia* **54:** 243-257

Berger P, Schaffitzel C, Berger I, Ban N, Suter U (2003) Membrane association of myotubularin-related protein 2 is mediated by a pleckstrin homology-GRAM domain and a coiled-coil dimerization module. *Proc Natl Acad Sci U S A* **100:** 12177-12182

Bertazzi DL, De Craene JO, Bar S, Sanjuan-Vazquez M, Raess MA, Friant S (2015a) [Phosphoinositides: lipidic essential actors in the intracellular traffic]. *Biol Aujourdhui* **209:** 97-109

Bertazzi DL, De Craene JO, Friant S (2015b) Myotubularin MTM1 Involved in Centronuclear Myopathy and its Roles in Human and Yeast Cells. *J Mol Genet Med*

Bertini E, D'Amico A, Gualandi F, Petrini S (2011) Congenital muscular dystrophies: a brief review. *Semin Pediatr Neurol* **18:** 277-288

Bevilacqua JA, Bitoun M, Biancalana V, Oldfors A, Stoltenburg G, Claeys KG, Lacene E, Brochier G, Manere L, Laforet P, Eymard B, Guicheney P, Fardeau M, Romero NB (2009) "Necklace" fibers, a new histological marker of late-onset MTM1-related centronuclear myopathy. *Acta Neuropathol* **117:** 283-291

Biancalana V, Beggs AH, Das S, Jungbluth H, Kress W, Nishino I, North K, Romero NB, Laporte J (2012) Clinical utility gene card for: Centronuclear and myotubular myopathies. *Eur J Hum Genet* **20**

Biancalana V, Scheidecker S, Miguet M, Laquerriere A, Romero NB, Stojkovic T, Abath Neto O, Mercier S, Voermans N, Tanner L, Rogers C, Ollagnon-Roman E, Roper H, Boutte C, Ben-Shachar S, Lornage X, Vasli N, Schaefer E, Laforet P, Pouget J, Moerman A, Pasquier L, Marcorelle P, Magot A, Kusters B, Streichenberger N, Tranchant C, Dondaine N, Schneider R, Gasnier C, Calmels N, Kremer V, Nguyen K, Perrier J, Kamsteeg EJ, Carlier P, Carlier RY, Thompson J, Boland A, Deleuze JF, Fardeau M, Zanoteli E, Eymard B, Laporte J (2017) Affected female carriers of MTM1 mutations display a wide spectrum of clinical and pathological involvement: delineating diagnostic clues. *Acta Neuropathol* **134:** 889-904

Bissig C, Hurbain I, Raposo G, van Niel G (2017) PIKfyve activity regulates reformation of terminal storage lysosomes from endolysosomes. *Traffic*

Bitoun M, Bevilacqua JA, Prudhon B, Maugenre S, Taratuto AL, Monges S, Lubieniecki F, Cances C, Uro-Coste E, Mayer M, Fardeau M, Romero NB, Guicheney P (2007) Dynamin 2 mutations cause sporadic centronuclear myopathy with neonatal onset. *Ann Neurol* **62:** 666-670

Bitoun M, Durieux AC, Prudhon B, Bevilacqua JA, Herledan A, Sakanyan V, Urtizberea A, Cartier L, Romero NB, Guicheney P (2009) Dynamin 2 mutations associated with human diseases impair clathrin-mediated receptor endocytosis. *Hum Mutat* **30:** 1419-1427

Bitoun M, Maugenre S, Jeannet PY, Lacene E, Ferrer X, Laforet P, Martin JJ, Laporte J, Lochmuller H, Beggs AH, Fardeau M, Eymard B, Romero NB, Guicheney P (2005) Mutations in dynamin 2 cause dominant centronuclear myopathy. *Nat Genet* **37:** 1207-1209

Blazeck J, Garg R, Reed B, Alper HS (2012) Controlling promoter strength and regulation in Saccharomyces cerevisiae using synthetic hybrid promoters. *Biotechnol Bioeng* **109:** 2884-2895

Blondeau F, Laporte J, Bodin S, Superti-Furga G, Payrastre B, Mandel JL (2000) Myotubularin, a phosphatase deficient in myotubular myopathy, acts on phosphatidylinositol 3-kinase and phosphatidylinositol 3-phosphate pathway. *Hum Mol Genet* **9:** 2223-2229

Blondelle J, Ohno Y, Gache V, Guyot S, Storck S, Blanchard-Gutton N, Barthelemy I, Walmsley G, Rahier A, Gadin S, Maurer M, Guillaud L, Prola A, Ferry A, Aubin-Houzelstein G, Demarquoy J, Relaix F, Piercy RJ, Blot S, Kihara A, Tiret L, Pilot-Storck F (2015) HACD1, a regulator of membrane composition and fluidity, promotes myoblast fusion and skeletal muscle growth. *J Mol Cell Biol* **7:** 429-440

Boal F, Mansour R, Gayral M, Saland E, Chicanne G, Xuereb JM, Marcellin M, Burlet-Schiltz O, Sansonetti PJ, Payrastre B, Tronchere H (2015) TOM1 is a PI5P effector involved in the regulation of endosomal maturation. *J Cell Sci* **128:** 815-827

Boal F, Puhar A, Xuereb J-M, Kunduzova O, Sansonetti PJ, Payrastre B, Tronchère H (2016) PI5P Triggers ICAM-1 Degradation in Shigella Infected Cells, Thus Dampening Immune Cell Recruitment. *Cell Reports* **14:** 750-759, 10.1016/j.celrep.2015.12.079

Bohm J, Biancalana V, Dechene ET, Bitoun M, Pierson CR, Schaefer E, Karasoy H, Dempsey MA, Klein F, Dondaine N, Kretz C, Haumesser N, Poirson C, Toussaint A, Greenleaf RS, Barger MA, Mahoney LJ, Kang PB, Zanoteli E, Vissing J, Witting N, Echaniz-Laguna A, Wallgren-Pettersson C, Dowling J, Merlini L, Oldfors A, Bomme Ousager L, Melki J, Krause A, Jern C, Oliveira AS, Petit F, Jacquette A, Chaussenot A, Mowat D, Leheup B, Cristofano M, Poza Aldea JJ, Michel F, Furby A, Llona JE, Van Coster R, Bertini E, Urtizberea JA, Drouin-Garraud V, Beroud C, Prudhon B, Bedford M, Mathews K, Erby LA, Smith SA, Roggenbuck J, Crowe CA, Brennan Spitale A, Johal SC, Amato AA, Demmer LA, Jonas J, Darras BT, Bird TD, Laurino M, Welt SI, Trotter C, Guicheney P, Das S, Mandel JL, Beggs AH, Laporte J (2012) Mutation spectrum in the large GTPase dynamin 2, and genotype-phenotype correlation in autosomal dominant centronuclear myopathy. *Hum Mutat* **33:** 949-959

Bonangelino CJ, Nau JJ, Duex JE, Brinkman M, Wurmser AE, Gary JD, Emr SD, Weisman LS (2002) Osmotic stress-induced increase of phosphatidylinositol 3,5-bisphosphate requires Vac14p, an activator of the lipid kinase Fab1p. *J Cell Biol* **156:** 1015-1028

Botstein D, Chervitz SA, Cherry JM (1997) Yeast as a model organism. *Science* **277:** 1259-1260

Buj-Bello A, Fougerousse F, Schwab Y, Messaddeq N, Spehner D, Pierson CR, Durand M, Kretz C, Danos O, Douar AM, Beggs AH, Schultz P, Montus M, Denefle P, Mandel JL (2008) AAV-mediated intramuscular delivery of myotubularin corrects the myotubular myopathy phenotype in targeted murine muscle and suggests a function in plasma membrane homeostasis. *Hum Mol Genet* **17:** 2132-2143

Buj-Bello A, Laugel V, Messaddeq N, Zahreddine H, Laporte J, Pellissier JF, Mandel JL (2002) The lipid phosphatase myotubularin is essential for skeletal muscle maintenance but not for myogenesis in mice. *Proc Natl Acad Sci U S A* **99:** 15060-15065

Calderon JC, Bolanos P, Caputo C (2014) The excitation-contraction coupling mechanism in skeletal muscle. *Biophys Rev* **6:** 133-160

Castets P, Lescure A, Guicheney P, Allamand V (2012) Selenoprotein N in skeletal muscle: from diseases to function. *J Mol Med (Berl)* **90:** 1095-1107

Chen S, Huang P, Qiu Y, Zhou Q, Li X, Zhu M, Hong D (2017) Phenotype variability and histopathological findings in patients with a novel DNM2 mutation. *Neuropathology*

Childers MK, Joubert R, Poulard K, Moal C, Grange RW, Doering JA, Lawlor MW, Rider BE, Jamet T, Daniele N, Martin S, Riviere C, Soker T, Hammer C, Van Wittenberghe L, Lockard M, Guan X, Goddard M, Mitchell E, Barber J, Williams JK, Mack DL, Furth ME, Vignaud A, Masurier C, Mavilio F, Moullier P, Beggs AH, Buj-Bello A (2014) Gene therapy prolongs survival and restores function in murine and canine models of myotubular myopathy. *Sci Transl Med* **6:** 220ra210

Chow CY, Zhang Y, Dowling JJ, Jin N, Adamska M, Shiga K, Szigeti K, Shy ME, Li J, Zhang X, Lupski JR, Weisman LS, Meisler MH (2007) Mutation of FIG4 causes neurodegeneration in the pale tremor mouse and patients with CMT4J. *Nature* **448:** 68-72

Claeys KG, Zuchner S, Kennerson M, Berciano J, Garcia A, Verhoeven K, Storey E, Merory JR, Bienfait HM, Lammens M, Nelis E, Baets J, De Vriendt E, Berneman ZN, De Veuster I, Vance JM, Nicholson G, Timmerman V, De Jonghe P (2009) Phenotypic spectrum of dynamin 2 mutations in Charcot-Marie-Tooth neuropathy. *Brain* **132:** 1741-1752

Cowling BS, Chevremont T, Prokic I, Kretz C, Ferry A, Coirault C, Koutsopoulos O, Laugel V, Romero NB, Laporte J (2014) Reducing dynamin 2 expression rescues X-linked centronuclear myopathy. *J Clin Invest* **124:** 1350-1363

Cowling BS, Prokic I, Tasfaout H, Rabai A, Humbert F, Rinaldi B, Nicot AS, Kretz C, Friant S, Roux A, Laporte J (2017) Amphiphysin (BIN1) negatively regulates dynamin 2 for normal muscle maturation. *J Clin Invest*

Cowling BS, Toussaint A, Amoasii L, Koebel P, Ferry A, Davignon L, Nishino I, Mandel JL, Laporte J (2011) Increased expression of wild-type or a centronuclear myopathy mutant of dynamin 2 in skeletal muscle of adult mice leads to structural defects and muscle weakness. *Am J Pathol* **178:** 2224-2235

Cowling BS, Toussaint A, Muller J, Laporte J (2012) Defective membrane remodeling in neuromuscular diseases: insights from animal models. *PLoS Genet* **8:** e1002595

Cui X, De Vivo I, Slany R, Miyamoto A, Firestein R, Cleary ML (1998) Association of SET domain and myotubularin-related proteins modulates growth control. *Nat Genet* **18:** 331-337

Cyert MS (2003) Calcineurin signaling in Saccharomyces cerevisiae: how yeast go crazy in response to stress. *Biochem Biophys Res Commun* **311:** 1143-1150

De Craene JO, Bertazzi DL, Bar S, Friant S (2017) Phosphoinositides, Major Actors in Membrane Trafficking and Lipid Signaling Pathways. *Int J Mol Sci* **18**

Denu JM, Dixon JE (1995) A catalytic mechanism for the dual-specific phosphatases. *Proc Natl Acad Sci U S A* **92:** 5910-5914

Doerks T, Strauss M, Brendel M, Bork P (2000) GRAM, a novel domain in glucosyltransferases, myotubularins and other putative membrane-associated proteins. *Trends Biochem Sci* **25:** 483-485

Dong XP, Shen D, Wang X, Dawson T, Li X, Zhang Q, Cheng X, Zhang Y, Weisman LS, Delling M, Xu H (2010) PI(3,5)P(2) controls membrane trafficking by direct activation of mucolipin Ca(2+) release channels in the endolysosome. *Nat Commun* **1:** 38

Dove SK, Cooke FT, Douglas MR, Sayers LG, Parker PJ, Michell RH (1997) Osmotic stress activates phosphatidylinositol-3,5-bisphosphate synthesis. *Nature* **390:** 187-192

Dove SK, Piper RC, McEwen RK, Yu JW, King MC, Hughes DC, Thuring J, Holmes AB, Cooke FT, Michell RH, Parker PJ, Lemmon MA (2004) Svp1p defines a family of phosphatidylinositol 3,5-bisphosphate effectors. *EMBO J* **23:** 1922-1933

Duex JE, Nau JJ, Kauffman EJ, Weisman LS (2006a) Phosphoinositide 5-phosphatase Fig 4p is required for both acute rise and subsequent fall in stress-induced phosphatidylinositol 3,5-bisphosphate levels. *Eukaryot Cell* **5:** 723-731

Duex JE, Tang F, Weisman LS (2006b) The Vac14p-Fig4p complex acts independently of Vac7p and couples PI3,5P2 synthesis and turnover. *J Cell Biol* **172:** 693-704

Durieux AC, Prudhon B, Guicheney P, Bitoun M (2010a) Dynamin 2 and human diseases. *J Mol Med (Berl)* **88:** 339-350

Durieux AC, Vassilopoulos S, Laine J, Fraysse B, Brinas L, Prudhon B, Castells J, Freyssenet D, Bonne G, Guicheney P, Bitoun M (2012) A centronuclear myopathy--dynamin 2 mutation impairs autophagy in mice. *Traffic* **13:** 869-879

Durieux AC, Vignaud A, Prudhon B, Viou MT, Beuvin M, Vassilopoulos S, Fraysse B, Ferry A, Laine J, Romero NB, Guicheney P, Bitoun M (2010b) A centronuclear myopathy-dynamin 2 mutation impairs skeletal muscle structure and function in mice. *Hum Mol Genet* **19:** 4820-4836

Efe JA, Botelho RJ, Emr SD (2007) Atg18 regulates organelle morphology and Fab1 kinase activity independent of its membrane recruitment by phosphatidylinositol 3,5-bisphosphate. *Mol Biol Cell* **18:** 4232-4244

Elverman M, Goddard MA, Mack D, Snyder JM, Lawlor MW, Meng H, Beggs AH, Buj-Bello A, Poulard K, Marsh AP, Grange RW, Kelly VE, Childers MK (2017) Long-term effects of systemic gene therapy in a canine model of myotubular myopathy. *Muscle Nerve* **56:** 943-953

Eugster A, Pecheur EI, Michel F, Winsor B, Letourneur F, Friant S (2004) Ent5p is required with Ent3p and Vps27p for ubiquitin-dependent protein sorting into the multivesicular body. *Mol Biol Cell* **15:** 3031-3041

Fabrizi GM, Ferrarini M, Cavallaro T, Cabrini I, Cerini R, Bertolasi L, Rizzuto N (2007) Two novel mutations in dynamin-2 cause axonal Charcot-Marie-Tooth disease. *Neurology* **69:** 291-295

Fendt SM, Sauer U (2010) Transcriptional regulation of respiration in yeast metabolizing differently repressive carbon substrates. *BMC Syst Biol* **4:** 12

Ferguson SM, De Camilli P (2012) Dynamin, a membrane-remodelling GTPase. *Nat Rev Mol Cell Biol* **13:** 75-88

Feyder S, De Craene JO, Bar S, Bertazzi DL, Friant S (2015) Membrane trafficking in the yeast Saccharomyces cerevisiae model. *Int J Mol Sci* **16:** 1509-1525

Foury F (1997) Human genetic diseases: a cross-talk between man and yeast. *Gene* **195:** 1-10

Fraysse B, Guicheney P, Bitoun M (2016) Calcium homeostasis alterations in a mouse model of the Dynamin 2-related centronuclear myopathy. *Biol Open* **5:** 1691-1696

Friant S, Pecheur EI, Eugster A, Michel F, Lefkir Y, Nourrisson D, Letourneur F (2003) Ent3p Is a PtdIns(3,5)P2 effector required for protein sorting to the multivesicular body. *Dev Cell* **5:** 499-511

Frijhoff J, Dagnell M, Godfrey R, Ostman A (2014) Regulation of protein tyrosine phosphatase oxidation in cell adhesion and migration. *Antioxid Redox Signal* **20:** 1994-2010

Fukumoto S, Fujimoto T (2002) Deformation of lipid droplets in fixed samples. *Histochem Cell Biol* **118:** 423-428

Gao D, Yang J, Wu Y, Wang Q, Wang Q, Lai EY, Zhu J (2016) Targeting Dynamin 2 as a Novel Pathway to Inhibit Cardiomyocyte Apoptosis Following Oxidative Stress. *Cell Physiol Biochem* **39:** 2121-2134

Gibney PA, Lu C, Caudy AA, Hess DC, Botstein D (2013) Yeast metabolic and signaling genes are required for heat-shock survival and have little overlap with the heat-induced genes. *Proc Natl Acad Sci U S A* **110:** E4393-4402

Gietz D, St Jean A, Woods RA, Schiestl RH (1992) Improved method for high efficiency transformation of intact yeast cells. *Nucleic Acids Res* **20:** 1425

Gillooly DJ, Morrow IC, Lindsay M, Gould R, Bryant NJ, Gaullier JM, Parton RG, Stenmark H (2000) Localization of phosphatidylinositol 3-phosphate in yeast and mammalian cells. *EMBO J* **19:** 4577-4588

Gonzalez-Jamett AM, Baez-Matus X, Olivares MJ, Hinostroza F, Guerra-Fernandez MJ, Vasquez-Navarrete J, Bui MT, Guicheney P, Romero NB, Bevilacqua JA, Bitoun M, Caviedes P, Cardenas AM (2017)

Dynamin-2 mutations linked to Centronuclear Myopathy impair actin-dependent trafficking in muscle cells. *Sci Rep* **7:** 4580

Gonzalez-Jamett AM, Momboisse F, Haro-Acuna V, Bevilacqua JA, Caviedes P, Cardenas AM (2013) Dynamin-2 Function and Dysfunction Along the Secretory Pathway. *Front Endocrinol (Lausanne)* **4:** 126

Gozani O, Karuman P, Jones DR, Ivanov D, Cha J, Lugovskoy AA, Baird CL, Zhu H, Field SJ, Lessnick SL, Villasenor J, Mehrotra B, Chen J, Rao VR, Brugge JS, Ferguson CG, Payrastre B, Myszka DG, Cantley LC, Wagner G, Divecha N, Prestwich GD, Yuan J (2003) The PHD finger of the chromatin-associated protein ING2 functions as a nuclear phosphoinositide receptor. *Cell* **114:** 99-111

Grainger DL, Tavelis C, Ryan AJ, Hinchliffe KA (2011) Involvement of phosphatidylinositol 5-phosphate in insulin-stimulated glucose uptake in the L6 myotube model of skeletal muscle. *Pflugers Arch* **462:** 723-732

Hasegawa J, Strunk BS, Weisman LS (2017) PI5P and PI(3,5)P2: Minor, but Essential Phosphoinositides. *Cell Struct Funct* **42:** 49-60

Haslam RJ, Koide HB, Hemmings BA (1993) Pleckstrin domain homology. *Nature* **363:** 309-310

Hatch AL, Gurel PS, Higgs HN (2014) Novel roles for actin in mitochondrial fission. *J Cell Sci* **127:** 4549-4560

Henne WM, Buchkovich NJ, Emr SD (2011) The ESCRT pathway. *Dev Cell* **21:** 77-91

Herman GE, Finegold M, Zhao W, de Gouyon B, Metzenberg A (1999) Medical complications in long-term survivors with X-linked myotubular myopathy. *J Pediatr* **134:** 206-214

Herrero E, Ros J, Belli G, Cabiscol E (2008) Redox control and oxidative stress in yeast cells. *Biochim Biophys Acta* **1780:** 1217-1235

Herrmann JM, Dick TP (2012) Redox Biology on the rise. *Biol Chem* **393:** 999-1004

Hessvik NP, Overbye A, Brech A, Torgersen ML, Jakobsen IS, Sandvig K, Llorente A (2016) PIKfyve inhibition increases exosome release and induces secretory autophagy. *Cell Mol Life Sci* **73:** 4717-4737

Hnia K, Tronchere H, Tomczak KK, Amoasii L, Schultz P, Beggs AH, Payrastre B, Mandel JL, Laporte J (2011) Myotubularin controls desmin intermediate filament architecture and mitochondrial dynamics in human and mouse skeletal muscle. *J Clin Invest* **121:** 70-85

Hnia K, Vaccari I, Bolino A, Laporte J (2012) Myotubularin phosphoinositide phosphatases: cellular functions and disease pathophysiology. *Trends Mol Med* **18:** 317-327

Hoepfner D, Schildknegt D, Braakman I, Philippsen P, Tabak HF (2005) Contribution of the endoplasmic reticulum to peroxisome formation. *Cell* **122:** 85-95

Hong NH, Qi A, Weaver AM (2015) PI(3,5)P2 controls endosomal branched actin dynamics by regulating cortactin-actin interactions. *J Cell Biol* **210:** 753-769

Hsu F, Mao Y (2015) The structure of phosphoinositide phosphatases: Insights into substrate specificity and catalysis. *Biochim Biophys Acta* **1851:** 698-710

Hyndman KA, Arguello AM, Morsing SK, Pollock JS (2016) Dynamin-2 is a novel NOS1beta interacting protein and negative regulator in the collecting duct. *Am J Physiol Regul Integr Comp Physiol* **310:** R570-577

Idrissi FZ, Geli MI (2014) Zooming in on the molecular mechanisms of endocytic budding by time-resolved electron microscopy. *Cell Mol Life Sci* **71:** 641-657

Ishida N, Nakamura Y, Tanabe K, Li SA, Takei K (2011) Dynamin 2 associates with microtubules at mitosis and regulates cell cycle progression. *Cell Struct Funct* **36:** 145-154

Izquierdo A, Casas C, Muhlenhoff U, Lillig CH, Herrero E (2008) Saccharomyces cerevisiae Grx6 and Grx7 are monothiol glutaredoxins associated with the early secretory pathway. *Eukaryot Cell* **7:** 1415-1426

Jeub M, Bitoun M, Guicheney P, Kappes-Horn K, Strach K, Druschky KF, Weis J, Fischer D (2008) Dynamin 2-related centronuclear myopathy: clinical, histological and genetic aspects of further patients and review of the literature. *Clin Neuropathol* **27:** 430-438

Jin N, Chow CY, Liu L, Zolov SN, Bronson R, Davisson M, Petersen JL, Zhang Y, Park S, Duex JE, Goldowitz D, Meisler MH, Weisman LS (2008) VAC14 nucleates a protein complex essential for the acute interconversion of PI3P and PI(3,5)P(2) in yeast and mouse. *EMBO J* **27:** 3221-3234

Jin N, Lang MJ, Weisman LS (2016) Phosphatidylinositol 3,5-bisphosphate: regulation of cellular events in space and time. *Biochem Soc Trans* **44:** 177-184

Jungbluth H, Gautel M (2014) Pathogenic mechanisms in centronuclear myopathies. *Front Aging Neurosci* **6:** 339

Jungbluth H, Wallgren-Pettersson C, Laporte J (2008) Centronuclear (myotubular) myopathy. *Orphanet J Rare Dis* **3:** 26

Jungbluth H, Zhou H, Sewry CA, Robb S, Treves S, Bitoun M, Guicheney P, Buj-Bello A, Bonnemann C, Muntoni F (2007) Centronuclear myopathy due to a de novo dominant mutation in the skeletal muscle ryanodine receptor (RYR1) gene. *Neuromuscul Disord* **17:** 338-345

Kachroo AH, Laurent JM, Yellman CM, Meyer AG, Wilke CO, Marcotte EM (2015) Evolution. Systematic humanization of yeast genes reveals conserved functions and genetic modularity. *Science* **348:** 921-925

Kamogashira T, Fujimoto C, Yamasoba T (2015) Reactive oxygen species, apoptosis, and mitochondrial dysfunction in hearing loss. *Biomed Res Int* **2015:** 617207

Kouwenberg C, Bohm J, Erasmus C, van Balken I, Vos S, Kusters B, Kamsteeg EJ, Biancalana V, Koch C, Dondaine N, Laporte J, Voermans N (2017) Dominant Centronuclear Myopathy with Early Childhood Onset due to a Novel Mutation in BIN1. *J Neuromuscul Dis* **4:** 349-355

Kuravi K, Nagotu S, Krikken AM, Sjollema K, Deckers M, Erdmann R, Veenhuis M, van der Klei IJ (2006) Dynamin-related proteins Vps1p and Dnm1p control peroxisome abundance in Saccharomyces cerevisiae. *J Cell Sci* **119:** 3994-4001

Kutchukian C, Lo Scrudato M, Tourneur Y, Poulard K, Vignaud A, Berthier C, Allard B, Lawlor MW, Buj-Bello A, Jacquemond V (2016) Phosphatidylinositol 3-kinase inhibition restores Ca2+ release defects and prolongs survival in myotubularin-deficient mice. *Proc Natl Acad Sci U S A* **113:** 14432-14437

Laporte J, Bedez F, Bolino A, Mandel JL (2003) Myotubularins, a large disease-associated family of cooperating catalytically active and inactive phosphoinositides phosphatases. *Hum Mol Genet* **12 Spec No 2:** R285-292

Laporte J, Blondeau F, Gansmuller A, Lutz Y, Vonesch JL, Mandel JL (2002) The PtdIns3P phosphatase myotubularin is a cytoplasmic protein that also localizes to Rac1-inducible plasma membrane ruffles. *J Cell Sci* **115:** 3105-3117

Laporte J, Hu LJ, Kretz C, Mandel JL, Kioschis P, Coy JF, Klauck SM, Poustka A, Dahl N (1996) A gene mutated in X-linked myotubular myopathy defines a new putative tyrosine phosphatase family conserved in yeast. *Nat Genet* **13:** 175-182

Laporte J, Kress W, Mandel JL (2001) Diagnosis of X-linked myotubular myopathy by detection of myotubularin. *Ann Neurol* **50:** 42-46

Lecompte O, Poch O, Laporte J (2008) PtdIns5P regulation through evolution: roles in membrane trafficking? *Trends Biochem Sci* **33:** 453-460

Lee JE, Westrate LM, Wu H, Page C, Voeltz GK (2016) Multiple dynamin family members collaborate to drive mitochondrial division. *Nature* **540:** 139-143

Lemmon MA (2007) Pleckstrin homology (PH) domains and phosphoinositides. *Biochem Soc Symp***:** 81-93

Lenk GM, Szymanska K, Debska-Vielhaber G, Rydzanicz M, Walczak A, Bekiesinska-Figatowska M, Vielhaber S, Hallmann K, Stawinski P, Buehring S, Hsu DA, Kunz WS, Meisler MH, Ploski R (2016) Biallelic Mutations of VAC14 in Pediatric-Onset Neurological Disease. *Am J Hum Genet* **99:** 188-194

Lenoir M, Kufareva I, Abagyan R, Overduin M (2015) Membrane and Protein Interactions of the Pleckstrin Homology Domain Superfamily. *Membranes (Basel)* **5:** 646-663

Li SC, Diakov TT, Xu T, Tarsio M, Zhu W, Couoh-Cardel S, Weisman LS, Kane PM (2014) The signaling lipid PI(3,5)P(2) stabilizes V(1)-V(o) sector interactions and activates the V-ATPase. *Mol Biol Cell* **25:** 1251-1262

Li X, Gould SJ (2003) The dynamin-like GTPase DLP1 is essential for peroxisome division and is recruited to peroxisomes in part by PEX11. *J Biol Chem* **278:** 17012-17020

Liu J, Hughes TE, Sessa WC (1997) The first 35 amino acids and fatty acylation sites determine the molecular targeting of endothelial nitric oxide synthase into the Golgi region of cells: a green fluorescent protein study. *J Cell Biol* **137:** 1525-1535

Lockshon D, Surface LE, Kerr EO, Kaeberlein M, Kennedy BK (2007) The sensitivity of yeast mutants to oleic acid implicates the peroxisome and other processes in membrane function. *Genetics* **175:** 77-91

Lorenzo O, Urbe S, Clague MJ (2005) Analysis of phosphoinositide binding domain properties within the myotubularin-related protein MTMR3. *J Cell Sci* **118:** 2005-2012

Lorenzo O, Urbe S, Clague MJ (2006) Systematic analysis of myotubularins: heteromeric interactions, subcellular localisation and endosome related functions. *J Cell Sci* **119:** 2953-2959

Mack DL, Poulard K, Goddard MA, Latournerie V, Snyder JM, Grange RW, Elverman MR, Denard J, Veron P, Buscara L, Le Bec C, Hogrel JY, Brezovec AG, Meng H, Yang L, Liu F, O'Callaghan M, Gopal N, Kelly VE, Smith BK, Strande JL, Mavilio F, Beggs AH, Mingozzi F, Lawlor MW, Buj-Bello A, Childers MK (2017) Systemic AAV8-Mediated Gene Therapy Drives Whole-Body Correction of Myotubular Myopathy in Dogs. *Mol Ther* 25: 839-854

Maehama T and Dixon JE (1998) The tumor suppressor, PTEN/MMAC1, dephosphorylates the lipid second messenger, phosphatidylinositol 3,4,5-trisphosphate. *J Biol Chem*. **273**:13375–13378.

Malinska D, Kudin AP, Bejtka M, Kunz WS (2012) Changes in mitochondrial reactive oxygen species synthesis during differentiation of skeletal muscle cells. *Mitochondrion* **12:** 144-148

Mayinger P (2012) Phosphoinositides and vesicular membrane traffic. *Biochim Biophys Acta* **1821:** 1104-1113

McNiven MA, Thompson HM (2006) Vesicle formation at the plasma membrane and trans-Golgi network: the same but different. *Science* **313:** 1591-1594

Mironova YA, Lenk GM, Lin JP, Lee SJ, Twiss JL, Vaccari I, Bolino A, Havton LA, Min SH, Abrams CS, Shrager P, Meisler MH, Giger RJ (2016) PI(3,5)P2 biosynthesis regulates oligodendrocyte differentiation by intrinsic and extrinsic mechanisms. *Elife* **5**

Morvan J, Rinaldi B, Friant S (2012) Pkh1/2-dependent phosphorylation of Vps27 regulates ESCRT-I recruitment to endosomes. *Mol Biol Cell* **23:** 4054-4064

Motley AM, Ward GP, Hettema EH (2008) Dnm1p-dependent peroxisome fission requires Caf4p, Mdv1p and Fis1p. *J Cell Sci* **121:** 1633-1640

Moustaq L, Smaczynska-de R, II, Palmer SE, Marklew CJ, Ayscough KR (2016) Insights into dynamin-associated disorders through analysis of equivalent mutations in the yeast dynamin Vps1. *Microb Cell* **3:** 147-158

Muller M, Lu K, Reichert AS (2015) Mitophagy and mitochondrial dynamics in Saccharomyces cerevisiae. *Biochim Biophys Acta* **1853:** 2766-2774

Nicolson TA, Weisman LS, Payne GS, Wickner WT (1995) A truncated form of the Pho80 cyclin redirects the Pho85 kinase to disrupt vacuole inheritance in S. cerevisiae. *J Cell Biol* **130:** 835-845

Nicot AS, Toussaint A, Tosch V, Kretz C, Wallgren-Pettersson C, Iwarsson E, Kingston H, Garnier JM, Biancalana V, Oldfors A, Mandel JL, Laporte J (2007) Mutations in amphiphysin 2 (BIN1) disrupt interaction with dynamin 2 and cause autosomal recessive centronuclear myopathy. *Nat Genet* **39:** 1134-1139

Niebuhr K, Giuriato S, Pedron T, Philpott DJ, Gaits F, Sable J, Sheetz MP, Parsot C, Sansonetti PJ, Payrastre B (2002) Conversion of PtdIns(4,5)P(2) into PtdIns(5)P by the S.flexneri effector IpgD reorganizes host cell morphology. *EMBO J* **21:** 5069-5078

North K (2008) What's new in congenital myopathies? *Neuromuscul Disord* **18:** 433-442

Numakawa T, Matsumoto T, Numakawa Y, Richards M, Yamawaki S, Kunugi H (2011) Protective Action of Neurotrophic Factors and Estrogen against Oxidative Stress-Mediated Neurodegeneration. *J Toxicol* **2011:** 405194

Nunes P, Demaurex N (2014) Redox regulation of store-operated Ca2+ entry. *Antioxid Redox Signal* **21:** 915-932

O'Grady GL, Best HA, Sztal TE, Schartner V, Sanjuan-Vazquez M, Donkervoort S, Abath Neto O, Sutton RB, Ilkovski B, Romero NB, Stojkovic T, Dastgir J, Waddell LB, Boland A, Hu Y, Williams C, Ruparelia AA, Maisonobe T, Peduto AJ, Reddel SW, Lek M, Tukiainen T, Cummings BB, Joshi H, Nectoux J, Brammah S, Deleuze JF, Ing VO, Ramm G, Ardicli D, Nowak KJ, Talim B, Topaloglu H, Laing NG, North KN, MacArthur DG, Friant S, Clarke NF, Bryson-Richardson RJ, Bonnemann CG, Laporte J, Cooper ST (2016) Variants in the Oxidoreductase PYROXD1 Cause Early-Onset Myopathy with Internalized Nuclei and Myofibrillar Disorganization. *Am J Hum Genet* **99:** 1086-1105

Obara K, Ohsumi Y (2011) PtdIns 3-Kinase Orchestrates Autophagosome Formation in Yeast. *J Lipids* **2011:** 498768

Odorizzi G, Babst M, Emr SD (1998) Fab1p PtdIns(3)P 5-kinase function essential for protein sorting in the multivesicular body. *Cell* **95:** 847-858

Oka OB, Bulleid NJ (2013) Forming disulfides in the endoplasmic reticulum. *Biochim Biophys Acta* **1833:** 2425-2429

Outten CE, Culotta VC (2004) Alternative start sites in the Saccharomyces cerevisiae GLR1 gene are responsible for mitochondrial and cytosolic isoforms of glutathione reductase. *J Biol Chem* **279:** 7785-7791

Palmer CP, Zhou XL, Lin J, Loukin SH, Kung C, Saimi Y (2001) A TRP homolog in Saccharomyces cerevisiae forms an intracellular Ca(2+)-permeable channel in the yeast vacuolar membrane. *Proc Natl Acad Sci U S A* **98:** 7801-7805

Pareyson D, Marchesi C (2009) Diagnosis, natural history, and management of Charcot-Marie-Tooth disease. *Lancet Neurol* **8:** 654-667

Parrish WR, Stefan CJ, Emr SD (2004) Essential role for the myotubularin-related phosphatase Ymr1p and the synaptojanin-like phosphatases Sjl2p and Sjl3p in regulation of phosphatidylinositol 3-phosphate in yeast. *Mol Biol Cell* **15:** 3567-3579

Payrastre B, Missy K, Giuriato S, Bodin S, Plantavid M, Gratacap M (2001) Phosphoinositides: key players in cell signalling, in time and space. *Cell Signal* **13:** 377-387

Pendaries C, Tronchere H, Arbibe L, Mounier J, Gozani O, Cantley L, Fry MJ, Gaits-Iacovoni F, Sansonetti PJ, Payrastre B (2006) PtdIns5P activates the host cell PI3-kinase/Akt pathway during Shigella flexneri infection. *EMBO J* **25:** 1024-1034

Pineau L, Bonifait L, Berjeaud JM, Alimardani-Theuil P, Berges T, Ferreira T (2008) A lipid-mediated quality control process in the Golgi apparatus in yeast. *Mol Biol Cell* **19:** 807-821

Puigpinos J, Casas C, Herrero E (2015) Altered intracellular calcium homeostasis and endoplasmic reticulum redox state in Saccharomyces cerevisiae cells lacking Grx6 glutaredoxin. *Mol Biol Cell* **26:** 104-116

Raess MA, Cowling BS, Bertazzi DL, Kretz C, Rinaldi B, Xuereb JM, Kessler P, Romero NB, Payrastre B, Friant S, Laporte J (2017a) Expression of the neuropathy-associated MTMR2 gene rescues MTM1-associated myopathy. *Hum Mol Genet* **26:** 3736-3748

Raess MA, Friant S, Cowling BS, Laporte J (2017b) WANTED - Dead or alive: Myotubularins, a large disease-associated protein family. *Adv Biol Regul* **63:** 49-58

Ramel D, Lagarrigue F, Pons V, Mounier J, Dupuis-Coronas S, Chicanne G, Sansonetti PJ, Gaits-Iacovoni F, Tronchere H, Payrastre B (2011) Shigella flexneri infection generates the lipid PI5P to alter endocytosis and prevent termination of EGFR signaling. *Sci Signal* **4:** ra61

Raymond CK, Howald-Stevenson I, Vater CA, Stevens TH (1992) Morphological classification of the yeast vacuolar protein sorting mutants: evidence for a prevacuolar compartment in class E vps mutants. *Mol Biol Cell* **3:** 1389-1402

Richter EA, Hargreaves M (2013) Exercise, GLUT4, and skeletal muscle glucose uptake. *Physiol Rev* **93:** 993-1017

Ross SH, Lindsay Y, Safrany ST, Lorenzo O, Villa F, Toth R, Clague MJ, Downes CP, Leslie NR (2007) Differential redox regulation within the PTP superfamily. *Cell Signal* **19:** 1521-1530

Ruotolo R, Marchini G, Ottonello S (2008) Membrane transporters and protein traffic networks differentially affecting metal tolerance: a genomic phenotyping study in yeast. *Genome Biol* **9:** R67

Sabha N, Volpatti JR, Gonorazky H, Reifler A, Davidson AE, Li X, Eltayeb NM, Dall'Armi C, Di Paolo G, Brooks SV, Buj-Bello A, Feldman EL, Dowling JJ (2016) PIK3C2B inhibition improves function and prolongs survival in myotubular myopathy animal models. *J Clin Invest* **126:** 3613-3625

Saimani U, Smothers J, McDermott H, Makaraci P, Kim K (2017) Yeast dynamin associates with the GARP tethering complex for endosome-to-Golgi traffic. *Eur J Cell Biol* **96:** 612-621

Salmeen A, Barford D (2005) Functions and mechanisms of redox regulation of cysteine-based phosphatases. *Antioxid Redox Signal* **7:** 560-577

Schaletzky J, Dove SK, Short B, Lorenzo O, Clague MJ, Barr FA (2003) Phosphatidylinositol-5-phosphate activation and conserved substrate specificity of the myotubularin phosphatidylinositol 3-phosphatases. *Curr Biol* **13:** 504-509

Scheckhuber CQ, Erjavec N, Tinazli A, Hamann A, Nystrom T, Osiewacz HD (2007) Reducing mitochondrial fission results in increased life span and fitness of two fungal ageing models. *Nat Cell Biol* **9:** 99-105

Schieber M, Chandel NS (2014) ROS function in redox signaling and oxidative stress. *Curr Biol* **24:** R453-462

Schmid SL, Frolov VA (2011) Dynamin: functional design of a membrane fission catalyst. *Annu Rev Cell Dev Biol* **27:** 79-105

Schrader M, Costello JL, Godinho LF, Azadi AS, Islinger M (2016) Proliferation and fission of peroxisomes - An update. *Biochim Biophys Acta* **1863:** 971-983

Schu PV, Takegawa K, Fry MJ, Stack JH, Waterfield MD, Emr SD (1993) Phosphatidylinositol 3-kinase encoded by yeast VPS34 gene essential for protein sorting. *Science* **260:** 88-91

Schulze RJ, McNiven MA (2014) A well-oiled machine: DNM2/dynamin 2 helps keep hepatocyte lipophagy running smoothly. *Autophagy* **10:** 388-389

Senderek J, Bergmann C, Weber S, Ketelsen UP, Schorle H, Rudnik-Schoneborn S, Buttner R, Buchheim E, Zerres K (2003) Mutation of the SBF2 gene, encoding a novel member of the myotubularin family, in Charcot-Marie-Tooth neuropathy type 4B2/11p15. *Hum Mol Genet* **12:** 349-356

Shewan AM, McCann RK, Lamb CA, Stirrat L, Kioumourtzoglou D, Adamson IS, Verma S, James DE, Bryant NJ (2013) Endosomal sorting of GLUT4 and Gap1 is conserved between yeast and insulin-sensitive cells. *J Cell Sci* **126:** 1576-1582

Shisheva A (2008) PIKfyve: Partners, significance, debates and paradoxes. *Cell Biol Int* **32:** 591-604

Sikosek T, Chan HS (2014) Biophysics of protein evolution and evolutionary protein biophysics. *J R Soc Interface* **11:** 20140419

Sivera R, Frasquet M, Lupo V, Garcia-Sobrino T, Blanco-Arias P, Pardo J, Fernandez-Torron R, de Munain AL, Marquez-Infante C, Villarreal L, Carbonell P, Rojas-Garcia R, Segovia S, Illa I, Frongia AL, Nascimento A, Ortez C, Garcia-Romero MDM, Pascual SI, Pelayo-Negro AL, Berciano J, Guerrero A, Casasnovas C, Camacho A, Esteban J, Chumillas MJ, Barreiro M, Diaz C, Palau F, Vilchez JJ, Espinos C, Sevilla T (2017) Distribution and genotype-phenotype correlation of GDAP1 mutations in Spain. *Sci Rep* **7:** 6677

Smirnova E, Shurland DL, Newman-Smith ED, Pishvaee B, van der Bliek AM (1999) A model for dynamin self-assembly based on binding between three different protein domains. *J Biol Chem* **274:** 14942-14947

Spiro AJ, Shy GM, Gonatas NK (1966) Myotubular myopathy. Persistence of fetal muscle in an adolescent boy. *Arch Neurol* **14:** 1-14

Staiano L, De Leo MG, Persico M, De Matteis MA (2015) Mendelian disorders of PI metabolizing enzymes. *Biochim Biophys Acta* **1851:** 867-881

Stowell MH, Marks B, Wigge P, McMahon HT (1999) Nucleotide-dependent conformational changes in dynamin: evidence for a mechanochemical molecular spring. *Nat Cell Biol* **1:** 27-32

Su Y (2014) Regulation of endothelial nitric oxide synthase activity by protein-protein interaction. *Curr Pharm Des* **20:** 3514-3520

Sun T, Wu XS, Xu J, McNeil BD, Pang ZP, Yang W, Bai L, Qadri S, Molkentin JD, Yue DT, Wu LG (2010) The role of calcium/calmodulin-activated calcineurin in rapid and slow endocytosis at central synapses. *J Neurosci* **30:** 11838-11847

Tang F, Liu W (2010) An age-dependent feedback control model of calcium dynamics in yeast cells. *J Math Biol* **60:** 849-879

Tasfaout H, Buono S, Guo S, Kretz C, Messaddeq N, Booten S, Greenlee S, Monia BP, Cowling BS, Laporte J (2017) Antisense oligonucleotide-mediated Dnm2 knockdown prevents and reverts myotubular myopathy in mice. *Nat Commun* **8:** 15661

Taylor GS, Maehama T, Dixon JE (2000) Myotubularin, a protein tyrosine phosphatase mutated in myotubular myopathy, dephosphorylates the lipid second messenger, phosphatidylinositol 3-phosphate. *Proc Natl Acad Sci U S A* **97:** 8910-8915

Thomas NS, Williams H, Cole G, Roberts K, Clarke A, Liechti-Gallati S, Braga S, Gerber A, Meier C, Moser H, et al. (1990) X linked neonatal centronuclear/myotubular myopathy: evidence for linkage to Xq28 DNA marker loci. *J Med Genet* **27:** 284-287

Tosch V, Rohde HM, Tronchere H, Zanoteli E, Monroy N, Kretz C, Dondaine N, Payrastre B, Mandel JL, Laporte J (2006) A novel PtdIns3P and PtdIns(3,5)P2 phosphatase with an inactivating variant in centronuclear myopathy. *Hum Mol Genet* **15:** 3098-3106

Tosch V, Vasli N, Kretz C, Nicot AS, Gasnier C, Dondaine N, Oriot D, Barth M, Puissant H, Romero NB, Bonnemann CG, Heller B, Duval G, Biancalana V, Laporte J (2010) Novel molecular diagnostic approaches for X-linked centronuclear (myotubular) myopathy reveal intronic mutations. *Neuromuscul Disord* **20:** 375-381

Tronchere H, Laporte J, Pendaries C, Chaussade C, Liaubet L, Pirola L, Mandel JL, Payrastre B (2004) Production of phosphatidylinositol 5-phosphate by the phosphoinositide 3-phosphatase myotubularin in mammalian cells. *J Biol Chem* **279:** 7304-7312

Trotter EW, Grant CM (2005) Overlapping roles of the cytoplasmic and mitochondrial redox regulatory systems in the yeast Saccharomyces cerevisiae. *Eukaryot Cell* **4:** 392-400

Tsujita K, Itoh T, Ijuin T, Yamamoto A, Shisheva A, Laporte J, Takenawa T (2004) Myotubularin regulates the function of the late endosome through the gram domain-phosphatidylinositol 3,5-bisphosphate interaction. *J Biol Chem* **279:** 13817-13824

Vaccari I, Dina G, Tronchere H, Kaufman E, Chicanne G, Cerri F, Wrabetz L, Payrastre B, Quattrini A, Weisman LS, Meisler MH, Bolino A (2011) Genetic interaction between MTMR2 and FIG4 phospholipid phosphatases involved in Charcot-Marie-Tooth neuropathies. *PLoS Genet* **7:** e1002319

Valderrama F, Babia T, Ayala I, Kok JW, Renau-Piqueras J, Egea G (1998) Actin microfilaments are essential for the cytological positioning and morphology of the Golgi complex. *Eur J Cell Biol* **76:** 9-17

Valderrama F, Luna A, Babia T, Martinez-Menarguez JA, Ballesta J, Barth H, Chaponnier C, Renau-Piqueras J, Egea G (2000) The golgi-associated COPI-coated buds and vesicles contain beta/gamma -actin. *Proc Natl Acad Sci U S A* **97:** 1560-1565

Vanhaesebroeck B, Leevers SJ, Ahmadi K, Timms J, Katso R, Driscoll PC, Woscholski R, Parker PJ, Waterfield MD (2001) Synthesis and function of 3-phosphorylated inositol lipids. *Annu Rev Biochem* **70:** 535-602

Vasli N, Bohm J, Le Gras S, Muller J, Pizot C, Jost B, Echaniz-Laguna A, Laugel V, Tranchant C, Bernard R, Plewniak F, Vicaire S, Levy N, Chelly J, Mandel JL, Biancalana V, Laporte J (2012a) Next generation sequencing for molecular diagnosis of neuromuscular diseases. *Acta Neuropathol* **124:** 273-283

Vasli N, Laugel V, Bohm J, Lannes B, Biancalana V, Laporte J (2012b) Myotubular myopathy caused by multiple abnormal splicing variants in the MTM1 RNA in a patient with a mild phenotype. *Eur J Hum Genet* **20:** 701-704

Vater CA, Raymond CK, Ekena K, Howald-Stevenson I, Stevens TH (1992) The VPS1 protein, a homolog of dynamin required for vacuolar protein sorting in Saccharomyces cerevisiae, is a GTPase with two functionally separable domains. *J Cell Biol* **119:** 773-786

Viaud J, Lagarrigue F, Ramel D, Allart S, Chicanne G, Ceccato L, Courilleau D, Xuereb JM, Pertz O, Payrastre B, Gaits-Iacovoni F (2014) Phosphatidylinositol 5-phosphate regulates invasion through binding and activation of Tiam1. *Nat Commun* **5:** 4080

Vicinanza M, Korolchuk VI, Ashkenazi A, Puri C, Menzies FM, Clarke JH, Rubinsztein DC (2015) PI(5)P regulates autophagosome biogenesis. *Mol Cell* **57:** 219-234

Vida TA, Emr SD (1995) A new vital stain for visualizing vacuolar membrane dynamics and endocytosis in yeast. *J Cell Biol* **128:** 779-792

Vizeacoumar FJ, Vreden WN, Fagarasanu M, Eitzen GA, Aitchison JD, Rachubinski RA (2006) The dynamin-like protein Vps1p of the yeast Saccharomyces cerevisiae associates with peroxisomes in a Pex19p-dependent manner. *J Biol Chem* **281:** 12817-12823

Walker DM, Urbe S, Dove SK, Tenza D, Raposo G, Clague MJ (2001) Characterization of MTMR3. an inositol lipid 3-phosphatase with novel substrate specificity. *Curr Biol* **11:** 1600-1605

Wang CH, Dowling JJ, North K, Schroth MK, Sejersen T, Shapiro F, Bellini J, Weiss H, Guillet M, Amburgey K, Apkon S, Bertini E, Bonnemann C, Clarke N, Connolly AM, Estournet-Mathiaud B, Fitzgerald D, Florence JM, Gee R, Gurgel-Giannetti J, Glanzman AM, Hofmeister B, Jungbluth H, Koumbourlis AC, Laing NG, Main M, Morrison LA, Munns C, Rose K, Schuler PM, Sewry C, Storhaug K, Vainzof M, Yuan N (2012) Consensus statement on standard of care for congenital myopathies. *J Child Neurol* **27:** 363-382

Wang YX, Zhao H, Harding TM, Gomes de Mesquita DS, Woldringh CL, Klionsky DJ, Munn AL, Weisman LS (1996) Multiple classes of yeast mutants are defective in vacuole partitioning yet target vacuole proteins correctly. *Mol Biol Cell* **7:** 1375-1389

Weisman LS (2003) Yeast vacuole inheritance and dynamics. *Annu Rev Genet* **37:** 435-460

Weisman LS, Emr SD, Wickner WT (1990) Mutants of Saccharomyces cerevisiae that block intervacuole vesicular traffic and vacuole division and segregation. *Proc Natl Acad Sci U S A* **87:** 1076-1080

Westermann B (2012) Bioenergetic role of mitochondrial fusion and fission. *Biochim Biophys Acta* **1817:** 1833-1838

Winzeler EA, Shoemaker DD, Astromoff A, Liang H, Anderson K, Andre B, Bangham R, Benito R, Boeke JD, Bussey H, Chu AM, Connelly C, Davis K, Dietrich F, Dow SW, El Bakkoury M, Foury F, Friend SH, Gentalen E, Giaever G, Hegemann JH, Jones T, Laub M, Liao H, Liebundguth N, Lockhart DJ, Lucau-Danila A, Lussier M, M'Rabet N, Menard P, Mittmann M, Pai C, Rebischung C, Revuelta JL, Riles L, Roberts CJ, Ross-MacDonald P, Scherens B, Snyder M, Sookhai-Mahadeo S, Storms RK, Veronneau S, Voet M, Volckaert G, Ward TR, Wysocki R, Yen GS, Yu K, Zimmermann K, Philippsen P, Johnston M, Davis RW (1999) Functional characterization of the S. cerevisiae genome by gene deletion and parallel analysis. *Science* **285:** 901-906

Yadav PK, Rajvanshi PK, Rajasekharan R (2017) The role of yeast m(6)A methyltransferase in peroxisomal fatty acid oxidation. *Curr Genet*

Yen K, Gitsham P, Wishart J, Oliver SG, Zhang N (2003) An improved tetO promoter replacement system for regulating the expression of yeast genes. *Yeast* **20:** 1255-1262

Yoon HS, Hajduk PJ, Petros AM, Olejniczak ET, Meadows RP, Fesik SW (1994) Solution structure of a pleckstrin-homology domain. *Nature* **369:** 672-675

Youn JY, Friesen H, Kishimoto T, Henne WM, Kurat CF, Ye W, Ceccarelli DF, Sicheri F, Kohlwein SD, McMahon HT, Andrews BJ (2010) Dissecting BAR domain function in the yeast Amphiphysins Rvs161 and Rvs167 during endocytosis. *Mol Biol Cell* **21:** 3054-3069

Yu X, Cai M (2004) The yeast dynamin-related GTPase Vps1p functions in the organization of the actin cytoskeleton via interaction with Sla1p. *J Cell Sci* **117:** 3839-3853

Zhang Y, Zolov SN, Chow CY, Slutsky SG, Richardson SC, Piper RC, Yang B, Nau JJ, Westrick RJ, Morrison SJ, Meisler MH, Weisman LS (2007) Loss of Vac14, a regulator of the signaling lipid phosphatidylinositol 3,5-bisphosphate, results in neurodegeneration in mice. *Proc Natl Acad Sci U S A* **104:** 17518-17523

Zuchner S, Noureddine M, Kennerson M, Verhoeven K, Claeys K, De Jonghe P, Merory J, Oliveira SA, Speer MC, Stenger JE, Walizada G, Zhu D, Pericak-Vance MA, Nicholson G, Timmerman V, Vance JM (2005) Mutations in the pleckstrin homology domain of dynamin 2 cause dominant intermediate Charcot-Marie-Tooth disease. *Nat Genet* **37:** 289-294

I. Introduction

Au cours de ma thèse, j'ai étudié au niveau moléculaire trois myopathies centronucléaires congénitales (CNM pour « centronuclear myopathy »). La myopathie centronucléaire liée à l'X (XLCNM) associée à des mutations dans le gène *MTM1*, la myopathie centronucléaire associée à des mutations dans *PYROXD1* et finalement la myopathie autosomique centronucléaire associée à des mutations dans *DNM2*. Ces trois myopathies ont quelques caractéristiques communes surtout au niveau de l'histologie du muscle du patient et de la physiopathologie des symptômes, mais elles ont aussi des différences. En effet, trois gènes différents sont affectés, et les protéines produites par leur expression sont impliquées dans des voies cellulaires spécifiques.

À mon avis, mieux nous comprenons un problème, plus nous serons en mesure de trouver une solution. Par conséquent, le but de ma thèse de doctorat était d'acquérir plus d'informations sur la fonction de ces protéines, pour mieux comprendre ces maladies et pour être à l'avenir en mesure de développer une thérapie adaptée et ciblée pour les patients affectés.

1.1. Les différentes myopathies centronucléaires

La myopathie fait référence à une pathologie affectant les muscles. Les origines sont multiples : congénitale, métabolique, immunologique ou inflammatoire, idiopathique, infectieuse, nutritionnelle, myopathies d'origine endocrinienne et myopathies médicamenteuses ou toxiques. La myopathie centronucléaire (CNM) appartient au grand groupe de myopathies congénitales (troubles neuromusculaires héréditaires) et comme indiqué par son nom, les noyaux des fibres musculaires du patient sont situés au centre, alors que dans le muscle adulte ils sont normalement situés à la périphérie.

Les myopathies congénitales peuvent être classées en 5 types, le tableau 1 montre les différents types de troubles et les gènes impliqués. (*Pour les autres figures citées dans ce résumé, se reporter à la thèse).

Dysfonction	Transmission	Protéine (gène) affectée
Myopathies congénitales associées aux protéines		
Accumulation		
Myopathie à la némaline	AD,AR	α-tropomyosine$_{SLOW}$ (TPM3)
	AR	nébuline (NEB)
	AD,AR	α-actine squelettique (ACTA1)

	AD	β-tropomyosine (TPM2)
	AR	troponine T (TNNT1)
	AR	cofiline (CLF2)
Cap maladie (variante de la myopathie némaline)	AD	β-tropomyosine (TPM2)
	AD	α-tropomyosine$_{SLOW}$ (TPM3)
	AD	α-actine squelettique (ACTA1)
Myopathie du corps zébré (variante de la némaline Myopathie)	AD	α-actine squelettique (ACTA1)
Myopathie de stockage de myosine (corps hyalin)	AD	chaîne lourde de myosine lente / β-cardiaque (MYH7)
Myopathies congénitales associées aux noyaux		
Maladie centrale du coeur	AD,AR	Récepteur de la ryanodine (RYR1)
Maladie multi-minicore	AD,AR	Récepteur de la ryanodine (RYR1)
Y compris la myopathie congénitale avec des noyaux (à la fois centrale et minicores)	AR	Sélénoprotéine N (SEPN1)
	AD	α-actine squelettique (ACTA1)
Myopathies congénitales associées aux noyaux et des tiges		
Myopathie core-rod	AD,AR	Récepteur de la ryanodine (RYR1)
	AD	Répétition Kelch BTB (POZ) domaine contenant 13 (KBTBD13)
	AR	Nebulin (NEB)
Myopathies congénitales associées à noyaux centralisés		
Myopathie myotubulaire	Liée à l'X	Myotubularine (MTM1)
Myopathie centronucléaire	AD	Dynamine 2 (DNM2)
	AR, AD	Amphiphysine 2 (BIN1)
	AR	Récepteur de la ryanodine (RYR1)
Myopathies congénitales associées uniquement à		

petites fibres de type I Disproportion de type de fibre congénitale	AD AD AR AD Liée à l'X	α-actine squelettique (ACTA1) α-tropomyosine$_{SLOW}$ (TPM3) Sélénoprotéine N (SEPN1) β-tropomyosine (TPM2) Xp22.13 à Xq22.1
Abréviations: AD autosomique dominante, AR autosomique récessive.		

Tableau 1. Classification des myopathies congénitales. La myopathie centronucléaire est un sous-groupe de ce type de troubles neuromusculaires. Les myopathies dues aux mutations du gène PYROXD1 ont des caractéristiques mixtes des 5 groupes. Adapté de (Nord,2008; Wang et al, 2012)

Le nombre de cas de nouveau-nés et / ou d'enfants (âge <18 ans) dans la population souffrant de myopathie centronucléaire a été estimé à <1 sur 100 000 répartis entre MTM1 (45%), DNM2 (15%), RYR1 (10-15%) et BIN1 (<5%) (Amburgey et al, 2011). Les 20% restant de cas ont probablement des mutations dans des gènes qu'il reste à identifier (Biancalana et al, 2012, Tosch et al, 2010). Actuellement, le séquençage de nouvelle génération est utilisé pour le diagnostic moléculaire de ces patients souffrant de myopathie centronucléaire mais sans gène causal identifié (Tosch et al, 2010; Vasli et al, 2012a).

1.1.1. Myopathie centronucléaire liée à l'X due à des mutations dans le gène MTM1

Le gène MTM1 est positionné sur le chromosome X, à la position Xq28 (Thomas et al, 1990). En raison de la transmission génétique liée au chromosome X, les mâles sont principalement affectés par cette myopathie appelée myopathie centronucléaire liée à l'X (XLCNM) ou myopathie myotubulaire liée à l'X (XLMTM). Cependant quelques rares des cas de femmes symptomatiques sont également décrits (Biancalana et al, 2017).

Les symptômes des patients sont une faiblesse musculaire généralisée, une hypotonie sévère et une détresse respiratoire, les patients survivent seulement jusqu'à l'enfance. Cependant, certains individus avec une forme moins grave de la maladie ont vécu jusqu'à l'âge adulte.

En 1996, Jocelyn Laporte et ses collègues ont identifié des mutations sur le gène *MTM1* comme responsable du XLCNM (Laporte et al, 1996). La protéine MTM1 appartient à la sous-famille des myotubularines, avec 14 représentants chez l'Homme dont certains portent des mutations dans le site catalytique les rendant inactifs (Raess et al, 2017b). Ces protéines appartiennent à la grande famille des lipides phosphatases, en particulier la protéine tyrosine phosphatase (PTP) à double spécificité phosphatase. Elles catalysent la réaction de déphosphorylation du phosphatidylinositol 3-

phosphate (PI3*P*) et du phosphatidylinositol (3,5) bisphosphate (PI(3,5)P_2) en position 3 du cycle inositol.

En 2012, environ 400 patients ont été décrits avec des mutations dans MTM1 et souffrant de XLCNM. Ces mutations incluent des mutations ponctuelles (faux-sens, non-sens et mutations au niveau du site d'épissage), des insertions et des délétions (Biancalana et al, 2012, Tosch et al, 2010). Beaucoup de mutations trouvées dans MTM1 sont associées à une perte de fonction avec souvent une diminution du niveau ou une absence de protéine MTM1 (Laporte et al, 2001; Vasli et al, 2012b).

Les domaines PH-GRAM et catalytique de la protéine MTM1

La myotubularine MTM1 est composée de six domaines (figure 8): PH/GRAM (Pleckstrin Homology-Glucosyltranferase, Rab-like GTPase activator and Myotubularin), RID (Rac-induced recruitment domain), PTP / DSP (Protein tyrosine phosphatase/Dual-specificity phosphatases), SID (SET-protein interaction domain), le site de liaison PDZ sert de médiateur des interactions protéine-protéine (PDS-95, une protéine postsynaptique, Discs-large, un suppresseur de tumeur de *Drosophila* et ZO-1, une protéine de jonction) et le domaine CC (coiled-coil) est important pour l'homodimérisation et/ou l'hétérodimérisation de la myotubularine (Bertazzi et al, 2015b, Laporte et al, 2003).

Pendant ma thèse j'ai focalisé mes études sur les domaines PH-GRAM (aa 1-170 de MTM1) et le catalytique PTP/DSP (aa 175-538 de MTM1).

Le domaine PH-GRAM

Les myotubularines humaines, même les catalytiques inactives, partagent en commun le domaine PH-GRAM qui est d'environ 70 acides aminés (Raess et al, 2017b). Dans la myotubularine MTM1, le domaine PH-GRAM est localisé à l'extrémité N-terminale. In vitro, le domaine PH-GRAM de MTM1 peut lier différents phosphoinositides (PIP) dont le PI(3,4,5)P_3, PI(3,5)P_2, PI5*P* et PI3*P* (Schaletzky et al., 2003; Tsujita et al, 2004). Cependant, il a été montré que la protéine MTM1 hydrolyse seulement PI3*P* et PI(3,5)P_2 via son activité 3-phosphatase (Taylor et al, 2000; Tronchere et al, 2004).

Il est intéressant de mentionner que même si l'on s'attend à ce que les domaines PH-GRAM se lient aux PIP, des données basées sur la structure cristalline de la myotubularine MTMR2, montrent que la taille et l'hydrophobicité de l'interface entre le domaine PH-GRAM de MTMR2 et la membrane restreignent son interaction avec les PIP (Begley et al, 2003). Des études ont montré que le domaine PH-GRAM est requis pour la liaison de la myotubularine MTMR2 avec la membrane (Berger et al,

2003). Cependant, il n'y avait pas de liaison avec les PIP observée dans la région du domaine PH-GRAM de MTMR2 dans la structure cristalline résolue en présence de PI(3,5)P_2 ou de PI3*P*. Ceci suggère une faible interaction d'affinité avec ces substrats, une caractéristique de la majorité des domaines PH (Pleckstrin Homology) (Berger et al, 2006). Comme la structure cristalline de MTM1 n'a pas été résolue dû à la difficulté de produire assez de protéine pure, les données de MTMR2 sont utilisées par modélisation pour mieux comprendre l'organisation tridimensionnelle de MTM1.

Le domaine catalytique

Le domaine catalytique de la phosphoinositide phosphatase PTP/DSP est très conservé parmi les différentes myotubularines, tant actives qu'inactives (Raess et al, 2017b).

La taille du domaine catalytique des myotubularines est beaucoup plus grande que celle observée pour les autres protéines tyrosine phosphatases PTP, constituées d'environ 400 acides aminés structurés dans un feuillet β central pris en sandwich par des hélices α (Begley et al, 2006) (figure 9). Les PTP sont caractérisées par la présence du motif consensus CX_5R dans le site actif, où X désigne n'importe quel acide aminé (Denu & Dixon, 1995). Cependant, les myotubularines ne déphosphorylent pas les résidus tyrosine, thréonine ou sérine comme le font les PTP, mais elles déphosphorylent les lipides phosphoinositides PI*P*, et sont appelées PTP/DSP pour « protein tyrosine phosphatase/ double specificity phosphatase ». Après avoir recherché pendant quatre ans le substrat protéique de la MTM1 phosphatase, il a finalement été montré en 2000 que la myotubularine MTM1 déphosphorylait le PI3*P* (Blondeau et al, 2000; Taylor et al, 2000). En 2004, Hélène Tronchère et ses collègues ont montré que in vitro et in vivo MTM1 déphosphorylait également un second type de PI*P*, le PI(3,5)P_2 et que le produit de cette réaction était le PI5*P* (Tronchere et al, 2004).

1.1.2. Myopathie centronucléaire due à des mutations du gène DNM2

Des mutations dans le gène *DNM2* sont impliquées dans la forme la plus bénigne de CNM, qui est autosomique dominante (ADCNM) également appelée myopathie centronucléaire 1 CNM1 (figure 3A). Le gène responsable est localisé à la position 19p13.2 (Bitoun et al, 2005). Des mutations de faux-sens hétérozygotes récurrentes et des mutations de novo ont été identifiées dans le gène *DNM2*. Les hommes et les femmes atteints ont des symptômes d'hypotonie, de faiblesse musculaire avec un visage allongé avec ptosis (paupière tombante) et une ophtalmoplégie. Plusieurs cas ont été rapportés présentant soit des phénotypes plus sévères avec apparition néonatale, soit des cas plus légers d'apparition tardive des symptômes dans l'enfance ou certaines formes moins sévères détectées à l'âge adulte (Abath Neto et al, 2015, Bitoun et al, 2007, Jeub et al, 2008).

Il est important de mentionner que des mutations dans le gène *DNM2* provoquent également une neuropathie (OMIM 606482), à savoir deux types de maladies de Charcot-Marie-Tooth (CMT): CMT dominante intermédiaire B (CMTDIB) et CMT axonale type 2M (Fabrizi et al, 2007; Zuchner et al, 2005) (figure 3B). Les neuropathies de Charcot-Marie-Tooth ont deux formes principales: démyélinisante et axonale. Dans ces formes, le défaut primaire réside dans les cellules de Schwann ou les neurones, respectivement (Pareyson & Marchesi, 2009). Cependant, un ensemble complexe de sous-types a été décrit comme le sous-type intermédiaire. Dans ce sous-type, il n'est pas clair si un trouble axonal ou démyélinisant est responsable de la maladie. La perte nerveuse de la conduction, la démyélinisation et l'hypermyélinisation focale sont les signes moléculaires de la maladie. En ce qui concerne les symptômes physiques, les patients présentent deux traits principaux: d'une part, les jambes présentant une apparence de bouteille de champagne inversée; deuxièmement, les déformations du pied et de la main. Cela pourrait s'expliquer par le fait que les muscles des membres ne peuvent pas recevoir correctement la transmission neuronale (Claeys et al, 2009).

La dynamine DNM2 est une protéine appartenant à la grande famille des GTPases. La DNM2 humaine est une protéine de 98 kDa codée par le gène *DNM2* situé sur le chromosome 19.

Dans les cellules de mammifères, il existe trois types différents de dynamine codés par trois gènes: DNM1 exprimé dans les cellules neuronales, DNM2 exprimé de façon ubiquitaire et DNM3 exprimé dans le cerveau, les testicules, les poumons et le cœur (Antonny et al, 2016).

La dynamine DNM2, une protéine GTPase

Les domaines de la protéine DNM2

La dynamine DNM2 est composée de 5 domaines (Figure 13). Le domaine catalytique GTPase en N-terminal est responsable de la liaison au GTP et de l'hydrolyse. Les analyses par microscopie électronique révèlent que l'hydrolyse du GTP induit un changement conformationnel de la protéine (Stowell et al, 1999). Le domaine du milieu est impliqué dans l'auto-assemblage de la dynamine (Smirnova et al, 1999). Le GED ou domaine effecteur GTPase et le domaine intermédiaire participent à l'oligomérisation et à la régulation de l'activité GTPase. Le domaine PH de DNM2 se lie aux membranes lipidiques mais ne montre pas de spécificité pour le PI(4,5)P_2 contrairement à ce qui avait été observé pour la dynamine DNM1 (Cowling et al, 2017). Le PRD ou domaine riche en proline en C-terminal se lie à des protéines contenant des domaines SH3 (Src homology 3); il est également nécessaire pour l'association aux microtubules. Pour DNM1 a été montré que les domaines PH et PRD coopèrent pour localiser la dynamine à des vésicules à manteau de clathrine.

DNM1 est le membre fondateur de la famille des dynamines et il joue un rôle important dans l'endocytose, le processus par lequel la cellule internalise le matériel extracellulaire par des invaginations dans la membrane plasmique. Sur la base de la conservation du domaine protéique, les différentes dynamines DNM1, DNM2 et DNM3 sont supposées jouer un rôle dans le remodelage membranaire et les phénomènes de fission membranaire.

Une étude récente a montré que DNM2 est également impliqué dans la fission des mitochondries, en coopération avec la GTPase DRP1/DNM1L associée à la dynamine cytoplasmique qui était auparavant considérée comme la seule dynamine requise pour la fission des mitochondries (Lee et al, 2016).

Maintenant, je vais décrire plus précisément certains des rôles connus de la dynamine DNM2 liée aux fonctions musculaires. En effet, il a été montré que DNM2 joue un rôle dans l'homéostasie du calcium dans le muscle (Durieux et al, 2010b ; Fraysse et al, 2016). Les expériences étaient faites sur un modèle de souris knock-in (KI) exprimant la mutation la plus fréquente dans la AD-CNM, la DNM2-R465W à un état hétérozygote DNM2-R465W/DNM2. Les résultats ont montré une concentration cytosolique plus élevée de Ca^{2+} dans les muscles EDL (extensor digitorum longus) et FDB (flexor digitorum brevis), une augmentation de la perméabilité sarcolemmique au Ca^{2+} et une teneur plus élevée en Ca^{2+} du réticulum sarcoplasmique dans les muscles EDL de ces souris hétérozygotes. Ceci suggère que l'augmentation de la concentration en calcium cytosolique n'est pas le résultat d'une fuite au niveau du réticulum sarcoplasmique. Fraysse et ses collègues proposent que la perméabilité de la membrane plasmique soit le principal facteur impliqué dans ces perturbations de l'homéostasie calcique (Fraysse et al, 2016). Cependant, il est important de mentionner qu'il n'y a pas eu d'altération des caractéristiques cinétiques du calcium en transit associé à l'activité musculaire contractile dans les muscles de ces souris Dnm2-R465W KI, qui ont une force musculaire plus faible. Ces différentes observations suggèrent que le défaut d'homéostasie du calcium n'est probablement pas la cause de l'altération contractile, même si les deux peuvent être corrélés.

Un rôle de DNM2 dans la production d'espèces réactives de l'oxygène ou ROS (reactive oxygen species) liée à l'apoptose induite par le stress oxydatif dans les cardiomyocytes a été récemment démontré (Gao et al, 2016). En effet, comme l'inhibition des dynamines DRP1 / DNM1L limite la production de ROS et l'apoptose dans les cardiomyocytes soumis à une lésion d'ischémie / reperfusion. Par conséquent, Gao et ses collègues ont analysé si l'inhibition de DNM2 limite également la production de ROS. Leurs résultats montrent que l'inhibition de DNM2 réduit la fission mitochondriale induite par le stress oxydatif et par conséquent réduit l'apoptose cellulaire

dans les cardiomyocytes (Gao et al, 2016). Ainsi, ces résultats suggèrent que DNM2 est lié à la production de ROS.

DNM2 est également impliqué dans l'autophagie (Durieux et al, 2012). Durieux et ses collègues ont montré que les souris Dnm2-R465W KI qui développent les phénotypes CNM présentent également un défaut d'autophagie néonatale avec une diminution du flux d'autophagie avant dégradation par l'autolysosome, un compartiment créé par la fusion de l'autophagosome mature et du lysosome (Durieux et al, 2012). Ils ont également observé que les fibroblastes embryonnaires des souris Dnm2 KI affichent un ratio accru d'autophagomes immatures lors de restrictions caloriques, des conditions induisant des niveaux élevés d'autophagie (Durieux et al, 2012).

1.1.3. Myopathie due à des mutations du gène PYROXD1

Des mutations dans le gène *PYROXD1* ont été identifiées comme une cause de myopathie myofibrillaire précoce (O'Grady et al, 2016). Les patients atteints présentent des symptômes caractérisés principalement par une faiblesse musculaire progressive, des difficultés à courir et à monter les escaliers, et une réduction de la masse musculaire. Ces symptomes apparaissent généralement dans l'enfance.

PYROXD1 est une protéine contenant un domaine pyridine-nucléotide-disulfure oxydoréductase (PNDR) et elle est classée comme une pyridine-nucléotide-disulfure oxydoréductase de classe I. Cependant contrairement aux autres PNDR humaines, PYROXD1 ne présente ni le motif redox du domaine oxydoréductase présent dans les glutathion réductases (GSR), dans les thioredoxine réductases 1,2 and 3 (TXNRD1,2,3) et dans les dihydrolipoamide déshydrogénase (DLD), ni le domaine de dimérisation conservé en C-terminal identifié dans les PNDR de classe I. Au lieu de cela, il présente un domaine nitrile réductase NADH-dépendant hautement conservé en C-terminal

---

De nos jours, aucun traitement n'est disponible pour les patients affectés par ces trois types de myopathies centronucléaires. Cependant, plusieurs laboratoires de recherche travaillent durement pour mieux comprendre ce type de myopathie et trouver un traitement adapté. En effet, certains traitements thérapeutiques pour la myopathie XLCNM sont en phase préclinique ou testés sur différents modèles animaux, avec des résultats prometteurs donnant de l'espoir aux patients et à leurs familles. Cependant, le mécanisme moléculaire de ces troubles et comment exactement les mutations au niveau des gènes impactent la fonction des protéines doivent être mieux compris.

1.2. La levure de boulanger *Saccharomyces cerevisiae*, le modèle de cette étude

La levure *Saccharomyces cerevisiae* est un eucaryote unicellulaire du groupe des ascomycètes appartenant au règne des Fungi. La levure *Saccharomyces cerevisiae* et plus spécifiquement la souche de laboratoire S288c a été le premier eucaryote dont le génome a été entièrement séquencé en 1996; après 4 ans d'un projet de séquençage regroupant plus de 100 laboratoires à travers le monde. De nos jours, c'est le génome eucaryote annoté le plus complet et les données de publication sur la régulation des gènes et le rôle des protéines sont stockées dans une base de données en libre accès, la base de données « Saccharomyces Genome Database » (https://www.yeastgenome.org/).

Cultiver des cellules de levure et manipuler son génome en laboratoire est bien décrit, rapide et peu coûteux. En outre, la collection de souches de délétion de levure englobant le knock-out de chaque gène de levure non essentiel est fournie pour la communauté scientifique par Euroscarf et décrit (http://www-sequence.stanford.edu/group/yeast_deletion_project/deletions3.html) (Winzeler et al, 1999). Cette collection regroupe l'ensemble des souches mutantes de délétion de levure portant le gène KanMX de résistance à la Kanamycin inséré dans plus de 6000 cadres de lecture ouverts (ORF) dans le génome de *S. cerevisiae*. Cette collection permet d'étudier la fonction cellulaire précise de chaque gène dans la souche de délétion correspondante (Winzeler et al, 1999).

Lors de ma thèse, j'ai utilisé l'humanisation de la levure pour étudier 3 protéines humaines impliquées dans des myopathies centronucléaires, à savoir la myotubularine MTM1, la dynamine DNM2 et l'oxydoréductase PYROXD1. L'humanisation de la levure consiste à transformer la levure avec des cDNA (ADN complémentaire) issus de gènes humains ou à remplacer un gène de la levure par son orthologue humain afin d'étudier sa fonction cellulaire dans cet eucaryote unicellulaire (Kachroo et al, 2015).

II. Résultats

2.1. La myotubularine MTM1 et son activité phosphatase dans la levure

2.1.1 Les interactions entre le PH/GRAM et le domaine catalytique de MTM1 reconstituent une myotubularine avec une activité phosphatase

Pour mieux comprendre la fonction cellulaire de MTM1, j'ai étudié les interactions *in vivo* entre les deux domaines principaux de cette protéine: le domaine de liaison lipidique en N-terminal PH-GRAM et le domaine en C-terminal phosphatase catalytique. Les deux domaines ont été fusionnés avec différents rapporteurs fluorescents (GFP (green fluorescent protein) et DsRed) et exprimés ou

co-exprimés dans des cellules de levure. J'ai visualisé par microscopie à fluorescence leurs effets cellulaires et leur localisation.

J'ai utilisé pour cette étude la souche de levure mutante *ymr1*Δ portant la délétion du seul gène codant pour une myotubularine présent chez la levure et nommé *YMR1* pour yeast myotubularine related 1. L'expression du cDNA codant pour MTM1 humain entraîne l'élargissement de la vacuole / lysosome de la souche de levure mutante *ymr1*Δ, une conséquence de son activité phosphatase (Amoasii et al, 2012). J'ai utilisé la taille vacuolaire comme marqueur de l'activité catalytique phosphatase de MTM1 *in vivo* dans la levure.

L'analyse de la localisation intracellulaire du domaine PH/GRAM lors de sa fusion avec la GFP en N- ou en C-terminal montre que sa localisation à la membrane est observée uniquement pour la construction PH-GRAM-GFP. La construction catalytique-GFP est observée dans des structures ponctuées à proximité des membranes vacuolaires fragmentées, indiquant que cette construction MTM1 sans le domaine PH-GRAM ne montre pas d'activité phosphatase *in vivo*. Ces résultats montrent que le domaine PH-GRAM en N-terminal est essentiel pour l'activité phosphatase de MTM1 *in vivo* dans les cellules de levure et que ce domaine doit être libre à son extrémité N-terminale pour sa localisation à la membrane.

Chez la levure, les phosphoinositides PI3*P* et PI(3,5)P_2, les deux substrats de MTM1, sont requis pour le tri des protéines vacuolaires, et en leur absence, la carboxypeptidase Y, CPY, est sécrétée dans le milieu extracellulaire, au lieu d'être adressée à la lumière vacuolaire (Mayinger, 2012). La sécrétion de CPY a été analysée dans les cellules de levure exprimant les différentes constructions de MTM1 portant une mutation faux-sens de patient atteint de CNM soit dans le domaine PH/GRAM, soit dans le domaine catalytique. Le taux de sécrétion de CPY dépend de l'activité catalytique de MTM1 révélée par la production de PI5*P*, avec la forme sauvage MTM1 montrant le plus haut niveau de sécrétion de CPY et les mutants catalytiques MTM1-C375S et MTM1-S376N portant des phosphatases défectueuses ne présentant aucune sécrétion de CPY. L'essai de sécrétion de CPY montre que MTM1-GFP est catalytique actif, quoique dans une moindre mesure comparé à la construction portant MTM1 libre et non fusionné à la GFP. Ce test de sécrétion CPY confirme également que ni le domaine PH-GRAM, ni le domaine catalytique ne sont catalytique actifs.

Les cellules mutantes de levure *ymr1*Δ ont été transformées avec des vecteurs portant PH/GRAM-DsRed et/ou le domaine catalytique-GFP pour observer leur localisation au sein des cellules. La lumière vacuolaire a été colorée en bleu avec le colorant CMAC (7-amino-4-chlorométhyl-coumarine) pour visualiser le phénotype vacuolaire. La myotubularine sauvage MTM1 et le mutant catalytique inactif MTM1-C375S ont été utilisés comme témoins. Le pourcentage de grandes

vacuoles au sein de la population de levures exprimant MTM1 ou MTM1-C375S est significativement différent (figure 2B), montrant une corrélation directe entre la taille de la vacuole et l'activité phosphatase de MTM1 *in vivo*. Comme observé précédemment sur le test de sécrétion de CPY, ni le domaine PH/GRAM, ni le domaine catalytique ne sont catalytiques actifs, car leur pourcentage de grandes vacuoles est similaire à celui observé pour le mutant catalytique inactif MTM1-C375S. Cependant, dans les cellules de levure co-exprimant le PH-GRAM et le domaine catalytique, ces deux domaines sont colocalisés dans une structure en forme de point, adjacente à la vacuole, et les vacuoles sont grandes. Seules les cellules de levure ayant les deux domaines colocalisés à côté de la vacuole ont des grandes vacuoles, alors que les autres cellules ont des vacuoles fragmentées (étoiles blanches, figure 2A). La quantification du phénotype vacuolaire montre que les cellules de levure co-exprimant le PH-GRAM et le domaine catalytique ont un pourcentage accru de grandes vacuoles par rapport aux vacuoles fragmentées (figure 2B). Ceci suggère que ces deux domaines interagissent et reconstituent une activité comparable à celle de la myotubularine MTM1 avec une phosphatase active.

Pour déterminer si les domaines PH/GRAM et catalytique interagissent, le domaine PH/GRAM a été immunoprécipité et la co-immunoprécipitation (coIP) du domaine catalytique a été évaluée par immunodétection en utilisant la technique du Western blot (figure 2C). Le domaine catalytique a été détecté dans l'extrait protéique total du contrôle mais pas dans la fraction immunoprécipitée (IP) indiquant qu'il ne se lie pas aux billes et n'a pas été reconnu par les anticorps monoclonaux 1G6 spécifiques de la région N-terminal MTM1. Le domaine catalytique interagit avec le PH/GRAM car il a été détecté dans la fraction IP uniquement en présence du domaine PH/GRAM (figure 2C). Ceci montre que ces deux domaines via leur interaction peuvent reconstituer une phosphatase fonctionnelle et active conduisant à l'élargissement des vacuoles de levure (Fig. 2B).

Pour déterminer si le domaine PH/GRAM complémente la perte d'activité de la MTM1 phosphatase non fonctionnelle, GFP-MTM1 a été co-exprimé avec le PH/GRAM-DsRed, et la protéine de fusion active MTM1-GFP a été utilisée comme contrôle (figure 3A). L'expression du domaine PH/GRAM permet d'associer GFP-MTM1 à plusieurs structures en points adjacentes à la vacuole (points jaunes) et les cellules de levure ont de grandes vacuoles (Fig. 3A), contrairement aux cellules transformées uniquement avec GFP-MTM1 dans lesquelles la vacuole reste fragmentée (Fig. 1A). Dans une seconde expérience, des cellules co-transformées avec le domaine catalytique-DsRed et les plasmides vides GFP, MTM1-GFP ou MTM1-C375S-GFP ont été observées par microscopie à fluorescence après coloration de la lumière vacuolaire avec le CMAC (bleu, Fig. 3B). Le domaine catalytique de MTM1 permet à la phosphatase non active catalytiquement MTM1-C375S-GFP de développer de grandes vacuoles (figure 3B), contrairement aux cellules de levure n'exprimant que

MTM1-C375S-GFP (figure 1A). Environ 700 à 800 cellules de chaque transformation ont été analysées pour classer leurs vacuoles en fonction de leur morphologie (vacuoles 1-large, 2-fragmentées et 3- petites, intermédiaires, un ou deux lobes) (figure 3C). Le pourcentage de grandes vacuoles de cellules co-exprimant MTM1-C375S et le domaine catalytique est significativement différent des cellules exprimant uniquement MTM1-C375S (figure 3C). Ce pourcentage accru de grandes vacuoles indique une activité de phosphatase catalytique, ce qui montre que le domaine catalytique restaure l'activité de la protéine catalytiquement inactive MTM1-C375S.

2.2. La dynamine humaine DNM2 et son étude dans les cellules de levure

Concernant le projet sur la dynamine DNM2, j'étais tuteur d'un stagiaire Erasmus, Roberto Silva Rojas (Université Complutense de Madrid, Espagne) qui a travaillé pendant 6 mois sur DNM2 avec moi. Des mutations dans le gène *DNM2* sont impliquées dans deux pathologies, la myopathie centronucléaire autosomique dominante et une neuropathie de type Charcot-Marie-Tooth intermédiaire. Cependant, les mutations dans *DNM2* conduisent à l'une ou l'autre maladie sans un schéma clair de mutations liées à chaque maladie. C'est pourquoi dans mon projet de recherche j'ai étudié la dynamine DNM2 pour mieux comprendre le lien entre les mutations et la maladie. Différentes dynamines humaines ont été étudiées dans les cellules de levure. Les dynamines de levure Vps1 et Dnm1 présentent une homologie fonctionnelle avec les dynamines humaines. De plus, l'équipe de Jocelyn Laporte a découvert une nouvelle isoforme de DNM2 spécifique aux muscles nommée DNM2 iso 12b. La dynamine de levure Vps1 a été décrit comme étant l'homologue de hDNM1 et la dynamine de levure Dnm1 comme l'homologue de hDNML1 (également appelé DRP1 ou DLP1). Ainsi, différentes stratégies de phénotypage des levures ont été testées afin de déterminer quels phénotypes pourraient être utilisés pour étudier les mutants de la protéine DNM2 impliqués dans la maladie. Un résumé des phénotypes étudiés est montré dans le Tableau 5. Nous avons utilisé deux souches de levures: *vps1*Δ et *dnm1*Δ. Vps1 et Dnm1 sont deux protéines de levures orthologues des dynamines humaines. Cependant, nos tests de complémentation suggèrent que ces protéines de levure ne sont pas des homologues fonctionnels des dynamines humaines. Ce résultat était inattendu puisque Vps1 et Dnm1 jouent des rôles similaires dans la levure à celle des dynamines humaines. Par exemple, Dnm1 est impliqué dans la fission des mitochondries tout comme hDNM2 dans les cellules humaines (Lee et al, 2016). J'ai fait un marquage fluorescent des mitochondries à l'aide du colorant Mitotracker de *dnm1*Δ exprimant ou non le hDNM2 iso1 humain, hDNM2 iso 12b, hDNM1 iso1, ou hDNM1L iso3. Ce marquage montre que les dynamines humaines ne rétablissent pas le phénotype caractéristique des cellules de levure de type sauvage avec un réseau mitochondrial ramifié et tubulaire. Même si, la coloration Mitotracker des mitochondries réalisée sur des cellules *dnm1*Δ transformées avec hDNM1L iso3

sous promoteur GPD présentait deux phénotypes différents avec certaines cellules montrant une complémentation. De plus, coloration Mitotracker des cellules *dnm1*Δ exprimant hDNM2 iso1 sous le promoteur TetO, a également montré certaines cellules avec un phénotype sauvage, donc une complémentation. Malheureusement, cette complémentation n'est pas assez efficace pour être utilisée pour faire un phénotypage avec les formes de hDNM2 portant des mutations de patients atteints de myopathie CNM ou de neuropathie CMT. Ces expériences ont été réalisées sur des cellules transformées avec des plasmides portant l'ADNc de la dynamine humaine sous le contrôle de deux promoteurs différents, donc pas sous le contrôle d'un promoteur de dynamine, ni intégré dans le génome de la levure. GPD est un promoteur fort constitutif de levure, tandis que le promoteur TetO est un promoteur dont le niveau d'expression peut être régulé par ajout de tétracycline (Blazeck et al, 2012; Yen et al, 2003). En effet, le niveau d'expression de hDNM2 iso1 dans les cellules *dnm1*Δ était 12 fois plus élevé pour le promoteur GPD par rapport au promoteur TetO. Cette surexpression de hDNM2 pourrait affecter sa fonction cellulaire dans les cellules de levure. En effet, le niveau d'expression de hDNM2 iso1 est fortement contrôlé chez les cellules humaines et dans les souris. De plus, des expériences récentes montrent que les souris Mtm1 KO sont guéries de la myopathie CNM en abaissant le niveau d'expression de DNM2 (Tasfaout et al, 2017). D'autres expériences devraient être réalisées avec le promoteur TetO en présence de différentes concentrations de tétracycline afin d'avoir des niveaux d'expression plus bas des dynamines humaines ou avec des plasmides permettant à l'ADNc de la dynamine humaine d'être intégré dans le génome de la levure au locus DNM1 ou VPS1 pour une expression endogène des dynamines humaines dans les cellules de levure. L'analyse de la morphologie des mitochondries réalisée sur la souche *vps1*Δ montre que ces cellules mutantes ont un phénotype de type sauvage. Fait intéressant, les cellules de type sauvage et les mutantes *vps1*Δ exprimant des niveaux élevés de hDNM1L iso3 étiqueté avec la GFP, et dont l'expression est placée sous le contrôle du promoteur GPD avaient un réseau de mitochondries anormal, avec un phénotype de mitochondrie de type *dnm1*Δ. Cela suggère un effet dominant probable de hDNM1L iso3 sur ces cellules de levure. Fait intéressant, l'observation au microscope à fluorescence des 3 dynamines humaines fusionnées avec la GFP exprimées dans les trois souches de levures *vps1*Δ, *dnm1*Δ et sauvage (BY4742) montrait une localisation intracellulaire similaire, c'est-à-dire, quelques points sur les mitochondries, même s'il y avait quelques différences. Dans les cellules *dnm1*Δ, les hDNM2 iso1 et iso 12b étiquetées avec la GFP ont présenté plusieurs points sur les mitochondries alors que hDNM1 iso1 a montré moins de points aux mitochondries et hDNM1L iso3 était principalement cytosolique. Dans les cellules *vps1*Δ il y avait une grande différence entre l'expression de hDNM1L iso3 et les trois autres dynamines; spécifiquement hDNM1L iso3 montrait un motif clairement cytosolique alors que hDNM1, hDNM2 iso1 et hDNM2 iso 12b ont montré des points situés à la mitochondrie. Ce

résultat était vraiment surprenant puisque hDNM1L iso3 est censé être l'homologue de Vps1 et son expression induit un défaut dominant mitochondrial dans les cellules *vps1*Δ. La question est de savoir comment la protéine hDNM1L qui est principalement cytosolique et non observée à la membrane mitochondriale dans les cellules de levure, est capable d'accomplir son rôle à la mitochondrie pour induire un phénotype de mitochondries anormales de type dnm1? Il serait intéressant d'effectuer des expériences de fractionnement subcellulaire afin de séparer les différents compartiments et d'identifier et de quantifier la dynamine hDNM1L présente dans la fraction mitochondriale par rapport à la fraction cytosolique. La souche *dnm1*Δ est caractérisée par un défaut de fission des mitochondries, conduisant à une anomalie du réseau mitochondrial. Des défauts dans la morphologie des mitochondries peuvent entraîner un dysfonctionnement mitochondrial, conduisant à une accumulation pathologique de ROS et par conséquent à la dissipation du potentiel de la membrane mitochondriale (Muller et al, 2015). L'augmentation du stress oxydatif et la perte du potentiel membranaire favorisent la mitophagie.

Nous avons effectué des tests de stress oxydatif en ajoutant du H_2O_2 aux milieux de culture des cellules de levure *dnm1*Δ exprimant ou non les différentes dynamines humaines pour observer l'effet du stress oxydatif sur ces cellules. Fait intéressant, dans des conditions normales sans stress (milieu riche YPD) à la fois les cellules de levure de type sauvage et les mutants *dnm1*Δ transformées ou non avec les plasmides d'expression des dynamines humaines, avaient des courbes de croissance similaires. Dans les conditions de stress oxydatif, il existe une extension de la phase de latence pour les cellules mutantes *dnm1*Δ, mais les pentes des courbes sont les mêmes. Cela suggère que les cellules mutantes *dnm1*Δ ont un retard dans l'adaptation aux conditions de stress. Cela pourrait être dû à un retard dans les voies redox du cytosol et des mitochondries médiées par la voie de la glutathion-NADH oxydoréductase dans les cellules *dnm1*Δ. Il serait intéressant de faire la même expérience mais en ajoutant le H_2O_2 dans les milieux de culture lorsque les cellules sont dans la phase exponentielle de croissance pour voir si les cellules *dnm1*Δ répondent différemment au stress oxydatif. Une autre expérience intéressante serait la visualisation du H_2O_2 en colorant les cellules avec de la dihydro-rhodamine, un réactif non chargé et non fluorescent indicateur des espèces oxygénées (ROS) (Scheckhuber et al, 2007); le potentiel de la membrane mitochondriale pourrait également être coloré en utilisant du $DiOC_6$. Ces deux colorants sont sélectifs des mitochondries et leur intensité de signal fluorescent permettrait d'étudier les levures exprimant ou non les dynamines humaines. J'ai également pu observer une complémentation des cellules *dnm1*Δ exprimant hDNM2 iso1 en présence de 4 mM H_2O_2, dans une culture sur plaque et avec le spectrofluorimètre. Malheureusement, ces premiers résultats très encourageants n'étaient plus reproductibles avec le nouveau lot de H_2O_2, et je ne peux donc pas conclure à ce sujet. Les cellules mutantes *vps1*Δ présentent des défauts de trafic membranaire, avec un retard dans la voie du trafic

vésiculaire entre l'appareil de Golgi et la vacuole, ou voie VPS pour « vacuolar protein sorting » conduisant à la sensibilité au cadmium observée dans les tests en goutte (Ruotolo et al, 2008). Cependant, il n'y avait pas de complémentation de ce phénotype *vps* par les dynamines humaines. D'autres tests liés au trafic membranaire ont été réalisé par la post doctorante Joelle Morvan qui était au laboratoire avant que je commence mon projet de thèse de doctorat. Ces tests consistaient en un test de sécrétion de CPY et des essais de sécrétion d'hydrolases vacuolaires sur des boites de lait. Joelle Morvan a observé qu'il n'y avait pas de complémentation du mutant *vps1*Δ par la dynamine humain DNM2 iso1, même si son expression était sous le promoteur TetO, donc sans une forte surexpression. Le défaut du nombre de peroxysomes observé dans les cellules *vps1*Δ n'a pas été rétabli par l'expression des dynamines humaines testées, pas même par hDNM1L, qui joue un rôle clé dans la biogenèse des peroxysomes dans les cellules humaines. Cette absence de complémentation pourrait être due au fait que la division peroxysomale dans des cellules humaines nécessite une protéine Mff pour cibler hDNM1L aux peroxysomes, tandis que les cellules de levure n'ont pas d'homologues Mff et utilisent d'autres adaptateurs (Schrader et al, 2016). Fait intéressant, en analysant les résultats de la coloration de peroxysome, nous avons réalisé que hDNM2 iso12b semble avoir un effet sur la taille et la forme vacuolaire. Les cellules mutantes *vps1*Δ ont des vacuoles anormales fragmentées, même si les mécanismes restent mal compris. Afin de caractériser davantage ce phénotype vacuolaire, une coloration vacuolaire devrait être faite en utilisant les colorants FM4-64® ou CellTracker ™ bleu CMAC qui colorent spécifiquement les vacuoles et ont été utilisés pour étudier la myotubularine humaine MTM1 dans les cellules de levure. Une possible complémentation du phénotype vacuolaire montrerait que les différences dans les séquences d'acides aminés entre les isoformes hDNM2 1 et 12b peuvent conduire à leur implication dans différentes voies.

Nos résultats montrent que les défauts dans les voies de trafic et les défauts de fission des peroxysomes de la souche mutante de levure vps1 ne peuvent pas être restaurés par une des dynamines humaines hDNM1, hDNM1L, hDNM2 ou hDNM2-12b musculaire.

2.3. PYROXD1 est une oxydoréductase impliquée dans une myopathie de type CNM

PYROXD1 (de l'anglais pyridine nucleotide-disulphide oxidoreductase [PNDR] domain-containing protein 1) est un nouveau gène impliqué dans des myopathies se caractérisant par des faiblesses musculaires précoces avec des noyaux situés au centre des cellules musculaires au lieu de la périphérie. Des mutations dans le gène *PYROXD1* ont été identifiées par séquençage d'exome chez neuf enfants de cinq familles par un consortium international de laboratoires entre l'Australie, la

France, la Turquie et les États-Unis; ce consortium était coordonné par Sandra T. Cooper (Australie) et Jocelyn Laporte (France). Deux mutations faux sens ont été détectées comme étant responsables de la maladie, ces deux mutations faux-sens induisent des changements d'acides aminés aux positions Gln372His et Asn155Ser. Cependant, la protéine PYROXD1 était de fonction inconnue et son activité d'oxydoréductase basée sur des homologies de séquences n'avait pas été testée auparavant. Par conséquent, Jocelyn Laporte a contacté Sylvie Friant pour participer à ce projet en utilisant le modèle de levure de boulanger et mon rôle dans ce projet de recherche était:

- D'abord, définir l'activité de cette nouvelle protéine en utilisant comme modèle la levure Saccharomyces cerevisiae

- Après, tester l'impact de ces deux mutations de patients sur l'activité de la protéine.

Mes données de levure ont été incluses dans un article que j'ai signé en tant que deuxième co-auteur et qui a été publié en 2016 dans l'American Journal of Human Genetics.

2.3.1 Humaniser la levure avec du PYROXD1 humain

Afin de tester l'activité redox de la PYROXD1 humaine dans la levure, j'ai dû considérer le système redox chez Saccharomyces cerevisiae. Les systèmes des glutarédoxines (GRX) et des thiorédoxines (TRX) sont deux voies d'oxydoréductase qui partagent certaines enzymes chez la levure. Ces systèmes sont indispensables pour maintenir l'équilibre redox de la cellule, en catalysant la réduction des protéines oxydées dans la cellule (voir figures 32 et 33 en introduction). Dans les premières expériences, j'ai établi un essai de complémentation dans la souche de levure mutante de délétion du gène *GLR1*. Le gène *GLR1* de levure code pour la glutathion réductase Glr1, une enzyme ayant une double localisation cellulaire au niveau du cytosol et de la mitochondrie. Glr1 participe à l'activité du système GRX en réduisant le glutathion GSSG en GSH.

Dans mes expériences, les cellules mutantes *glr1*Δ ont été transformées avec des plasmides de levure exprimant l'ADNc de la PYROXD1 humaine étiqueté avec la GFP ou non marqué, cet ADNc codait soit la protéine sauvage, soit PYROXD1 portant des mutations de patients Q372H ou N155S. J'ai d'abord vérifié leur expression dans la levure par immunodétection selon la technique du Western blot avec des anticorps spécifiques pour PYROXD1. La figure 3 de l'article inclut le western blot des plasmides d'expression pour PYROXD1. Deuxièmement, afin de déterminer la localisation de la PYROXD1 humaine dans des cellules de levure, j'ai observé les cellules de levure transformées exprimant les différentes constructions de PYROXD1 étiquetées avec la GFP (Fig. 3D, article). La protéine sauvage PYROXD1-GFP et les formes mutantes du patient PYROXD1-Q372H et PYROXD1-N155S ont une localisation similaire avec une coloration cytoplasmique et

aussi un signal plus faible dans le noyau, comme observé pour la coloration de PYROXD1 dans des cultures de cellules COS7 (figure 6). J'ai aussi fait un western blot pour vérifier l'expression des constructions de PYROXD1 étiquetées par GFP, ce western blot est montré dans mon manuscrit de thèse après la publication (figure 53). La protéine sauvage PYROXD1 et les deux formes mutantes du patient sont tous détectées dans des extraits de protéines de levure, montrant que les mutations de patient ne nuisent pas à l'expression de l'ADNc de PYROXD1 et n'aboutissent pas à une instabilité de la protéine (figure 53). Les tests de croissance en gouttes montrent que la souche mutante *glr1*Δ ne pousse pas en présence d'un stress oxydant H_2O_2 (figure 53). Fait intéressant, l'expression de la PYROXD1 humaine complémente cette sensibilité au H_2O_2, montrant que la PYROXD1 humaine agit comme une protéine protectrice du stress oxydatif dans les cellules de levure (figure 53). Par contre, les deux formes de PYROXD1 Q372H ou N155S portant de mutations de patients complémentent moins efficacement cette sensibilité au H_2O_2 de la souche mutante *glr1*Δ, montrant que l'activité oxydoréductase de pYROXD1 est altérée par les mutations de patients atteints de myopathie.

Pour voir si cette complémentation était spécifique de la glutathion réductase Glr1, j'ai également étudié Grx6 qui est une glutarexodine de levure. Grx6 protège la cellule contre le stress oxydatif dû aux ROS (Herrero et al, 2008). Grx6 catalyse la réduction du disulfure de protéine ou du disulfure mixte de glutathion-protéine lié en utilisant un système couplé avec du glutathion, du NADPH et de la glutathion réductase telle que Glr1. Le glutathion réduit GSH agit comme donneur d'hydrogène et la glutathion réductase utilise des électrons du NADPH pour régénérer le glutathion oxydé (GSSG) (figures 32 et 33) (Herrero et al, 2008).

Les cellules mutantes *grx6*Δ présentent un déséquilibre dans l'homéostasie du Ca^{2+} avec une accumulation de Ca^{2+} dans le cytosol et un appauvrissement en Ca^{2+} du lumen du réticulum endoplasmique RE (Puigpinos et al, 2015). Ce phénotype de calcium lié à une activité oxydoréductase est très intéressant puisque le calcium est nécessaire pour la fonction musculaire; donc, j'ai également utilisé la souche mutante *grx6*Δ pour des études d'humanisation avec la PYROXD1. Malheureusement, je n'ai pas pu reproduire les résultats de Puigpinos et ses collègues qui montrent une régulation à la hausse de la voie dépendante du calcium ou CDRE (calcium dependant response element) en absence de Grx6 (Puigpinos et al, 2015). Ainsi, j'ai testé si la souche mutante *grx6*Δ était sensible au stress oxydatif pour valider ma souche mutante. Les tests de croissance montrent que la souche mutante *grx6*Δ ne pousse pas en présence d'un stress oxydant H_2O_2 (figure 54). Fait intéressant, l'expression de la PYROXD1 humaine a complémenté cette sensibilité au H_2O_2, montrant que la PYROXD1 humaine agit comme une protéine protectrice du stress oxydatif dans les cellules de levure (figure 54). De futures expériences seront effectuées en

utilisant des cellules de levure pour tester une nouvelle mutation de patient atteint de myopathie et identifié dans le gène PYROXD1 par le laboratoire de Sandra Cooper (Australie). De plus, d'autres souches de levures mutantes portant des délétions dans la voie de redox (souches grx, trx, trr, figures 32 et 33) seront testées pour la complémentation par PYROXD1, pour déterminer quelles voies peuvent être sauvées, et quelles sont les limites de sauvetage de l'enzyme humaine exprimée dans les cellules de levure. Ces études sur les levures aideront à mieux comprendre les fonctions cellulaires et moléculaires de l'enzyme PYROXD1 humaine.

III. Pensées finales et conclusion

3.1. Humanisation des cellules de levure et arrière-plan des souches de levure

3.1.1. Contexte des souches de levure, un paramètre à considérer

Dans le projet sur la myotubularine MTM1, la souche de levure SEY6210 a été utilisée comme type sauvage. Cette souche a été construite par Scott Emr en croisant les souches de 5 laboratoires différents (Gerry Fink, Ron Davis, David Botstein, Fred Sherman, Randy Schekman). Scott Emr a utilisé cette souche dans les études sur l'autophagie et le tri des protéines. Le mutant *ymr1*Δ que j'ai utilisé pendant ma thèse est un dérivé de cette souche SEY6210. Cette *ymr1*Δ a une vacuole fragmentée avec plusieurs petits lobes, contrairement au type sauvage SEY6210, qui a une vacuole unilobée. Ce phénotype vacuolaire était central pour les expériences réalisées sur la myotubularine MTM1 tout au long de ma thèse. Il convient de noter que le mutant *ymr1*Δ issu de la collecte systématique de suppressions de levures fournie par Euroscarf pour la communauté scientifique a un fond génétique différent. Ce *ymr1*Δ est un mutant dérivé de la souche de laboratoire BY4742. Il a été montré par Dimitri Bertazzi au cours de sa thèse que cette souche mutante *ymr1*Δ dans le fond BY4742 ne présente pas de vacuoles fragmentées, une caractéristique de l'augmentation dans les niveaux de PI3*P* observé dans le *ymr1*Δ avec le fond SEY6210. Par conséquent pour étudier MTM1 et d'autres myotubularines, seule la souche *ymr1*Δ dans le fond SEY6210 était utilisée.

Dans le projet sur la dynamine DNM2, j'ai utilisé 3 souches de la collection de délétion systématique de levure, la souche sauvage de référence nommée BY4742 et les souches mutantes de délétion *vps1*Δ et *dnm1*Δ. Ces souches sont dérivées de S288C. J'ai essayé de complémenter différents phénotypes des souches *vps1*Δ et *dnm1*Δ par leurs homologues humains afin d'étudier la dynamine DNM2 humaine dont le gène est muté dans des myopathies et des neuropathies. Cependant, les différents phénotypes que j'ai testés n'ont pas été restaurés par la dynamine humaine DNM2 malgré la réalisation de différentes expériences. Je n'ai pas réussi à valider un phénotype de

complémentation qui permettrait de réaliser des expériences sur les mutations dans DNM2 des patients atteints de CNM ou de CMT. Considérant ces résultats négatifs et la nécessité de trouver un phénotype afin d'utiliser la levure humanisée pour étudier la dynamine humaine DNM2, il serait intéressant d'utiliser une autre souche de levure. Il serait possible de créer le mutant *vps1*Δ dans le fond SEY6210. En effet, le fond génétique SEY6210 a été utilisé par Scott Emr pour les études de trafic vésiculaire des protéines et Vps1 (vacuolar protein sorting 1) est une protéine de levure impliquée dans le trafic membranaire vers la vacuole. Donc il serait intéressant d'établir le phénotype des cellules *vps1*Δ avec le fond SEY6210 et de les humaniser avec hDNM2. En outre, DNM2 pourrait jouer un rôle dans le trafic membranaire (Ishida et al, 2011). De même, il serait possible de créer le mutant de délétion *dnm1*Δ dans le fond SEY6210. La souche SEY6210 a été utilisée dans des études d'autophagie et DNM2 est important pour l'autophagie des lipid droplets ou LD, des vésicules lipidiques de stockage accumulées dans le cytoplasme des levures. Il serait intéressant d'effectuer des expériences sur l'autophagie avec la dynamine DNM2, ainsi qu'avec la myotubularine MTM1. Malheureusement, je n'ai pas pu reproduire le défaut redox de la souche *grx6*Δ observé par Puigpinos et ses collègues (Puigpinos et al, 2015). Une explication possible serait qu'ils ont utilisé la souche *grx6*Δ construite dans le fond W303-1A. Cette souche W303-1A a une mutation dans le gène *YBP1*, qui abolit sa fonction requise pour l'oxydation, augmentant ainsi sa sensibilité au stress oxydatif (Base de données SGD). Par conséquent, je devrais également analyser la réponse au stress oxydatif dans les souches mutantes de délétion *grx6*Δ et *dnm1*Δ construites dans le fond W303-1A.

3.1.2. Étudier les protéines humaines dans des cellules de levure

Tout au long de l'histoire de la biologie moléculaire et de la génétique, la levure a été largement utilisée comme modèle dans différents laboratoires pour étudier différentes voies dans les cellules eucaryotes. Plusieurs découvertes faites dans la levure ont été extrapolées plus tard aux cellules humaines, permettant l'acquisition de nouvelles connaissances. Cependant, l'humanisation des cellules de levure est une approche récente utilisée dans la recherche pour accéder aux fonctions cellulaires de protéines humaines. Même si cette approche est vraiment puissante, elle est également complexe et ne fonctionne pas toujours, comme j'ai pu l'observer pour l'étude des dynamines humaines dans les cellules de levure. En effet, dans une étude systématique d'humanisation de la levure *Saccharomyces cerevisiae* seulement environ 50% des gènes de levure ont été humanisés avec succès (Kachroo et al, 2015).

Dans une étude récente, différentes mutations de patients atteints de CMT (neuropathie Charcot-Marie-Tooth) tels que DNM2-G358R ont été introduites dans la protéine orthologue de levure Vps1 et analysées, comme le mutant vps1-G397R par exemple, afin d'étudier l'effet de ces mutations

dans la fonction moléculaire et cellulaire de la dynamine de levure Vps1 (Moustaq et al, 2016). Cette approche en ciblant des mutations de patients dans DNM2 et en produisant des mutations équivalentes dans la protéine Vps1 de levure est efficace et a démontré que certaines de ces mutations CMT perturbaient l'oligomérisation de Vps1, l'endocytose ou la liaison de Vps1 aux lipides (Moustaq et al, 2016). Cependant, sur la base de mes études montrant que la DNM2 humaine ne complémente pas les défauts du trafic des cellules de levure mutante *vps1*Δ, peut-être que ces résultats de levure ne reproduisent pas les défauts du patient CNM de la DNM2 humaine. De plus, cette approche en introduisant les mutations du patient dans la protéine de levure est également limitée par la mauvaise conservation en acides aminés entre la levure et les protéines humaines, comme indiqué par les alignements de protéines et études de conservation que j'ai réalisé au cours de ma thèse (figures 29 et 35). Au vu des résultats que j'ai obtenus dans le projet DNM2, il serait possible d'imaginer une différence d'évolution des dynamines entre les protéines de la levure et de l'Homme. Pour cela, il est nécessaire de tenir compte du fait que les protéines de levure Vps1 et Dnm1 n'ont pas les domaines PH et PRD, contrairement aux dynamines humaines hDNM1, hDNM2 iso1 et hDNM2 iso 12b. L'organisation en domaine de la dynamine humaine pourrait être le résultat de l'évolution via des réarrangements de séquences comme l'évolution par acquisition/perte de domaines protéiques, la fusion de petits fragments peptidiques ou la recombinaison "chimérique" de fragments (Sikosek & Chan, 2014).

3.2. Myopathies centronucléaires

Les myopathies centronucléaires liées aux mutations des gènes MTM1, DNM2 et PYROXD1 provoquent une hypotonie et une faiblesse musculaire. Les cas les plus graves souffrent d'insuffisance respiratoire; d'autres patients ont besoin d'une ventilation respiratoire ou d'un fauteuil roulant. Diverses causes peuvent conduire à des altérations du couplage excitation-contraction dans les muscles; et plusieurs facteurs, comme les organites ou les voies intracellulaires jouent un rôle. Nous pouvons considérer les troubles neuromusculaires comme résultant de problèmes de production d'énergie où les mitochondries pourraient être impliquées, ou dans un déséquilibre potentiel électrochimique où le Golgi pourrait être impliqué. Les patients atteints de myopathies centronucléaires ne sont pas capables de contracter leurs muscles ou de maintenir leur tonicité. Les symptômes sont les conséquences de déficiences macromoléculaires dans les cellules et/ou entre les cellules. Pour mieux comprendre les myopathies centronucléaires, il est important de mieux caractériser les dysfonctionnements des muscles au niveau moléculaire. Mon opinion est que nous pourrions utiliser les connaissances sur les dysfonctionnements moléculaires présents dans ces maladies et les relier aux symptômes observés chez les patients par les médecins, car cette approche intégrée pourrait aider à découvrir de nouveaux symptômes qui n'ont peut-être pas été pris en

compte et cela pourrait aussi aider la recherche fondamentale pour aller plus loin et développer de nouvelles lignes de recherches basées sur le diagnostic des médecins. Les fibres musculaires de type I sont les fibres principales affectées par ces myopathies centronucléaires. Ces fibres de type I sont caractérisées par une plus grande concentration de mitochondries, ce qui est cohérent avec les défauts mitochondriaux observés dans les muscles des patients atteints de myopathies centronucléaires. En plus, les mitochondries sont les organites principaux produisant l'énergie sous forme d'ATP, et les muscles et les neurones ont besoin de beaucoup d'énergie pour remplir correctement leurs fonctions. Par conséquent, les fibres de type I ont également la plus forte concentration d'enzymes oxydatives. Fait intéressant, ils ont aussi une haute concentration dans les lipides, et les lipides sont oxydés par β-oxydation dans les mitochondries et les peroxysomes; deux organelles affectées dans les maladies neuromusculaires. Le modèle de l'activité des motoneurones est une clé déterminante de la spécification de la fibre musculaire: les fibres lentes, comme les fibres de type I, expérimentent une stimulation neuronale plus fréquente que les fibres rapides, et cela se traduit par des niveaux plus élevés de $[Ca^{2+}]_{cyt}$ présents dans les fibres lentes par rapport aux fibres rapides. Fait intéressant, in vitro, les fibres rapides peuvent être converties en fibres lentes par exposition à une stimulation électrique fréquente qui imite le modèle d'activité neuronale d'une fibre lente (Cyert, 2003). Compte tenu de ces propriétés des fibres de type I et de l'organisation des sarcomères dans les muscles, j'ai essayé de connecter différentes fonctions cellulaires observées dans les muscles: les espèces réactives de l'oxygène (ROS), la β-oxydation des lipides et la peroxydation lipidique, la courbure de la membrane et la dynamique des membranes ainsi que la composition lipidique des membranes. De plus, le flux de calcium qui déclenche la contraction musculaire à travers le potentiel d'action et favorise par exemple la translocation de GLUT4, inhibe également la mobilité de la myosine pendant la contraction. Enfin, le stress du réticulum endoplasmique et la réponse au stress liée à l'accumulation de protéines mal repliées est liée à l'autophagie, elle-même affectée par des défauts dans le trafic membranaire vers le lysosome/vacuole et par un déséquilibre ionique comme c'est le cas du calcium dans les myopathies centronucléaires liées au RYR ou au STIM. Si nous pensons que le potentiel d'action est un potentiel électrochimique et que les patients ont des déficiences dans la contraction musculaire en raison de déficiences dans la formation d'énergie via la production d'ATP; je pense qu'il est important de se demander d'où vient cette énergie et quels sont les facteurs impliqués? C'est une question générale qui ouvre une grande diversité de possibilités, qui pourraient être étudiées dans le futur.

Je m'excuse si dans les paragraphes suivants, je fais des erreurs d'interprétation des symptômes observés chez les patients. En effet, je ne suis pas médecin et mon idée est plutôt de connecter la recherche fondamentale en biologie avec la médecine, en posant des questions dont les réponses pourraient aider à éclaircir les dysfonctionnements moléculaires et cellulaires liés aux myopathies centronucléaires CNM.

Les patients affectés par une CNM présentent-ils des symptômes liés au stress oxydatif? La fibrose est-elle observée dans l'histologie musculaire des patients CNM comme cela a été observé pour la dystrophie musculaire de Duchenne (figure 55), et cela pourrait-il être la conséquence d'un stress oxydatif (figure 55)?

Les patients ont-ils un problème de calcium dans les os et dans les dents et cela pourrait-il être progressif?

Y a-t-il des rapports de problèmes électrochimiques chez les patients? Le potentiel d'action des neurones a-t-il été mesuré? Et dans la jonction neuromusculaire?

3.3. Les troubles musculaires avec des caractéristiques de stress oxydatif.

Il a été démontré que DNM2 interagit avec l'oxyde nitrique synthase endothéliale, eNOS ou NOS3 (Su, 2014), ainsi qu'avec le nNOS dans les canaux collecteurs du rat (isoforme neuronale ou NOS1) (Hyndman et al, 2016). Les deux isoformes synthétisent constitutivement l'oxyde nitrique de la L-arginine d'une manière dépendante de la calmoduline. L'oxyde nitrique (NO) est un radical libre qui, en biologie, est appelé espèce d'azote réactif (RNS). L'isoforme nNOS est situé au niveau du tissu nerveux (système nerveux périphérique et central) et du muscle squelettique de type II. L'isoforme eNOS est situé à l'endothélium, génère du NO dans les vaisseaux sanguins et est impliqué dans la régulation de la vascularisation. Fait intéressant, eNOS est localisé au niveau de l'appareil de Golgi et dans les cavéoles des cellules endothéliales (Liu et al, 1997).

Les patients CNM ont-ils des problèmes dans les fonctions rénales?

Est-ce que les patients CNM ont des problèmes dans la formation des vaisseaux sanguins et des capillaires dans certains cas spécifiques du tissu? Qu'en est-il de la vascularisation du muscle squelettique?

Dans les cellules de mammifères, il est connu que le cytosquelette d'actine est nécessaire pour la morphologie et positionnement cellulaire de l'appareil de Golgi, et qu'une perturbation du cytosquelette d'actine provoque un effondrement concomitant de l'appareil de Golgi (figure 56) (Valderrama et al, 1998; Valderrama et al, 2000). Chez la levure Saccharomyces cerevisiae, Vps1 a

été identifié comme un nouveau facteur dans le TGN requis pour l'organisation normale de l'actine (Yu & Cai, 2004). Ces données montrent également lien entre le transport des protéines et l'organisation du cytosquelette d'actine. De nouvelles expériences pourraient être effectuées avec la souche *vps1*Δ concernant le lien entre le Golgi et le cytosquelette d'actine afin de trouver un phénotype qui pourrait être complémenté par hDNM2.

3.4. Stress oxydatif et neuropathies.

D'autres gènes que le *DNM2* liés au système d'oxydation-réaction ont été impliqués dans les troubles de Charcot-Marie, comme par exemple *GDAP1*. Le gène *GDAP1* code pour une protéine appartenant à la sous-famille des enzymes de la glutathion S-transférase (GST). Des mutations autosomiques récessives dans ce gène *GDAP1* provoquent des formes axonales, intermédiaires et démyélinisantes de la maladie. Même si l'activité enzymatique GST de cette protéine doit être démontrée, la protéine GDAP1 joue un rôle dans la fission des peroxysomes, la régulation de la dynamique mitochondriale et l'homéostasie calcique (Sivera et al, 2017). En effet, dans les cellules de mammifères, le mécanisme de croissance et de division des peroxysomes est initié par un processus de remodelage de la membrane similaire à la mitochondrie et régulé par de protéines de la morphologie peroxysomale telles que Pex11, DLP1/Drp1, Fis1, Mff, et GDAP1, qui à l'exception de Pex11, sont partagées avec les mitochondries (Schrader et al, 2016). De plus, la calcineurine phosphatase dépendante du calcium/calmoduline peut déphosphoryler des protéines de la machinerie de l'endocytose comme la dynamine (Sun et al, 2010).

La calcineurine pourrait jouer un rôle dans l'endocytose rapide et lente observé aux synapses. Il est à noter que la modulation de l'homéostasie intracellulaire du Ca^{2+} par la régulation redox des thiols des transporteurs est conservée dans l'évolution chez les eucaryotes (Oka & Bulleid, 2013; Puigpinos et al, 2015). Par conséquent, il serait intéressant de mener de nouvelles expériences reliant la régulation du calcium et du redox chez la levure dans la souche *dnm1*Δ.

PIKFyve participe à la translocation de GLUT4 à la membrane dans des cellules de mammifères et DNM2 joue également un rôle dans la translocation GLUT4. Fab1 est l'homologue de levure de PIKFyve et la protéine Gap1 dans la levure est l'homologue de GLUT4. Gap1 interagit avec le GSH1 qui catalyse la première étape de synthèse du GSH et avec Pis1 (phosphatidylinositol synthase) (Shewan et al, 2013). Il serait intéressant d'analyser le trafic Gap1 dans les souches *dnm1*Δ ou *vps1*Δ. Fait intéressant dans les cellules de levure, le stress déclenche l'accumulation de triacylglycérol dans les lipid droplets ou LD. Les LD sont physiquement connectées aux différents organites tels que le réticulum endoplasmique, les mitochondries et les peroxysomes (Yadav et al, 2017). Cependant, la pertinence physiologique de ces interactions physiques doit être approfondie.

Quoi qu'il en soit, il a été montré que des altérations dans la fonction de DNM2 conduisent à une accumulation de LD dans les hépatocytes (Schulze & McNiven, 2014).

Est-ce que la translocation de Glut4 au niveau des membranes a été mesurée chez les patients et si oui est-elle efficace? Qu'en est-il de l'accumulation de gouttes lipidiques dans les hépatocytes chez les patients?

Il pourrait y avoir une relation entre le pourcentage de graisse dans les membranes et les problèmes de courbure des membranes chez les patients CNM. Récemment, des études dans le laboratoire de Fanny Pilot-Storck ont montré que des anomalies dans la synthèse des acides gras très longs sont liées à la fusion des myoblastes et à des anomalies dans la crête mitochondriale (Blondelle et al, 2015). Des études connexes ont été réalisés en levure par Ludovic Pineau lors de sa thèse de doctorat où des défauts dans les voies de synthèse de l'acide gras insaturé et de l'ergostérol ont provoqué un stress dans la courbure de la membrane, diminuant ainsi la courbure de la membrane et affectant le trafic membranaire du Golgi à la vacuole (Pineau et al, 2008).

Des problèmes dans le métabolisme des graisses ont-ils été observés chez les patients?

3.5. Conclusion

En conclusion générale, les myopathies centronucléaires sont des maladies génétiques complexes dans lesquelles les fonctions contractiles des muscles squelettiques sont altérées. Ce qui est le plus surprenant dans ces maladies génétiques est que les gènes portant les mutations sont ubiquitaires, puisque leur expression n'est pas restreinte aux tissus nerveux et aux muscles squelettiques. Cependant, le système nerveux et le muscle squelettique sont les tissus affectés par la maladie. La myotubularine MTM1 est une phosphoinositide 3- phosphatase et des mutations dans le gène MTM1 sont responsables de la myopathie centronucléaire liée à l'X. Les myotubularines de la même famille que MTM1 dont certaines sont très similaires à MTM1 au niveau de la séquence en acides aminés telles que MTMR2 sont associées à une neuropathie de Charcot-Marie Tooth (Raess et al, 2017b). Des mutations dans le gène *DNM2* sont également associées soit à une myopathie, soit à une neuropathie, les mutations faux-sens étant parfois seulement éloignées de quelques acides aminés (figure 13). De plus, il n'y a pas de corrélation entre la position des mutations dans un domaine spécifique de la protéine DNM2 et le type de maladie résultante CNM ou CMT (figure 13). Pour le moment, il n'y a pas d'explications au niveau moléculaire permettant de comprendre pourquoi certaines mutations conduisent à une myopathie et d'autres à une neuropathie. Peut-être qu'il y a une caractéristique tissulaire spécifique due à l'association avec une protéine spécifique, ou due à certains variantes d'épissage spécifiques comme l'isoforme musculaire DNM2 12b, récemment identifié par Belinda Cowling dans le laboratoire de Jocelyn Laporte (Cowling et al,

2017). En effet, DNM2 pourrait interagir avec différents partenaires en fonction du tissu, comme il a été observé pour MTM1 qui interagit avec la desmine, une protéine spécifique du muscle (Hnia et al, 2011). Il pourrait aussi y avoir des changements de conformation en fonction des conditions environnementales. Par exemple, un pH différent pourrait provoquer des changements dans le repliement des protéines permettant l'interaction avec une protéine spécifique, ou une modification de la localisation de la protéine. Le stress oxydatif a un effet différent sur les différentes phosphoinositide 3-phosphatases, puisque les ROS ont un fort impact sur l'activité de la phosphatase PTEN comparativement aux myotubularines qui sont peu affectées par les ROS (Ross et al, 2007). Un déséquilibre ionique pourrait également conduire à des changements dans les charges électriques, qui à leur tour modifieraient la capacité d'interaction entre les enzymes et leurs substrats ou entre deux protéines en interaction. En tenant compte des symptômes des patients CNM, il serait peut-être possible de concevoir de nouvelles expériences de biologie moléculaire ou cellulaire et en utilisant des cellules de levure ou un autre organisme modèle mammifère afin de mettre en évidence les caractéristiques moléculaires impliquées dans ces maladies humaines.

Myriam Sanjuán Vázquez

Study of proteins implicated in centronuclear myopathies by using the model of yeast *Saccharomyces cerevisiae*

Résumé

La myopathie centronucléaire (CNM) est un groupe de maladies génétiques caractérisées au niveau histologique par des noyaux au centre des myofibres au lieu de la périphérie. Des mutations dans trois gènes (MTM1, DNM2 et BIN1) sont associées à cette pathologie. Récemment, l'implication d'un nouveau gène a été révélée dans une myopathie congénitale, le gène PYROXD1.

Cependant, la base moléculaire responsable du déséquilibre à l'intérieur de la cellule reste incertaine et la relation entre le niveau histologique et les symptômes chez les patients n'est pas comprise. De plus, aucun traitement n'est disponible pour ces maladies.

Au cours de ma thèse, j'ai centré mon travail sur l'utilisation du modèle de levure S. cerevisiae pour comprendre trois protéines associées au CNM: la myotubularine Mtm1, l'oxydoréductase Pyroxd1 et la dynamine Dnm2. Ces données révèlent qu'il est possible d'utiliser une simple cellule eucaryote afin d'élucider certains aspects moléculaires de ces protéines impliquées dans des maladies humaines.

Mots-clés: myopathie centronucléaire, interactions intramoléculaires, phosphoinositides, stress oxydatif, *Saccaromyces cerevisiae*

Abstract

Centronuclear myopathy (CNM) is a group of genetic disorders characterized at the histological level by nuclei at the center of the myofibers instead of the periphery. Mutations in three genes (MTM1, DNM2 and BIN1) are associated with this pathology. Recently the implication of a new gene has been revealed in a congenital myopathy, the PYROXD1 gene.

However, the molecular basis responsible for the imbalance inside the cell remains unclear and the relation between the histological level and the symptoms in patients is not understood. Moreover, there is no treatment available for these diseases.

During my thesis I have focused my work on using yeast *S. cerevisiae* model to understand three proteins associated to CNM: the myotubularin Mtm1, the oxidoreductase Pyroxd1 and the dynamin Dnm2. These data reveal that it is possible to use a single eukaryote cell to elucidate some molecular aspects of these proteins implicated in human disorders.

Key words: centronuclear myopathy, intramolecular interactions, phosphoinositides, oxidative stress, *Saccaromyces cerevisiae.*